

2
AD-A233 150

The Pennsylvania State University
APPLIED RESEARCH LABORATORY
P.O. Box 30
State College, PA 16804

DATA FILE COPY

THE EFFECT OF COMPLIANT WALLS ON
THREE-DIMENSIONAL PRIMARY AND
SECONDARY INSTABILITIES IN
BOUNDARY LAYER TRANSITION

by

R. D. Joslin

Technical Report No. TR 91-003
April 1991

Supported by:
Space and Naval Warfare Systems Command

L.R. Hettche, Director
Applied Research Laboratory

Approved for public release; distribution unlimited

Q 1 1 2 5 0 8 3

REPORT DOCUMENTATION PAGE

Form Approved
OMB No. 0704-0188

The reporting burden for this collection of information is estimated to average 1 hour per response, including the time for reviewing instructions, searching existing data sources, gathering and maintaining the data needed, and completing and reviewing the collection of information. Send comments regarding this burden estimate or any other aspect of this collection of information, including suggestions for reducing this burden, to Washington Headquarters Service, Directorate for Information Operations and Reports, 1215 Jefferson Davis Highway, Suite 1202, Arlington, VA 22202-4302, and to the Office of Management and Budget, Paperwork Reduction Project (0704-0188), Washington, DC 20503.

AGENCY USE ONLY (Leave blank)		2. REPORT DATE April 1991	3. REPORT TYPE AND DATES COVERED
TITLE AND SUBTITLE The Effect of Compliant Walls on Three-Dimensional Primary and Secondary Instabilities in Boundary Layer Transition		5. FUNDING NUMBERS	
AUTHOR(S) Ronald D. Joslin			
PERFORMING ORGANIZATION NAME(S) AND ADDRESS(ES) Applied Research Laboratory The Pennsylvania State University P. O. Box 30 State College, PA 16804		8. PERFORMING ORGANIZATION REPORT NUMBER TR#91-003	
SPONSORING/MONITORING AGENCY NAME(S) AND ADDRESS(ES) Space and Naval Warfare Systems Command Department of the Navy Washington, DC 20363-5100		10. SPONSORING/MONITORING AGENCY REPORT NUMBER N00039-88-C-0051	
11. SUPPLEMENTARY NOTES			
12. DISTRIBUTION/AVAILABILITY STATEMENT Unlimited		12b. DISTRIBUTION CODE	
13. ABSTRACT (Maximum 200 words) The use of passive devices to obtain drag and noise reduction or transition delays in boundary layers is highly desirable. One such device that shows promise for hydrodynamic applications is the compliant coating. In previous two-dimensional studies with a mechanical model representing the compliant wall, coatings were found that provided significant transition delays. The present study extends the mechanical model to allow for three-dimensional waves. Previous studies were concerned with the initial linear stage of transition. In this study we also look at the effect of compliant walls on three-dimensional secondary instabilities.			
14. SUBJECT TERMS boundary layer, compliant coating, three-dimensional waves, secondary instabilities			
15. NUMBER OF PAGES		16. PRICE CODE	
17. SECURITY CLASSIFICATION OF REPORT Unclassified		18. SECURITY CLASSIFICATION OF THIS PAGE Unclassified	
19. SECURITY CLASSIFICATION OF ABSTRACT Unclassified		20. LIMITATION OF ABSTRACT Unlimited	

Abstract (cont'd.)

For the initial stage of this analysis, two- and three-dimensional primary instabilities propagate over compliant coatings. Results over the compliant walls are compared with the rigid wall case. Three-dimensional instabilities are found to dominate transition over the compliant walls considered. However, transition delays are still obtained compared with transition delay predictions for rigid walls. The angles of wave propagation are plotted with Reynolds number and frequency. Low frequency waves are found to be highly three-dimensional. Waves of all frequencies approach two-dimensional dominance as they propagate downstream. Calculations at fixed Reynolds numbers are also presented. The results indicate that the dominant mode for the coatings considered occurs for an oblique angle of approximately 40°-60°. Other modes of instability namely Travelling-Wave Flutter and Static-Divergence that arise as a result of the wall compliance are shown to remain marginally stable for oblique waves.

In the second stage of this study, the effect of compliant walls on secondary instabilities in boundary layer transition is determined. A theory developed by Herbert to represent secondary instabilities for two-dimensional primary instabilities is extended to allow for three-dimensional waves. Results for the secondary instabilities with the dominant two-dimensional and three-dimensional primary instabilities over compliant walls are compared with the rigid wall results.

The effect of the variation of amplitude and spanwise wavenumber on the secondary instabilities is examined. Similar to the rigid wall results, the subharmonic mode of secondary instability dominates low amplitude disturbances for compliant walls. Both isotropic and non-isotropic compliant walls lead to reduced secondary growth rates compared with the rigid wall results. For three-dimensional primary instabilities, real and complex conjugate eigenvalues no longer occur. As the angle of wave propagation increases the shift in the phase velocity of the modes of instability increase. For fixed properties, the growth rates for oblique waves decrease for the rigid and compliant walls. Two- and three-dimensional e^z calculations for secondary instabilities were carried out. The compliant walls suppress the amplification of the secondary instabilities. Thus by suppressing the amplification of primary instabilities, the onset of the explosive growth of the secondary instabilities can be delayed.

W-1

Calculations at fixed Reynolds numbers are also presented. These results indicate that the dominant mode for the coatings considered occurs for an oblique angle of approximately 40° - 60° . Other modes of instability namely Travelling-Wave Flutter and Static-Divergence that arise as a result of the wall compliance are shown to remain marginally stable for oblique waves.

In the second stage of this study, the effect of compliant walls on secondary instabilities in boundary layer transition is determined. A theory developed by Herbert to represent secondary instabilities for two-dimensional primary instabilities is extended to allow for three-dimensional waves. Results for the secondary instabilities with the dominant two-dimensional and three-dimensional primary instabilities over compliant walls are compared with the rigid wall results.

The effect of the variation of amplitude and spanwise wavenumber on the secondary instabilities is examined. Similar to the rigid wall results, the subharmonic mode of secondary instability dominates low amplitude disturbances for compliant walls. Both isotropic and non-isotropic compliant walls lead to reduced secondary growth rates compared with the rigid wall results. For three-dimensional primary instabilities, real and complex conjugate eigenvalues no longer occur. As the angle of wave propagation increases the shift in the phase velocity of the modes of instability increase. For fixed properties, the growth rates for oblique waves decrease for the rigid and compliant walls. Two- and three-dimensional e^n calculations for secondary instabilities were carried out. The compliant walls suppress the amplification of the secondary instabilities. Thus by suppressing the amplification of primary instabilities, the onset of the explosive growth of the secondary instabilities can be delayed.

TABLE OF CONTENTS

	<u>Page</u>
LIST OF SYMBOLS	viii
LIST OF TABLES	xiii
LIST OF FIGURES	xvi
ACKNOWLEDGMENTS	xxvi
CHAPTER	
1. INTRODUCTION	1
1.1 Review of Boundary Layer Transition	1
1.2 Review of Compliant Wall Research	12
1.3 Motivation and Scope of Present Research	25
2. DERIVATION OF GOVERNING EQUATIONS	28
2.1 Introduction	28
2.2 Primary Instability Equations	28
2.3 Secondary Instability Equations	34
3. FORMULATION OF COMPLIANT WALL MODEL	45
3.1 Introduction	45
3.2 Primary Wall Equations	45
3.3 Secondary Wall Equations	55
4. NUMERICAL METHODS OF SOLUTION	65
4.1 Introduction	65
4.2 Spectral Method for Primary Instabilities	65
4.2.1 Linear Companion Matrix Method	73
4.2.2 Bernoulli Iteration Method	75
4.2.3 Traub Iteration Method	76

4.2.4 Lancaster's Refinement Method	78
4.3 Shooting Method for Primary Instabilities	79
4.4 Spectral Method for Secondary Instabilities	84
4.4.1 Solution for the Subharmonic Disturbance	84
4.4.2 Solution for the Fundamental Disturbance	89
4.5 Shooting Method for Secondary Instabilities	94
4.5.1 Solution for the Subharmonic Disturbance	94
4.5.2 Solution for the Fundamental Disturbance	96
5. RESULTS OF THE PRIMARY INSTABILITY ANALYSIS	99
5.1 Rigid Wall Verification	99
5.2 Introduction of Wall Compliance	105
5.3 Curves of Neutral Stability	110
5.4 Fixed Reynolds Number Results	116
5.5 Travelling-Wave Flutter	129
5.6 Static-Divergence	140
5.7 2D and 3D e^n Method Calculations	141
6. RESULTS OF THE SECONDARY INSTABILITY ANALYSIS	160
6.1 Rigid Wall Verification	160
6.1.1 Subharmonic Disturbance	160
6.1.2 Fundamental Disturbance	163
6.2 Introduction of Wall Compliance	166
6.2.1 Subharmonic Disturbance	166
6.2.2 Fundamental Disturbance	168
6.3 Results for 2D Primary Waves	169
6.4 Results for 3D Primary Waves	196
7. CONCLUSIONS AND RECOMMENDATIONS	214

7.1 Conclusions	214
7.2 Recommendations for Future Studies	218
REFERENCES	221
APPENDIX A: SECONDARY INSTABILITY EQUATIONS	237
APPENDIX B: SECONDARY COMPLIANT WALL EQUATIONS	248
APPENDIX C: CHEBYSHEV SERIES FORMULAS	267
APPENDIX D: NUMERICAL ALGORITHMS	277
APPENDIX E: A PROPOSED FORMULATION FOR THE TURBULENT BOUNDARY LAYER	280

LIST OF SYMBOLS

a_*	right eigenvector
a_i, b_i, c_i	general coefficients of compliant wall equations
b	plate thickness
\bar{b}	spanwise wavenumber for secondary instability, $= \beta/R \times 10^3$
c_r	phase velocity of primary instability
c_x	streamwise phase velocity of primary instability, $= c_r \cos \phi$
c_z	spanwise phase velocity of primary instability, $= c_r \sin \phi$
f	similarity variable for Blasius profile, $f' = U_o(y)$
g	acceleration due to gravity, $\simeq 32.2 \text{m/s/s}$
i	imaginary index, $=(0,1)$
$m(z)$	metric, $= dz/dy = (1 - z)^2/2L$ or $= dz/dy = 2/y_{max}$
p_1	pressure of primary instability
u_1	streamwise velocity of primary instability
v_1	normal velocity of primary instability
w_1	spanwise velocity of primary instability
p_3	pressure of secondary instability
u_3	streamwise velocity of secondary instability
v_3	normal velocity of secondary instability
w_3	spanwise velocity of secondary instability
p	instantaneous pressure
u	instantaneous streamwise velocity
v	instantaneous normal velocity
w	instantaneous spanwise velocity
t	time variable

x, y, z	Cartesian coordinate system
\tilde{x}, \tilde{z}	laboratory reference frame for secondary analysis
x', z'	transformed reference frame for secondary analysis
y_{max}	normal distance used for shooting method
A	amplitude of primary instability
B	amplitude of secondary instability
B_x	streamwise flexural rigidity of plate
B_z	spanwise flexural rigidity of plate
B_{xz}	transverse flexural rigidity of plate, $=\sqrt{B_x B_z}$
C_i	nondimensional coefficients of compliant wall properties, $i = M, B_x, B_{xz}, B_z, K, K_s, T_x, T_z$
C_i	combined matrices of the OS and S equations $2(N \times N)$, $i = 0, 1, \dots, 5$
\bar{C}_i	constants of integration, $i = 0, 1, \dots, 5$
D_i	lambda matrix, $i = 3, 4, 5, 7$, or 10
E_x	streamwise modulus of elasticity of plate
E_z	spanwise modulus of elasticity of plate
E_i, F_i, G_i	coefficient matrices of Orr-Sommerfeld equation $N \times N$
Fr	frequency of disturbance, $=\omega/R \times 10^6$
G_n	G-polynomials in Traub iteration
H_i, I_i, J_i	coefficient matrices of Squire's equation $N \times N$
I	identity matrix
K	streamwise-normal spring stiffness
K_E	effective streamwise spring stiffness, $=K - g(\rho - \rho_s) \cos \theta$
K_s	spanwise spring stiffness
N	order of Chebyshev series
P	pressure of mean flow

R_δ	displacement thickness Reynolds number, $= U_\infty \delta^* / \nu$
R_δ	boundary layer thickness Reynolds number, $= U_\infty \delta / \nu$
T_n	Chebyshev polynomials of order n
$T_r \{ \}$	trace of matrix
U	streamwise velocity of mean flow
V	normal velocity of mean flow
W	spanwise velocity of mean flow
U_0	Blasius velocity solution, $= f'$
W_0	component of Blasius velocity, $= -U_0 \sin \phi$
U_∞	freestream velocity
Y	right solvent in factorization methods
α	wavenumber of the primary instability, $= 2\pi/\lambda_r = \alpha_r + i\alpha_i = \alpha^* \delta^*$
α^*	dimensional wavenumber of primary instability
α^+	streamwise wavenumber of primary instability
$\bar{\alpha}_n$	$\partial/\partial x$ (secondary instability)
β	spanwise wavenumber of secondary instability
β^*	dimensional spanwise wavenumber of secondary instability
β^+	spanwise wavenumber of primary instability
$\bar{\beta}_n$	$\partial/\partial z$ (secondary instability)
δ	boundary layer thickness
δ^*	displacement thickness
$\delta\theta$	angular displacement of surface element
ℓ	length of rigid-member support
ϵ_v	streamwise vorticity
Ω	normal vorticity
ρ_v	spanwise vorticity

γ	spatial growth rate of the secondary instability
λ_r	wavelength of primary instability
λ_x	streamwise wavelength of primary instability, $=\lambda_r \cos \phi$
λ_z	spanwise wavelength of primary instability, $=\lambda_r \sin \phi$
λ	transformed eigenvalue, $= 1/(\bar{\alpha} - s)$ or $= (\sigma + t)/(\sigma + s)$
s and t	are arbitrary constants
μ	viscosity
ν	kinematic viscosity, $=\rho/\mu$
ν_x	streamwise Poisson's ratio, $=0.5$
ν_z	spanwise Poisson's ratio, $=0.5$
ω	frequency of disturbance, $= \omega_r + i\omega_i = \omega^* \delta^* / U_\infty$
ω^*	dimensional frequency of disturbance
ϕ	angle of wave propagation of disturbance
ρ	density
ρ_m	plate density
ρ_s	substrate density
σ	temporal growth rate of secondary instability
θ	angle between horizontal and rigid-member of compliant wall
τ_{yx}	streamwise viscous shear stress perturbation on plate surface
τ_{yy}	normal viscous stress perturbation on plate surface
τ_{yz}	spanwise viscous shear stress perturbation on plate surface
ξ	dummy variable, $= mv'$
ξ	streamwise surface displacement
η	normal surface displacement
ζ	spanwise surface displacement
Δ_n	$\partial^2 / \partial x^2 + \partial^2 / \partial z^2$ (secondary instability)

∇	operator, $= \partial/\partial x + \partial/\partial y + \partial/\partial z$
Γ_i	coefficient matrices of G_n -polynomial, $i = 1, 2, \dots, 5$
$(\)'$	derivative with respect to y
∞	infinity
{}	defines vector
[]	defines matrices
\int	integral
\sum	summation

LIST OF TABLES

<u>Table</u>		<u>Page</u>
5.1	Spectral convergence of a TSI wavenumber over a rigid wall for $R_{\delta^*} = 998$ and $\omega = 0.1122$ by the Linear Companion Matrix method. (VAX 8550)	100
5.2	Spectral convergence of a TSI wavenumber over a rigid wall for $R_{\delta^*} = 998$ and $\omega = 0.1122$ by Bernoulli Iteration. (VAX 8550)	101
5.3	Spectral convergence of a TSI wavenumber over a rigid wall for $R_{\delta^*} = 998$ and $\omega = 0.1122$ by Traub Iteration (stage 1:stage 2). (VAX 8550)	101
5.4	Isotropic and non-isotropic compliant wall properties optimized at $R_{\delta^*} = 2240$ and $R_{\delta^*} = 5000$ with $\rho_m = 1000\text{kg/m}^3$ (Carpenter and Morris; 1990).	105
5.5	Spectral convergence of a TSI wavenumber over a rigid wall ($C_M \rightarrow \infty$) by the Linear Companion Matrix method. (IBM 3090-vectorized,V, and non-vectorized,NV)	107
5.6	Spectral convergence of the two-dimensional TSI and TWF wavenumbers over a $\theta = 60^\circ$ (2240) wall by the Linear Companion Matrix method. (IBM 3090-vectorized,V, and non-vectorized,NV)	107
5.7	Spectral convergence of the two-dimensional TSI and TWF wavenumbers over a $\theta = 60^\circ$ (2240) wall by Lancaster's method. (IBM 3090-vectorized,V, and non-vectorized,NV)	108
5.8	Spectral convergence of a three-dimensional TSI wavenumber over a $\theta = 60^\circ$ (2240) wall/isotropic plate by the Linear Companion Matrix method. (IBM 3090-vectorized,V, and non-vectorized,NV) (10° angle of wave propagation)	109
5.9	Spectral convergence of a three-dimensional TSI wavenumber over a $\theta = 60^\circ$ (2240) wall/isotropic plate by Lancaster's method. (IBM 3090-vectorized,V, and non-vectorized,NV) (10° angle of wave propagation)	109

6.10	Spectral convergence of temporal eigenvalues for the subharmonic mode of secondary instability for a two-dimensional primary wave over a rigid wall for $R_\delta = 880$, $Fr = 58.8$, $A = 0.00695$, $\beta = 0.214$ and $\alpha = 0.15488 - i0.005504$. (IBM 3090)	161
6.11	Variation of the spanwise wavenumber β for the subharmonic mode of secondary instability for a two-dimensional primary wave over a rigid wall for $R_\delta = 880$, $Fr = 58.8$, $A = 0.00695$, and $\alpha = 0.15488 - i0.005504$. (IBM 3090)	161
6.12	Comparison of the present results with Herbert (1983) for the unstable modes of the subharmonic mode of secondary instability for a two-dimensional primary wave over a rigid wall for $R_\delta = 826.36$, $Fr = 83$, $\beta = 0.18$ and $\alpha = 0.1949$. (IBM 3090)	162
6.13	Spectral convergence of temporal eigenvalues for the fundamental mode of secondary instability for a two-dimensional primary wave over a rigid wall for $R_\delta = 880$, $Fr = 58.8$, $A = 0.00695$, $\beta = 0.214$ and $\alpha = 0.15488 - i0.005504$. (Cray Y/MP)	165
6.14	Variation of the spanwise wavenumber β for the fundamental mode of secondary instability for a two-dimensional primary wave over a rigid wall for $R_\delta = 880$, $Fr = 58.8$, $A = 0.00695$, and $\alpha = 0.15488 - i0.005504$. (IBM 3090)	165
6.15	Spectral convergence of temporal eigenvalues for the subharmonic mode of secondary instability for a two-dimensional primary wave over a rigid wall ($C_M \rightarrow \infty$) for $R_\delta = 880$, $Fr = 58.8$, $A = 0.00695$, $\beta = 0.214$ and $\alpha = 0.15488 - i0.005504$ by the Bernoulli method with three iterations. (IBM 3090)	167
6.16	Spectral convergence of temporal eigenvalues for the subharmonic mode of secondary instability for a two-dimensional primary wave over the $\theta = 0^\circ$ (2240) wall/isotropic plate for $R_\delta = 880$, $Fr = 58.8$, $A = 0.00695$, $\beta = 0.214$ and $\alpha = 0.15212 - i0.004853$ by the Bernoulli method with three iterations. (IBM 3090)	167

6.17 Spectral convergence of temporal eigenvalues for the fundamental mode of secondary instability for a two-dimensional primary wave over a rigid wall ($C_M \rightarrow \infty$) for $R_\delta = 880$, $Fr = 58.8$, $A = 0.00695$, $\beta = 0.214$ and $\alpha = 0.15488 - i0.005504$ by the Bernoulli method with three iterations. (Cray Y/MP) 168

6.18 Spectral convergence of temporal eigenvalues for the fundamental mode of secondary instability for a two-dimensional primary wave over the isotropic wall for $R_\delta = 880$, $Fr = 58.8$, $A = 0.00695$, $\beta = 0.214$ and $\alpha = 0.15212 - i0.004853$ by the Bernoulli method with three iterations. (Cray Y/MP) 169

LIST OF FIGURES

<u>Figure</u>		<u>Page</u>
1.1	A sketch of transition to turbulence in a boundary layer: a-amplification of plane disturbances; b-phase modulation of the wave while three-dimensional effects appear; c-amplitude modulation of waves with peak and valley formation; d-organized longitudinal vortex system; e-intensity changes of vorticity and active formation of spots developing into a turbulent boundary layer (Yurchenko, Babenko, and Kozlov; 1984)	5
1.2	A sketch of the a-subharmonic and b-fundamental modes of secondary instability (Bertolotti; 1985)	7
1.3	Cross-section of the epidermis of a dolphin (Kramer; 1965) . . .	14
1.4	A sketch of Kramer's rubber coating (Kramer; 1965).	16
1.5	Static-Divergence waves of a compliant wall under a boundary layer flow (Gad-el-Hak, Blackwelder, and Riley; 1984)	20
1.6	A sketch of the Grosskreutz compliant coating (Grosskreutz; 1975)	22
1.7	Mechanical model representing the Grosskreutz compliant coating (Carpenter and Morris; 1985)	24
5.1	A comparison of the v_1 -eigenvector solution by the - \times -, spectral approach; —, shooting approach; with - \circ -, Jordinson (1970) for $Re_{\delta^*} = 998$, $\alpha = 0.3086 - i0.0057$ and $\omega = 0.1122$	103
5.2	Curves of neutral stability for the rigid wall determined by —, present calculations; - \circ -, Jordinson (1970); and - \times -, Van Stijn and Van de Vooren (1980)	104
5.3	Real versus imaginary phase velocity for a two-dimensional TSI wave over a $\theta = 0^\circ$ (2240) compliant wall for $Re_{\delta^*} = 2240$ and $\omega = 0.065$ (o, N=48 and \times , N=52)	111

5.4	Curves of neutral stability over a —, rigid wall; — — —, $\theta = 0^\circ$ (2240); and — · —, $\theta = 60^\circ$ (2240) compliant walls	112
5.5	Curves of neutral stability over a —, rigid wall; — — —, $\theta = 0^\circ$ (5000); and — · —, $\theta = 60^\circ$ (5000) compliant walls	114
5.6	Curves of neutral stability over a —, rigid wall; — · —, $\theta = 60^\circ$ (2240); and · · ·, $\theta = -60^\circ$ (2240) compliant walls	115
5.7	Curves of neutral stability over a —, rigid wall; — · —, 2D $\theta = 60^\circ$ (2240) wall; and · · ·, 3D $\theta = 60^\circ$ (2240) wall/isotropic plate at $\phi = 20^\circ$	117
5.8	Two-dimensional growth rates as a function of frequency for TSI waves over a —, rigid wall; — o —, $\theta = 0^\circ$ (2240) wall; and — × —, $\theta = 60^\circ$ (2240) wall at $Re_{\delta^*} = 2240$	118
5.9	Growth rates as a function of frequency for TSI waves over a $\theta = 0^\circ$ (2240) wall/isotropic plate at $Re_{\delta^*} = 2240$ for oblique wave angles of —, 0° ; · · ·, 10° ; — — —, 20° ; — · —, 30° ; — o —, 40° ; · · · × · · ·, 50° ; — △ —, 60° ; — × —, 70°	119
5.10	Growth rates as a function of frequency for TSI waves over a $\theta = 60^\circ$ (2240) wall/isotropic plate at $Re_{\delta^*} = 2240$ for oblique wave angles of —, 0° ; · · ·, 10° ; — — —, 20° ; — · —, 30° ; — o —, 40° ; · · · × · · ·, 50° ; — △ —, 60° ; — × —, 70°	120
5.11	Growth rates as a function of frequency for TSI waves over a $\theta = 0^\circ$ (2240) wall/orthotropic plate at $Re_{\delta^*} = 2240$ for oblique wave angles of —, 0° ; · · ·, 10° ; — — —, 20° ; — · —, 30° ; — o —, 40° ; · · · × · · ·, 50° ; — △ —, 60° ; — × —, 70°	122
5.12	Growth rates as a function of frequency for TSI waves over a $\theta = 60^\circ$ (2240) wall/orthotropic plate at $Re_{\delta^*} = 2240$ for oblique wave angles of —, 0° ; · · ·, 10° ; — — —, 20° ; — · —, 30° ; — o —, 40° ; · · · × · · ·, 50° ; — △ —, 60° ; — × —, 70°	123

5.13	Growth rates as a function of frequency for TSI waves over a $\theta = 60^\circ$ (2240) wall/isotropic plate at $Re_{\delta^*} = 5000$ for oblique wave angles of —, 0° ; — —, 20° ; — · —, 30° ; — o —, 40° ; · · · x · · ·, 50° ; — — —, 60°	125
5.14	Growth rates as a function of frequency for TSI waves over a $\theta = 60^\circ$ (2240) wall/orthotropic plate at $Re_{\delta^*} = 5000$ for oblique wave angles of —, 0° ; · · ·, 10° ; — — —, 20° ; — · —, 30° ; — o —, 40° ; · · · x · · ·, 50° ; — — —, 60°	126
5.15	Two-dimensional growth rates as a function of frequency for TSI waves over a —, rigid wall; — o —, $\theta = 0^\circ$ (5000) wall; and — x —, $\theta = 60^\circ$ (5000) wall at $Re_{\delta^*} = 5000$	127
5.16	Growth rates as a function of frequency for TSI waves over a $\theta = 60^\circ$ (5000) wall/isotropic plate at $Re_{\delta^*} = 5000$ for oblique wave angles of —, 0° ; · · ·, 10° ; — — —, 20° ; — · —, 30° ; — o —, 40° ; · · · x · · ·, 50° ; — △ —, 60° ; — x —, 70°	128
5.17	Growth rates as a function of frequency for TSI waves over a $\theta = 60^\circ$ (5000) wall/orthotropic plate at $Re_{\delta^*} = 5000$ for oblique wave angles of —, 0° ; · · ·, 10° ; — — —, 20° ; — · —, 30° ; — o —, 40° ; · · · x · · ·, 50° ; — △ —, 60° ; — x —, 70°	130
5.18	Growth rates as a function of frequency for TSI waves over a $\theta = 0^\circ$ (5000) wall/isotropic plate at $Re_{\delta^*} = 5000$ for oblique wave angles of —, 0° ; · · ·, 10° ; — — —, 20° ; — · —, 30° ; — o —, 40° ; · · · x · · ·, 50° ; — △ —, 60° ; — x —, 70°	131
5.19	Growth rates as a function of frequency for TSI waves over a $\theta = 0^\circ$ (5000) wall/orthotropic plate at $Re_{\delta^*} = 5000$ for oblique wave angles of —, 0° ; · · ·, 10° ; — — —, 20° ; — · —, 30° ; — o —, 40° ; · · · x · · ·, 50° ; — △ —, 60° ; — x —, 70°	132
5.20	Temporal growth rates as a function of wavenumber for TWF over a $\theta = 0^\circ$ (2240) wall/isotropic plate at $Re_{\delta^*} = 2240$ for oblique wave angles of —, 0° ; — — —, 15° ; — · —, 30° ; — — —, 45° ; · · ·, 60° . (Carpenter; 1990b)	133

5.21	Temporal growth rates as a function of wavenumber for TWF over a $\theta = 0^\circ$ (2240) wall/orthotropic plate at $Re_{\delta^*} = 2240$ for oblique wave angles of —, 0° ; — —, 15° ; - · -, 30° ; - — -, 45° ; · · ·, 60° . (Carpenter; 1990b)	135
5.22	Temporal growth rates as a function of wavenumber for TWF over a $\theta = 60^\circ$ (2240) wall/isotropic plate at $Re_{\delta^*} = 2240$ for oblique wave angles of —, 0° ; — —, 15° ; - · -, 30° ; - — -, 45° ; · · ·, 60° . (Carpenter; 1990b)	136
5.23	Temporal growth rates as a function of wavenumber for TWF over a $\theta = 60^\circ$ (2240) wall/orthotropic plate at $Re_{\delta^*} = 2240$ for oblique wave angles of —, 0° ; — —, 15° ; - · -, 30° ; - — -, 45° ; · · ·, 60° . (Carpenter; 1990b)	137
5.24	Temporal growth rates as a function of wavenumber for TWF over a $\theta = 60^\circ$ (5000) wall/isotropic plate at $Re_{\delta^*} = 5000$ for oblique wave angles of —, 0° ; — —, 15° ; - · -, 30° ; - — -, 45° ; · · ·, 60° . (Carpenter; 1990b)	138
5.25	Temporal growth rates as a function of wavenumber for TWF over a $\theta = 60^\circ$ (5000) wall/orthotropic plate at $Re_{\delta^*} = 5000$ for oblique wave angles of —, 0° ; — —, 15° ; - · -, 30° ; - — -, 45° ; · · ·, 60° . (Carpenter; 1990b)	139
5.26	Two-dimensional curves of maximum amplification for TSI waves over a —, rigid wall; - — -, $\theta = 0^\circ$ (2240) wall; and - · -, $\theta = 60^\circ$ (2240) wall.	145
5.27	Two-dimensional curves of maximum amplification for TSI waves over a —, rigid wall; - — -, $\theta = 0^\circ$ (2240) wall; and - · -, $\theta = 60^\circ$ (2240) wall. Frequencies of: $Fr = -o-, 25.6$; $-x-, 15.4$; and $-\Delta-, 8.1$ over the $\theta = 60^\circ$ (2240) compliant wall	146
5.28	Two- and three-dimensional curves of maximum amplification for TSI waves over a —, 2D rigid wall; - · -, 2D $\theta = 60^\circ$ (2240) wall; — —, 3D $\theta = 60^\circ$ (2240) wall/orthotropic plate; and · · ·, 3D $\theta = 60^\circ$ (2240) wall/isotropic plate	147

5.29	Two- and three-dimensional curves of maximum amplification for TSI waves over a —, 2D rigid wall; - - -, 2D $\theta = 0^\circ$ (2240) wall; — —, 3D $\theta = 0^\circ$ (2240) wall/orthotropic plate; and · · ·, 3D $\theta = 0^\circ$ (2240) wall/isotropic plate	148
5.30	Two-dimensional curves of maximum amplification for TSI waves over a —, rigid wall; - - -, $\theta = 0^\circ$ (5000) wall; and - · -, $\theta = 60^\circ$ (5000) wall	150
5.31	Two-dimensional curves of maximum amplification for TSI waves over a —, rigid wall; - - -, $\theta = 0^\circ$ (2240) wall; and · · ·, $\theta = 0^\circ$ (5000) wall	151
5.32	Two-dimensional curves of maximum amplification for TSI waves over a —, rigid wall; - - -, $\theta = 60^\circ$ (2240) wall; and · · ·, $\theta = 60^\circ$ (5000) wall	152
5.33	Two- and three-dimensional curves of maximum amplification for TSI waves over a —, 2D rigid wall; - - -, 2D $\theta = 60^\circ$ (5000) wall; — —, 3D $\theta = 60^\circ$ (5000) wall/orthotropic plate; and · · ·, 3D $\theta = 60^\circ$ (5000) wall/isotropic plate. (o-calculated values)	154
5.34	The angle of wave propagation as a function of Reynolds number for the most unstable TSI wave over a $\theta = 60^\circ$ (2240) wall/isotropic plate for frequencies of: $Fr = - \times -$, 99.3; —, 89.5; - · -, 67.0; · · ·, 42.3; — —, 20.9; and - - -, 9.8	155
5.35	The angle of wave propagation as a function of Reynolds number for the most unstable TSI wave over a $\theta = 60^\circ$ (2240) wall/orthotropic plate for frequencies of: $Fr = - \times -$, 99.3; —, 89.5; - · -, 67.0; · · ·, 42.3; — —, 20.9; and - - -, 9.8	156
5.36	The angle of wave propagation as a function of Reynolds number for the most unstable TSI wave over a $\theta = 0^\circ$ (2240) wall/isotropic plate for frequencies of: $Fr = - \times -$, 99.7; —, 82.4; - · -, 62.0; · · ·, 41.1; and — —, 15.8	157
5.37	The angle of wave propagation as a function of Reynolds number for the most unstable TSI wave over a $\theta = 0^\circ$ (2240) wall/orthotropic plate for frequencies of: $Fr = - \times -$, 99.7; —, 82.4; - · -, 62.0; · · ·, 41.1; — —, 15.8; and - - -, 8.0	158

6.1	Comparison of the u_3 -distribution of a subharmonic disturbance at $R_\delta = 608$, $Fr = 124$, and $\bar{b} = 0.33$ for the —, shooting method; — \times —, spectral method; and o, Kachanov and Levchenko (1984)	164
6.2	Growth rates of the secondary instabilities as a function of spanwise wavenumber for $R_\delta = 2240$, $Fr \simeq 29.0$, and $A = 0.01$. subharmonic: — o —, rigid wall; \cdots o \cdots , isotropic wall and fundamental: — \times —, rigid wall; \cdots \times \cdots , isotropic wall	172
6.3	Growth rates of the subharmonic disturbance versus spanwise wavenumber for $R_\delta = 2240$, $Fr \simeq 24.5$, and $A = 0.01$. —, rigid wall and — \cdot —, non-isotropic wall	173
6.4	Real versus imaginary temporal eigenvalue of the subharmonic mode for a two-dimensional primary wave over a rigid wall with $R_\delta = 2240$, $Fr \simeq 24.5$, $A = 0.01$, and $\beta = 0.2$. (o, N=40 and \times , N=45)	174
6.5	Real versus imaginary temporal eigenvalue of the subharmonic mode for a two-dimensional primary wave over a non-isotropic wall with $R_\delta = 2240$, $Fr \simeq 24.5$, $A = 0.01$, and $\beta = 0.2$. (o, N=40 and \times , N=45)	176
6.6	Real versus imaginary temporal eigenvalue of the subharmonic mode for a two-dimensional primary wave over a o, rigid wall and \times , non-isotropic wall with $R_\delta = 2240$, $Fr \simeq 24.5$, $A = 0.01$, and $\beta = 0.2$	177
6.7	Real versus imaginary temporal eigenvalue for growing modes of the subharmonic mode for a two-dimensional primary wave over a o, rigid wall and \times , non-isotropic wall with $R_\delta = 2240$, $Fr \simeq 24.5$, $A = 0.01$, and $\beta = 0.2$	178
6.8	Real versus imaginary temporal eigenvalue of the subharmonic mode for a two-dimensional primary wave over a isotropic wall with $R_\delta = 2240$, $Fr \simeq 24.5$, $A = 0.01$, and $\beta = 0.2$. (o, N=40 and \times , N=45)	179

6.9	Real versus imaginary temporal eigenvalue of the subharmonic mode for a two-dimensional primary wave over a o, rigid wall and x, isotropic wall with $R_{\delta^*} = 2240$, $Fr \approx 29.0$, $A = 0.01$, and $\beta = 0.25$	180
6.10	Real versus imaginary temporal eigenvalue for growing modes of the subharmonic mode for a two-dimensional primary wave over a o, rigid wall and x, isotropic wall with $R_{\delta^*} = 2240$, $Fr \approx 29.0$, $A = 0.01$, and $\beta = 0.25$	181
6.11	Amplitude growth with Reynolds number of the subharmonic mode (B) of a two-dimensional primary wave (A) over a rigid wall at $Fr = 124$, $A_o = 0.0044$, $B_o = 1.86 \times 10^{-5}$, and $\bar{b} = 0.33$. —, theory and (x,o), Kachanov and Levchenko (1984) . . .	183
6.12	Two-dimensional curves of maximum amplification for TSI waves over a —, rigid wall; — — —, isotropic wall; and — · —, non-isotropic wall and —o—, waves of $Fr \approx 53$	184
6.13	Amplitude growth with Reynolds number of the subharmonic mode (B) of a two-dimensional primary wave (A) at $Fr \approx 53$, $A_o = 0.004$, $B_o = 1 \times 10^{-5}$, and $\bar{b} = 0.15$ over a —, rigid wall; — — —, isotropic wall; and — · —, non-isotropic wall	186
6.14	Amplitude growth with Reynolds number of the subharmonic mode (B) of a two-dimensional primary wave (A) at $Fr \approx 53$, $A_o = 0.004$, and $\bar{b} = 0.15$ over a —, rigid wall and — · —, non-isotropic wall with B_o : — · —, 1×10^{-5} ; — — —, 2×10^{-5} ; — — —, 3×10^{-5} ; — · —, 4×10^{-5} ; and —o—, 5×10^{-5}	187
6.15	Amplitude growth with Reynolds number of the subharmonic mode (B) of a two-dimensional primary wave (A) at $Fr \approx 53$, $B_o = 1 \times 10^{-5}$, and $\bar{b} = 0.15$ over a —, rigid wall with $A_o = 0.004$; — · —, non-isotropic wall with $A_o = 0.004$; and — — —, non-isotropic wall with $A_o = 0.008$	188
6.16	Velocity distribution of the subharmonic mode of a two-dimensional primary wave over a rigid wall at $R_{\delta^*} = 1771$, $A = 0.18$, $\bar{b} = 0.15$, and $B = 0.0015$ for a- u_3 velocity profiles and b-(v_3, w_3) velocity vectors versus spanwise position . . .	190

6.17	Velocity distribution of the subharmonic mode of a two-dimensional primary wave over a rigid wall at $R_{\delta^*} = 1871$, $A = 0.27$, $\bar{b} = 0.15$, and $B = 1.0$ for a- u_3 velocity profiles and b- (v_3, w_3) velocity vectors versus spanwise position	191
6.18	Velocity distribution of the subharmonic mode of a two-dimensional primary wave over a isotropic wall at $R_{\delta^*} = 1760$, $A = 0.12$, $\bar{b} = 0.15$, and $B = 0.0025$ for a- u_3 velocity profiles and b- (v_3, w_3) velocity vectors versus spanwise position	192
6.19	Velocity distribution of the subharmonic mode of a two-dimensional primary wave over a isotropic wall at $R_{\delta^*} = 1860$, $A = 0.15$, $\bar{b} = 0.15$, and $B = 1.0$ for a- u_3 velocity profiles and b- (v_3, w_3) velocity vectors versus spanwise position	193
6.20	Velocity distribution of the subharmonic mode of a two-dimensional primary wave over a non-isotropic wall at $R_{\delta^*} = 1559$, $A = 0.08$, $\bar{b} = 0.15$, and $B = 0.21$ for a- u_3 velocity profiles and b- (v_3, w_3) velocity vectors versus spanwise position	194
6.21	Velocity distribution of the subharmonic mode of a two-dimensional primary wave over a non-isotropic wall at $R_{\delta^*} = 1659$, $A = 0.09$, $\bar{b} = 0.15$, and $B = 1.0$ for a- u_3 velocity profiles and b- (v_3, w_3) velocity vectors versus spanwise position	195
6.22	Real versus imaginary temporal eigenvalue of the subharmonic mode for two- and three-dimensional primary waves over a rigid wall with $R_{\delta^*} = 2240$, $Fr \simeq 24.5$, $A = 0.01$, and $\beta = 0.2$. (o, 2D and \times , 3D at $\phi = 10^\circ$)	198
6.23	Real versus imaginary temporal eigenvalue of the subharmonic mode for a three-dimensional primary wave at $\phi = 10^\circ$ over a non-isotropic wall with $R_{\delta^*} = 2240$, $Fr \simeq 24.5$, $A = 0.01$, and $\beta = 0.2$. (o, N=40 and \times , N=45)	199
6.24	Real versus imaginary temporal eigenvalue of the subharmonic mode for two- and three-dimensional primary waves over a non-isotropic wall with $R_{\delta^*} = 2240$, $Fr \simeq 24.5$, $A = 0.01$, and $\beta = 0.2$. (o, 2D and \times , 3D at $\phi = 10^\circ$)	200

6.25	Real versus imaginary temporal eigenvalue of the subharmonic mode for a three-dimensional primary wave at $\phi = 10^\circ$ over a o, rigid wall and \times , non-isotropic wall with $R_{\delta^*} = 2240$, $Fr \simeq 24.5$, $A = 0.01$, and $\beta = 0.2$	201
6.26	Real versus imaginary temporal eigenvalue of the subharmonic mode for a three-dimensional primary wave at $\phi = 10^\circ$ over a isotropic wall with $R_{\delta^*} = 2240$, $Fr \simeq 24.5$, $A = 0.01$, and $\beta = 0.25$. (o, N=40 and \times , N=45)	202
6.27	Real versus imaginary temporal eigenvalue of the subharmonic mode for two- and three-dimensional primary waves over a isotropic wall with $R_{\delta^*} = 2240$, $Fr \simeq 29.0$, $A = 0.01$, and $\beta = 0.25$. (o, 2D and \times , 3D at $\phi = 10^\circ$)	203
6.28	Real versus imaginary temporal eigenvalue of the subharmonic mode for a three-dimensional primary wave at $\phi = 10^\circ$ over a o, rigid wall and \times , isotropic wall with $R_{\delta^*} = 2240$, $Fr \simeq 29.0$, $A = 0.01$, and $\beta = 0.25$	204
6.29	Growth rates of the subharmonic disturbance for two- and three-dimensional primary waves over the non-isotropic wall as a function of spanwise wavenumber for $R_{\delta^*} = 2240$, $Fr \simeq 17.9$, and $A = 0.01$. —, $\phi = 0^\circ$; \cdots , $\phi = 10^\circ$; and — —, $\phi = 20^\circ$	206
6.30	Frequency shift of the subharmonic disturbance for a three-dimensional primary wave over the non-isotropic wall as a function of spanwise wavenumber for $R_{\delta^*} = 2240$, $Fr \simeq 17.9$, and $A = 0.01$. \cdots , $\phi = 10^\circ$ and — —, $\phi = 20^\circ$	207
6.31	Growth rates of the subharmonic disturbance for two- and three-dimensional primary waves over the isotropic wall as a function of spanwise wavenumber for $R_{\delta^*} = 2240$, $Fr \simeq 22.3$, and $A = 0.01$. —, $\phi = 0^\circ$; \cdots , $\phi = 10^\circ$; and — —, $\phi = 20^\circ$	208
6.32	Frequency shift of the subharmonic disturbance for a three-dimensional primary wave over the isotropic wall as a function of spanwise wavenumber for $R_{\delta^*} = 2240$, $Fr \simeq 22.3$, and $A = 0.01$. \cdots , $\phi = 10^\circ$ and — —, $\phi = 20^\circ$	209

6.33	Growth rates of the subharmonic disturbance for two- and three-dimensional primary waves over the non-isotropic wall as a function of spanwise wavenumber for $R_{\delta^*} = 2788$ and $Fr \approx 21.0$ for —, $\phi = 0^\circ$ with $A = 0.007$ and $\dots, \phi = 50^\circ$ with $A = 0.045$	210
6.34	Growth rates of the subharmonic disturbance for two- and three-dimensional primary waves over the isotropic wall as a function of spanwise wavenumber for $R_{\delta^*} = 1760$ and $Fr \approx 30.2$ for —, $\phi = 0^\circ$ with $A = 0.010$ and $\dots, \phi = 45^\circ$ with $A = 0.031$	211
6.35	Amplitude growth with Reynolds number of the subharmonic mode (B) of a two- and three-dimensional primary wave (A) at $Fr \approx 53$, $B_o = 1 \times 10^{-5}$, $A_o = 0.004$, and $\bar{b} = 0.15$ over a —, rigid wall; - - -, 2D non-isotropic wall; and $\dots, 3D$ non-isotropic wall	213

CHAPTER 1

INTRODUCTION

1.1 Review of Boundary Layer Transition

A review of Boundary Layer Theory is a formidable task. To mention all of the notable papers in this subject is an impossible undertaking. In this section we will not even attempt such a review. Instead we will discuss a few of the investigations in boundary layer theory that form some of the pieces, which when combined, lead to a better understanding of the physical processes involved in boundary layer transition.

The problem of transition from laminar to turbulent flow in boundary layers is of practical interest. Laminar boundary layers have a much lower skin friction compared with the turbulent counter part. This makes the presence of a laminar boundary layer flow more desirable than the turbulent in many circumstances. In application, a savings of fuel would be obtained if laminar flow can be maintained for high speed vehicles such as airplanes since skin friction drag accounts for a significant percentage of the total drag. Additionally, a laminar boundary layer produces less noise which is important for underwater vehicles such as submarines and projectiles such as torpedoes. Although laminar boundary layers are preferred, some circumstances, such as adverse pressure gradients, lead to separation or large Reynolds number flows where turbulent flow is inevitable. In the previous case turbulent boundary layers are preferred. Therefore it is highly desirable to predict and control whether the flow is laminar or turbulent. Decades of research have focused on this problem. Smith (1956) and Smith and Gamberoni (1956) and van Ingen (1956) developed a method known as the e^n -criterion for transition prediction. It is empirical and therefore must be limited to a known

data base of information. This became the standard tool in engineering practice for lack of anything else. Numerical transition simulations have gained reliability in the past decade. Theoretical tools hold an important place in identifying mechanisms and structures of transition and turbulent flows which have been observed but not yet explained or understood. Stability theory is one of these important theoretical tools which has made some progress since its beginning.

Since there is a multitude of external forces (i.e. noise, particles, roughness, etc.) that can affect the boundary layer, a general theory of transition has yet to be developed. How the mechanisms are ingested into the boundary layer is denoted as "receptivity." Receptivity is the means by which a particular disturbance enters the viscous boundary layer and the nature by which it leaves its impact on the disturbance flow. If these disturbance levels are sufficiently small, they will tend to excite free disturbances which are normal modes such as the Tollmien-Schlichting wave. The study of receptivity is a major area of interest in itself and will not be addressed here. For a review of receptivity refer to Reshotko (1984). We concentrate on the situation in which receptivity has established low level disturbances inside the boundary layer. These disturbances have a sufficiently small amplitude so nonlinear modifications of the mean flow are negligible and the dynamic behavior of the normal modes are governed by linearized disturbance equations which form an eigenvalue problem. We further focus our discussion on boundary layers over flat plates which have two-dimensional mean flows. This in fact neglects the centrifugal instabilities of Görtler vortices, cross-flow vortices and the various modes of interaction. A review of the understanding of these three-dimensional instabilities is given by Reed and Saric (1986).

In the study of stability of a fluid, the basic equations take the form of nonlinear partial differential equations. Due to the complications with such systems,

simplifications are made. In order to proceed in the understanding of the system, linear approximations are made. The first major theoretical contributions to the study of this field, labelled *Hydrodynamic Stability Theory*, was made by Helmholtz (1868), Reynolds (1883), Kelvin (1880), and Rayleigh (1878, 1880, 1887). These initial investigations neglected the effects of viscosity. Viscous terms and the term with the second derivative of the mean velocity proved to be of key importance in explaining boundary layers.

Boundary layer disturbances in the initial stages of transition are governed by linearized dynamic equations. The instabilities are commonly referred to as Tollmien-Schlichting instability waves(TSI) after the work of Tollmien (1926) and Schlichting (1933). Experiments confirming their studies were conducted by Liepmann (1943) and Schubauer and Skramstad (S&S) (1947). Experiments require a low background of disturbance level and the introduction of controlled oscillations. A small two-dimensional disturbance was introduced by a vibrating ribbon for the experiments of S&S. The equations governing linear instabilities for locally parallel flows are the Orr-Sommerfeld equation after the work of Orr (1907) and Sommerfeld (1908) and the Squire's equation after the work of Squire (1933). Squire highlighted the two-dimensional wave using a transformation from three to two dimensions since he showed that an equivalent two-dimensional problem may be formulated. He showed that the dominant instability is two-dimensional. However, oblique waves or streamwise vortices cannot be considered irrelevant as we will emphasize in the present study.

A view of the instability picture consists of an irregular pattern of three-dimensional wave packets with non-uniform frequencies. Usually assumptions are made to simplify the analysis of studies since the total solution is unattainable presently. If nonlinear coupling is ignored, individual components of the frequency

spectrum may be studied. More over, most studies make this assumption and it will be employed in this investigation. Similarly, the rigid wall theoretical analysis begins with two-dimensional travelling TSI waves. The TSI waves are referred to as *primary* instabilities since additional instabilities arise as a result of the vorticity of this instability. Temporal and spatial stability concepts change the streamwise growth slightly but provide a common curve of neutral stability. This curve marks the region where a disturbance neither grows nor decays in frequency-Reynolds number space. This marks the region of growth for disturbances with suitable frequencies. The disturbance enters the region of growth as it travels downstream. At the upper portion of the curve it ceases to growth and becomes damped after crossing the curve. Further discussion of the neutral curves will be given in a later section. This concept outlines spatially growing waves since Gaster (1962) showed that growth rate predictions made spatially were quantitatively more correct than temporal. Several studies have been conducted on the effects of non-parallelism. Among these are Gaster (1974), Saric and Nayfeh (1977), Bridges and Morris (1984b), and Fasel and Konzelmann (1990). The major conclusion of these studies was that the effect of non-parallelism is to enlarge the neutral curve moderately, most predominantly for high frequencies.

An accurate process of transition from a laminar to turbulent boundary layer can best be qualitatively understood by observations. A sketch of transition from the initial two-dimensional travelling wave to turbulence is given by Yurchenko, Babenko, and Kozlov (1984) and shown in Figure 1.1. The most significant effect of the TSI waves is the breakup of the uniform flow (Figure 1.1b-c). This is characterized by a redistribution of the spanwise vorticity into periodic concentrations near the critical layer. The critical layer ends at the location in which the

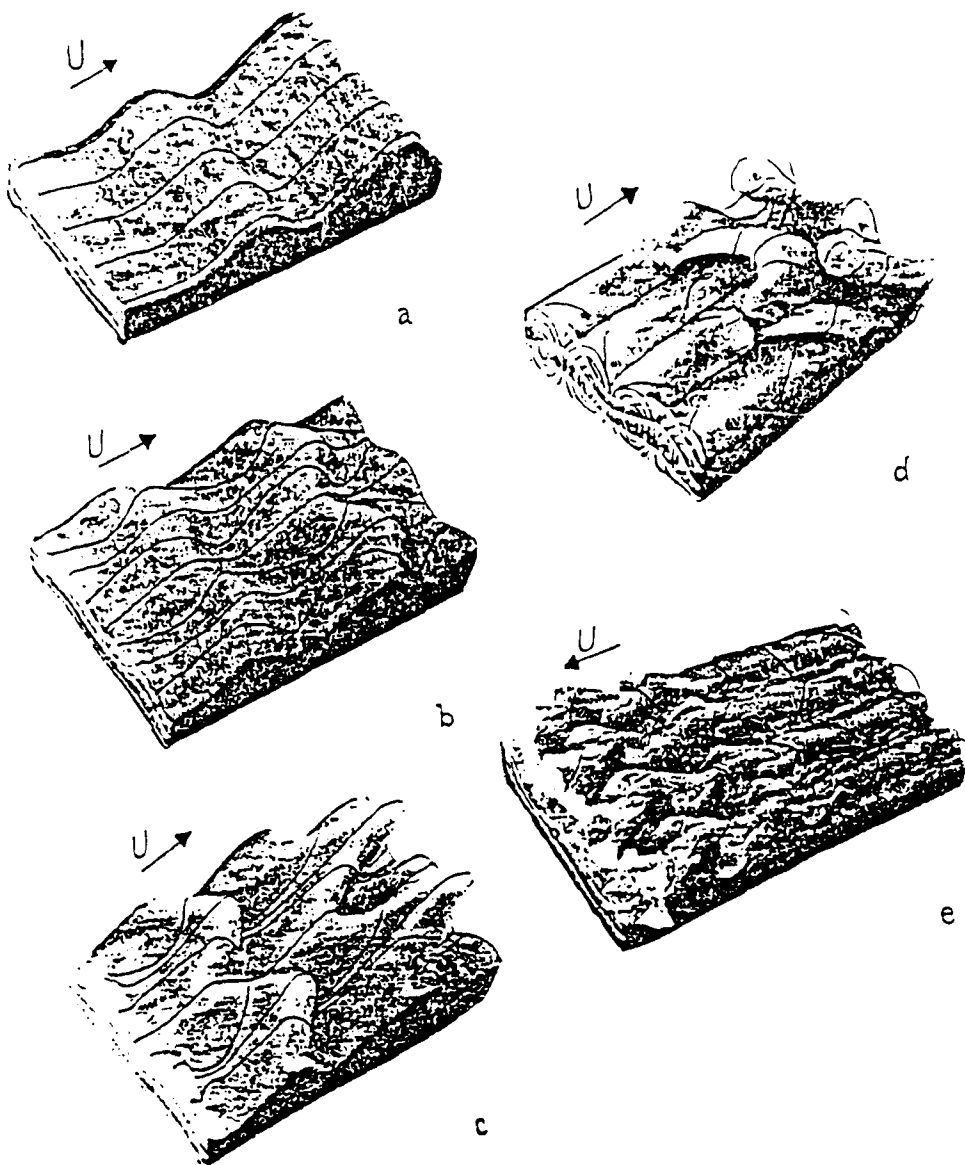
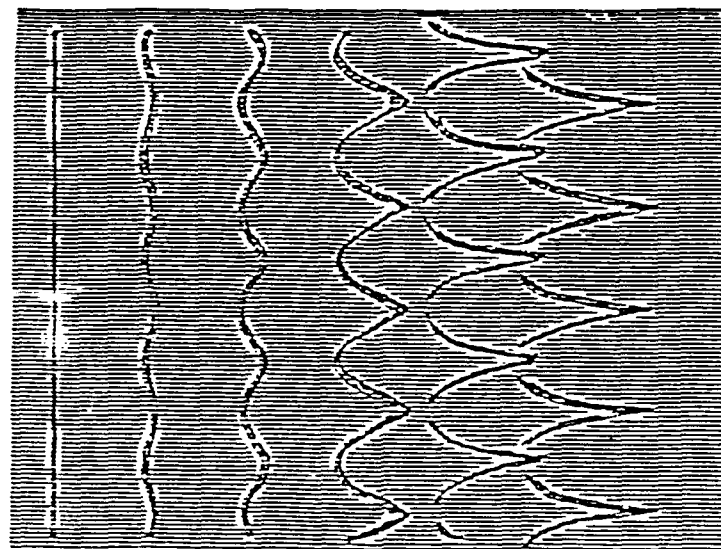


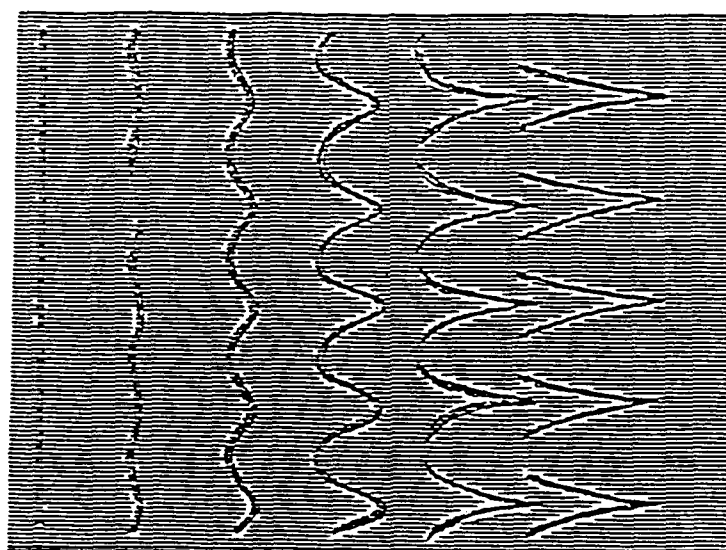
Figure 1.1 A sketch of transition to turbulence in a boundary layer: a-amplification of plane disturbances; b-phase modulation of the wave while three-dimensional effects appear; c-amplitude modulation of waves with peak and valley formation; d-organized longitudinal vortex system; e-intensity changes of vorticity and active formation of spots developing into a turbulent boundary layer (Yurchenko, Babenko, and Kozlov; 1984).

wave speed equals the mean velocity. These waves grow on a slow viscous scale between the neutral curve, then decay. The question then arises as to how these two-dimensional waves which grow and decay are related to turbulence which is violent, three-dimensional and of high frequency. Other than the concern of "receptivity," this is the major question that is addressed today in boundary layer transition. A partial answer to this question is available and given in the remaining portion of this review.

As with the observations of Yurchenko et al., a number of experiments were conducted on transition. The pioneering investigation was conducted by Klebanoff, Tidstrom (1959), and Sargent (1962) where they observed the three-dimensional nature of interest. They observed a distinct arrangement of Λ -shaped vortices which are characterized as aligned in rows. These are referred to as fundamental mode or peak-valley splitting. An alternative distinct three-dimensional mode consists of Λ -shaped vortices which are staggered. This is referred to as subharmonic mode or peak-valley alignment. This later three-dimensional mode was observed and measured using a hot-wire by Kachanov, Levchenko, and Kozlov (1979, 84) and Saric, Kozlov, and Levchenko (1984). A sketch of the subharmonic and fundamental modes of secondary instability is shown in Figure 1.2. A combination of these three-dimensional instabilities can occur also. These are referred to as detuned modes. At sufficiently low amplitude of the TSI wave, the wave grows and decays. At a larger amplitude, this three-dimensional structure evolves. After the three-dimensionality sets in, the highly inflectional instantaneous velocity profiles become unstable with respect to high-frequency disturbances. This causes "spikes" in the hot-wire signal. Eventually breakdown to turbulence occurs.



a



b

Figure 1.2 A sketch of the a-subharmonic and b-fundamental modes of secondary instability (Bertolotti; 1985).

Out of these experiments numerous attempts have been made to try to explain the three-dimensional phenomena by using weakly nonlinear models. Among these Benney and Lin (1960) proposed a nonresonant model in which a two-dimensional wave with wavenumber $(\alpha^+, 0)$ interacts with two oblique waves $(\alpha^+, \pm\beta^+)$. Further work on the nonresonant model was conducted by Benney (1964) and discussed more recently in a review by Benney and Chow (1987). This nonresonant model is crude and has its limitations as Benney admits. However, the approach does predict flow patterns qualitatively. Stuart (1962) criticized the Benney-Lin model. He argued that a phase change would occur between the waves due to the different wave speeds. This would not agree with observations. Herbert and Morkovin (1979) proposed a model of the two-dimensional wave $(\alpha^+, 0)$ interacting with longitudinal vorticity $(0, \beta^+)$. Both interaction models have failed to fully reproduce the characteristics of the peak-valley splitting.

Another weakly nonlinear theory was suggested by Craik (1971). He proposed a resonant triad model which consists of a TSI wave $(\alpha^+, 0)$ and two subharmonic oblique waves $(\alpha^+/2, \pm\beta^+)$ with twice the spanwise wavelength of the TSI wave. Craik's results suited the experiments by Klebanoff et al. at a high frequency. Subharmonic resonance was found for peak-valley alignment, but the application of Craik's model is limited and does not explain the behavior of the three-dimensional modes.

These weakly nonlinear theories fail to model the physical phenomena. Additionally, since these are of the perturbation family, the accuracy and convergence of the solution is dependent on whether the perturbation "parameter" is sufficiently small.

Direct numerical simulations of boundary layer transition have been performed by Wray and Hussaini (1980) and Zang and Hussaini (1988, 1989). This

is possible due only to advances in computers and computational methods. Additionally a spatial growing analysis has been performed by Fasel, Rist, and Konzelmann (1987). Numerous obstacles remain with simulations of this type. Insufficient resolution is present for the nonlinear stages of the three-dimensional development. Additionally, computations suffer from the inability to specify outflow conditions properly. Although numerical and experimental results are similar, the numerical studies have lacked the ability of predicting the point of transition. This is due to the fact that most studies have been performed temporally.

Up to this point, several experiments have been performed identifying the occurrence of peak-valley splitting (fundamental), peak-valley alignment (sub-harmonic) and combination (detuned) modes of three-dimensional instabilities. A revised picture of how these modes occur was suggested by Orszag and Patera (1980, 1981) and Herbert (1981). Previously, the three-dimensionality was attributed to spanwise differential amplifications of the TSI wave and the onset of spikes were considered to arise from secondary instabilities. They suggested that the exponential growth of the small three-dimensionality was due to a secondary instability mechanism. The initial proposal was solved for channel flow through use of Floquet theory. This new theory was later introduced by Herbert (1983) to solve the boundary layer stability problem that provided results consistent with the experiments of Klebanoff et al. for peak-valley splitting and Kachanov et al. for peak-valley alignment. This theory of secondary instability agreed with the numerical simulations of Spalart and Yang (1987). Herbert's theory is based on the assumption that the mean flow is not altered by the primary instability. The mean and primary flow form the basic flow upon which a disturbance (secondary) is imposed. The coordinate reference frame is transformed to one moving with the

primary wave. This gives a periodic wave with a constant amplitude. This is valid with the assumption that the secondary instability grows much faster than the primary. A form of solution is found from Floquet theory. Herbert has shown the application of this new theory and when previous models (i.e. Craik, Benney and Lin) apply. The main results that are found from this new theory are as follows. First, three-dimensional secondary instabilities can lead to different disturbance characteristics. Peak-valley splitting arising from primary resonance with the TSI wave occurs when the TSI amplitude reaches some threshold. Subharmonic resonance (peak-valley alignment) can occur at even smaller amplitudes. Secondly, these secondary instabilities originate from the redistribution of spanwise vorticity into regions of streamwise periodicity near the critical layer. Growth of the three-dimensional modes arise from vortex stretching and tilting. Next a link exists between the primary instability and the three-dimensional modes. Finally, the calculated growth rates and velocities are consistent with experiments.

A series of recent experiments have been conducted by Corke (1987) and Mangano (1987). As with the previous theory, these experiments are directed at measuring the resonant interactions in the boundary layer instabilities. Resonant growth occurs through the simultaneous forcing of plane TSI waves $(\alpha^+, 0)$ and oblique waves $(\alpha^+/2, \pm\beta^+)$. This promotes the interaction of other modes of the form $(3\alpha^+/2, \pm\beta^+)$, $(5\alpha^+/2, \pm\beta^+)$, $(\alpha^+/2, \pm 2\beta^+)$, and $(0, \pm 2\beta^+)$. Both subharmonic and fundamental secondary modes were found to exist in the Blasius boundary layer. The parametric interaction led to a loss of phase locking and a rapid spectral filling associated with transition to turbulence.

The alternative root to transition was not addressed but is of importance. If the amplitude of the ingested disturbance is large enough, the linear region of transition is by-passed and nonlinearities dominate. Murdock (1977) and Mur-

dock and Taylor (1977) looked at this large amplitude nonlinear wave interactions. Similar studies were conducted by Fasel (1974, 1976) using direct numerical simulations. The results of this system are amplitude dependent.

A significant number of investigations have been undertaken with the goal of understanding and predicting transition. This review noted only a few of the many important contributions. These were limited to two-dimensional TSI waves introduced into a mean flow over a flat plate. Further, theories were discussed to model the secondary instability mechanism. In the past decade significant progress has been made in modeling the physical mechanisms that make up transition. There are still many more problems to be considered and overcome including modeling the fully nonlinear mechanisms as well as come up with a more comprehensive theory to predict transition.

We have only touched on the subject of transition to turbulence in a boundary layer. A number of other investigations have focused on transition and turbulence, but were not discussed. Some of these are Stuart (1958, 1960), Raetz (1959), Maseev (1968), Landahl (1972), Saric and Reynolds (1979), Blackwelder (1979), Nayfeh and Bozatli (1979), Nayfeh and Padhye (1979), Nayfeh (1985), Thomas (1986), Hall and Smith (1988), and Smith (1988). Only a few of the numerous important papers could be listed in this text. More complete reviews are given by Dryden (1955), Stewartson (1975), Tani (1977), Maslowe (1981), Morkovin (1983), Reshotko (1986), Herbert (1988b), and Bayly, Orszag and Herbert (1988).

In the present investigation we will make use of the linear and secondary instability theories for the study of boundary layer transition over a compliant wall. Before the compliant wall model and the motivation and goal of this study are introduced, a review of compliant wall research will be given below.

1.2 Review of Compliant Wall Research

There is an ever-increasing demand for new technologies to increase the efficiency of commercial and military transportation (i.e. aircraft, ships, submarines, etc.). This arises from the increasing costs of fuel. For aircraft, ships, and underwater vehicles, skin friction drag can account for a considerable percentage of the total drag. Any decrease in viscous drag would lead to a more efficient vehicle and corresponding fuel savings. And since laminar boundary layer flows have a much lower skin friction than turbulent, it is highly desirable to maintain laminar flow if possible. One such passive device that shows promise in delaying this onset of turbulence is the compliant wall. In practise, the use of a compliant wall to delay transition to turbulence would occur for small projectiles where turbulent flow would otherwise occupy a small percentage of the surface. In the present study, a compliant wall will be used with this limitation in mind. Before we discuss the goals of this investigation, a review of the use of compliant walls for transition delays will be given.

The road to understanding a physical process can best be undertaken by observing the process as it occurs in nature. It is through these observations that we may form our understanding of a phenomenon. This is precisely what led to the proposed theories for instabilities in transition that were discussed in the previous section. This is also how compliant coating research began.

The particulars concerning the shapes, sizes, and speeds of fish and various marine mammals began as early as 1919. Since then expeditions and studies have been conducted to eliminate conflicting reports. The results of these studies have inspired further work concerned with understanding the propulsive and flow characteristics of these fish and mammals. Gawn (1948) did a study on

the propulsive efficiency of the whale. Similarly, Gray (1957) talked about the efficiencies of various fish, a dolphin, and a whale. Gray was clever to focus on a seeming inconsistency between nature and what was currently known about hydrodynamics. Gray notes that for the speeds that the dolphin and whale achieve, physiologists argue that an intolerable strain would be placed on their hearts in order to generate sufficient power for motion through turbulence. On the other hand, the power was sufficient for laminar flow. Most aerodynamic and hydrodynamic engineers would consider an absence of turbulence at the dolphin and whale speeds unlikely. So we have a seeming controversy between the physiologist and engineer concerning these mammals. This was known as Gray's Paradox. An explanation of Gray's Paradox was suggested by Lang and Pryor (1966). Some of the observations of dolphins swimming at high speeds resulted from assisted locomotion where the ships' waves or the bow pressure field added to the thrust of the animals. It has been argued that many of the sighted short-term bursts of speed can be explained by the great power output of the muscles that go into a state of "oxygen debt." Finally, it was demonstrated that the speed and time duration are linked and that the power required for the speeds in the range reported by Gray could be attained for a few seconds. Ending this comment on Gray's Paradox, let us continue with the review.

It was not until the mid 1950's that an explanation was proposed by Kramer (1957-65). He attempted to exploit the "dolphin's secret" technologically. Kramer made detailed observations and experiments of the properties and characteristics of the dolphin's epidermis. Shown in Figure 1.3 is the complex structure imbedded in the dolphin skin. The epidermis consists of several layers. In general, the outer most layer may be compared to a plate of soft rubber. The next layer contains many thin ribs which connect the top "plate" with the hide. Between the ribs are

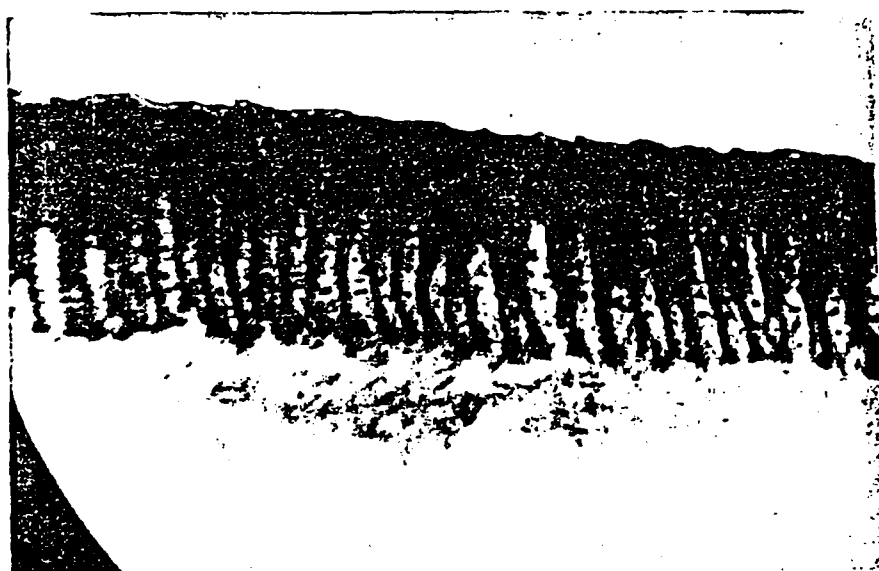


Figure 1.3 Cross-section of the epidermis of a dolphin (Kramer; 1965).

narrow ducts which contain soft spongy material that are water logged. These ducts are aligned parallel to the flow direction. Although, Kramer had an imperfect understanding of the structure and function of the dolphin epidermis, he designed a rubber coating (i.e. compliant) based on his observations. From a series of experiments conducted in Long Beach Harbor, California U.S.A., Kramer was able to achieve a 60 percent drag reduction with one of his coatings covering a projectile compared to the uncoated projectile. The Kramer coating consisted of a thin rubber diaphragm supported by short rubber stubs. A sketch of Kramer's coating is given in Figure 1.4. The space between the stubs was filled with a viscous fluid. This coating has many of the characteristics of the dolphin skin. Kramer's initial postulation that the dolphin was able to sustain a laminar flow was changed. Instead Kramer suggested that the transition to turbulence could be suppressed, or delayed, by viscous damping within the wall. For viscous damping in the wall to work, the wall compliance must be soft enough for the wall to respond favorably to the fluctuations due to the disturbance in the flow. If a transition delay over these coatings was achieved, then significant drag reductions may be realized as a result of lower skin friction.

Kramer's compliant invention is of great importance for hydrodynamic applications. A reduced drag means a savings of energy expended. Further a transition delay means that bodies may move with greater speeds prior to turbulence. These coatings would have distinct advantages acoustically since laminar flows are quieter than turbulent flows.

Since Kramer's results were so astounding and the prospective applications so great, several experimental and theoretical studies were undertaken to duplicate and explain Kramer's findings. Experiments in the 1960-70's were conducted by Gregory and Love (1961), Babenko (1973), and others. No experimental results

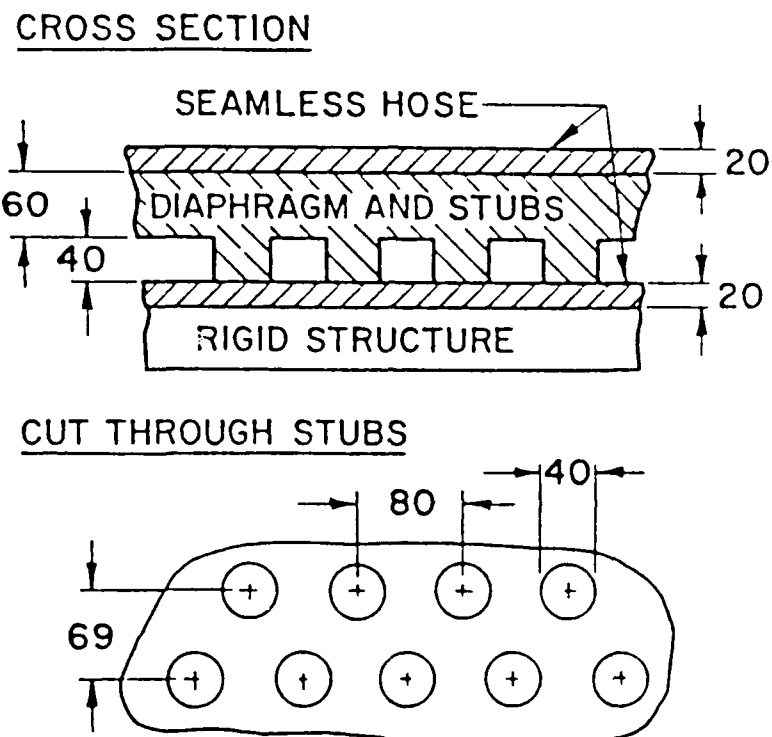


Figure 1.4 A sketch of Kramer's rubber coating (Kramer; 1965).

to date have affirmed Kramer's results. It is pertinent that an appropriate choice of wall properties be used. These experiments may not have used appropriate coatings for their studies. Only recently, experiments have been conducted by Daniel (1984-86), Willis (1986), and Gaster (1987) that show favorable results using compliance. Their experiments were conducted in a long water towing tank at BMT in the United Kingdom. A disturbance was introduced by injecting air through a hundred tiny holes at the leading edge of the test section. Disturbances are detected by foil gauges surface mounted at the trailing edge of the test section. Using a compliant coating, approximately a 60 percent reduction in the foil response occurred as compared to the rigid wall results. A similar reduction was found theoretically. Other recent experiments have been conducted by Hansen and Hunston (1983) and Gad-el-Hak, Blackwelder, and Riley (1980,84). Although they failed to obtain favorable effects from compliance, they did demonstrate an additional wall-mode instability that may arise with the use of compliance.

With little success in obtaining drag reductions and transition delays, interest was extended to investigating the possible effects of compliant walls on turbulent boundary layer flows. In the 1970's research programs were sponsored by NASA Langley Research Center and in the 1980's the Office of Naval Research to determine if drag reductions were possible using compliance. These studies indicate that drag increases occur prior to surface deformation. Further, emphasis was placed primarily on turbulent drag reduction. Investigations carried out by these organizations are described by Bushnell(1984), Hefner, and Ash (1977) and Reischman (1984). The experiments in the 1960-70's have been discounted for many reasons. Some contend the results of these experiments due to experimental bias or imperfections.

At the same time that experiments were being conducted to confirm

Kramer's results, researchers were at work trying to explain these findings theoretically. Early theoretical studies were performed by Benjamin (1960,63,64), Landahl (1962), Betchov (1959), and Gyorgyfalvy (1967). Benjamin and Landahl identified and separated modes of instability that may arise from the fluid/wall interaction of flow over a compliant wall. These were named Class A, Class B, and Class C. The Class A instability was shown by Benjamin to be destabilized by wall damping while Class B instabilities were stabilized. Additionally, Class A instabilities require an extraction of energy from the initially unperturbed system for their activation and consequently are destabilized by dissipation. The opposite is true of the Class B instability. The stability of these waves is determined by the net effect of irreversible processes which include dissipation and energy transfer from non-conservative hydrodynamic forces. Class C instabilities involve conservative forces and thus conservative energy transfers from the flow to the wall. They are inviscid and an example of which is the Kelvin-Helmholtz instability. The present study will involve three instabilities. The first is the common Tollmien-Schlichting Instability (TSI), which is a Class A instability. This instability is a slow moving wave (slower than the freestream velocity) which is present over rigid and compliant walls. The second is the Travelling-Wave Flutter (TWF) which is a Class B instability. This instability is a fast moving wave (faster than the freestream velocity) and is a surface-induced instability. The third is Static-Divergence which is a Class C instability. This instability is a result of the compliant wall. When this instability is present, any potential transition delay characteristics which the coating may possess is destroyed.

Another study was conducted by Kaplan (1964). The important results in corrected form were given by Landahl and Kaplan (1965). They found significant reduced spatial growth rates over spring-backed membranes compared to the rigid

wall case. Little else was attempted for transition in the remainder of the 1960's and 1970's except for some possible European and Russian investigators (i.e. Babenko et al., 1971-79). Work during this period was concerned with the effect of compliant walls for turbulent drag reduction. In the 1980's a re-assessment of Kramer's work began. This occurred, in part, due to the arguments made by Carpenter and Garrad (1985,86). Although much controversy still exists concerning Kramer's results, Carpenter and Garrad have demonstrated with two-dimensional theory that substantial transition delays were possible with Kramer's coatings. Further, a careful assessment of other experimental tests revealed deficiencies in the facilities and methods used. Additionally they were able to duplicate Landahl and Kaplan's results. To accomplish this an error had to be intentionally made in the scaling. This indicated that Landahl and Kaplan had made a minor scaling error. Finally, they showed that the Class C instability, Static-Divergence, could be represented by a function of the wall properties and that there was a characteristic critical or onset speed for Divergence. If the flow speed was below the critical speed, Divergence was stable and did not occur. If the flow speed was above the critical onset speed, Divergence resulted and any potential transition delay was destroyed. Gad-el-Hak et al. and Hansen et al. experimentally verified that the onset of Divergence occurred only after the flow speed reached some threshold. The observed surface deformation arising as Static-Divergence is shown if Figure 1.5.

There has also been some work done on the stability of inviscid flows over flexible coatings. Many of these were done with the turbulent flow interacting with the coating. The inviscid stability of a potential flow over a viscoelastic wall was studied by Evrensel and Kalnins (1985). A similar study with the addition of a pressure perturbation correction was done by Duncan, Waxman, and Tulin

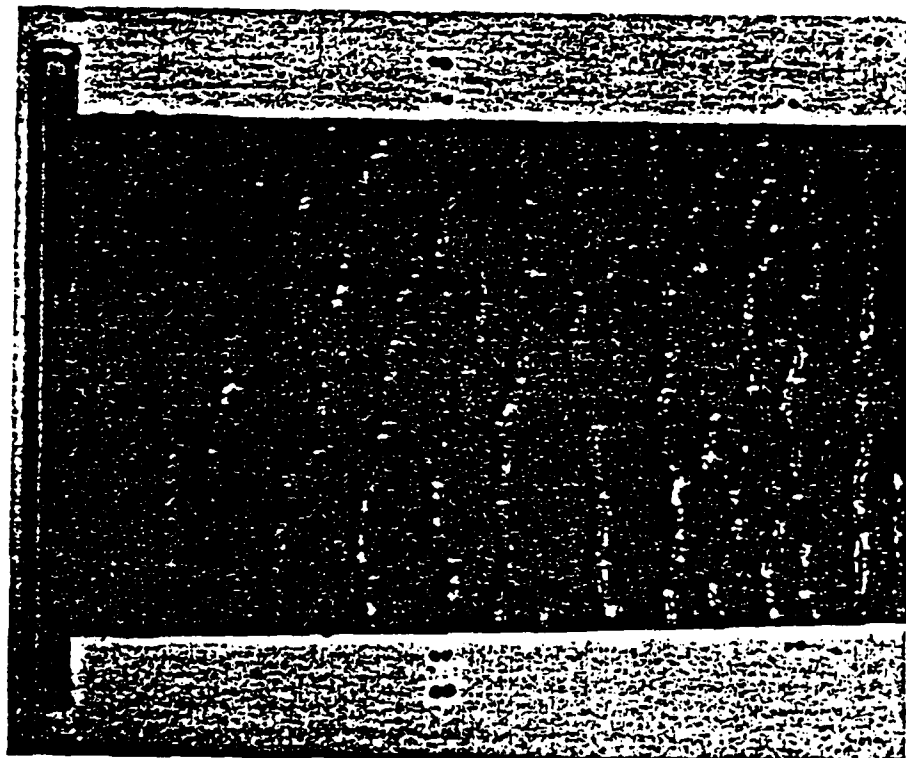


Figure 1.5 Static-Divergence waves of a compliant wall under a boundary layer flow (Gad-el-Hak, Blackwelder, and Riley; 1984).

(1985). The main feature that their models lack is the viscosity of the fluid.

A theoretical framework for the study of multilayered walls was given by Yeo (1986, 1988). This approach accounts for solid, elastic, and viscous fluid sublayers. Yeo concluded that the use of multilayers gives a measure of control over the stability of the flow not available to single layers and that potential delays of transition are attainable. Additionally, Yeo looked at the influence of oblique waves on the critical Reynolds number. He found that lower critical Reynolds numbers were achieved for oblique waves. Fraser and Carpenter (1985) investigated the linear stability of boundary layers over a single- and two-layer elastic wall model.

An alternative approach to studying specific walls to determine their linear stability characteristics and delay of transition potential was used by Sen and Arora (1988). They studied stability implications for specified values of the eigenfunction of the Orr-Sommerfeld equation at the wall. They obtained results by using a kinematic model which is used to back-calculate the material properties corresponding to any chosen model for the dynamical behavior of the wall. This problem used a two-dimensional wall that involved only vertical displacements. This resulted in four parameters to be determined.

In addition to the investigations of transitional boundary layers over compliant walls, some studies were conducted with turbulent boundary layers. It is beyond the scope of this project to review the turbulent boundary layer studies. A review is given by Bushnell et al. (1977). However, we introduce one study conducted by Grosskreutz (1971,1975). He introduced a compliant wall which linked the streamwise and normal surface displacements. A sketch of the model is shown in Figure 1.6. He suggested that this link could produce a negative production of Reynolds stress in the near-wall region of the turbulent boundary

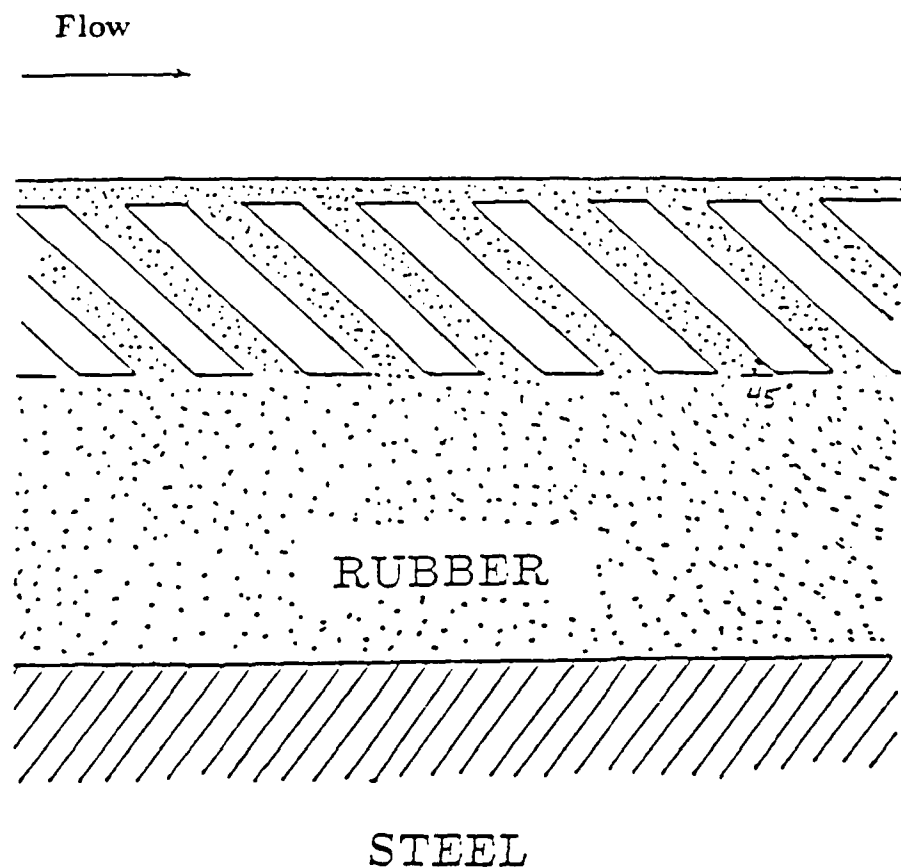


Figure 1.6 A sketch of the Grosskreutz compliant coating (Grosskreutz; 1975).

layer. Although his results were disappointing, the concept and coating appear promising for reducing the growth rates in laminar boundary layers leading to transition delays. The use of Grosskreutz's compliant wall model for transition studies was suggested by Carpenter and Morris (1985). The model is designed to represent isotropic and non-isotropic coatings. A sketch of the model is given in Figure 1.7. They found, that with an appropriate choice of wall properties, significant reductions in the growth rates of the TSI waves were found compared to the rigid wall. Carpenter and Morris (1985-90) performed additional studies involving the wall-induced instabilities and the effect of damping in the coatings. They found that damping destabilizes the Class A-TSI and stabilizes the Class B-TWF. Additionally, Carpenter and Morris used the e^n -criteria by Smith and Gamberoni to compute transition predictions for the compliant coatings. They found that the Reynolds number at which transition occurs (or is imminent) increases by a factor of 4-10 times that of the rigid wall. Using the same wall model Joslin and Morris (1987, 1989) and Joslin (1987) determined the sensitivity of the flow and wall instabilities to changes in the compliant wall properties. They found that the stiffness of the coatings investigated has the greatest influence on the instabilities.

A number of other investigations have been carried out over the past ten years, most of which have considered isotropic compliant-wall models or one- or two-layer isotropic coatings. The general consensus is that compliant coatings can lead to reductions in the instability growth rates and delays of transition. A number of studies have considered turbulent as well as transitional boundary layers over wall compliance but were not discussed for brevity sake. Some of these are Semenov (1971), Orszag (1977,1979), Balasubramanian (1978), Hansen, Hunston, Ni, Reischman, and Hoyt (1979, 1980), Bushnell (1980), Sengupta and

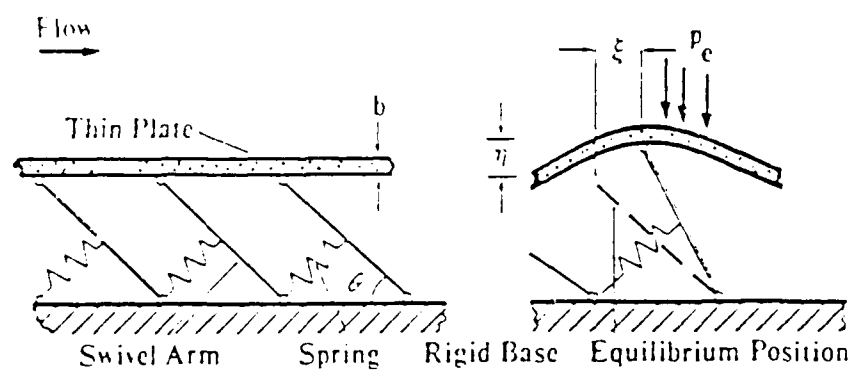


Figure 1.7 Mechanical model representing the Grosskreutz compliant coating (Carpenter and Morris; 1985).

Lekoudis (1985), Nakao (1985), Yeo and Dowling (1987), Thomas and Craik (1988), Breuer, Haritonidis and Landahl (1989), and Rotenberry (1989). These studies are listed as a reference for the reader.

Several notable contributions have been given concerning boundary layer transition over compliant walls. This list is far from complete. More in depth reviews are given by Gad-el-Hak et al. (1985, 1987), Dowell (1985), Riley et al. (1988), and Carpenter (1990).

Our understanding of transitional or turbulent boundary layer flows over compliant walls is far from complete. The problem is parametrically very complex and no obvious solutions lend themselves. This is not to say that progress has not been made since the pioneering days of Kramer. The days when arbitrary compliant walls are put into a tunnel and studied are over. Due to the high cost of performing these experiments, a more economical and realistic approach must be made. This involves the use of theoretical tools and computers. The cost involved with performing a number of numerical studies with different coatings is insignificant compared with an experimental test. The present investigation involves using some of these theoretical tools to model transition over compliant walls.

1.3 Motivation and Scope of Present Research

In the previous two sections reviews were given for compliant wall research and transitional boundary layer theory. These reviews did not discuss or encompass every study undertaken. Rather, some of the investigations familiar to the authors were mentioned to give the reader a broad representation of the ideas and concepts that have been examined. The following investigation is based on some of these approaches that have proved successful.

From the compliant wall review, a compliant wall model was discussed that showed promise for transition delays in boundary layers. It is from the significant transition delays found by using this model (and other similar models) along with the resent experimental findings of Daniel (1985-87), Willis (1986), and Gaster (1987) that we continue investigations in this direction. In the present study, the Grosskreutz (1971,1975) coating and the mechanical model of Carpenter and Morris (1985) are used. The analysis extends the wall model to account for oblique waves. The role of three-dimensional waves in transitional boundary layers is determined. This is done using linear stability theory.

After determining the importance of three-dimensional instabilities, a secondary instability theory is introduced and used to determine the effect of wall compliance on these instabilities. From the review of nonlinear instability theory, a model proposed by Herbert (1983) matches well with experiments. This theory provided a much needed explanation to the three-dimensional phenomenon found in experiments. In the secondary analysis for the present study, Herbert's theory for two-dimensional primary waves is extended to include three-dimensional primary waves. Suitable compliant wall boundary conditions are developed for the secondary instability analysis.

In the present investigation, the effect of wall compliance on three-dimensional primary and secondary instabilities is determined. We begin this by a review of past studies. This has been given in chapter 1. In chapter 2, the dynamic equations are derived for the primary and secondary instabilities. The appropriate compliant wall equations are derived in chapter 3. In chapter 4, numerical methods of solution are introduced to solve the eigenvalue problems that result from the analysis. In chapter 5, the results are presented for two- and three-dimensional primary instability waves that propagate over compliant

walls and compared to the rigid wall case. In chapter 6, results for the secondary instability analysis are presented. In chapter 7, the conclusions are outlined along with proposed few future compliant wall projects. Additionally, appendices are included removing from the main text the lengthy equations and other details which are pertinent to this study. In the final appendix, a proposed formulation for the turbulent boundary layer problem is outlined.

CHAPTER 2

DERIVATION OF GOVERNING EQUATIONS

2.1 Introduction

In this chapter, the dynamic equations are derived for the three-dimensional primary and secondary instabilities in a transitional boundary layer. The disturbances are represented by travelling waves which may grow or decay as they propagate. Nonlinear coupling is ignored so that individual components of the frequency spectrum may be studied. Additionally, the growth of the boundary layer is neglected so that a parallel flow assumption may be made. With this in mind, the derivation of the respective equations proceeds. In the next section, the equations for the primary instabilities are derived. In the final section, the equations describing the secondary instabilities are derived.

2.2 Primary Instability Equations

The problem we consider consists of an incompressible laminar boundary layer flow over a smooth flat wall. The equations governing the flow are the Navier-Stokes equations. These consist of the momentum and continuity equations given as

$$\frac{\partial}{\partial t}u + (\bar{v} \cdot \nabla)u = -\frac{1}{\rho} \frac{\partial}{\partial x}p + \nu \nabla^2 u \quad 2.2.1a$$

$$\frac{\partial}{\partial t}v + (\bar{v} \cdot \nabla)v = -\frac{1}{\rho} \frac{\partial}{\partial y}p + \nu \nabla^2 v \quad 2.2.1b$$

$$\frac{\partial}{\partial t}w + (\bar{v} \cdot \nabla)w = -\frac{1}{\rho} \frac{\partial}{\partial z}p + \nu \nabla^2 w \quad 2.2.1c$$

$$\nabla \cdot \bar{v} = 0 \quad 2.2.2$$

where $\nabla = \frac{\partial}{\partial x} + \frac{\partial}{\partial y} + \frac{\partial}{\partial z}$, x, y, z correspond respectively to the streamwise, normal, and spanwise coordinate directions, $\bar{v} = (u, v, w)$ are the streamwise, normal, and spanwise velocity components, and p is the pressure. ρ is the fluid density and ν is the kinematic viscosity. u, v, w and p are the instantaneous flow properties. A small-amplitude disturbance is introduced into the laminar flow. In general, the flow components may be given by

$$u(x, y, z, t) = U(x, y, z, t) + A u_1(x, y, z, t) \quad 2.2.3a$$

$$v(x, y, z, t) = V(x, y, z, t) + A v_1(x, y, z, t) \quad 2.2.3b$$

$$w(x, y, z, t) = W(x, y, z, t) + A w_1(x, y, z, t) \quad 2.2.3c$$

$$p(x, y, z, t) = P(x, y, z, t) + A p_1(x, y, z, t) \quad 2.2.3d$$

where u_1, v_1, w_1 and p_1 are the disturbance properties; A is the finite small-amplitude of the disturbance; and U, V, W and P are the mean flow properties. For the problem at hand, simplifications may be made. The mean velocity profile is assumed two-dimensional and self-similar. This stipulation defines a class of flows known as *parallel* flows. This implies that U is the streamwise component and $V = W = 0$. A description for this flow was described many years ago by Blasius (1908). Blasius introduced a similarity variable. The change in coordinates is $y = y/xR_x^{1/2}$ where hereafter y is the similarity coordinate. The equation governing the mean flow known as the Blasius profile is given by

$$f''' + \frac{1}{2}ff'' = 0 \quad 2.2.4$$

with

$$f(0) = f''(0) = 0 \quad \text{and} \quad f' \rightarrow 1 \quad \text{as} \quad y \rightarrow \infty$$

where f' is the nondimensional mean velocity, U_0 , and $(\cdot)' = d/dy$. For the rigid wall case, a three-dimensional disturbance motion may be represented by an equivalent most dominant two-dimensional problem as shown by Squire (1933). This is not proven for non-rigid walls, so we retain the three-dimensional nature of the equations describing the disturbance. The resulting flow with the mean flow assumptions has components given by

$$u(x, y, z, t) = U(y) + A u_1(x, y, z, t) \quad 2.2.5a$$

$$v(x, y, z, t) = A v_1(x, y, z, t) \quad 2.2.5b$$

$$w(x, y, z, t) = A w_1(x, y, z, t) \quad 2.2.5c$$

$$p(x, y, z, t) = P(y) + A p_1(x, y, z, t) \quad 2.2.5d$$

These are substituted into (2.2.1-2). Only linear terms in A are retained. The resulting system of equations is

$$\frac{\partial u_1}{\partial t} + U \frac{\partial u_1}{\partial x} + v_1 \frac{dU}{dy} = -\frac{1}{\rho} \frac{\partial p_1}{\partial x} + \nu \nabla^2 u_1 \quad 2.2.6a$$

$$\frac{\partial v_1}{\partial t} + U \frac{\partial v_1}{\partial x} = -\frac{1}{\rho} \frac{\partial p_1}{\partial y} + \nu \nabla^2 v_1 \quad 2.2.6b$$

$$\frac{\partial w_1}{\partial t} + U \frac{\partial w_1}{\partial x} = -\frac{1}{\rho} \frac{\partial p_1}{\partial z} + \nu \nabla^2 w_1 \quad 2.2.6c$$

$$\nabla \cdot \vec{v} = 0 \quad 2.2.7$$

The pressure component is eliminated by differentiating and subtracting the above equations resulting in the vorticity equations, or

$$\left[\frac{\partial}{\partial t} + U \frac{\partial}{\partial x} - \nu \nabla^2 \right] \left(\frac{\partial w_1}{\partial y} - \frac{\partial v_1}{\partial z} \right) + \frac{dU}{dy} \frac{\partial w_1}{\partial x} = 0 \quad 2.2.8a$$

$$\left[\frac{\partial}{\partial t} + U \frac{\partial}{\partial x} - \nu \nabla^2 \right] \left(\frac{\partial u_1}{\partial z} - \frac{\partial w_1}{\partial x} \right) + \frac{dU}{dy} \frac{\partial v_1}{\partial z} = 0 \quad 2.2.8b$$

$$\left[\frac{\partial}{\partial t} + U \frac{\partial}{\partial x} - \nu \nabla^2 \right] \left(\frac{\partial v_1}{\partial x} - \frac{\partial u_1}{\partial y} \right) + \frac{dU}{dy} \frac{\partial w_1}{\partial z} - \frac{d^2 U}{dy^2} v_1 = 0 \quad 2.2.8c$$

We further reduce these to two equations by introducing the definition of vorticity normal to the wall, $\Omega = \partial u / \partial z - \partial w / \partial x$, and perform the following operation: $\partial / \partial z$ (2.2.8a) – $\partial / \partial x$ (2.2.8c). The equations are then nondimensionalized by the freestream velocity (U_∞), density (ρ), and a characteristic length scale such as the boundary layer thickness (δ). The resulting equations are

$$\left[\frac{1}{R_\delta} \nabla^2 - U_o \frac{\partial}{\partial x} - \frac{\partial}{\partial t} \right] \Omega_1 - \frac{dU_o}{dy} \frac{\partial v_1}{\partial z} = 0 \quad 2.2.9$$

$$\left[\frac{1}{R_\delta} \nabla^2 - U_o \frac{\partial}{\partial x} - \frac{\partial}{\partial t} \right] \nabla^2 v_1 - \frac{d^2 U_o}{dy^2} \frac{\partial v_1}{\partial x} = 0 \quad 2.2.10$$

where R_δ is the boundary layer thickness Reynolds number given as $R_\delta = U_\infty \delta / \nu$ and U_o is the nondimensional mean velocity profile.

The disturbance introduced into the boundary layer may be represented in the form of a travelling wave. A normal mode representation is given as

$$\{v_1, \Omega_1\}(x, y, z, t) = \{\hat{v}_1, \hat{\Omega}_1\}(y) E + c.c. \quad 2.2.11$$

where \hat{v}_1 and $\hat{\Omega}_1$ are the complex eigenfunctions of normal velocity and vorticity. In the general case

$$E = \exp[i(\alpha^+ x + \beta^+ z - \omega t)] \quad 2.2.12$$

where α^+ and β^+ are complex wavenumbers and ω is the complex frequency. There are two general cases, or classes, of solution given by

- (i) Temporal Instability. For this case α_r^+ and β_r^+ are specified and $\alpha_i^+ = \beta_i^+ = 0$. The frequency of the disturbance is determined and given by ω_r and ω_i is the temporal growth rate. The imaginary part of the complex frequency or

phase velocity determines the growth or decay rate of the wave. For $\omega_i > 0$ the wave is unstable; for $\omega_i < 0$ the wave is stable; and for $\omega_i = 0$ the wave neither grows nor decays and is referred to as neutrally stable.

(ii) Spatial Instability. In this case the wave frequency is given by ω_r and $\omega_i = 0$. The determination of the wavenumbers depends on the study being considered. If one is interested in the streamwise growth then β_r^+ is specified, $\beta_i^+ = 0$, and α_r^+ is the streamwise wavenumber and α_i^+ is the growth rate. The imaginary part of the wavenumber is a measure of the growth or decay rate of the wave. For $\alpha_i^+ < 0$ the wave is unstable and grows exponentially, for $\alpha_i^+ > 0$ the wave is stable and decays, and for $\alpha_i^+ = 0$ the wave neither grows nor decays and is referred to as neutrally stable. We are interested in the growth rate and the wave growth in the direction of the wave propagation. So α_i^+ and β_i^+ are determined. The description of this approach is explained below.

We follow the ideology behind the spatial stability approach since Gaster (1962) showed that spatial growth rate predictions are quantitatively more correct. We follow Mack (1980) and define two real vectors, a wavenumber vector (α_r^+, β_r^+) making an angle ϕ_r to the x -axis and a second growth rate vector (α_i^+, β_i^+) making an angle ϕ_i to the x -axis. In general these two vectors are not the same, but in the present study we consider the special case where $\phi_r = \phi_i = \phi$. This allows an alternative representation to (2.2.12) or

$$E = \exp[i(\alpha \cos \phi x + \alpha \sin \phi z - \omega t)] \quad 2.2.13$$

where $\alpha^+ = \alpha \cos \phi$ and $\beta^+ = \alpha \sin \phi$. In this case there is a single complex wavenumber and eigenvalue α . Additionally, the nondimensional to dimensional relations are given as: $\alpha = \alpha^* \delta$ is the complex nondimensional wavenumber;

$c_r = \omega/\alpha_r$ is the phase velocity of the wave; $\omega = \omega^* \delta/U_\infty$ is the nondimensional frequency; and ϕ is the angle of wave propagation.

If we substitute (2.2.11, 13) into (2.2.9-10), the resulting system is

$$\hat{v}_1'' + a_1(y)\hat{v}_1'' + a_2(y)\hat{v}_1 = 0 \quad 2.2.14$$

where

$$a_1(y) = -iR_\delta\alpha(U_o(y)\cos\phi - c_r) - 2\alpha^2$$

$$a_2(y) = iR_\delta\alpha^3(U_o(y)\cos\phi - c_r) + iR_\delta\alpha\cos\phi U_o''(y) + \alpha^4$$

and

$$\hat{\Omega}_1'' + a_3(y)\hat{\Omega}_1 + a_4(y)\hat{v}_1 = 0 \quad 2.2.15$$

where

$$a_3(y) = -\alpha^2 - iR_\delta\alpha(U_o(y)\cos\phi - c_r)$$

$$a_4(y) = -iR_\delta\alpha\sin\phi U_o'(y)$$

These equations are referred to as the Orr-Sommerfeld and Squire's equations, respectively. These equations were originally derived by Orr (1907), Sommerfeld (1908), and Squire (1933). This is a system of coupled, non-constant coefficient equations. The problem is of an eigenvalue nature where the spatial eigenvalue appears to the fourth power and the temporal eigenvalue appears to the first power. The system requires six boundary conditions. The disturbance fluctuations and their derivatives vanish as infinity is approached in the normal, or cross-stream, direction. This gives the three boundary conditions.

$$\hat{v}_1(y), \hat{v}_1'(y), \hat{\Omega}_1(y) \rightarrow 0 \quad \text{as} \quad y \rightarrow \infty \quad 2.2.16$$

In the next chapter the remaining boundary conditions will be determined. These conditions are enforced at the wall. Before we introduce the compliant wall model, the equations governing the secondary instabilities in the flow will be derived. This is examined in the next section.

2.3 Secondary Instability Equations

As we have outlined in the first chapter, the procedure we follow is a generalization of a theory by Herbert (1983). Herbert's theory is extended to allow for three-dimensional primary instabilities and introduce wall compliance.

An incompressible flow that is governed by the Navier-Stokes equations (2.2.1-2) with appropriate boundary conditions is considered. A basic flow $\bar{v}_2 = (u_2, v_2, w_2)$ subject to a three-dimensional disturbance $\bar{v}_3 = (u_3, v_3, w_3)$ which is termed a secondary instability is introduced. The instantaneous velocity and pressure components are given as

$$u(\bar{x}, y, \bar{z}, t) = u_2(\bar{x}, y, \bar{z}, t) + B u_3(\bar{x}, y, \bar{z}, t) \quad 2.3.1a$$

$$v(\bar{x}, y, \bar{z}, t) = v_2(\bar{x}, y, \bar{z}, t) + B v_3(\bar{x}, y, \bar{z}, t) \quad 2.3.1b$$

$$w(\bar{x}, y, \bar{z}, t) = w_2(\bar{x}, y, \bar{z}, t) + B w_3(\bar{x}, y, \bar{z}, t) \quad 2.3.1c$$

$$p(\bar{x}, y, \bar{z}, t) = p_2(\bar{x}, y, \bar{z}, t) + B p_3(\bar{x}, y, \bar{z}, t) \quad 2.3.1d$$

and the basic flow is given as

$$u_2(\bar{x}, y, \bar{z}, t) = U_o(y) + A u_1(\bar{x}, y, \bar{z}, t) \quad 2.3.2a$$

$$v_2(\bar{x}, y, \bar{z}, t) = A v_1(\bar{x}, y, \bar{z}, t) \quad 2.3.2b$$

$$w_2(\bar{x}, y, \bar{z}, t) = W_o(y) + A w_1(\bar{x}, y, \bar{z}, t) \quad 2.3.2c$$

$$p_2(\bar{x}, y, \bar{z}, t) = A p_1(\bar{x}, y, \bar{z}, t) \quad 2.3.2d$$

The basic flow is left in a general form. The values of each component of the basic flow are varied as the choice of coordinate reference frame is changed. For the reference frame in which \bar{x} is in the mean flow direction, (u_1, v_1, w_1) are the

primary wave solution which is determined from the dynamic equations in the previous section. In this reference frame, the mean spanwise velocity component, W_0 , is zero. The primary instability is of the wave form (i.e. periodic in t and periodic in (\tilde{x}, \tilde{z}) with wavelength $\lambda_r = 2\pi/\alpha_r$) and travelling with phase velocity $c_r = (c_x, 0, c_z) = (c_r, 0)$ where

$$c_x = \omega_r/\alpha_r \cos \phi \quad \text{and} \quad c_z = \omega_r/\alpha_r \sin \phi$$

If transforming to a coordinate reference frame moving with the wave we have

$$\bar{v}_1(\tilde{x}, y, \tilde{z}) = \bar{v}_1(x, y, z) = \bar{v}_1(x + \lambda_x, y, z + \lambda_z) \quad 2.3.3$$

where (\tilde{x}, \tilde{z}) is the fixed laboratory reference frame and (x, z) is the reference frame moving with the primary wave. By a proper normalization of (u_1, v_1, w_1) the amplitude A directly measures the maximum streamwise *rms* fluctuation. This is given by

$$\max_{0 \leq y < \infty} |u(y)|^2 = |u(y_m)|^2 = 1/2 \quad 2.3.4$$

The key element of this theory of secondary instabilities is that the primary wave is periodic in the (x, z) plane at a finite-amplitude A of the TSI wave. Use of the shape assumption noted by Stuart (1960) is made. This assumes that the primary wave is governed by a linear system of equations. This is justifiable since observations indicate that secondary instabilities occur at small amplitudes. These instabilities are assumed to originate due to a redistribution of vorticity and not Reynolds stresses. With the shape assumption, the normal velocity and normal vorticity of the primary wave are given by

$$\{v_1, \Omega_1\}(x, y, z) = \{v_1, \Omega_1\}(y) e^{i\alpha_r (x \cos \phi + z \sin \phi)} + \{v_{-1}, \Omega_{-1}\}(y) e^{-i\alpha_r (x \cos \phi + z \sin \phi)} \quad 2.3.5$$

where $v_1 = v_{-1}^*$ in order to obtain a real solution and $*$ denotes the complex conjugate. v_1, Ω_1 are eigenfunctions of the Orr-Sommerfeld and Squire's equations. This problem was outlined in the previous section. The solution of the primary problem gives the eigenfunctions and primary surface displacements.

Using the primary solution as being sufficiently adequate for the secondary instability analysis assumes that the secondary instability grows at a much faster rate than the primary. This is a result of assuming that the primary amplitude does not vary in space for spatial analysis and in time for temporal analysis. Thus, Herbert assimilated the comparison that the primary instability grows at a viscous time scale while the secondary instability grows convectively.

At this point, the governing equations for the secondary instability analysis are derived. The instantaneous velocities and pressure (2.3.1) are substituted into the Navier-Stokes equations and linearized on the secondary amplitude, B . This yields the nondimensional equations for \bar{v}_3

$$\frac{\partial}{\partial t} \bar{v}_3 + (\bar{v}_2 \cdot \nabla) \bar{v}_3 + (\bar{v}_3 \cdot \nabla) \bar{v}_2 = -\Delta p_3 + \frac{1}{R_\delta} \nabla^2 \bar{v}_3 \quad 2.3.6$$

The pressure terms are eliminated by appropriate differentiation and subtraction of (2.3.6). The vorticity equations result

$$\left[\frac{1}{R_\delta} \nabla^2 - \frac{\partial}{\partial t} \right] \bar{\Omega}_3 - (\bar{v}_2 \cdot \nabla) \bar{\Omega}_3 - (\bar{v}_3 \cdot \nabla) \bar{\Omega}_2 + (\bar{\Omega}_2 \cdot \nabla) \bar{v}_3 + (\bar{\Omega}_3 \cdot \nabla) \bar{v}_2 = 0 \quad 2.3.7$$

along with the continuity equation

$$\nabla \cdot \bar{v}_3 = 0. \quad 2.3.8$$

As with the primary problem, the equations in terms of the normal velocity and vorticity are sought. This is an extension of Herbert's two-dimensional analysis. Introducing the streamwise, normal, and spanwise vorticity gives.

$$\epsilon_v = \frac{\partial w}{\partial y} - \frac{\partial v}{\partial z} \quad \Omega = \frac{\partial u}{\partial z} - \frac{\partial w}{\partial x} \quad \rho_v = \frac{\partial v}{\partial x} - \frac{\partial u}{\partial y}$$

Only normal vorticity terms will remain when the analysis is complete.

One equation results by substituting the basic flow \bar{v}_2 into (2.3.7). This gives

$$\begin{aligned} & \left[\frac{1}{R} \nabla^2 - \frac{\partial}{\partial t} - (U_o - c_x) \frac{\partial}{\partial x} - (W_o - c_z) \frac{\partial}{\partial z} \right] \Omega_3 - \frac{dU_o}{dy} \frac{\partial v_3}{\partial z} + \frac{dW_o}{dy} \frac{\partial v_3}{\partial x} \\ & + A \left\{ -(\bar{v}_1 \cdot \nabla) \Omega_3 - (\bar{v}_3 \cdot \nabla) \Omega_1 + (\epsilon_1 + \frac{\partial v_1}{\partial z}) \frac{\partial v_3}{\partial x} \right. \\ & \left. + \Omega_1 \frac{\partial v_3}{\partial y} + (\rho_1 - \frac{\partial v_1}{\partial x}) \frac{\partial v_3}{\partial z} - \frac{\partial v_1}{\partial z} \frac{\partial u_3}{\partial y} + \frac{\partial v_1}{\partial x} \frac{\partial w_3}{\partial y} \right\} = 0 \end{aligned} \quad 2.3.9$$

The other equation is found by taking $\partial/\partial z$ (streamwise vorticity)- $\partial/\partial x$ (spanwise vorticity). This results in the remaining equation describing the dynamic system.

$$\begin{aligned} & \left[\frac{1}{R} \nabla^2 - \frac{\partial}{\partial t} - (U_o - c_x) \frac{\partial}{\partial x} - (W_o - c_z) \frac{\partial}{\partial z} \right] \nabla^2 v_3 + \frac{d^2 U_o}{dy^2} \frac{\partial v_3}{\partial x} + \frac{d^2 W_o}{dy^2} \frac{\partial v_3}{\partial z} \\ & + A \left\{ [-(\bar{v}_1 \cdot \nabla) \nabla^2 - \frac{\partial}{\partial y} \nabla^2 v_1 - (\frac{\partial^2 u_1}{\partial x^2} + \frac{\partial^2 u_1}{\partial z^2} - \frac{\partial^2 u_1}{\partial y^2} + 2 \frac{\partial^2 v_1}{\partial x \partial y}) \frac{\partial}{\partial x} \right. \\ & + (\frac{\partial^2 v_1}{\partial z^2} - \frac{\partial^2 v_1}{\partial x^2} + \frac{\partial^2 v_1}{\partial y^2} + 2 \frac{\partial^2 u_1}{\partial x \partial y}) \frac{\partial}{\partial y} + (\frac{\partial^2 w_1}{\partial y^2} - \frac{\partial^2 w_1}{\partial x^2} + \frac{\partial^2 u_1}{\partial x \partial z} \\ & - \frac{\partial^2 v_1}{\partial y \partial z}) \frac{\partial}{\partial z} + (\frac{\partial v_1}{\partial y} + 2 \frac{\partial u_1}{\partial x}) (\frac{\partial^2}{\partial z^2} - \frac{\partial^2}{\partial x^2} + \frac{\partial^2}{\partial y^2}) - 2 \frac{\partial v_1}{\partial x} \frac{\partial^2}{\partial x \partial y} - 2 (\frac{\partial u_1}{\partial z} \\ & + \frac{\partial w_1}{\partial x}) \frac{\partial^2}{\partial x \partial z} - \frac{\partial v_1}{\partial z} \frac{\partial^2}{\partial y \partial z}] v_3 \\ & + [-\frac{\partial}{\partial x} (\nabla^2 v_1) + 2 (\frac{\partial^2 v_1}{\partial z^2} - \frac{\partial^2 v_1}{\partial x^2} + \frac{\partial^2 v_1}{\partial y^2} + 2 \frac{\partial^2 u_1}{\partial x \partial y}) \frac{\partial}{\partial x} + 2 (\frac{\partial^2 w_1}{\partial x \partial y} \\ & - \frac{\partial^2 v_1}{\partial x \partial z}) \frac{\partial}{\partial z} - \frac{\partial v_1}{\partial x} (\frac{\partial^2}{\partial x^2} + \frac{\partial^2}{\partial z^2} - \frac{\partial^2}{\partial y^2}) + 2 (\frac{\partial v_1}{\partial y} + 2 \frac{\partial u_1}{\partial x}) \frac{\partial^2}{\partial x \partial y} \\ & + 2 \frac{\partial w_1}{\partial x} \frac{\partial^2}{\partial y \partial z} + \frac{\partial v_1}{\partial z} \frac{\partial^2}{\partial x \partial z}] u_3 \\ & + [-\frac{\partial}{\partial z} (\nabla^2 v_1) + 2 (\frac{\partial u_1}{\partial y \partial z} - \frac{\partial^2 v_1}{\partial x \partial z}) \frac{\partial}{\partial x} - \frac{\partial v_1}{\partial z} (\frac{\partial^2}{\partial x^2} - \frac{\partial^2}{\partial y^2}) \\ & \left. + 2 \frac{\partial u_1}{\partial z} \frac{\partial^2}{\partial x \partial y}] w_3 \right\} = 0 \end{aligned} \quad 2.3.10$$

This equation involves terms with all components of secondary velocity. In order to reduce this equation to normal velocity and vorticity only without integral

representations, normal modes are introduced. Then as with the primary problem, the continuity equation and the definition of vorticity are employed. As with the primary problem, the disturbance quantities v_3 , Ω_3 and $\partial v_3 / \partial y$ vanish far from the wall and at the wall for the rigid wall case. The compliant wall equations govern the boundary conditions for the compliant case. Additionally, note that the primary amplitude, A , is a parameter in the equations. As $A \rightarrow 0$ the Orr-Sommerfeld and Squire's equations result for oblique waves with the basic flow now being only the Blasius flow. For the case of interest where $A \neq 0$, the primary eigenfunctions (u_1, v_1, w_1) appear in the equations as coefficients. To solve the secondary problem, an appropriate normal mode representation is sought.

For a two-dimensional primary instability, the coefficients of (2.3.9) and (2.3.10) are independent of z and t , we can apply the following normal mode concept

$$v_3(x, y, z, t) = e^{\sigma t} e^{i\beta z} V(x, y) \quad 2.3.11$$

where the spanwise wavenumber $\beta = 2\pi/\lambda_z$ is real and $\sigma = \sigma_r + i\sigma_i$ is complex. $V(x, y)$ is the function representing the class of modes. Floquet theory suggests a form of solution for periodic systems. A discussion of Floquet theory is given by Floqu t (1883), Arscott (1964), Coppel (1965), and Herbert (1984d). For the present problem Floquet theory gives

$$V(x, y) = e^{\gamma x} \tilde{V}(x, y) \quad 2.3.12$$

where $\gamma = \gamma_r + i\gamma_i$ is the characteristic exponent and $\tilde{V}(x, y)$ is periodic in the x direction and may be represented by a Fourier series. So the normal mode representation of the secondary instability for a two-dimensional basic flow is

$$v_3 = e^{\sigma t + i\beta z + \gamma x} \sum_{n=-\infty}^{\infty} \hat{v}_n(y) e^{i(n/2)\alpha_r z} \quad 2.3.13$$

For three-dimensional primary instabilities the problem is more complex and the form of solution depends on the situation under consideration. By simply introducing an oblique wave and transform (2.3.13) the following normal mode form arises

$$v_3 = e^{\sigma t + i\beta(z \cos \phi - x \sin \phi) + \gamma(x \cos \phi + z \sin \phi)} \sum_{n=-\infty}^{\infty} \hat{v}_n(y) e^{i(n/2)\alpha, (x \cos \phi + z \sin \phi)} \quad 2.3.14$$

This leads to an infinite system of ordinary differential equations. The system consists of two distinct classes of solution. This occurs since even and odd modes decouple. This results in

$$v_f = e^{\sigma t + i\beta(z \cos \phi - x \sin \phi) + \gamma(x \cos \phi + z \sin \phi)} \sum_{n=even} \hat{v}_n(y) e^{i(n/2)\alpha, (x \cos \phi + z \sin \phi)} \quad 2.3.15a$$

and

$$v_s = e^{\sigma t + i\beta(z \cos \phi - x \sin \phi) + \gamma(x \cos \phi + z \sin \phi)} \sum_{n=odd} \hat{v}_n(y) e^{i(n/2)\alpha, (x \cos \phi + z \sin \phi)} \quad 2.3.15b$$

By observation

$$\tilde{v}_f(x + \lambda_z, y, z + \lambda_z) = \tilde{v}(x, y, z)$$

$$\tilde{v}_s(x + 2\lambda_z, y, z + 2\lambda_z) = \tilde{v}(x, y, z)$$

The fundamental mode is associated with primary resonance and the subharmonic mode with parametric resonance. A problem may arise with this formulation since the periodic form is no longer unidirectional. A question arises as to what periodic exponents are appropriate. Namely, are the forms of the solution simply related by the relation $\gamma = \gamma(x \cos \phi + z \sin \phi)$?

To retain periodicity in one direction, the coordinate reference frame for the secondary instabilities is rotated to the direction of the wave as well as changed

to move with the wave. The form of the solution is then

$$v_3 = e^{\sigma t + i\beta z' + \gamma z'} \sum_{n=-\infty}^{\infty} \hat{v}_n(y) e^{i(n/2)\alpha, z'} \quad 2.3.16$$

where

$$x' = x \cos \phi + z \sin \phi \quad \text{and} \quad z' = z \cos \phi - x \sin \phi$$

Solutions are then obtained in the (x', z') frame. In this reference frame, the basic flow changes to

$$u_2 = \bar{U}_o(y) + A\bar{u}_1(x, y, z, t) \quad 2.3.17a$$

$$v_2 = A\bar{v}_1(x, y, z, t) \quad 2.3.17b$$

$$w_2 = \bar{W}_o(y) \quad 2.3.17c$$

where

$$\bar{U}_o = U_o \cos \phi$$

$$\bar{u}_1 = u_1 \cos \phi + w_1 \sin \phi$$

$$\bar{W}_o = -U_o \sin \phi$$

With this reference frame the form of the solution is the same as the two-dimensional problem. To obtain a real solution in this reference frame, $\hat{u}_m = \hat{u}_{-m}^*$, $\hat{v}_m = \hat{v}_{-m}^*$, and $\hat{w}_m = -\hat{w}_{-m}^*$ where $*$ indicates complex conjugate.

Either form of the solution gives two complex quantities σ and γ which leads to an ambiguity similar to that found with the Orr-Sommerfeld/Squire problem. Four unknowns, $\sigma_r, \sigma_i, \gamma_r, \gamma_i$ result. Two can be determined while two must be chosen in some other way. There are three general cases, or classes, of solution that have a physical interpretation and a fourth case whose interpretation is yet unclear. We consider the form of the solution given in (2.3.14) since it is more general and may easily be transformed to (2.3.16).

(i) Spatial growing tuned modes. For this case the spatial growth rate is related to the laboratory reference frame. Transforming from the frame moving with the primary wave to a fixed frame, we find

$$e^{\sigma t} e^{\gamma(x \cos \phi + z \sin \phi)} = e^{(\sigma - \gamma c_r)t} e^{\gamma(\hat{x} \cos \phi + \hat{z} \sin \phi)} \quad 2.3.18$$

To suppress any temporal effects, we choose $\sigma = \gamma c_r$. The γ_r provides the spatial growth rate in the direction of the primary wave in the laboratory frame and γ_i is the shift in the wavenumber.

(ii) Temporal growing tuned modes. The temporal growth rate is σ_r , and σ_i can be interpreted as a shift in frequency. In this case we choose $\gamma_r = \gamma_i = 0$. If $\sigma_i = 0$ then we can say that the secondary mode is travelling synchronously with the basic flow.

(iii) Temporal growing detuned modes. In this case $\gamma_r = 0$ and $\gamma_i = \Delta\omega$. σ_r and σ_i are defined as in (ii).

(iv) Spatial growing detuned modes. In this case $\sigma_r = \gamma c_r$. The γ_r provides the spatial growth rate in the direction of the primary wave and γ_i provides a shift in the wavenumber. $\sigma_i = \Delta\omega$ is a frequency shift. It is unclear as to how this frequency shift might occur.

At this point the final form of equations governing the subharmonic and fundamental modes of instability may be obtained. If we substitute (2.3.5) where $m = \pm 1$ as the general exponential superscript and (2.3.14) into (2.3.9,10), the equations in normal modes result. These are given as

$$\begin{aligned}
& \left\{ \frac{1}{R} \hat{\Omega}_n'' + \left[\frac{1}{R} \Delta_n - \sigma - (U_o - c_z) \bar{\alpha}_n - (W_o - c_z) \bar{\beta}_n \right] \hat{\Omega}_n + (W_o' \bar{\alpha}_n - U_o' \bar{\beta}_n) \hat{v}_n \right\} e^N \\
& + A \left\{ \left[-1 - im\alpha \sin \phi \frac{\bar{\beta}_n}{\Delta_n} - im\alpha \cos \phi \frac{\bar{\alpha}_n}{\Delta_n} \right] v_m \hat{\Omega}_n' + \left[(-\bar{\alpha}_n \right. \right. \\
& \left. \left. + m^2 \alpha^2 \cos \phi \sin \phi \frac{\bar{\beta}_n}{\Delta_n} - m^2 \alpha^2 \frac{\bar{\alpha}_n}{\Delta_n} \right) u_m + (1 + im\alpha \cos \phi \frac{\bar{\alpha}_n}{\Delta_n}) v_m' \right. \\
& \left. - (\bar{\beta}_n + m^2 \alpha^2 \cos^2 \phi \frac{\bar{\beta}_n}{\Delta_n}) w_m \right] \hat{\Omega}_n + \left[im\alpha \sin \phi \frac{\bar{\alpha}_n}{\Delta_n} \right. \\
& \left. - im\alpha \cos \phi \frac{\bar{\beta}_n}{\Delta_n} \right] v_m \hat{v}_n'' + \left[(-m^2 \alpha^2 \cos \phi \sin \phi \frac{\bar{\alpha}_n}{\Delta_n} - m^2 \alpha^2 \frac{\bar{\beta}_n}{\Delta_n} \right. \\
& \left. + im\alpha \sin \phi) u_m + im\alpha \cos \phi \frac{\bar{\beta}_n}{\Delta_n} v_m' + (m^2 \alpha^2 \cos^2 \phi \frac{\bar{\alpha}_n}{\Delta_n} \right. \\
& \left. - im\alpha \cos \phi) w_m \right] \hat{v}_n' - [im\alpha \sin \phi u_m' - im\alpha \cos \phi w_m' \\
& \left. - \bar{\alpha}_n w_m' + \bar{\beta}_n u_m' \right] \hat{v}_n \right\} e^{M+N} = 0
\end{aligned} \tag{2.3.19}$$

and

$$\begin{aligned}
& \left\{ \frac{1}{R} \hat{v}_n^{iv} + \left[\frac{2}{R} \Delta_n - \sigma - (U_o - c_z) \bar{\alpha}_n - (W_o - c_z) \bar{\beta}_n \right] \hat{v}_n'' + \left[\frac{1}{R} \Delta_n^2 - \sigma \Delta_n \right. \right. \\
& \left. \left. - (U_o - c_z) \bar{\alpha}_n \Delta_n - (W_o - c_z) \bar{\beta}_n \Delta_n + W_o'' \bar{\beta}_n + U_o'' \bar{\alpha}_n \right] \hat{v}_n \right\} e^N \\
& + A \left\{ - \left[\frac{\bar{\alpha}_n}{\Delta_n} im\alpha \cos \phi + 1 + \frac{\bar{\beta}_n}{\Delta_n} im\alpha \sin \phi \right] v_m \hat{v}_n''' - \left[\left(\frac{\bar{\alpha}_n}{\Delta_n} 4im\alpha \cos \phi \bar{\alpha}_n \right. \right. \\
& \left. \left. + \bar{\alpha}_n - 2im\alpha \cos \phi + \frac{\bar{\beta}_n}{\Delta_n} 2im\alpha \sin \phi \bar{\alpha}_n \right) u_m + \left(\frac{\bar{\alpha}_n}{\Delta_n} 2\bar{\alpha}_n - 1 \right) v_m' \right. \\
& \left. + \left(\frac{\bar{\alpha}_n}{\Delta_n} 2im\alpha \cos \phi \bar{\beta}_n + \bar{\beta}_n \right) w_m \right] \hat{v}_n'' + \left[-\frac{\bar{\alpha}_n}{\Delta_n} \{ (im^3 \alpha^3 \cos \phi \right. \right. \\
& \left. \left. + 2m^2 \alpha^2 \cos 2\phi \bar{\alpha}_n + 2m^2 \alpha^2 \cos \phi \sin \phi \bar{\beta}_n - im\alpha \cos \phi \Delta_n \right. \right. \\
& \left. \left. + im\alpha \sin \phi \bar{\alpha}_n \bar{\beta}_n \right) v_m - (im\alpha \cos \phi - 2\bar{\alpha}_n) v_m'' + 4im\alpha \cos \phi \bar{\alpha}_n u_m' \right. \\
& \left. + 2im\alpha \cos \phi \bar{\beta}_n w_m' \right\} - (\Delta_n - m^2 \alpha^2 \cos 2\phi + 2im\alpha \cos \phi \bar{\alpha}_n \\
& + im\alpha \sin \phi \bar{\beta}_n) v_m + v_m'' + 2im\alpha \cos \phi u_m' - \frac{\bar{\beta}_n}{\Delta_n} \{ im\alpha \sin \phi (m^2 \alpha^2 \\
& - 2im\alpha \cos \phi \bar{\alpha}_n - \bar{\alpha}_n^2) v_m - im\alpha \sin \phi v_m'' + 2im\alpha \sin \phi \bar{\alpha}_n u_m' \} \right] \hat{v}_n'
\end{aligned}$$

$$\begin{aligned}
& + \left[(-\bar{\alpha}_n \Delta_n + m^2 \alpha^2 \bar{\alpha}_n - m^2 \alpha^2 \sin \phi \cos \phi \bar{\beta}_n + 2im\alpha \cos \phi (\bar{\beta}_n^2 - \bar{\alpha}_n^2) \right. \\
& - 2im\alpha \sin \phi \bar{\alpha}_n \bar{\beta}_n) u_m + (m^2 \alpha^2 - 2im\alpha \cos \phi \bar{\alpha}_n - im\alpha \sin \phi \bar{\beta}_n \\
& + \bar{\beta}_n^2 - \bar{\alpha}_n^2) v'_m + \bar{\alpha}_n u''_m - (\bar{\beta}_n \Delta_n - m^2 \alpha^2 \cos^2 \phi \bar{\beta}_n \\
& \left. + 2im\alpha \cos \phi \bar{\alpha}_n \bar{\beta}_n) w_m - v'''_m + \bar{\beta}_n w''_m \right] \hat{v}_n + \left[\frac{\bar{\beta}_n}{\Delta_n} im\alpha \cos \phi \right. \\
& - \frac{\bar{\alpha}_n}{\Delta_n} im\alpha \sin \phi \left. \right] v_m \hat{\Omega}''_n + \left[\frac{\bar{\beta}_n}{\Delta_n} (2\bar{\alpha}_n v'_m + 4im\alpha \cos \phi \bar{\alpha}_n u_m \right. \\
& \left. + 2im\alpha \cos \phi \bar{\beta}_n w_m) - \frac{\bar{\alpha}_n}{\Delta_n} (2im\alpha \sin \phi \bar{\alpha}_n u_m) \right] \hat{\Omega}'_n + \left[\frac{\bar{\beta}_n}{\Delta_n} \{ (im^3 \alpha^3 \cos \phi \right. \right. \\
& \left. \left. + 2m^2 \alpha^2 \cos 2\phi \bar{\alpha}_n + 2m^2 \alpha^2 \cos \phi \sin \phi \bar{\beta}_n - im\alpha \cos \phi \Delta_n \right. \right. \\
& \left. \left. + im\alpha \sin \phi \bar{\alpha}_n \bar{\beta}_n) v_m - (im\alpha \cos \phi - 2\bar{\alpha}_n) v''_m + 4im\alpha \cos \phi \bar{\alpha}_n u'_m \right. \right. \\
& \left. \left. + 2im\alpha \cos \phi \bar{\beta}_n w'_m \right\} - \frac{\bar{\alpha}_n}{\Delta_n} \{ im\alpha \sin \phi (m^2 \alpha^2 - 2im\alpha \cos \phi \bar{\alpha}_n - \bar{\alpha}_n^2) v_m \right. \\
& \left. \left. - im\alpha \sin \phi v''_m + 2im\alpha \sin \phi \bar{\alpha}_n u'_m \right\} \right] \hat{\Omega}_n \} e^{N+M} = 0
\end{aligned} \tag{2.3.20}$$

In the above equations the variables referenced to the secondary instability are defined as

$$\bar{\alpha}_n = \frac{\partial}{\partial x} \quad \bar{\beta}_n = \frac{\partial}{\partial z} \quad \Delta_n = \frac{\partial^2}{\partial x^2} + \frac{\partial^2}{\partial z^2} \tag{2.3.21a}$$

$$e^N = e^{i(n/2)\alpha, (x \cos \phi + z \sin \phi)} = e^{i(n/2)\alpha, x'} \tag{2.3.21b}$$

$$e^M = e^{im\alpha, (x \cos \phi + z \sin \phi)} = e^{im\alpha, x'} \tag{2.3.21c}$$

Only a few terms of the Fourier series are used since Herbert (1976), Bertolotti, and Santos (1985) showed that this provided sufficient accuracy. By comparing terms with like exponentials in (2.3.19-20), the following two distinct classes of solution are found and defined by

Subharmonic: $m = \pm 1, n = \pm 1$

Fundamental: $m = \pm 1, n = 0, \pm 2$

Due to the size of the resulting equations for the subharmonic and fundamental modes, a listing is postponed and presented in Appendix A.

The boundary conditions for these equations are

$$\hat{v}_n, \hat{v}'_n, \hat{\Omega}_n \rightarrow 0 \quad \text{as} \quad y \rightarrow \infty \quad 2.3.22$$

along with the compliant wall boundary conditions or for the rigid wall

$$\hat{v}_n, \hat{v}'_n, \hat{\Omega}_n = 0 \quad \text{at} \quad y = 0 \quad 2.3.23$$

This completes the formation of the equations of motion for the three-dimensional primary and secondary instabilities in a laminar boundary layer. In the next chapter, a compliant wall model is introduced from which the wall boundary conditions will be derived.

CHAPTER 3

FORMULATION OF COMPLIANT WALL MODEL

3.1 Introduction

A number of different compliant, or flexible, wall models have been introduced to represent physically realistic coatings. Some of these were noted in the first chapter. A simple mechanical model that has shown significant delays of transition in theoretical studies by Carpenter and Morris (1990) is chosen. In some cases, up to ten times the transitional x -Reynolds number of the rigid wall was achieved. These results were obtained using a two-dimensional stability analysis. In the present paper, the mechanical model is extended to three dimensions. With this extension we look at the role of oblique primary waves on transition. The equations for the wall are derived in the next section. Additionally, we look at the effect of wall compliance on secondary instabilities. The boundary conditions required for this fluid/wall interaction study are derived in the third section.

3.2 Primary Wall Equations

The model was introduced by Grosskreutz (1971, 1975) in his drag reduction studies with turbulent boundary layers. A sketch of this compliant coating is shown in Figure 1.6. He suggested that the link between streamwise and normal surface displacements would cause a negative production of turbulence near the wall. Although his results were disappointing, in theory the surface may react to the fluid fluctuations in such a way as to produce a reduced or negative production of instability growth. The surface would then be attractive for potentially delaying transition in laminar boundary layers.

The mechanical model consists of a thin, elastic plate supported by hinged and sprung rigid members inclined to the horizontal and facing upstream at an angle, θ , when in equilibrium. A sketch of the mechanical wall is shown in Figure 1.7. The motion of the plate is treated such that each element of the plate can oscillate in pendulum like motion about its rigid member. The distance between each member is assumed much smaller than a characteristic wavelength of the flow instability. This mechanical model may be regarded as an approximate model for a flexible plate supported by fibre-composite sheets, or a thin plate supported by ribs that extend spanwise. Thus, it becomes comparatively stiff in the spanwise direction.

The derivation of the boundary conditions is begin by enforcing the continuity of motion between the fluid and wall. The streamwise, normal, and spanwise continuity equations are given by

$$\frac{\partial \xi}{\partial t} = u(x, y, z, t) \quad 3.2.1a$$

$$\frac{\partial \eta}{\partial t} = v(x, y, z, t) \quad 3.2.1b$$

$$\frac{\partial \zeta}{\partial t} = w(x, y, z, t) \quad 3.2.1c$$

where (ξ, η, ζ) are the streamwise, normal, and spanwise surface displacements and (u, v, w) are the velocity components as defined earlier. The instantaneous quantities are given by

$$\xi = \xi_0 + A\xi_1 \quad \text{and} \quad u = U_0 + Au_1 \quad 3.2.2a$$

$$\eta = \eta_0 + A\eta_1 \quad \text{and} \quad v = Av_1 \quad 3.2.2b$$

$$\zeta = \zeta_0 + A\zeta_1 \quad \text{and} \quad w = Aw_1 \quad 3.2.2c$$

It is assumed that there is no mean surface deformation implying, $(\xi_o, \eta_o, \zeta_o) = (0, 0, 0)$. By expanding the surface displacement in a Taylor series about $(\xi_1, \eta_1, \zeta_1) = (0, 0, 0)$ and substituting into (3.2.2) we find

$$A \frac{\partial \xi_1}{\partial t} = (U_o + Au_1) + A \xi_1 \frac{\partial Au_1}{\partial x} + A \eta_1 \frac{\partial (U_o + Au_1)}{\partial y} + h.o.t \quad 3.2.3a$$

$$A \frac{\partial \eta_1}{\partial t} = Av_1 + A\xi_1 \frac{\partial Av_1}{\partial x} + A\eta_1 \frac{\partial Av_1}{\partial y} + A\zeta_1 \frac{\partial Av_1}{\partial z} + h.o.t. \quad 3.2.3b$$

$$A \frac{\partial \zeta_1}{\partial t} = Aw_1 + A\xi_1 \frac{\partial Aw_1}{\partial x} + A\eta_1 \frac{\partial Aw_1}{\partial y} + A\zeta_1 \frac{\partial Aw_1}{\partial z} + h.o.t. \quad 3.2.3c$$

Linearizing the equations on the primary wave amplitude, A , the resulting continuity equations are

$$\frac{\partial \xi_1}{\partial t} = u_1 + \eta_1 U'_o \quad 3.2.4a$$

$$\frac{\partial \eta_1}{\partial t} = v_1 \quad 3.2.4b$$

$$\frac{\partial \zeta_1}{\partial t} = w_1 \quad 3.2.4c$$

At this point we may elect to make an assumption relative to the wall model being used. Since the swivel-arm, or rib, for a given element's orientation is such that the streamwise and normal wall motion will have a much greater freedom of motion than the spanwise, we can assume the following

$$\zeta_1 \ll \eta_1, \xi_1 \quad 3.2.5$$

So we let $\zeta_1 = 0$. From equation (3.2.4c), the spanwise fluctuation at the wall is zero, or $w_1 = 0$. This is consistent with the Grosskreutz coating since the stiff ribs extend in the spanwise direction thus allowing for little or no motion. But for a more conventional coating where stiffened fibers are imbedded in a soft matrix equation, (3.2.5) may not hold. So to retain some freedom with the

coating behavior, we do not choose to assume (3.2.5) and proceed with the full three-dimensional model which allows spanwise surface displacements.

For small displacements of an element out of equilibrium, the mechanical surface can be thought to move in a direction perpendicular to the rigid swivel-arm, or rib element, since the horizontal and vertical displacements are linked. The equation of motion for the element in the streamwise direction is given such that the total force acting on the surface by the fluid fluctuations balances with the force due to the wall. This equation is given by

$$\begin{aligned} \rho_m b \frac{\partial^2 \eta_1}{\partial t^2} + (B_z \frac{\partial^4 \eta_1}{\partial x^4} + 2B_{xz} \frac{\partial^4 \eta_1}{\partial x^2 \partial z^2} + B_z \frac{\partial^4 \eta_1}{\partial z^4}) \cos^2 \theta + K_E \eta_1 \\ - E_z b \frac{\partial^2 \xi_1}{\partial x^2} \sin \theta \cos \theta \\ = - p \cos^2 \theta + \tau_{yy} \cos^2 \theta + \tau_{yz} \sin \theta \cos \theta \end{aligned} \quad 3.2.6$$

The terms on the left hand side of (3.2.6) refer to mechanical forces and the terms on the right refer to fluid motion forces due to viscous stress and pressure fluctuations. For the case where the ribs are aligned at $\theta = 0^\circ$ the wall becomes isotropic and reduces to the theoretical model studied by Carpenter and Garrad (1985, 1986). Otherwise the wall is referred to as non-isotropic and the rib angle is determined by θ . For $E_z = E_x$ the plate is described as isotropic and for $E_z \neq E_x$ the plate is orthotropic. The effect of an isotropic and of an orthotropic plate with $E_z = 0$ combined with both isotropic ($\theta = 0^\circ$) and non-isotropic ($\theta > 0^\circ$) walls supporting substrates, on three-dimensional disturbances will be investigated.

The physical meaning of each term in (3.2.6) is given, respectively, as

- (1) rate of change of momentum of the surface element
- (2) resistance due to the bending stiffness in the streamwise direction
- (3) resistance due to the bending stiffness in the transverse ($\theta = 45^\circ$) direction
- (4) resistance due to the bending stiffness in the spanwise direction

- (5) resistance due to effective spring stiffness, or stiffness of the ribs, and the resistance to their motion due to the matrix, or substrate
- (6) tension force induced by relative motion of adjacent rigid member, or rib, in the streamwise direction
- (7) force due to the dynamic pressure fluctuations
- (8) force due to the normal viscous stress fluctuations
- (9) force due to the streamwise viscous shear stress fluctuations

The variables of the mechanical model may be defined as: $\delta\theta$ is the angular displacement of the element relative to the equilibrium position; ℓ is the rigid member length in the mechanical model; ρ_m and b are the plate density and thickness; (B_x, B_{xz}, B_z) are the flexural rigidities of the plate in the streamwise, transverse and spanwise directions; (E_x, E_z) are the moduli of elasticity of the plate; K_E is the effective spring stiffness; and p , τ_{yy} and τ_{yz} are the pressure, normal viscous stress, and streamwise viscous shear stress fluctuations in the fluid acting on the wall.

The effective spring stiffness incorporates the body forces such that

$$K_E = K - g(\rho - \rho_s) \cos \theta \quad 3.2.7$$

where K is the spring stiffness, g is the acceleration due to gravity, ρ_s is the substrate density. In this investigation the case where $(\rho = \rho_s)$ is considered, so $K_E = K$.

In addition, the flexural rigidities may be found by the relations

$$B_x = \frac{E_x b^3}{12(1 - \nu_x \nu_z)} \quad \text{and} \quad B_z = \frac{E_z b^3}{12(1 - \nu_x \nu_z)} \quad 3.2.8$$

The materials used to manufacture a practical compliant coating would most likely have Poisson ratios that are very close to 0.5. It is therefore assumed

$\nu_x = \nu_z = 0.5$. A reasonable approximation for B_{zz} is given by

$$B_{zz} = \sqrt{B_x B_z} \quad 3.2.9$$

The necessary equations of motion for the surface are coupled by a relationship between the tangential and normal displacements (ξ_1, η_1) with the angular displacement $(\delta\theta)$ such that

$$\xi_1 = \ell\delta\theta \sin\theta \quad \text{and} \quad \eta_1 = \ell\delta\theta \cos\theta \quad 3.2.10a$$

or

$$\xi_1 = \eta_1 \tan\theta \quad 3.2.10b$$

The displacement of the surface is assumed to take the same normal mode form as equation (2.2.11,13), or

$$\{\xi_1, \eta_1, \zeta_1\}(x, y, z, t) = \{\hat{\xi}_1, \hat{\eta}_1, \hat{\zeta}_1\}(y) \cdot \exp[i\alpha(x \cos\phi + z \sin\phi - c_r t)] + c.c. \quad 3.2.11$$

Substituting into the streamwise force balance equation for the wall and nondimensionalizing, we find

$$\begin{aligned} & \left[-C_M \omega^2 + (C_{Bz} \cos^4 \phi + 2C_{Bzz} \sin^2 \phi \cos^2 \phi + C_{Bz} \sin^4 \phi) \alpha^4 \cos^2 \theta \right. \\ & \quad \left. + C_K + C_{Tz} \alpha^2 \sin^2 \theta \cos^2 \phi \right] \hat{\eta}_1 \\ & = -\hat{p} \cos^2 \theta + \hat{\tau}_{yy} \cos^2 \theta + \hat{\tau}_{yz} \sin \theta \cos \theta \end{aligned} \quad 3.2.12$$

where

$$\begin{aligned} C_{Bz} &= \frac{B_z}{\rho_\infty U_\infty \delta^3} & C_{Bzz} &= \frac{B_{zz}}{\rho_\infty U_\infty \delta^3} & C_{Bz} &= \frac{B_z}{\rho_\infty U_\infty \delta^3} \\ C_M &= \frac{\rho_m b}{\rho_\infty \delta^3} & C_K &= \frac{K \delta^3}{\rho_\infty U_\infty^2} & C_{Tz} &= \frac{E_t b}{\rho_\infty U_\infty^2 \delta^3} \end{aligned}$$

In order to obtain equations for the wall motion in terms of the normal velocity (v) and vorticity (Ω), relations for u and w are formulated from the fluid continuity

equation and the definition of normal vorticity. For the primary instability this gives

$$\hat{u}_1 = \frac{i}{\alpha} [\cos \phi \hat{v}'_1 - \sin \phi \hat{\Omega}_1] \quad 3.2.13a$$

and

$$\hat{w}_1 = \frac{i}{\alpha} [\sin \phi \hat{v}'_1 + \cos \phi \hat{\Omega}_1] \quad 3.2.13b$$

Similarly, substituting (3.2.11) and (3.2.13) into the linearized continuity equations results in

$$\alpha(U'_o \cos \theta + i\omega \sin \theta) \hat{\eta}_1 = i [\sin \phi \hat{\Omega}_1 - \cos \phi \hat{v}'_1] \cos \theta \quad 3.2.14a$$

$$\hat{\eta}_1 \omega = i \hat{v}_1 \quad 3.2.14b$$

$$\alpha \omega \hat{\zeta}_1 = - [\sin \phi \hat{v}'_1 + \cos \phi \hat{\Omega}_1] \quad 3.2.14c$$

This along with the following relations for viscous and pressure fluctuations at the wall are then substituted into (3.2.12) resulting in a boundary condition for the wall.

The stress tensor is given by

$$\tau_{ij} = \mu \left(\frac{\partial u_i}{\partial x_j} + \frac{\partial u_j}{\partial x_i} \right) \quad 3.2.15$$

The normal viscous stress at the wall is found from (3.2.15) to be

$$\tau_{yy} = 2\mu \frac{\partial v}{\partial y} \quad 3.2.16a$$

or nondimensionally

$$\hat{\tau}_{yy} = \frac{2}{R_\delta} \hat{v}'_1 \quad 3.2.16b$$

The streamwise viscous shear stress at the wall from (3.2.15) is

$$\tau_{yz} = \mu \left(\frac{\partial v}{\partial x} + \frac{\partial u}{\partial y} \right) \quad 3.2.17a$$

or nondimensionally in normal modes

$$\hat{\tau}_{yz} = \frac{1}{R_\delta} (i\alpha \cos \phi \hat{v}_1 + \hat{u}'_1) \quad 3.2.17b$$

Substituting equation (3.2.13) in for u gives

$$\hat{\tau}_{yz} = \frac{i}{\alpha R_\delta} [\cos \phi \hat{v}_1'' + \alpha^2 \cos \phi \hat{v}_1 - \sin \phi \hat{\Omega}'_1] \quad 3.2.18$$

The pressure fluctuation is found from the linearized streamwise and spanwise components of the Navier-Stokes equations. In normal components this is

$$\hat{p} = \frac{1}{\alpha^2 R_\delta} [\hat{v}_1''' + (i\omega R_\delta - \alpha^2) \hat{v}_1' + i\alpha \cos \phi R_\delta U'_o \hat{v}_1] \quad 3.2.19$$

Substituting the above relations for pressure and stress fluctuations into (3.2.12) yields

$$\begin{aligned} & \left[-C_M \omega^2 + (C_{Bz} \cos^4 \phi + 2C_{Bzz} \sin^2 \phi \cos^2 \phi + C_{Bz} \sin^4 \phi) \alpha^4 \cos^2 \theta \right. \\ & \quad \left. + C_K + C_{Tz} \alpha^2 \sin^2 \theta \cos^2 \phi \right] \frac{(\sin \phi \hat{\Omega}_1 - \cos \phi \hat{v}_1') \cos \theta}{(U'_o \cos \theta + i\omega \sin \theta)} \\ & \quad + \frac{\cos^2 \theta}{\alpha^2 R_\delta} \left[\hat{v}_1''' + (i\omega R_\delta - \alpha^2) \hat{v}_1' + i\alpha \cos \phi R_\delta U'_o \hat{v}_1 \right] - \frac{2 \cos^2 \theta}{R_\delta} \hat{v}'_1 \\ & \quad - \frac{i \sin \theta \cos \theta}{\alpha R_\delta} \left[\cos \phi \hat{v}_1'' + \alpha^2 \cos \phi \hat{v}_1 - \sin \phi \hat{\Omega}'_1 \right] = 0 \quad 3.2.20 \end{aligned}$$

By rearranging (3.2.20) the resulting boundary condition may be obtained.

$$\begin{aligned}
 & \alpha^5 \left[(C_{Bz} \cos^4 \phi + 2C_{Bzz} \cos^2 \phi \sin^2 \phi + C_{Bz} \sin^4 \phi) \cos^2 \theta \right] (\cos^2 \phi \hat{v}'_1 \\
 & - \sin \phi \cos \phi \hat{\Omega}_1) + \left[\alpha^3 C_{Tz} \sin^2 \theta \cos^2 \phi + \alpha (C_K - \omega^2 C_M) \right] (\cos^2 \phi \hat{v}'_1 \\
 & - \sin \phi \cos \phi \hat{\Omega}_1) + \frac{\alpha^2 \cos \theta \cos \phi}{R_\delta} \left[(2\omega \sin \theta - 3iU'_o \cos \theta) + \omega^2 \sin \theta \sin^2 \phi \right] \hat{v}'_1 \\
 & - (U'_o \cos \theta \sin^2 \phi + i\omega \sin \theta) \omega \cos \theta \cos \phi \hat{v}'_1 \\
 & + \alpha (U'_o \cos \theta + i\omega \sin \theta) \frac{\sin \theta \cos^2 \phi}{R_\delta} \hat{v}''_1 + \frac{i \cos \theta \cos \phi}{R_\delta} (U'_o \cos \theta + i\omega \sin \theta) \hat{v}'''_1 \\
 & + (\omega \sin \theta \frac{\alpha^2}{R_\delta} - U'_o \cos \theta) \omega \cos \theta \cos^2 \phi \sin \phi \hat{\Omega}_1 \\
 & - \sin \theta \sin \phi \cos \phi \frac{\alpha}{R_\delta} (U'_o \cos \theta + i\omega \sin \theta) \hat{\Omega}'_1 = 0
 \end{aligned} \tag{3.2.21}$$

The second boundary condition may be obtained by combining (3.2.14a) and (3.2.14b). This gives

$$\alpha (U'_o \cos \theta + i\omega \sin \theta) \hat{v}_1 + \omega \cos \theta [\cos \phi \hat{v}'_1 - \sin \phi \hat{\Omega}_1] = 0 \tag{3.2.22}$$

The final boundary condition accounts for the spanwise motion and the continuity given by (3.2.14c). In order to remove the spanwise surface displacement ζ_1 , an additional equation must be found. This equation results from the balance of forces in the spanwise direction and is given as

$$\rho_m b \frac{\partial^2 \zeta_1}{\partial t^2} + K_s \zeta_1 - E_z b \frac{\partial^2 \zeta_1}{\partial z^2} = \tau_{yz} \tag{3.2.23}$$

where the first term is the spanwise rate of change of momentum of the surface element; the second term is the resistance due to an effective spanwise spring stiffness with K_s as an effective stiffening parameter; the third term is a tension force induced by the relative motion of an adjacent rib; and the final term is the fluid force due to the spanwise viscous shear stress fluctuation. This equation is a result of assuming that the rigid member is normal to the plate. For the

Grosskreutz coating, K_s , would be very large resulting in no spanwise surface displacement. This results in (3.2.5) being acceptable, or the spanwise displacement is insignificant as compared to the normal and streamwise surface motion.

Proceeding to obtain the final boundary condition, equation (3.2.23) is nondimensionalized and normal modes are introduced, giving

$$[-C_M \omega^2 + C_{K_s} + C_{T_z} \alpha^2 \sin^2 \phi] \hat{\zeta}_1 = \hat{\tau}_{yz} \quad 3.2.24$$

where

$$C_{K_s} = \frac{K_s \delta^*}{\rho_\infty U_\infty^2} \quad \text{and} \quad C_{T_z} = \frac{E_z b}{\rho_\infty U_\infty^2 \delta^*}$$

From the stress tensor (3.2.15) the following results.

$$\tau_{yz} = \mu \left(\frac{\partial v}{\partial z} + \frac{\partial w}{\partial y} \right) \quad 3.2.25a$$

or

$$\hat{\tau}_{yz} = \frac{i}{\alpha R} [\sin \phi \hat{v}_1'' + \alpha^2 \hat{v}_1 + \cos \phi \hat{\Omega}_1'] \quad 3.2.25b$$

To arrive at the final form of the boundary condition the shear stress (3.2.25) and the continuity equation (3.2.14c) are substituted into (3.2.24). This gives

$$\begin{aligned} & [C_{K_s} - C_M \omega^2 + C_{T_z} \alpha^2 \sin^2 \phi] (\cos \phi \hat{\Omega}_1 + \sin \phi \hat{v}_1') \\ & + \frac{i\omega}{R} (\sin \phi \hat{v}_1'' + \alpha^2 \sin \phi \hat{v}_1 + \cos \phi \hat{\Omega}_1') = 0 \end{aligned} \quad 3.2.26$$

To simulate the rigid wall case, let $C_M \rightarrow \infty$ or C_B and $C_K \rightarrow \infty$. In this way the above boundary conditions reduce to that of the flat plate. To simulate the Grosskreutz coating, let $C_{K_s} \rightarrow \infty$. This implies that $\zeta_1 = w_1(0) = 0$. For the $\theta = 0^\circ$ case, an isotropic wall is simulated. And for the $\theta \neq 0^\circ$ case, a non-isotropic wall is found.

3.3 Secondary Wall Equations

In this section the compliant wall boundary equations will be derived for secondary instabilities. The analysis follows the same route as was taken for the primary instabilities, except a number of additional terms arise. These are due to the primary wave, and thus the wall motion is parametrically driven by the primary flow. This is consistent with the derivations and discussion of the secondary fluid equations of motion in the previous chapter. As with the fluid equations, the derivations below are for the reference frame moving with the primary wave. Some of the equations are repeated from the previous section. This is done to maintain a flow of the derivations since the equations are quite large and the analysis becomes tedious.

For the secondary fluid/wall interaction and subsequent wall motion, we begin with the same general governing equations as with the primary. Thus, we have continuity of fluid and wall motion in each direction as well as the equations of force balance in the streamwise and spanwise directions. The continuity of motion between the fluid and wall implies

$$\frac{\partial \xi}{\partial t} = u(x, y, z, t) \quad 3.3.1a$$

$$\frac{\partial \eta}{\partial t} = v(x, y, z, t) \quad 3.3.1b$$

$$\frac{\partial \zeta}{\partial t} = w(x, y, z, t) \quad 3.3.1c$$

where the independent variables are in a reference frame moving with the primary wave at phase speed, $(c_x, 0, c_z)$. Consistent with the fluid equations, the amplitude of the primary wave is locally non-varying. The instantaneous velocity and surface displacements are

$$\xi = \xi_0 + A\xi_1 + B\xi_3 \quad \text{and} \quad u = U_0 + Au_1 + Bu_3 \quad 3.3.2a$$

$$\eta = \eta_o + A\eta_1 + B\eta_3 \quad \text{and} \quad v = Av_1 + Bv_3 \quad 3.3.2b$$

$$\zeta = \zeta_o + A\zeta_1 + B\zeta_3 \quad \text{and} \quad w = Aw_1 + Bw_3 \quad 3.3.2c$$

Expand the surface displacements in a Taylor series about $(\xi, \eta, \zeta) = (0, 0, 0)$.

This gives

$$\frac{\partial \xi}{\partial t} = u + \xi \frac{\partial u}{\partial x} + \eta \frac{\partial u}{\partial y} + \zeta \frac{\partial u}{\partial z} + h.o.t \quad 3.3.3a$$

$$\frac{\partial \eta}{\partial t} = v + \xi \frac{\partial v}{\partial x} + \eta \frac{\partial v}{\partial y} + \zeta \frac{\partial v}{\partial z} + h.o.t \quad 3.3.3b$$

$$\frac{\partial \zeta}{\partial t} = w + \xi \frac{\partial w}{\partial x} + \eta \frac{\partial w}{\partial y} + \zeta \frac{\partial w}{\partial z} + h.o.t \quad 3.3.3c$$

Consistent with the fluid equations, the primary fluid/wall interaction is assumed exactly represented by the respective equations. Thus, by substitution and linearization on the secondary amplitude B , the continuity equations result.

$$\frac{\partial \xi_3}{\partial t} = u_3 + \eta_3 U'_o + A \left\{ \xi_1 \frac{\partial u_3}{\partial x} + \eta_1 \frac{\partial u_3}{\partial y} + \zeta_1 \frac{\partial u_3}{\partial z} + \xi_3 \frac{\partial u_1}{\partial x} + \eta_3 \frac{\partial u_1}{\partial y} + \zeta_3 \frac{\partial u_1}{\partial z} \right\} \quad 3.3.4a$$

$$\frac{\partial \eta_3}{\partial t} = v_3 + A \left\{ \xi_1 \frac{\partial v_3}{\partial x} + \eta_1 \frac{\partial v_3}{\partial y} + \zeta_1 \frac{\partial v_3}{\partial z} + \xi_3 \frac{\partial v_1}{\partial x} + \eta_3 \frac{\partial v_1}{\partial y} + \zeta_3 \frac{\partial v_1}{\partial z} \right\} \quad 3.3.4b$$

$$\frac{\partial \zeta_3}{\partial t} = w_3 + \eta_3 W'_o + A \left\{ \xi_1 \frac{\partial w_3}{\partial x} + \eta_1 \frac{\partial w_3}{\partial y} + \zeta_1 \frac{\partial w_3}{\partial z} + \xi_3 \frac{\partial w_1}{\partial x} + \eta_3 \frac{\partial w_1}{\partial y} + \zeta_3 \frac{\partial w_1}{\partial z} \right\} \quad 3.3.4c$$

With these equations, some parallels are drawn with the fluid equations. First, if the primary amplitude, A , goes to zero, the primary compliant boundary equations result. This occurs similarly with the fluid equations. Secondly, the terms in the equations that are amplitude dependent involve coefficients that are functions of the primary wave. So as with the fluid, the wall is dependent on the primary wave development. The difference between the fluid equations and boundary conditions that does arise makes the analysis very tedious. Equations (3.3.4) involve six unknowns for the velocity fluctuations and surface displacement in a

highly coupled system. The goal, as with the primary boundary conditions, is to arrive at a set of equations which represent the surface motion in terms of the normal velocity and vorticity.

The first step to accomplish this involves representing (3.3.4) in normal modes. This form is the same as (2.3.14), or

$$\{\xi_3, \eta_3, \zeta_3\} = e^{\sigma t + i\beta(z \cos \phi - x \sin \phi) + \gamma(x \cos \phi + z \sin \phi)} \sum_{n=-\infty}^{\infty} \{\hat{\xi}_n, \hat{\eta}_n, \hat{\zeta}_n\} e^N \quad 3.3.5$$

where as before this and subsequent equations will involve symbols listed in (2.3.21). This is done to simplify the equations. Equations (2.3.5, 14) and (3.3.5) are substituted into the linearized continuity equations giving

$$\begin{aligned} \sigma \hat{\xi}_n e^N &= (\hat{u}_n + U'_o \hat{\eta}_n) e^N \\ &+ A \left\{ \xi_m \bar{\alpha}_n \hat{u}_n + \eta_m \hat{u}'_n + \zeta_m \bar{\beta}_n \hat{u}_n + im\alpha \cos \phi u_m \hat{\xi}_n \right. \\ &\left. + u'_m \hat{\eta}_n + im\alpha \sin \phi u_m \hat{\zeta}_n \right\} e^{N+M} \end{aligned} \quad 3.3.6a$$

$$\begin{aligned} \sigma \hat{\eta}_n e^N &= \hat{v}_n e^N \\ &+ A \left\{ \xi_m \bar{\alpha}_n \hat{v}_n + \eta_m \hat{v}'_n + \zeta_m \bar{\beta}_n \hat{v}_n + im\alpha \cos \phi v_m \hat{\xi}_n \right. \\ &\left. + v'_m \hat{\eta}_n + im\alpha \sin \phi v_m \hat{\zeta}_n \right\} e^{N+M} \end{aligned} \quad 3.3.6b$$

$$\begin{aligned}
\sigma \hat{\zeta}_n e^N &= (\hat{w}_n + W_o' \hat{\eta}_n) e^N \\
&+ A \left\{ \xi_m \bar{\alpha}_n \hat{w}_n + \eta_m \hat{w}'_n + \zeta_m \bar{\beta}_n \hat{w}_n + im\alpha \cos \phi w_m \hat{\zeta}_n \right. \\
&\left. + w'_m \hat{\eta}_n + im\alpha \sin \phi w_m \hat{\zeta}_n \right\} e^{N+M}
\end{aligned} \tag{3.3.6c}$$

From the mechanical model a relationship between the normal and streamwise displacement is found and given in equation (3.2.10). From the mass continuity and vorticity we find

$$\hat{u}_n = \left[\frac{\bar{\beta}_n}{\Delta_n} \hat{\Omega}_n - \frac{\bar{\alpha}_n}{\Delta_n} \hat{v}'_n \right] \tag{3.3.7a}$$

$$\hat{w}_n = - \left[\frac{\bar{\alpha}_n}{\Delta_n} \hat{\Omega}_n + \frac{\bar{\beta}_n}{\Delta_n} \hat{v}'_n \right] \tag{3.3.7b}$$

Substituting (3.2.10) and (3.3.7) into (3.3.6) reduces the unknown dependent variables to four. This results in

$$\begin{aligned}
(\sigma \tan \theta - U_o') \hat{\eta}_n e^N &= \left(\frac{\bar{\beta}_n}{\Delta_n} \hat{\Omega}_n - \frac{\bar{\alpha}_n}{\Delta_n} \hat{v}'_n \right) e^N \\
&+ A \left\{ (\eta_m \tan \theta \bar{\alpha}_n + \zeta_m \bar{\beta}_n) \left(\frac{\bar{\beta}_n}{\Delta_n} \hat{\Omega}_n - \frac{\bar{\alpha}_n}{\Delta_n} \hat{v}'_n \right) \right. \\
&+ \eta_m \left(\frac{\bar{\beta}_n}{\Delta_n} \hat{\Omega}'_n - \frac{\bar{\alpha}_n}{\Delta_n} \hat{v}''_n \right) + (\tan \theta im\alpha \cos \phi u_m + u'_m) \hat{\eta}_n \\
&\left. + im\alpha \sin \phi u_m \hat{\zeta}_n \right\} e^{N+M}
\end{aligned} \tag{3.3.8a}$$

$$\begin{aligned}
\sigma \hat{\eta}_n e^N &= \hat{v}_n e^N + A \left\{ (\eta_m \tan \theta \bar{\alpha}_n + \zeta_m \bar{\beta}_n) \hat{v}_n + \eta_m \hat{v}'_n \right. \\
&\left. + (\tan \theta im\alpha \cos \phi v_m + v'_m) \hat{\eta}_n + im\alpha \sin \phi v_m \hat{\zeta}_n \right\} e^{N+M}
\end{aligned} \tag{3.3.8b}$$

$$\begin{aligned}
\sigma \hat{\zeta}_n e^N = & - \left(\frac{\bar{\alpha}_n}{\Delta_n} \hat{\Omega}_n + \frac{\bar{\beta}_n}{\Delta_n} \hat{v}'_n \right) e^N + W'_o \hat{\eta}_n e^N \\
& - A \left\{ (\eta_m \tan \theta \bar{\alpha}_n + \zeta_m \bar{\beta}_n) \left(\frac{\bar{\alpha}_n}{\Delta_n} \hat{\Omega}_n + \frac{\bar{\beta}_n}{\Delta_n} \hat{v}'_n \right) \right. \\
& + \eta_m \left(\frac{\bar{\alpha}_n}{\Delta_n} \hat{\Omega}'_n + \frac{\bar{\beta}_n}{\Delta_n} \hat{v}''_n \right) - (\tan \theta i m \alpha \cos \phi w_m + w'_m) \hat{\eta}_n \\
& \left. - i m \alpha \sin \phi w_m \hat{\zeta}_n \right\} e^{N+M} \quad 3.3.8c
\end{aligned}$$

To further reduce the number of unknown dependent variables, additional equations must be used.

The equation representing the balance of forces between the fluid and wall in the spanwise direction is introduced.

$$\rho_m b \frac{\partial^2 \zeta_3}{\partial t^2} + K_s \zeta_3 - E_z b \frac{\partial^2 \zeta_3}{\partial z^2} = \tau_{yz} \quad 3.3.9$$

This is the same form as equation (3.2.23) for the primary wall. From the stress tensor (3.2.15) we find

$$\hat{\tau}_{yz} = \frac{1}{R_\delta} \left(\frac{\partial v_3}{\partial z} + \frac{\partial w_3}{\partial y} \right) \quad 3.3.10a$$

or in normal modes

$$\hat{\tau}_{yz} = \frac{1}{R_\delta} (\bar{\beta}_n \hat{v}_n + \hat{w}'_n) e^N \quad 3.3.10b$$

Substituting for \hat{w}' gives

$$\hat{\tau}_{yz} = \frac{1}{R_\delta} \left(\bar{\beta}_n \hat{v}_n - \frac{\bar{\alpha}_n}{\Delta_n} \hat{\Omega}'_n - \frac{\bar{\beta}_n}{\Delta_n} \hat{v}''_n \right) e^N \quad 3.3.10c$$

In nondimensional and normal modes and substituting in the stress relation (3.3.10) the spanwise surface displacement is given by

$$\hat{\zeta}_n = \frac{1}{R_\delta} \left(\bar{\beta}_n \hat{v}_n - \frac{\bar{\alpha}_n}{\Delta_n} \hat{\Omega}'_n - \frac{\bar{\beta}_n}{\Delta_n} \hat{v}''_n \right) / (C_M \sigma^2 + C_{K_s} - C_{T_z} \bar{\beta}_n^2) e^N \quad 3.3.11$$

where

$$C_M = \frac{\rho_m b}{\rho_\infty \delta^*} \quad C_{Ks} = \frac{K_s \delta^*}{\rho_\infty U_\infty^2} \quad C_{Tz} = \frac{E_z b}{\rho_\infty U_\infty^2 \delta^*}$$

This relation for the spanwise surface displacement is substituted into (3.3.8) to give

$$\begin{aligned} & \left[\frac{\bar{\alpha}_n}{\Delta_n} \hat{v}'_n - \frac{\bar{\beta}_n}{\Delta_n} \hat{\Omega}_n + (\sigma \tan \theta - U'_o) \hat{\eta}_n \right] e^N \\ &= A \left\{ (\eta_m \tan \theta \bar{\alpha}_n + \zeta_m \bar{\beta}_n) \left(\frac{\bar{\beta}_n}{\Delta_n} \hat{\Omega}_n - \frac{\bar{\alpha}_n}{\Delta_n} \hat{v}'_n \right) \right. \\ &+ \eta_m \left(\frac{\bar{\beta}_n}{\Delta_n} \hat{\Omega}'_n - \frac{\bar{\alpha}_n}{\Delta_n} \hat{v}''_n \right) + (\tan \theta i m \alpha \cos \phi u_m + u'_m) \hat{\eta}_n \\ &+ \frac{i m \alpha \sin \phi u_m}{R_\delta (C_M \sigma^2 + C_{Ks} - C_{Tz} \bar{\beta}_n^2)} \left(\bar{\beta}_n \hat{v}_n - \frac{\bar{\alpha}_n}{\Delta_n} \hat{\Omega}'_n \right. \\ & \left. \left. - \frac{\bar{\beta}_n}{\Delta_n} \hat{v}''_n \right) \right\} e^{N+M} \end{aligned} \quad 3.3.12a$$

$$\begin{aligned} (\sigma \hat{\eta}_n - \hat{v}_n) e^N &= A \left\{ (\eta_m \tan \theta \bar{\alpha}_n + \zeta_m \bar{\beta}_n) \hat{v}_n + \eta_m \hat{v}'_n \right. \\ &+ (\tan \theta i m \alpha \cos \phi v_m + v'_m) \hat{\eta}_n \\ &+ \frac{i m \alpha \sin \phi v_m}{R_\delta (C_M \sigma^2 + C_{Ks} - C_{Tz} \bar{\beta}_n^2)} \left(\bar{\beta}_n \hat{v}_n - \frac{\bar{\alpha}_n}{\Delta_n} \hat{\Omega}'_n - \frac{\bar{\beta}_n}{\Delta_n} \hat{v}''_n \right) \right\} e^{N+M} \end{aligned} \quad 3.3.12b$$

$$\begin{aligned} & \left[\frac{\sigma}{R_\delta} \left(\bar{\beta}_n \hat{v}_n - \frac{\bar{\alpha}_n}{\Delta_n} \hat{\Omega}'_n - \frac{\bar{\beta}_n}{\Delta_n} \hat{v}''_n \right) + (C_M \sigma^2 + C_{Ks} - C_{Tz} \bar{\beta}_n^2) \left(\frac{\bar{\alpha}_n}{\Delta_n} \hat{\Omega}_n + \frac{\bar{\beta}_n}{\Delta_n} \hat{v}'_n \right) \right] e^N \\ &+ W'_o \hat{\eta}_n e^N = -A (C_M \sigma^2 + C_{Ks} - C_{Tz} \bar{\beta}_n^2) \left\{ (\eta_m \tan \theta \bar{\alpha}_n + \zeta_m \bar{\beta}_n) \left(\frac{\bar{\alpha}_n}{\Delta_n} \hat{\Omega}_n + \frac{\bar{\beta}_n}{\Delta_n} \hat{v}'_n \right) \right. \\ &+ \eta_m \left(\frac{\bar{\alpha}_n}{\Delta_n} \hat{\Omega}'_n + \frac{\bar{\beta}_n}{\Delta_n} \hat{v}''_n \right) - \hat{\eta}_n (\tan \theta i m \alpha \cos \phi w_m + w'_m) \\ & \left. - \frac{i m \alpha \sin \phi w_m}{R_\delta (C_M \sigma^2 + C_{Ks} - C_{Tz} \bar{\beta}_n^2)} \left(\bar{\beta}_n \hat{v}_n - \frac{\bar{\alpha}_n}{\Delta_n} \hat{\Omega}'_n - \frac{\bar{\beta}_n}{\Delta_n} \hat{v}''_n \right) \right\} e^{N+M} \end{aligned} \quad 3.3.12c$$

Thus, the above continuity equations are in terms of the normal velocity, normal vorticity, and normal surface displacement only.

The final necessary boundary equation is derived from a balance of fluid and wall forces in the streamwise direction. A balance of forces yields

$$\begin{aligned} & \left[\rho_m b \frac{\partial^2}{\partial t^2} + \left(B_z \frac{\partial^4}{\partial x^4} + 2B_{zz} \frac{\partial^4}{\partial x^2 \partial z^2} + B_z \frac{\partial^4}{\partial z^4} \right) \cos^2 \theta \right. \\ & \quad \left. + K_E - E_z b \frac{\partial^2}{\partial x^2} \sin^2 \theta \right] \eta_3 \\ & = - p \cos^2 \theta + \tau_{yy} \cos^2 \theta + \tau_{yz} \sin \theta \cos \theta \end{aligned} \quad 3.3.13$$

or nondimensionally

$$\begin{aligned} & \left[C_M \frac{\partial^2}{\partial t^2} + \left(C_{Bz} \frac{\partial^4}{\partial x^4} + 2C_{Bzz} \frac{\partial^4}{\partial x^2 \partial z^2} + C_{Bz} \frac{\partial^4}{\partial z^4} \right) \cos^2 \theta \right. \\ & \quad \left. + C_K - C_{Tz} \frac{\partial^2}{\partial x^2} \sin^2 \theta \right] \eta_3 \\ & = - \hat{p} \cos^2 \theta + \hat{\tau}_{yy} \cos^2 \theta + \hat{\tau}_{yz} \sin \theta \cos \theta \end{aligned} \quad 3.3.14$$

The normal stress is given as

$$\hat{\tau}_{yy} = \frac{2}{R_\delta} \frac{\partial v}{\partial y} \quad 3.3.15a$$

or

$$\hat{\tau}_{yy} = \frac{2}{R_\delta} \hat{v}'_n e^N \quad 3.3.15b$$

The streamwise shear stress is given by

$$\hat{\tau}_{yz} = \frac{1}{R_\delta} \left(\frac{\partial v}{\partial x} + \frac{\partial u}{\partial y} \right) \quad 3.3.16a$$

In normal modes and replacing u by the appropriate velocity-vorticity relation gives

$$\hat{\tau}_{yz} = \frac{1}{R_\delta} \left(\bar{\alpha}_n \hat{v}_n - \frac{\bar{\alpha}_n}{\Delta_n} \hat{v}''_n + \frac{\bar{\beta}_n}{\Delta_n} \hat{\Omega}'_n \right) e^N \quad 3.3.16b$$

The pressure fluctuation at the wall is found from the linearized streamwise and spanwise momentum equations. This results in the following pressure in normal modes

$$\begin{aligned} \Delta_n \hat{p} = & \left\{ -\left[\frac{1}{R_\delta} \Delta_n - \sigma + c_x \bar{\alpha}_n + c_z \bar{\beta}_n \right] \hat{v}' - \frac{1}{R} \hat{v}''' - (U'_o \bar{\alpha}_n + W'_o \bar{\beta}_n) \hat{v}_n \right\} e^N \\ & + A \left\{ (u_m \bar{\alpha}_n + w_m \bar{\beta}_n) \hat{v}'_n + v_m \hat{v}''_n - (u'_m \bar{\alpha}_n + w'_m \bar{\beta}_n) \hat{v}_n \right. \\ & + im\alpha \cos \phi (u_m \bar{\alpha}_n + w_m \bar{\beta}_n) \left(\frac{\bar{\alpha}_n}{\Delta_n} \hat{v}'_n - \frac{\bar{\beta}_n}{\Delta_n} \hat{\Omega}_n \right) \\ & \left. + im\alpha \sin \phi (u_m \bar{\alpha}_n + w_m \bar{\beta}_n) \left(\frac{\bar{\beta}_n}{\Delta_n} \hat{v}'_n + \frac{\bar{\alpha}_n}{\Delta_n} \hat{\Omega}_n \right) \right\} e^{N+M} \end{aligned} \quad 3.3.17$$

Substituting the normal mode relation (3.3.5) along with the stress and pressure relations (3.3.15-17) into (3.3.14), the final necessary equation to complete the boundary conditions results. This is given as

$$\begin{aligned} & [C_M \sigma^2 + (C_{Bx} \bar{\alpha}_n^4 + 2C_{Bzz} \bar{\alpha}_n^2 \bar{\beta}_n^2 + C_{Bz} \bar{\beta}_n^4) \cos^2 \theta + C_K \\ & - C_{Tx} \bar{\alpha}_n^2 \sin^2 \theta] \hat{\eta}_n \Delta_n e^N \\ & - \left\{ \left[\frac{3}{R_\delta} \Delta_n - \sigma + c_x \bar{\alpha}_n + c_z \bar{\beta}_n \right] \hat{v}'_n + \frac{1}{R} \hat{v}'''_n + (U'_o \bar{\alpha}_n + W'_o \bar{\beta}_n) \hat{v}_n \right. \\ & - \frac{\Delta_n \tan \theta}{R_\delta} \left(\frac{\bar{\alpha}_n}{\Delta_n} \hat{v}''_n - \bar{\alpha}_n \hat{v}_n - \frac{\bar{\beta}_n}{\Delta_n} \hat{\Omega}'_n \right) \left. \right\} e^N \\ & + A \left\{ (u_m \bar{\alpha}_n + w_m \bar{\beta}_n) \hat{v}'_n + v_m \hat{v}''_n - (u'_m \bar{\alpha}_n + w'_m \bar{\beta}_n) \hat{v}_n \right. \\ & + im\alpha \cos \phi (u_m \bar{\alpha}_n + w_m \bar{\beta}_n) \left(\frac{\bar{\alpha}_n}{\Delta_n} \hat{v}'_n - \frac{\bar{\beta}_n}{\Delta_n} \hat{\Omega}_n \right) \\ & \left. + im\alpha \sin \phi (u_m \bar{\alpha}_n + w_m \bar{\beta}_n) \left(\frac{\bar{\beta}_n}{\Delta_n} \hat{v}'_n + \frac{\bar{\alpha}_n}{\Delta_n} \hat{\Omega}_n \right) \right\} \cos^2 \theta e^{N+M} = 0 \quad 3.3.18 \end{aligned}$$

The complete boundary conditions are the system of equations given by (3.3.12, 18). This must be reduced to three equations in terms of the normal

velocity and normal vorticity prior to obtaining solutions. This elimination of $(\hat{\eta}_n)$ from the boundary conditions is in itself not trivial. Great care must be maintained with the subscripts (n and m). They identify which Fourier mode is being represented. So in order to obtain a general closed form for the three boundary conditions in terms of velocity and vorticity only, a number of "redefinitions" must be carried out for the subscripts depending on the modes being considered. Since we are interested in solving for only two modes for the subharmonic and three for the fundamental, we choose to avoid this index redefinition route. Instead, by the use of equation (3.3.12b) and identifying the modes of interest, relations can be found for the modes representing the normal surface displacement in terms of velocity and vorticity only. These are then substituted into (3.3.12a, 12b, 18) and the final form of the boundary conditions is determined. The complete derivations and a listing of these boundary conditions are given in Appendix B.

Before the solution methods are discussed, a few general observations of these equations should be noted. First, no simplifications or assumptions have been made concerning the eigenmode calculations. Either a spatial or temporal analysis may be made. Second, two- or three-dimensional primary waves may be used. Finally, a not so positive attribute is found with the order of the eigenvalue present. For the subharmonic mode represented by two Fourier modes, the temporal eigenvalue (σ), appears to the seventh order. For the fundamental mode with three Fourier modes, the temporal eigenvalue (σ) appears to the tenth order. So as more Fourier modes are included, the order of the eigenvalue subsequently increases considerably and, in fact, leads to an overbearing problem computationally. So we find that in parallel with the primary problem, the highest order of the eigenvalue appears in the boundary conditions. With these considerations

noted, we focus our attention on obtaining solutions to the above coupled system of fluid and wall equations.

In the next chapter, spectral and shooting approaches are introduced to solve for the three-dimensional primary and secondary instabilities over compliant walls.

CHAPTER 4

NUMERICAL METHODS OF SOLUTION

4.1 Introduction

In this chapter, two numerical approaches are introduced to solve the above formed system of equations and boundary conditions representing transition over a compliant wall. The first is a spectral approximation. Both global and local schemes are outlined. The second approach is a shooting method. The spectral method enables the capture of the discrete spectrum of the eigenvalues. For a given eigenvalue, the local method enables an efficient tracking of the mode downstream or over the frequency range of interest. In the next two sections local and global approaches are outlined for the primary instability problem. In the final sections, local and global approaches are discussed for the secondary instability problem.

4.2 Spectral Method for Primary Instabilities

A spectral method may be defined as a series solution approximation whose basis is made up of an orthogonal set of polynomials. In particular, we make use of Chebyshev polynomials which are defined and discussed in Appendix C. Gottlieb and Orszag (1977) have shown that the use of Chebyshev polynomials in a series leads to good resolution near the boundaries. This is of great importance in our investigation due to the fluid/wall motion which occurs. Additionally, the rate of convergence for the series is exponential with the number of polynomials as compared to trigonometric series which are algebraic.

The technique used to formulate the numerical approximation for two-dimensional, laminar boundary-layer flow over a flat plate was previously studied

by Bridges and Morris (1984a) and Bridges (1984). This amounted to an eigenvalue problem which is nonlinear in the eigenvalue to fourth-order. The approach which will be discussed has also been used to study the two-dimensional compliant wall problem by Carpenter and Morris (1985), Morris (1987), Joslin and Morris (1987, 1989), and Joslin (1987). In the present discussion, the method is extended to allow for three-dimensional instabilities. With this, the eigenvalue spectrum is looked closely at. From this approach all unstable modes become evident. Through a tracking procedure spurious modes may be identified and neglected while the modes of physical significance can be accurately obtained.

The domain of the physical problem extends from zero at the wall to infinity in the normal, or cross-stream, direction. To solve the problem numerically using the spectral method approximation, a transformation is employed to obtain a finite domain. One reason for doing this is made evident by Boyd (1982), where he found that in the infinite domain the optimum number of series polynomials is directly dependent on the finite distance from the wall chosen for the far field boundary conditions. So a transformation is chosen to enable a reasonable computation domain. Grosch and Orszag (1977) have performed a study of this subject and suggest an algebraic transformation. We use

$$z = \frac{y - L}{y + L} \quad \text{or} \quad y = L \frac{1 + z}{1 - z} \quad 4.2.1$$

where $z \in [-1, 1]$ and $y \in [0, \infty)$. A value of $L = 2$ was suggested by Bridges and Morris (1984a) and is used in this study. The resulting metric takes the form of

$$m(z) = \frac{dz}{dy} = \frac{(1 - z)^2}{2L} \quad 4.2.2$$

A problem arises for the far field boundary condition. In the transformed domain we have

$$m(z) \hat{v}'_1(z) = \frac{(1 - z)^2}{2L} \cdot \frac{d\hat{v}_1}{dz} \rightarrow 0 \quad \text{as} \quad z \rightarrow 1 \quad 4.2.3$$

This introduces an ambiguity for $\hat{v}'(1)$ since the metric approaches zero as $z \rightarrow 1$. In order to temporarily avoid such a problem, an additional dependent variable (ξ) is introduced and defined such that

$$\hat{\xi}_1 - m\hat{v}'_1 = 0 \quad 4.2.4$$

This leads to the following transformed system consisting of the Orr-Sommerfeld (2.2.14) and Squire's (2.2.15) equations.

$$m(m(m\hat{\xi}'_1)')' + ma_1\hat{\xi}'_1 + a_2\hat{v}_1 = 0 \quad 4.2.5$$

$$m(m\hat{\Omega}'_1)' + a_3\hat{\Omega}_1 + a_4\hat{v}_1 = 0 \quad 4.2.6$$

where

$$a_1(z) = -2\alpha^2 - iR_\delta\alpha(\cos\phi U_o(z) - c_r)$$

$$a_2(z) = \alpha^4 + i\alpha^3 R_\delta(\cos\phi U_o(z) - c_r) + iR_\delta\alpha\cos\phi m(z)[m(z)U'_o(z)]'$$

$$a_3(z) = -\alpha^2 - iR_\delta\alpha(\cos\phi U_o(z) - c_r)$$

$$a_4(z) = -iR_\delta\alpha\sin\phi m(z)U'_o(z)$$

with far field boundary conditions

$$\hat{v}(1) = \hat{\xi}(1) = \hat{\Omega}(1) = 0 \quad 4.2.7$$

and compliant wall conditions

$$\begin{aligned} & \alpha^5 \left[(C_{Bz} \cos^4 \phi + 2C_{Bzz} \cos^2 \phi \sin^2 \phi + C_{Bz} \sin^4 \phi) \cos^2 \theta \hat{v}'_1(-1) \right] \\ & + \alpha^3 \left[C_{Tz} \sin^2 \theta \cos^2 \phi + \alpha(C_K - \omega^2 C_M) \right] [\cos^2 \hat{\xi}_1(-1) - \sin \phi \cos \phi \hat{\Omega}_1(-1)] \\ & + \frac{\alpha^2 \cos \theta \cos \phi}{R_\delta} \left[(2\omega \sin \theta - 3im(-1)U'_o(-1) \cos \theta) + \omega^2 \sin \theta \sin^2 \phi \right] \hat{\xi}_1(-1) \\ & - \left[m(-1)U'_o(-1) \cos \theta \sin^2 \phi + i\omega \sin \theta \right] \cos \theta \cos \phi \hat{\xi}_1(-1) \end{aligned}$$

$$\begin{aligned}
& + \alpha \left[m(-1)U'_o(-1) \cos \theta + i\omega \sin \theta \right] \frac{\sin \theta \cos^2 \phi}{R_\delta} m(-1) \hat{\xi}'(-1) \\
& + \frac{i \cos \theta \cos \phi}{R_\delta} \left[m(-1)U'_o(-1) \cos \theta + i\omega \sin \theta \right] m(-1) (m(-1) \hat{\xi}'_1(-1))' \\
& + \left[\omega \sin \theta \frac{\alpha^2}{R_\delta} - m(-1)U'_o(-1) \cos \theta \right] \omega \cos \theta \cos^2 \phi \sin \phi \hat{\Omega}_1(-1) \\
& - \sin \theta \sin \phi \cos \phi \frac{\alpha}{R_\delta} \left[m(-1)U'_o(-1) \cos \theta + i\omega \sin \theta \right] m(-1) \hat{\Omega}'_1(-1) = 0 \quad 4.2.8
\end{aligned}$$

and

$$\begin{aligned}
& \alpha \cos \phi (m(-1)U'_o(-1) \cos \theta + i\omega \sin \theta) \hat{v}(-1) \\
& + i\omega [\sin \phi \hat{\Omega}_1(-1) - \cos \phi \hat{\xi}_1(-1)] \cos \theta = 0 \quad 4.2.9
\end{aligned}$$

and

$$\begin{aligned}
& \left[-C_M \omega^2 + C_{Ks} + C_{Tz} \alpha^2 \sin^2 \phi \right] (\cos \phi \hat{\Omega}_1(-1) + \sin \phi \hat{\xi}_1(-1)) \\
& + \frac{i\omega}{R_\delta} \left[\sin \phi m(-1) \hat{\xi}'_1(-1) + \alpha^2 \sin \phi \hat{v}_1(-1) \right. \\
& \left. + \cos \phi m(-1) \hat{\Omega}'_1(-1) \right] = 0 \quad 4.2.10
\end{aligned}$$

where the nondimensional coefficients were previously defined as

$$\begin{aligned}
C_{Bz} &= \frac{Bz}{\rho_\infty U_\infty \delta^3} & C_{Bzz} &= \frac{Bzz}{\rho_\infty U_\infty \delta^3} & C_{Bz} &= \frac{Bz}{\rho_\infty U_\infty \delta^3} \\
C_M &= \frac{\rho_m b}{\rho_\infty \delta^3} & C_K &= \frac{K_F \delta^3}{\rho_\infty U_\infty^2} & C_{Tz} &= \frac{E_t b}{\rho_\infty U_\infty^2 \delta^3} \\
C_{Ks} &= \frac{K_F \delta^3}{\rho_\infty U_\infty^2} & C_{Tz} &= \frac{E_t b}{\rho_\infty U_\infty^2 \delta^3}
\end{aligned}$$

The primes in equations (4.2.4-10) denote derivatives with respect to the transformed independent variable, z , and $U_o(z)$ is the Blasius velocity profile in the transformed domain.

A spectral approach known as a finite Chebyshev series approximation is sought as a means of solution. Properties of Chebyshev polynomials are given

by Gottlieb and Orszag (1977); Fox and Parker (1968); Canuto, Hussaini, Quarteroni, and Zang (1988); Gottlieb, Hussaini, and Orszag (1984). Necessary transformations and integrations for this investigation are given by Joslin (1987) and in Appendix C.

A Chebyshev series expansion for the disturbance in equations (4.2.4-6) is given by

$$\{\hat{v}_1, \hat{\xi}_1, \hat{\Omega}_1\} = \sum_{n=0}^N {}' \{v_n, \xi_n, \Omega_n\} T_n(z) \quad 4.2.11$$

where v_n, ξ_n, Ω_n are coefficients of the series; $T_n(z)$ are Chebyshev polynomials of order n ; and the prime on the summation signifies that the leading term of the series is to be halved. The Blasius profile is expanded in a similar manner

$$U_o = \sum_{n=0}^{\infty} {}' u_n T_n(z) \quad 4.2.12$$

Details of how a known function may be represented by a Chebyshev series is given in Appendix C.

Three basic approaches arise as a means of solution for spectral methods. These are collocation, Galerkin, and tau. Collocation (or pseudo-collocation) methods involve solving the equations at discrete points determined by the cosine trigonometric function. In other words, a function is represented by only one term of the series at the collocation point. This leads to a simplified manner of computing a numerical solution. Instead of a dense matrix, diagonally dominant systems are found. This is inviting except that a problem may arise with enforcing the boundary conditions. Difficulties are encountered with using a collocation approach for the Orr-Sommerfeld equation with rigid wall boundary conditions. This was discussed by Canuto et al. (1988). To avoid any complications with the more complex compliant wall, we will use the tau method which was previously

used by Morris (1987) and Tsoi (1987). Details about the tau method will be given shortly; first the equations will be placed in a more useful form.

Due to the properties of the Chebyshev polynomial and the tau method, it is convenient to pose the governing equations (4.2.4-6) in integral form. The following equations result.

$$\int \hat{\xi} - m\hat{v} + \int m'\hat{v} = \bar{C}_1 \quad 4.2.13$$

$$\begin{aligned} P_0\hat{\xi} + \int P_1\hat{\xi} + \int \int P_2\hat{\xi} + \int \int \int P_3\hat{\xi} + \int \int ma_1\hat{\xi} - \int \int \int (ma_1)'\hat{\xi} \\ + \int \int \int a_2\hat{v} = \bar{C}_2 + \bar{C}_3z + \bar{C}_4z^2 \end{aligned} \quad 4.2.14$$

$$P_4\hat{\Omega} + \int P_5\hat{\Omega} + \int \int P_6\hat{\Omega} + \int \int a_3\hat{\Omega} + \int \int a_4\hat{v} = \bar{C}_5 + \bar{C}_6z \quad 4.2.15$$

and

$$\begin{aligned} P_0 &= m^3 & P_4 &= m^2 \\ P_1 &= -6m^2m' & P_5 &= -3mm' \\ P_2 &= 7m(m')^2 + 4m^2m'' & P_6 &= (m')^2 + mm'' \\ P_3 &= -(m(mm')')' \end{aligned}$$

The tau method was introduced by Lanczos (1938). A detailed sample problem explaining the tau method is given by Bridges and Morris (1984a). Equation (4.2.4) which has one constant of integration is used for our explanation. By equating coefficients of the Chebyshev polynomials of equal order, a system of linear equations result. The tau method involves the addition of one term of the

form $\tau T_{N+1}(z)$ to the right hand side of (4.2.4) to close the system of equations. The equation involving the polynomial $T_o(z)$ serves to determine the constant of integration only and need not be explicitly calculated for the problem at hand. The added "tau" term need not be explicitly calculated either. The resulting system then consists of N equations and one boundary constraint. When combined an $N + 1$ system of equations results with $N + 1$ unknowns.

The tau method and the Chebyshev product and integral formulas are used. The metric (4.2.2) represented by a Chebyshev series is

$$m(z) = \frac{3}{2L} T_o(z) - \frac{1}{L} T_1(z) + \frac{1}{4L} T_2(z) \quad 4.2.16$$

The Chebyshev series are substituted into (4.2.13-15). This results in a system of equations with vectors of unknown Chebyshev coefficients and unknown eigenvalues. Using the far field condition, $\hat{\xi}(1) = 0$, with equation (4.2.13) the follow results

$$\{\xi\} = [T]\{v\} \quad 4.2.17$$

where $\{\xi\}$ and $\{v\}$ are column vectors containing the unknown Chebyshev coefficients and $[T]$ is a real square $N + 1$ matrix. Three of the remaining boundary conditions along with equation (4.2.14) give

$$\left[\sum_{k=0}^4 E_k \alpha^{4-k} \right] \{v\} + \left[\sum_{\substack{k=0 \\ k \neq 1}}^5 F_k \alpha^{5-k} \right] \{\xi\} + \left[\sum_{k=0}^2 G_k \alpha^{2-k} \right] \{\Omega\} = \{0\} \quad 4.2.18$$

where $[E_k]$, $[F_k]$ and $[G_k]$ are complex square matrices of order $N + 1$ which are functions of ω, R, ϕ and the compliant wall properties. $[G_k]$ are singular and contain a compliant boundary condition only. The vorticity boundary conditions with equation (4.2.15) give

$$\left[\sum_{k=0}^2 H_k \alpha^{2-k} \right] \{\Omega\} + \left[\sum_{k=0}^1 I_k \alpha^{1-k} \right] \{v\} + \left[\sum_{\substack{k=0 \\ k \neq 1}}^2 J_k \alpha^{2-k} \right] \{\xi\} = \{0\} \quad 4.2.19$$

where $[H_k]$, $[I_k]$ and $[J_k]$ are complex square matrices of order $N + 1$ which are functions of ω, R, ϕ and the compliant wall properties. $[J_k]$ are singular and contain a compliant boundary condition only. $\{\xi\}$ can now be removed from the system by the use of (4.2.17). Combining (4.2.18,19) the following system results.

$$\begin{pmatrix} \sum_{k=0}^5 E_k \alpha^{5-k} & \sum_{k=0}^2 G_k \alpha^{2-k} \\ \sum_{k=0}^2 I_k \alpha^{2-k} & \sum_{k=0}^2 H_k \alpha^{2-k} \end{pmatrix} \begin{Bmatrix} v_n \\ \Omega_n \end{Bmatrix} = \{0\} \quad 4.2.20$$

In this form, the two- and three-dimensional problems are compared. For a two-dimensional problem, the above matrix is reduced to solving the first element of the matrix involving only the Chebyshev coefficients, v_n . This would be a $N + 1$ by $N + 1$ matrix eigenvalue problem. With the introduction of a third dimension, the problem order increases by a factor of two as shown in equation (4.2.20). This leads to a significant increase in the required computational storage and time as will be discussed in the next chapter.

Continuing with the three-dimensional problem, we find that the system (4.2.20) can be replaced by a simpler form as

$$D_5(\alpha) \begin{Bmatrix} v_n \\ \Omega_n \end{Bmatrix} = \{0\} \quad 4.2.21$$

where

$$D_5(\alpha) = C_0 \alpha^5 + C_1 \alpha^4 + C_2 \alpha^3 + C_3 \alpha^2 + C_4 \alpha + C_5$$

The complex square matrices are now of order $2(N + 1)$. This forms the Chebyshev series discretization of the Orr-Sommerfeld and Squire's equations with compliant boundary conditions.

4.2.1 Linear Companion Matrix Method

The eigenvalue problem derived above is nonlinear in the eigenvalue to the degree of five. In this section, a global method will be discussed to solve such a problem. With this method the spectrum of eigenvalues may be determined. The importance of this will be outlined in the results section.

The global method is referred to as the Linear Companion Matrix method. It was given by Gohberg, Lancaster, and Rodman (1982). The Orr-Sommerfeld problem over a rigid wall has been solved by Benney and Orszag (1977) and Bridges and Morris (1984a). Additionally, Joslin and Morris (1987, 1989) have used this approach for the two-dimensional compliant wall problem. The description is detailed in either of the above references but will be given here for completeness.

The linear companion matrix is a linearization of the given nonlinear eigenvalue problem. If the coefficient matrices are of order m then the linearized companion matrix is of order m times the order of the eigenvalue problem at hand. For our problem, the order of the companion matrix would be $5m$, or $10(N + 1)$. For a generalized eigenvalue problem the form is given as

$$Aa_* = \alpha Ba_* \quad 4.2.22$$

where α is the eigenvalue and a_* represents the corresponding right eigenvector. The eigenvalues are found from the following condition

$$\text{Det}|A - \alpha B| = 0 \quad 4.2.23$$

For the present problem, the coefficients matrices are arranged as

$$\left\{ \begin{bmatrix} -C_1 & -C_2 & -C_3 & -C_4 & -C_5 \\ I & 0 & 0 & 0 & 0 \\ 0 & I & 0 & 0 & 0 \\ 0 & 0 & I & 0 & 0 \\ 0 & 0 & 0 & I & 0 \end{bmatrix} - \alpha \begin{bmatrix} C_o & 0 & 0 & 0 & 0 \\ 0 & I & 0 & 0 & 0 \\ 0 & 0 & I & 0 & 0 \\ 0 & 0 & 0 & I & 0 \\ 0 & 0 & 0 & 0 & I \end{bmatrix} \right\} \begin{bmatrix} \alpha^4 a_* \\ \alpha^3 a_* \\ \alpha^2 a_* \\ \alpha a_* \\ a_* \end{bmatrix} = \{0\} \quad 4.2.24$$

If B in equation (4.2.23) is invertible then a more efficient and equivalent form is given by

$$\text{Det}|B^{-1}A - \alpha I| = 0 \quad 4.2.25$$

The leading coefficient matrix, $[C_o]$, is singular since the only elements are due to the compliant boundary condition where $[C_o]$ is

$$C_o = \begin{pmatrix} 0 & 0 & \dots & 0 & \dots & 0 \\ 0 & 0 & \dots & 0 & \dots & 0 \\ \vdots & \vdots & \ddots & \vdots & \dots & \vdots \\ a_{N-1,0} & a_{N-1,1} & \dots & a_{N-1,N} & \dots & 0 \\ \vdots & \vdots & \vdots & \vdots & \ddots & \vdots \\ 0 & 0 & \dots & 0 & \dots & 0 \end{pmatrix} \quad 4.2.26$$

To remove the singularity, an algebraic transformation is introduced.

$$\lambda = \frac{1}{\alpha - s} \quad 4.2.27$$

where s is a real constant taken in this analysis to be $(\omega/0.35)$. This transformation performs a shift in the eigenvalue spectrum. With this the coefficient matrix, $[C_o]$, becomes dense and invertible. Equation (4.2.24) is rearranged enabling the following

$$B^{-1}A = \begin{pmatrix} -C_o^{-1}C_1 & -C_o^{-1}C_2 & -C_o^{-1}C_3 & -C_o^{-1}C_4 & -C_o^{-1}C_5 \\ I & 0 & 0 & 0 & 0 \\ 0 & I & 0 & 0 & 0 \\ 0 & 0 & I & 0 & 0 \\ 0 & 0 & 0 & I & 0 \end{pmatrix} \quad 4.2.28$$

The eigenvalues of (4.2.28) may be obtained in an efficient manner by the use of the QR algorithm. This method provides a means to determine the spectrum of eigenvalues without requiring an initial guess. As we will discuss later, this approach identifies any other unstable modes which may be present. The next method is also a global method. The formulation is given in the following.

4.2.2 Bernoulli Iteration Method

The second method to determine the discrete spectrum is derived by a matrix equivalent to synthetic division to compute the dominant solvent. The following results for the Lambda matrix

$$D_5(\lambda) = Q_4(\lambda)(\lambda I - Y) + R_r \quad 4.2.29$$

where

$$\begin{aligned} Q_4(\lambda) = & C_0\lambda^4 + (C_0Y + C_1)\lambda^3 + (C_0Y^2 + C_1Y + C_2)\lambda^2 \\ & + (C_0Y^3 + C_1Y^2 + C_2Y + C_3)\lambda \\ & + (C_0Y^4 + C_1Y^3 + C_2Y^2 + C_3Y + C_4) \end{aligned}$$

and

$$R_r = C_0Y^5 + C_1Y^4 + C_2Y^3 + C_3Y^2 + C_4Y + C_5$$

$[Q_4]$ is the right quotient and $[R_r]$ is the right remainder of the division of $D_5(\lambda)$ by $(\lambda I - Y)$. For $(\lambda I - Y)$ to be a factor of $D_5(\lambda)$, $[R_r]$ must be zero. To satisfy this the following requirement holds.

$$C_0Y^5 + C_1Y^4 + C_2Y^3 + C_3Y^2 + C_4Y + C_5 = 0 \quad 4.2.30$$

The unknown square matrix, $[Y]$, is referred to as the right solvent. To compute the dominant solvent the Bernoulli iteration method is used. The iteration formula is given as

$$Y_{i+1} = -C_0^{-1}(C_1 + (C_2 + (C_3 + (C_4 + C_5Y_{i-3}^{-1})Y_{i-2}^{-1})Y_{i-1}^{-1})Y_i^{-1}) \quad 4.2.31$$

where

$$Y_0 = Y_1 = Y_2 = Y_3 = 0 \quad \text{and} \quad Y_4 = -C_o^{-1} C_1$$

Unlike the companion matrix method, this approach is iterative and convergence is usually attained in from three to ten iterations. The eigenvalues of the right solvent are determined by the QR algorithm.

4.2.3 Traub Iteration Method

The final global method considered was developed by Dennis, Traub, and Weber (1978) to compute the dominant solvent. The algorithm is a generalization of the algorithm for scalar polynomials by Traub (1966). The method consists of two iteration steps. The first consists of constructing the equivalent G -polynomial. First, consider the matrix polynomial.

$$M(Y) = Y^m + A_1 Y^{m-1} + \cdots + A_m \quad 4.2.32$$

where $[A_i]$ are the known complex square coefficient matrices. The dominant solvent (right solvent in this formulation) $[S]$ gives $M(S) = 0$. The first step to compute this is defined as

$$G_o(Y) = I \quad 4.2.33a$$

$$G_{n+1}(Y) = G_n(Y)Y - \Gamma_1^{(n)} D_5(\lambda) \quad 4.2.33b$$

where

$$G_n(Y) = \Gamma_1^{(n)} Y^4 + \Gamma_2^{(n)} Y^3 + \Gamma_3^{(n)} Y^2 + \Gamma_4^{(n)} Y + \Gamma_5^{(n)}$$

and $[\Gamma_1^{(n)}]$ in (4.2.33) is the leading coefficient matrix of $[G_n(Y)]$.

This method may be somewhat difficult to understand. The mathematical discussion is given by Dennis et al. Here an example of the formulation is given.

Consider the polynomial

$$M(Y) = Y^3 + A_1 Y^2 + A_2 Y + A_3 \quad 4.2.34$$

For $n = 0$:

$$G_o = \Gamma_1^o Y^2 + \Gamma_2^o Y + \Gamma_3^o = Y^2 \quad 4.2.35a$$

$$\Gamma_1^o = I \quad \Gamma_2^o = \Gamma_3^o = 0 \quad 4.2.35b$$

Making use of (4.2.33), we find for $n = 1$:

$$\begin{aligned} G_1 &= G_o(Y)Y - \Gamma_1^o M(Y) \\ &= \Gamma_1^o Y^3 + \Gamma_2^o Y^2 + \Gamma_3^o Y \\ &\quad + \Gamma_1^o [Y^3 + A_1 Y^2 + A_2 Y + A_3] \\ &= [\Gamma_2^o - \Gamma_1^o A_1] Y^2 + [\Gamma_3^o - \Gamma_1^o A_2] Y - \Gamma_1^o A_3 \end{aligned} \quad 4.2.36$$

For the next iteration of the G -polynomial build-up, the new coefficients are given by

$$\Gamma_1^1 = \Gamma_2^o - \Gamma_1^o A_1 \quad 4.2.37a$$

$$\Gamma_2^1 = \Gamma_3^o - \Gamma_1^o A_2 \quad 4.2.37b$$

$$\Gamma_3^1 = -\Gamma_1^o A_3 \quad 4.2.37c$$

After each iteration the coefficients $[\Gamma]$ are normalized with respect to the lead coefficient, $[\Gamma_1]$. After the G -polynomial build-up, the second stage requires the final L -iteration coefficients $[\Gamma^{(L)}]$ and the previous coefficients $[\Gamma^{(L-1)}]$. These are then used to iterate for the dominant solvent.

The second stage is given by

$$Y_o = (\Gamma_1^{(L)}) (\Gamma_1^{(L-1)})^{-1} \quad 4.2.38a$$

$$Y_{i+1} = G_L(Y_i)G_{L-1}^{-1}(Y_i) \quad 4.2.38b$$

where i is the iteration level and L is the final G -polynomial built-up. The first stage is equivalent to the Bernoulli method. For the second stage, convergence is linear but the error may be made as small as desired by increasing the number of first stage iterations. Usually a sufficient number of iterations for convergence is taken as three to five for the first stage and three for the second stage.

A subset of the discrete eigenvalue spectrum may be obtained by using an efficient eigenvalue solver, such as the QR algorithm. The next and final spectral method is a local method which means a sufficiently accurate initial guess is required and may be obtained from a global method.

4.2.4 Lancaster's Refinement Method

This method is a locally convergent algorithm which requires a sufficiently good initial guess for the refinement of a single eigenvalue. The approach is a modification of Newton's method which has quadratic convergence. The method is attributed to Lancaster (1964). Bridges and Morris (1984a) have used the method for the rigid wall problem and Joslin (1987) for the two-dimensional compliant wall problem. The iterative formula is given by

$$\alpha_{i+1} = \alpha_i - 2f(\alpha_i)/\{f^2(\alpha_i) - f^{(1)}(\alpha_i)\} \quad 4.2.39$$

where

$$f(\alpha_i) = T_r\{D^{-1}(\alpha_i)D^{(1)}(\alpha_i)\}$$

and

$$f^{(1)}(\alpha_i) = T_r\{D^{-1}(\alpha_i)D^{(2)}(\alpha_i) - [D^{-1}(\alpha_i)D^{(1)}(\alpha_i)]^2\}$$

$T_r\{s\}$ denotes the trace of matrix $[s]$; D^{-1} is the inverse of D and $D^{(i)}$ denotes the i th derivative of D with respect to α . After converging upon the eigenvalue of interest, the eigenvector may efficiently be obtained from the following inverse iteration formula.

$$[D_5(\alpha)]\{a_*^{k+1}\} = \sigma \{a_*^k\} \quad 4.2.40$$

where σ is a normalizing factor. The procedure usually converges in two or three iterations using an initial guess of $\{a_*^0\} = [1, 1, 1, \dots, 1]^T$.

The above methods provide a useful means to identify and track instabilities using spectral methods. We have used all of these methods earlier for the two-dimensional primary problem. They are described again since they are employed, not only for the present problem, but for the secondary instability analysis. This is pertinent for the global schemes since the spectrum is yet unknown for the secondary instabilities over wall compliance.

4.3 Shooting Method for Primary Instabilities

The following is a description of a local shooting method. Beginning at the wall boundary conditions we march using a Runge-Kutta integration scheme across the boundary layer. Outside of the boundary layer the numerical solution vectors match with the asymptotic limit. The eigenvalue is altered until the condition is satisfied. Upon convergence the eigenvectors can be obtained with one additional pass across the boundary layer.

The Orr-Sommerfeld equation (2.2.14) and Squire's equation (2.2.15) may be arranged in the following system of first order ordinary differential equations.

$$D \begin{Bmatrix} \hat{v}_1''' \\ \hat{v}_1'' \\ \hat{v}_1' \\ \hat{v}_1 \\ \hat{\Omega}_1' \\ \hat{\Omega}_1 \end{Bmatrix} = \begin{pmatrix} 0 & -d_1 & 0 & -d_2 & 0 & 0 \\ 1 & 0 & 0 & 0 & 0 & 0 \\ 0 & 1 & 0 & 0 & 0 & 0 \\ 0 & 0 & 1 & 0 & 0 & 0 \\ 0 & 0 & 0 & -d_4 & 0 & -d_3 \\ 0 & 0 & 0 & 0 & 0 & 1 \end{pmatrix} \begin{Bmatrix} \hat{v}_1''' \\ \hat{v}_1'' \\ \hat{v}_1' \\ \hat{v}_1 \\ \hat{\Omega}_1' \\ \hat{\Omega}_1 \end{Bmatrix} \quad 4.3.1$$

This is the form for the Runge-Kutta integration routine which is listed in Appendix D. In general, the form of the compliant wall boundary conditions given by (3.2.21, 22, 26) is

$$a_1 \hat{v}_1'(0) + a_2 \hat{v}_1''(0) + a_3 \hat{v}_1'''(0) + a_4 \hat{\Omega}_1(0) + a_5 \hat{\Omega}_1'(0) = 0 \quad 4.3.2$$

$$b_1 \hat{v}_1(0) + b_2 \hat{v}_1'(0) + b_3 \hat{v}_1''(0) + b_4 \hat{\Omega}_1(0) + b_5 \hat{\Omega}_1'(0) = 0 \quad 4.3.3$$

$$c_1 \hat{v}_1(0) + c_2 \hat{v}_1'(0) + c_3 \hat{\Omega}_1(0) = 0 \quad 4.3.4$$

The general form of solution for the sixth-order system may be written

$$\begin{Bmatrix} \hat{v}_1''' \\ \hat{v}_1'' \\ \hat{v}_1' \\ \hat{v}_1 \\ \hat{\Omega}_1' \\ \hat{\Omega}_1 \end{Bmatrix} = A_1 \begin{Bmatrix} 1 \\ 0 \\ 0 \\ 0 \\ 0 \\ 0 \end{Bmatrix} + A_2 \begin{Bmatrix} 0 \\ 1 \\ 0 \\ 0 \\ 0 \\ 0 \end{Bmatrix} + \dots + A_6 \begin{Bmatrix} 0 \\ 0 \\ 0 \\ 0 \\ 0 \\ 1 \end{Bmatrix} \quad 4.3.5$$

Using the rigid wall boundary conditions three of the unknown coefficients may be eliminated giving three linearly independent solutions at the wall of the form

$$\begin{Bmatrix} \hat{v}_1''' \\ \hat{v}_1'' \\ \hat{v}_1' \\ \hat{v}_1 \\ \hat{\Omega}_1' \\ \hat{\Omega}_1 \end{Bmatrix} = A \begin{Bmatrix} 0 \\ 1 \\ 0 \\ 0 \\ 0 \\ 0 \end{Bmatrix} + B \begin{Bmatrix} 1 \\ 0 \\ 0 \\ 0 \\ 0 \\ 0 \end{Bmatrix} + C \begin{Bmatrix} 0 \\ 0 \\ 0 \\ 0 \\ 0 \\ 1 \end{Bmatrix} \quad 4.3.6$$

where \hat{v}'' , \hat{v}''' and $\hat{\Omega}'$ are not initially known. In this formulation, the boundary conditions are satisfied and the higher order derivatives are left arbitrary. Alternatively, we can introduce a wall motion caused by the disturbance, the boundary

conditions (4.3.2-4) are used to eliminate three unknown coefficients in (4.3.5).

The boundary conditions then take the form of

$$\begin{Bmatrix} \hat{v}_1''' \\ \hat{v}_1'' \\ \hat{v}_1' \\ \hat{v}_1 \\ \hat{\Omega}_1' \\ \hat{\Omega}_1 \end{Bmatrix} = A \begin{Bmatrix} 0 \\ 1 \\ v_1' \\ v_1 \\ 0 \\ \Omega_1 \end{Bmatrix} + B \begin{Bmatrix} 1 \\ 0 \\ v_2' \\ v_2 \\ 0 \\ \Omega_2 \end{Bmatrix} + C \begin{Bmatrix} 0 \\ 0 \\ v_3' \\ v_3 \\ 1 \\ \Omega_3 \end{Bmatrix} \quad 4.3.7$$

where

$$v_1' = [\frac{b_3 c_1 a_4}{b_4 c_1 - b_1 c_3} - a_2] / [a_1 + \frac{a_4 (b_1 c_2 - c_1 b_2)}{b_4 c_1 - b_1 c_3}]$$

$$\Omega_1 = \frac{b_1 c_2 - c_1 b_2}{b_4 c_1 - b_1 c_3} v_1' - \frac{b_3 c_1}{b_4 c_1 - b_1 c_3} \quad v_1 = -\frac{1}{c_1} [c_2 v_1' + c_3 \Omega_1]$$

$$v_2' = -a_3 / [a_1 + \frac{a_4 (b_1 c_2 - c_1 b_2)}{b_4 c_1 - b_1 c_3}]$$

$$\Omega_2 = \frac{b_1 c_2 - c_1 b_2}{b_4 c_1 - b_1 c_3} v_2' \quad v_2 = -\frac{1}{c_1} [c_2 v_2' + c_3 \Omega_2]$$

$$v_3' = [\frac{b_5 c_1 a_4}{b_4 c_1 - b_1 c_3} - a_5] / [a_1 + \frac{a_4 (b_1 c_2 - c_1 b_2)}{b_4 c_1 - b_1 c_3}]$$

$$\Omega_3 = \frac{b_1 c_2 - c_1 b_2}{b_4 c_1 - b_1 c_3} v_3' - \frac{b_5 c_1}{b_4 c_1 - b_1 c_3} \quad v_3 = -\frac{1}{c_1} [c_2 v_3' + c_3 \Omega_3]$$

Beginning with these vectors at the wall we integrate across the boundary layer. The numerical vectors retain linear independence by using the Gram-Schmidt orthonormalization. The orthonormalization is implemented whenever a vector's magnitude exceeds 10^3 . A final orthonormalization is applied at the outer edge of the boundary layer.

Outside the boundary layer the asymptotic solutions satisfying the boundary conditions at infinity (2.2.16) may be written

$$v_1 = B_1 e^{-\alpha y} + B_2 e^{-\bar{\alpha} y} \quad 4.3.8$$

and

$$\Omega_1 = B_3 e^{-\bar{\alpha}y} \quad 4.3.9$$

where

$$\bar{\alpha} = \sqrt{\alpha^2 + iR_\delta \alpha (U_\infty \cos \phi - c_r)} \quad \text{and} \quad R\{\bar{\alpha}\} > 0$$

The numerical solutions are matched with the three linearly independent solution vectors formed from (4.3.8-9) at the edge of the boundary layer. This gives the following 6×6 homogeneous system of equations for the unknown coefficients, A, B, C, B_1, B_2, B_3 .

$$A \begin{Bmatrix} v_1''' \\ v_1'' \\ v_1' \\ v_1 \\ \Omega_1' \\ \Omega_1 \end{Bmatrix} + B \begin{Bmatrix} v_2''' \\ v_2'' \\ v_2' \\ v_2 \\ \Omega_2' \\ \Omega_2 \end{Bmatrix} + C \begin{Bmatrix} v_3''' \\ v_3'' \\ v_3' \\ v_3 \\ \Omega_3' \\ \Omega_3 \end{Bmatrix} = B_1 \begin{Bmatrix} -\alpha^3 \\ \alpha^2 \\ -\alpha \\ 1 \\ 0 \\ 0 \end{Bmatrix} + B_2 \begin{Bmatrix} -\bar{\alpha}^3 \\ \bar{\alpha}^2 \\ -\bar{\alpha} \\ 1 \\ 0 \\ 0 \end{Bmatrix} + B_3 \begin{Bmatrix} 0 \\ 0 \\ 0 \\ 0 \\ 1 \\ -\bar{\alpha} \end{Bmatrix} \quad 4.3.10$$

For a nontrivial solution the determinant of the system must be zero. At a fixed Reynolds number and frequency, the wavenumber is altered until this condition is met.

In this approach the viscous solution vectors contaminate the inviscid vector. This effectively makes the solution non-orthogonal. Thus, in order to maintain linearly independent (orthogonal) vectors, a method referred to as the Gram-Schmidt orthonormalization given by Courant and Hilbert (1953) is used. The formula removes the contamination and leaves the vectors normalized. The procedure is listed as follows.

(1.1) Normalize vector f_1 : $g_1 = f_1 / \|f_1\|$

(1.2) Normalize previous points: $f_1(0 - y)$ by $\|f_1\|$

(2.1) Remove contamination: $g_2 = f_2 - (g_1 \cdot f_2)g_1$

(2.2) Remove contamination from previous points:

$$g_2(0 - y) = f_2(0 - y) - (g_1(0 - y) \cdot f_2(0 - y))g_1(0 - y)$$

(3.1) Normalize vector: $g_2 = g_2 / \|g_2\|$

(3.2) Normalize previous points: $g_2(0 - y) = g_2(0 - y) / \|g_2\|$

(4.1) Save values and continue: $f_1 = g_1 \quad f_2 = g_2$

g_1 and g_2 are the vectors resulting from the orthonormalization and f_1 and f_2 are the initial numerical vectors. This can be performed on any number of vectors which, is of course, problem dependent. The general formula for this is given as

$$g_1 = f_1 / \|f_1\|$$

$$g_n = \left[f_n - \sum_{j=1}^{n-1} (f_n \cdot g_j)g_j \right] / \|f_n - \sum_{j=1}^{n-1} (f_n \cdot g_j)g_j\| \quad 4.3.11$$

The $\| \cdot \|$ is the magnitude of the vector. In the above formulation, $(f \cdot g)$ is the scalar product. For orthogonal vectors this would be zero. But since the viscosity contaminates the inviscid solution, the formula removes this amount of error made evident through the dot product. The above procedure is not performed at every step in marching across the boundary layer. This in itself may lead to an "over-kill" of the procedure leading to an error which would grow with the number of orthonormalizations. Instead, a criterion is used to determine when to orthonormalize. This criterion was tested by Conti (1966) in which orthonormalization is performed when a vector reaches a designated magnitude. In our problem 10^3 is used. This is sufficient for the degree of stiffness present in the Orr-Sommerfeld/Squire system of equations. This is, however, problem dependent as we will find in the secondary analysis.

In order to obtain the corresponding eigenvectors one final integration across the boundary layer is made. At each step the value of the solution vectors are saved and orthonormalized at the appropriate times. The coefficients of (4.3.10) are then solved for and the eigenvectors (u_1, v_1, w_1) are computed.

As with the spectral method approximation, this method has distinct advantages and disadvantages which will be discussed in the next chapter. We reserve the comparative discussion until results can be presented for all approaches.

4.4 Spectral Method for Secondary Instabilities

The spectral method approach is similar to that for the primary problem, except the equations are more complex and a different metric is used. We will describe the subharmonic problem in the first section and the fundamental in the second section.

4.4.1 Solution for the Subharmonic Disturbanc.

For the secondary system of equations involved, the temporal eigenvalue problem, by observation, is easier to solve than the spatial. In the fluid equations the temporal eigenvalue, σ , appears linearly in two terms of each equation while the spatial eigenvalue, γ , appears nonlinearly throughout. So we choose to solve for the temporal eigenvalue. This may be done with some confidence since Bertolotti (1985) has shown for the rigid wall that at most, only a few percent error occurs as a result of using Gaster's transformation for the temporal-spatial conversion. Yet, even though this becomes easier for the fluid equations, a problem remains with the boundary conditions. If no further simplifications are made

the resulting system for the eigenvalue will be

$$D_7(\sigma) \begin{Bmatrix} \bar{V}_1 \\ \bar{V}_{-1} \\ \bar{\Omega}_1 \\ \bar{\Omega}_{-1} \end{Bmatrix} = \{0\} \quad 4.4.1$$

where

$$D_7(\sigma) = A_0\sigma^7 + A_1\sigma^6 + \cdots + A_7$$

and

$$\bar{\Omega}_n = (\hat{\Omega}'_n, \hat{\Omega}_n) \quad \text{and} \quad \bar{V}_n = (\hat{v}_n'''', \hat{v}_n'', \hat{v}_n', \hat{v}_n)$$

The $[A_i]$ are known coefficient matrices most of which are singular. This would lead to a considerable demand for virtual memory and computer time to solve the equations. The main goal in using this method is to enable an efficient identification of the spectrum. From this a local method can then be used for tracking whichever eigenvalue is of interest. By looking at the boundary conditions we find that if the primary wave were two-dimensional, the order of σ reduces to three. So the computational burden is lifted, somewhat.

A similar reduction in the order of the eigenvalue problem can be obtained while retaining the three-dimensional primary wave form if an assumption is made concerning the spanwise surface motion. The spanwise surface displacement is given by (3.3.11) or

$$\zeta \sim \frac{1}{K_s} \quad 4.4.2$$

As we have already discussed, the Grosskreutz coating may be assumed to have no spanwise surface displacement, or $K_s \rightarrow \infty$. If this assumption is made, (4.4.1) reduces to a third-order eigenvalue problem given by

$$D_3(\sigma) \begin{Bmatrix} \bar{V}_1 \\ \bar{V}_{-1} \\ \bar{\Omega}_1 \\ \bar{\Omega}_{-1} \end{Bmatrix} = \{0\} \quad 4.4.3$$

where

$$D_3(\sigma) = A_0\sigma^3 + A_1\sigma^2 + A_2\sigma + A_3$$

In choosing the second assumption, three-dimensional primary instabilities are permitted.

Since the parameters for the primary problem are known, we will use the computationally more efficient local shooting method to describe the primary eigenvalue, eigenfunctions, and wall displacements.

For the spectral approach we must transform the domain from $y \in [0, y_{max}]$ to the Chebyshev domain $z \in [-1, 1]$. This suggests a transformation

$$z = \frac{2y - y_{max}}{y_{max}} \quad \text{and} \quad y = \frac{y_{max}(z + 1)}{2} \quad 4.4.4$$

The corresponding metric is

$$m(z) = \frac{dz}{dy} = \frac{2}{y_{max}} \quad 4.4.5$$

As opposed to the present route of shooting primary/spectral secondary approach, one might choose spectral primary/spectral secondary which requires a different metric. In that case the metric would involve transforming from a semi-infinite domain to a finite domain. As was shown in Section 4.2, this results in an ambiguity in the far-field boundary condition. To avoid this, a dummy variable was introduced. So in order to generalize this solution and allow for alternative metrics, we introduce the same dummy variable defined as

$$\hat{\xi}_n = m\hat{v}'_n \quad 4.4.6$$

where subscript n is the Fourier mode. The transformed system is then found by substituting (4.4.5) and (4.4.6) into the equations giving

$$\begin{aligned} m(m(m\hat{\xi}'_n)')' + a_{1n}m\hat{\xi}'_n + a_{2n}\hat{v}_n + A \{ & a_{3n}m(m\hat{\xi}'_o)' + a_{4n}m\hat{\xi}'_o + a_{5n}\hat{\xi}_o \\ & + a_{6n}\hat{v}_o + a_{7n}m(m\hat{\Omega}'_o)' + a_{8n}m\hat{\Omega}'_o + a_{9n}\hat{\Omega}_o \} = 0 \end{aligned} \quad 4.4.7$$

and

$$m(m(\hat{\Omega}'_n)' + c_{1n}\hat{\Omega}_n + c_{2n}\hat{v}_n + A \left\{ c_{3n}m\hat{\Omega}'_o + c_{4n}\hat{\Omega}_o + c_{5n}m\hat{\xi}'_o + c_{6n}\hat{\xi}_o + c_{7n}\hat{v}_o \right\}) = 0 \quad 4.4.8$$

We again use the tau method. Further, the equations placed in integral form are given by

$$\int \hat{\xi}_n = m\hat{v}_n - \int m'\hat{v}_n \quad 4.4.9$$

and

$$\begin{aligned} P_o\hat{\xi}_n + \int P_1\hat{\xi}_n + \int \int P_2\hat{\xi}_n + \int \int \int P_3\hat{\xi}_n + \int \int a_{1n}m\hat{\xi}_n \\ - \int \int \int (a_{1n}m)' \hat{\xi}_n + \int \int \int a_{2n}\hat{v}_n + A \left\{ \int a_{3n}m^2\hat{\xi}_o \right. \\ - \int \int (2a'_{3n}m^2 + 3mm'a_{3n})\hat{\xi}_o + \int \int \int (m(ma_{3n})')'\hat{\xi}_o \\ + \int \int a_{4n}m\hat{\xi}_o - \int \int \int (ma_{4n})'\hat{\xi}_o + \int \int \int a_{5n}\hat{\xi}_o \\ + \int \int \int a_{6n}\hat{v}_o + \int a_{7n}m^2\hat{\Omega}_o - \int \int (2a'_{7n}m^2 \\ + 3mm'a_{7n})\hat{\Omega}_o + \int \int \int (m(ma_{7n})')'\hat{\Omega}_o + \int \int a_{8n}m\hat{\Omega}_o \\ \left. - \int \int \int (ma_{8n})'\hat{\Omega}_o + \int \int \int a_{9n}\hat{\Omega}_o \right\} \\ = \bar{C}_1 z^2 + \bar{C}_2 z + \bar{C}_3 \end{aligned} \quad 4.4.10$$

and

$$\begin{aligned} P_4\hat{\Omega}_n + \int P_5\hat{\Omega}_n + \int \int P_6\hat{\Omega}_n + \int \int c_{1n}\hat{\Omega}_n + \int \int c_{2n}\hat{v}_n \\ + A \left\{ \int c_{3n}m\hat{\Omega}_o - \int \int (mc_{3n})'\hat{\Omega}_o + \int \int c_{4n}\hat{\Omega}_o + \int mc_{5n}\hat{\xi}_o \right. \end{aligned}$$

$$\begin{aligned}
& - \int \int (m c_{5n})' \hat{\xi}_o + \int \int c_{6n} \hat{\xi}_o + \int \int c_{7n} \hat{v}_o \Big\} \\
& = \bar{C}_4 z + \bar{C}_5
\end{aligned} \tag{4.4.11}$$

where for the subharmonic, $n = \pm 1$ and the coefficients are non-constant and

$$\begin{aligned}
P_0 &= m^3 & P_4 &= m^2 \\
P_1 &= -6m^2 m' & P_5 &= -3mm' \\
P_2 &= 7m(m')^2 + 4m^2 m'' & P_6 &= (mm')' \\
P_3 &= -(m(m(mm')')')
\end{aligned}$$

The boundary conditions are transformed but not listed. Each Fourier mode is represented by a finite Chebyshev series expansion. This is given as

$$\{\hat{\rho}_n, \hat{v}_n, \hat{\Omega}_n\} = \sum_{m=0}^N ' \{\rho_{m,n}, v_{m,n}, \Omega_{m,n}\} T_m(z) \tag{4.4.12}$$

The prime on the summation signifies that the leading term of the series is to be halved. The Blasius velocity profile is expanded in a similar manner

$$U_o(z) = \sum_{m=0}^{\infty} u_m T_m(z) \tag{4.4.13}$$

The eigenfunctions of the primary wave are expanded in the same manner as the Blasius profile. Details of representing a known function by a Chebyshev series are given in Appendix C.

The series (4.4.12-13) and the series representing the eigenfunctions are substituted into (4.4.9-11) along with the boundary conditions. The dummy variable is then eliminated by back substitution. This results in the following complex matrix eigenvalue problem in terms of the nonlinear eigenvalue, σ .

$$D_3(\sigma) \begin{Bmatrix} v_{m,1} \\ v_{m,-1} \\ \Omega_{m,1} \\ \Omega_{m,-1} \end{Bmatrix} = \{0\} \tag{4.4.14}$$

where

$$D_3(\sigma) = C_0\sigma^3 + C_1\sigma^2 + C_2\sigma + C_3$$

and $[C_i]$ are complex square matrices of order $4(N+1)$. $[C_0]$ and $[C_1]$ are singular and contain only compliant boundary conditions. To remove the singularity which prevents the solution, a transformation is introduced

$$\lambda = \frac{\sigma + t}{\sigma + s} \quad \text{and} \quad \sigma = \frac{t - \lambda s}{\lambda - 1} \quad 4.4.15$$

where s and t are arbitrary constants taken as $s = -.01$ and $t = 1.0$. In this way all of the matrices become non-singular and solutions can be obtained by methods discussed in Section 4.2. This completes the Chebyshev discretization of the subharmonic problem.

4.4.2 Solution for the Fundamental Disturbance

In the same manner as the subharmonic problem, the temporal eigenvalue problem is solved. Again a problem arises with the boundary conditions. If no further simplifications are made, the resulting system for the eigenvalue will be

$$D_{10}(\sigma) \begin{Bmatrix} \frac{\bar{V}_2}{\bar{V}_0} \\ \frac{\bar{V}_{-2}}{\bar{\Omega}_2} \\ \frac{\bar{\Omega}_0}{\bar{\Omega}_{-2}} \end{Bmatrix} = \{0\} \quad 4.4.16$$

where

$$D_{10}(\sigma) = A_0\sigma^{10} + A_1\sigma^9 + \cdots + A_{10}$$

and

$$\bar{\Omega}_n = (\hat{\Omega}'_n, \hat{\Omega}_n) \quad \text{and} \quad \bar{V}_n = (\hat{v}_n'''', \hat{v}_n'', \hat{v}_n', \hat{v}_n)$$

The $[A_i]$ are known coefficient matrices most of which are singular. As we have already discussed, the Grosskreutz coating may be assumed to have no spanwise surface displacement, or $K_s \rightarrow \infty$. If this assumption is made, (4.4.16) reduces to a fourth-order eigenvalue problem given by

$$D_4(\sigma) \begin{Bmatrix} \frac{\bar{V}_2}{\bar{V}_0} \\ \frac{\bar{V}_{-2}}{\bar{\Omega}_2} \\ \frac{\bar{\Omega}_2}{\bar{\Omega}_0} \\ \frac{\bar{\Omega}_0}{\bar{\Omega}_{-2}} \end{Bmatrix} = \{0\} \quad 4.4.17$$

where

$$D_4(\sigma) = A_0\sigma^4 + A_1\sigma^3 + A_2\sigma^2 + A_3\sigma + A_4$$

To generalize this solution and allow for alternative metrics, the dummy variable is introduced giving

$$\hat{\xi}_n = m\hat{v}'_n \quad 4.4.18$$

where subscript n is the Fourier mode. The transformed system is then found by substituting (4.4.5) and (4.4.18) into the equations giving

$$m(m(m\hat{\xi}'_o)')' + b_{1o}m\hat{\xi}'_o + b_{2o}\hat{v}_o + A \left\{ b_{\pm 3}m(m\hat{\xi}'_{\pm 2})' + b_{\pm 4}m\hat{\xi}'_{\pm 2} + b_{\pm 5}\hat{\xi}_{\pm 2} \right. \\ \left. + b_{\pm 6}\hat{v}_{\pm 2} + b_{\pm 7}m(m\hat{\Omega}'_{\pm 2})' + b_{\pm 8}m\hat{\Omega}'_{\pm 2} + b_{\pm 9}\hat{\Omega}_{\pm 2} \right\} = 0 \quad 4.4.19$$

and

$$m(m(\hat{\Omega}'_o)')' + d_{1o}\hat{\Omega}_o + d_{2o}\hat{v}_o + A \left\{ d_{\pm 3}m\hat{\Omega}'_{\pm 2} + d_{\pm 4}\hat{\Omega}_{\pm 2} \right. \\ \left. + d_{\pm 5}m\hat{\xi}'_{\pm 2} + d_{\pm 6}\hat{\xi}_{\pm 2} + d_{\pm 7}\hat{v}_{\pm 2} \right\} = 0 \quad 4.4.20$$

for the $n = 0$ Fourier mode and

$$m(m(m\hat{\xi}'_n)')' + a_{1n}m\hat{\xi}'_n + a_{2n}\hat{v}_n + A \left\{ a_{3n}m(m\hat{\xi}'_o) + a_{4n}m\hat{\xi}'_o + a_{5n}\hat{\xi}_o \right. \\ \left. + a_{6n}\hat{v}_o + a_{7n}m(m\hat{\Omega}'_o) + a_{8n}m\hat{\Omega}'_o + a_{9n}\hat{\Omega}_o \right\} = 0 \quad 4.4.21$$

and

$$m(m(\hat{\Omega}'_n)' + c_{1n}\hat{\Omega}_n + c_{2n}\hat{v}_n + A\left\{c_{3n}m\hat{\Omega}'_o + c_{4n}\hat{\Omega}_o + c_{5n}m\hat{\xi}'_o + c_{6n}\hat{\xi}_o + c_{7n}\hat{v}_o\right\}) = 0 \quad 4.4.22$$

for the $n = \pm 2$ Fourier modes. The \pm implies that the terms $n = +$ are summed with the $n = -$ terms. We again use the tau method. Further the equations placed in integral form are given by

$$\int \hat{\xi}_n = m\hat{v}_n - \int m'\hat{v}_n \quad 4.4.23$$

and

$$\begin{aligned} P_o\hat{\xi}_o + \int P_1\hat{\xi}_o + \int \int P_2\hat{\xi}_o + \int \int \int P_3\hat{\xi}_o + \int \int b_{1o}m\hat{\xi}_o \\ - \int \int \int (b_{1o}m)'\hat{\xi}_o + \int \int \int b_{2o}\hat{v}_o + A\left\{ \int b_{\pm 3}m^2\hat{\xi}_{\pm 2} \right. \\ - \int \int (2m^2b'_{\pm 3} + 3mm'b_{\pm 3})\hat{\xi}_{\pm 2} + \int \int \int (m(mb_{\pm 3})')'\hat{\xi}_{\pm 2} \\ + \int \int b_{\pm 4}m\hat{\xi}_{\pm 2} - \int \int \int (mb_{\pm 4})'\hat{\xi}_{\pm 2} + \int \int \int b_{\pm 5}\hat{\xi}_{\pm 2} \\ + \int \int \int b_{\pm 6}\hat{v}_{\pm 2} + \int b_{\pm 7}m^2\hat{\Omega}_{\pm 2} - \int \int (2m^2b'_{\pm 7} \\ + 3mm'b_{\pm 7})\hat{\Omega}_{\pm 2} + \int \int \int (m(mb_{\pm 7})')'\hat{\Omega}_{\pm 2} + \int \int b_{\pm 8}m\hat{\Omega}_{\pm 2} \\ \left. - \int \int \int (mb_{\pm 8})'\hat{\Omega}_{\pm 2} + \int \int \int b_{\pm 9}\hat{\Omega}_{\pm 2} \right\} \\ = \bar{C}_1z^2 + \bar{C}_2z + \bar{C}_3 \end{aligned} \quad 4.4.24$$

and

$$\begin{aligned} P_4\hat{\Omega}_o + \int P_5\hat{\Omega}_o + \int \int P_6\hat{\Omega}_o + \int \int d_{1o}\hat{\Omega}_o + \int \int d_{2o}\hat{v}_o \\ + A\left\{ \int md_{\pm 3}\hat{\Omega}_{\pm 2} - \int \int (md_{\pm 3})'\hat{\Omega}_{\pm 2} + \int \int d_{\pm 4}\hat{\Omega}_{\pm 2} \right. \end{aligned}$$

$$\begin{aligned}
& + \int m d_{\pm 5} \hat{\xi}_{\pm 2} - \int \int (m d_{\pm 5})' \hat{\xi}_{\pm 2} + \int \int d_{\pm 6} \hat{\xi}_{\pm 2} \\
& + \int \int d_{\pm 7} \hat{v}_{\pm 2} \Big\} = \bar{C}_4 z + \bar{C}_5
\end{aligned} \tag{4.4.25}$$

for the $n = 0$ Fourier mode and

$$\begin{aligned}
& P_0 \hat{\xi}_n + \int P_1 \hat{\xi}_n + \int \int P_2 \hat{\xi}_n + \int \int \int P_3 \hat{\xi}_n + \int \int a_{1n} m \hat{\xi}_n \\
& - \int \int \int (a_{1n} m)' \hat{\xi}_n + \int \int \int a_{2n} \hat{v}_n + A \left\{ \int a_{3n} m^2 \hat{\xi}_o \right. \\
& - \int \int (2a'_{3n} m^2 + 3mm' a_{3n}) \hat{\xi}_o + \int \int \int (m(ma_{3n})')' \hat{\xi}_o \\
& + \int \int a_{4n} m \hat{\xi}_o - \int \int \int (ma_{4n})' \hat{\xi}_o + \int \int \int a_{5n} \hat{\xi}_o \\
& + \int \int \int a_{6n} \hat{v}_o + \int a_{7n} m^2 \hat{\Omega}_o - \int \int (2a'_{7n} m^2 \\
& + 3mm' a_{7n}) \hat{\Omega}_o + \int \int \int (m(ma_{7n})')' \hat{\Omega}_o + \int \int a_{8n} m \hat{\Omega}_o \\
& \left. - \int \int \int (ma_{8n})' \hat{\Omega}_o + \int \int \int a_{9n} \hat{\Omega}_o \right\} \\
& = \bar{C}_1 z^2 + \bar{C}_2 z + \bar{C}_3
\end{aligned} \tag{4.4.26}$$

and

$$\begin{aligned}
& P_4 \hat{\Omega}_n + \int P_5 \hat{\Omega}_n + \int \int P_6 \hat{\Omega}_n + \int \int c_{1n} \hat{\Omega}_n + \int \int c_{2n} \hat{v}_n \\
& + A \left\{ \int c_{3n} m \hat{\Omega}_o - \int \int (mc_{3n})' \hat{\Omega}_o + \int \int c_{4n} \hat{\Omega}_o + \int mc_{5n} \hat{\xi}_o \right. \\
& - \int \int (mc_{5n})' \hat{\xi}_o + \int \int c_{6n} \hat{\xi}_o + \int \int c_{7n} \hat{v}_o \Big\} \\
& = \bar{C}_4 z + \bar{C}_5
\end{aligned} \tag{4.4.27}$$

for the $n = \pm 2$ Fourier modes. As before the coefficients are non-constant and

$$\begin{aligned}
 P_0 &= m^3 & P_4 &= m^2 \\
 P_1 &= -6m^2m' & P_5 &= -3mm' \\
 P_2 &= 7m(m')^2 + 4m^2m'' & P_6 &= (mm')' \\
 P_3 &= -(m(m(mm')')') \\
 \end{aligned}$$

The boundary conditions are transformed but not listed. Each Fourier mode is represented by a finite Chebyshev series expansion (4.4.12). The Blasius velocity profile and primary eigenfunctions are expanded in a similar manner.

The series (4.4.12-13) and the series representing the eigenfunctions are substituted into (4.4.23-27) along with the boundary conditions. The dummy variable is then eliminated by back substitution. This results in the following complex matrix eigenvalue problem in terms of the nonlinear eigenvalue, σ .

$$D_4(\sigma) \begin{Bmatrix} v_{m,2} \\ v_{m,0} \\ v_{m,-2} \\ \Omega_{m,2} \\ \Omega_{m,0} \\ \Omega_{m,-2} \end{Bmatrix} = \{0\} \quad 4.4.28$$

where

$$D_4(\sigma) = C_0\sigma^4 + C_1\sigma^3 + C_2\sigma^2 + C_3\sigma + C_4$$

and $[C_i]$ are complex square matrices of order $6(N + 1)$. $[C_0]$, $[C_1]$ and $[C_2]$ are singular and contain only compliant boundary conditions. To remove the singularity which prevents the solution, a transformation (4.4.15) is introduced. In this way all of the matrices become non-singular and solutions can be obtained by methods discussed in Section 4.2. This completes the Chebyshev discretization of the fundamental problem.

4.5 Shooting Method for Secondary Instabilities

The procedure for the local method is the same for the primary instability problem. A difference lies in the size of the system of equations and boundary conditions. For the fundamental mode we have a system of eighteen first-order ordinary differential equations, while the subharmonic involves twelve equations. These are arranged in the form similar to equation (4.3.1). We will outline this method for the subharmonic and fundamental modes below.

4.5.1 Solution for the Subharmonic Disturbance

The complementary system to (4.3.1) for the subharmonic mode is

$$D \begin{Bmatrix} \bar{\Omega}_1 \\ \bar{\Omega}_{-1} \end{Bmatrix} \begin{pmatrix} I_1 & I_2 & \cdots & I_{12} \\ J_1 & J_2 & \cdots & J_{12} \\ \vdots & \vdots & \ddots & \vdots \\ L_1 & L_2 & \cdots & L_{12} \end{pmatrix} \begin{Bmatrix} \bar{V}_1 \\ \bar{V}_{-1} \\ \bar{\Omega}_1 \\ \bar{\Omega}_{-1} \end{Bmatrix} \quad 4.5.1a$$

and

$$D \begin{Bmatrix} \bar{V}_1 \\ \bar{V}_{-1} \end{Bmatrix} \begin{pmatrix} A_1 & A_2 & \cdots & A_{12} \\ B_1 & B_2 & \cdots & B_{12} \\ \vdots & \vdots & \ddots & \vdots \\ H_1 & H_2 & \cdots & H_{12} \end{pmatrix} \begin{Bmatrix} \bar{V}_1 \\ \bar{V}_{-1} \\ \bar{\Omega}_1 \\ \bar{\Omega}_{-1} \end{Bmatrix} \quad 4.5.1b$$

The system must be solved in the order shown since the solution of (4.5.1a) is required to solve (4.5.1b). A fixed step Runge-Kutta routine is used to solve the system. In general the form of solution is given as

$$\begin{Bmatrix} \bar{V}_1 \\ \bar{V}_{-1} \\ \bar{\Omega}_1 \\ \bar{\Omega}_{-1} \end{Bmatrix} = \bar{A}_1 \begin{Bmatrix} 1 \\ 0 \\ \vdots \\ 0 \end{Bmatrix} + \bar{A}_2 \begin{Bmatrix} 0 \\ 1 \\ \vdots \\ 0 \end{Bmatrix} + \cdots + \bar{A}_{12} \begin{Bmatrix} 0 \\ 0 \\ \vdots \\ 1 \end{Bmatrix} \quad 4.5.2$$

By the use of the compliant wall boundary conditions listed in Appendix B, six of the twelve unknown coefficients may be eliminated to give the following system at the wall.

$$\begin{pmatrix} a_1 & a_2 & \cdots & a_6 \\ b_1 & b_2 & \cdots & b_6 \\ \vdots & \vdots & \ddots & \vdots \\ f_1 & f_2 & \cdots & f_6 \end{pmatrix} \begin{Bmatrix} \hat{v}'_1 \\ \hat{v}'_1 \\ \hat{\Omega}'_1 \\ \hat{v}'_{-1} \\ \hat{\Omega}'_{-1} \end{Bmatrix} = \{H_i\} \quad 4.5.3$$

where $\{H_i\}, i = 1 \rightarrow 6$ depending on which numerical vector the boundary conditions are representing. For all of the vectors

$$\hat{v}'' = \hat{v}'_1 = \hat{v}'_{-1} = \hat{v}'_{-1} = \hat{\Omega}'_1 = \hat{\Omega}'_{-1} = 0 \quad 4.5.4a$$

except

$$\hat{v}'_1 = 1 \quad \hat{v}'_{-1} = 1 \quad \hat{\Omega}'_1 = 1 \quad 4.5.4b$$

$$H_1 = \begin{Bmatrix} 0 \\ 0 \\ 0 \\ 0 \\ -e_7 \\ 0 \end{Bmatrix} \quad H_2 = \begin{Bmatrix} -a_8 \\ -b_8 \\ -c_8 \\ -d_8 \\ -e_8 \\ -f_8 \end{Bmatrix} \quad H_3 = \begin{Bmatrix} -a_9 \\ -b_9 \\ -c_9 \\ -d_9 \\ -e_9 \\ -f_9 \end{Bmatrix} \quad 4.5.4c$$

$$\hat{v}'_{-1} = 1 \quad \hat{v}'_{-1} = 1 \quad \hat{\Omega}'_{-1} = 1 \quad 4.5.4d$$

$$H_4 = \begin{Bmatrix} 0 \\ 0 \\ 0 \\ 0 \\ -e_{10} \\ 0 \end{Bmatrix} \quad H_5 = \begin{Bmatrix} -a_{11} \\ -b_{11} \\ -c_{11} \\ -d_{11} \\ -e_{11} \\ -f_{11} \end{Bmatrix} \quad H_6 = \begin{Bmatrix} -a_{12} \\ -b_{12} \\ -c_{12} \\ -d_{12} \\ -e_{12} \\ -f_{12} \end{Bmatrix} \quad 4.5.4e$$

Beginning with these vectors at the wall we integrate across the boundary layer. Using the Gram-Schmidt orthonormalization as before, linear independent numerical vectors are maintained. Orthonormalization is performed whenever a vector exceeds a magnitude of 10^6 . This criterion is sufficient for the amount of stiffness in this system. A final orthonormalization is performed at the outer edge of the boundary layer before the solution vectors are matched with the following asymptotic solutions which satisfy the far-field boundary conditions.

$$\hat{v}_n = B_{1n} e^{-\sqrt{\Delta_n} y} + B_{2n} e^{-\sqrt{\bar{\Delta}_n} y} \quad 4.5.5a$$

$$\hat{\Omega}_n = B_{3n} e^{-\sqrt{\Delta_n} y} \quad 4.5.5b$$

where

$$\overline{\Delta_n} = \sqrt{-\Delta_n + \sigma R_\delta + \bar{\alpha}_n R_\delta (U_0 - c_x) + R \bar{\beta}_n (W_0 - c_z)} \quad \text{and} \quad \text{Re}\{\overline{\Delta_n}\} > 0$$

For a nontrivial solution the determinant for the system must be zero. For a given primary instability, the secondary eigenvalue is altered until the matching condition is satisfied.

4.5.2 Solution for the Fundamental Disturbance

In the same manner as described for the subharmonic mode, the complementary system to (4.3.1) for the fundamental mode is

$$D \begin{Bmatrix} \bar{\Omega}_2 \\ \bar{\Omega}_0 \\ \bar{\Omega}_{-2} \end{Bmatrix} \begin{pmatrix} J_1 & J_2 & \cdots & J_{18} \\ Q_1 & Q_2 & \cdots & Q_{18} \\ \vdots & \vdots & \ddots & \vdots \\ R_1 & R_2 & \cdots & R_{18} \end{pmatrix} \begin{Bmatrix} \bar{V}_2 \\ \bar{V}_0 \\ \bar{V}_{-2} \\ \bar{\Omega}_2 \\ \bar{\Omega}_0 \\ \bar{\Omega}_{-2} \end{Bmatrix} \quad 4.5.6a$$

and

$$D \begin{Bmatrix} \bar{V}_2 \\ \bar{V}_0 \\ \bar{V}_{-2} \end{Bmatrix} \begin{pmatrix} A_1 & A_2 & \cdots & A_{18} \\ B_1 & B_2 & \cdots & B_{18} \\ \vdots & \vdots & \ddots & \vdots \\ I_1 & I_2 & \cdots & I_{18} \end{pmatrix} \begin{Bmatrix} \bar{V}_2 \\ \bar{V}_0 \\ \bar{V}_{-2} \\ \bar{\Omega}_2 \\ \bar{\Omega}_0 \\ \bar{\Omega}_{-2} \end{Bmatrix} \quad 4.5.6b$$

The system must be solved in the order shown since the solution of (4.5.6a) is required to solve (4.5.6b). The fixed step Runge-Kutta routine is used to solve the system. In general the form of solution is given as

$$\begin{Bmatrix} \bar{V}_2 \\ \bar{V}_0 \\ \bar{V}_{-2} \\ \bar{\Omega}_2 \\ \bar{\Omega}_0 \\ \bar{\Omega}_{-2} \end{Bmatrix} = \bar{A}_1 \begin{Bmatrix} 1 \\ 0 \\ \vdots \\ 0 \end{Bmatrix} + \bar{A}_2 \begin{Bmatrix} 0 \\ 1 \\ \vdots \\ 0 \end{Bmatrix} + \cdots + \bar{A}_{18} \begin{Bmatrix} 0 \\ 0 \\ \vdots \\ 1 \end{Bmatrix} \quad 4.5.7$$

By the use of the compliant wall boundary conditions listed in Appendix B, nine of the eighteen unknown coefficients may be eliminated to give the following system at the wall.

$$\begin{pmatrix} a_1 & a_2 & \cdots & a_9 \\ b_1 & b_2 & \cdots & b_9 \\ \vdots & \vdots & \ddots & \vdots \\ h_1 & h_2 & \cdots & h_9 \\ i_1 & i_2 & \cdots & i_9 \end{pmatrix} \begin{Bmatrix} \hat{v}'_2 \\ \hat{v}_2 \\ \hat{\Omega}_2 \\ \hat{v}'_0 \\ \hat{v}_0 \\ \hat{\Omega}_0 \\ \hat{v}'_{-2} \\ \hat{v}_{-2} \\ \hat{\Omega}_{-2} \end{Bmatrix} = \{H_i\} \quad 4.5.8$$

where $\{H_i\}, i = 1 \rightarrow 9$ depending on which numerical vector the boundary conditions are representing. For all of the vectors

$$\hat{v}_2''' = \hat{v}_2'' = \hat{v}_0''' = \hat{v}_0'' = \hat{v}_{-2}''' = \hat{v}_{-2}'' = \hat{\Omega}'_2 = \hat{\Omega}'_0 = \hat{\Omega}'_{-2} = 0 \quad 4.5.9a$$

except

$$\hat{v}_2''' = 1 \quad \hat{v}_2'' = 1 \quad \hat{\Omega}'_2 = 1 \quad 4.5.9b$$

$$H_1 = \begin{Bmatrix} 0 \\ 0 \\ 0 \\ 0 \\ 0 \\ 0 \\ -e_{10} \\ 0 \\ 0 \end{Bmatrix} \quad H_2 = \begin{Bmatrix} -a_{11} \\ -b_{11} \\ -c_{11} \\ -d_{11} \\ -e_{11} \\ -f_{11} \\ -g_{11} \\ -h_{11} \\ -i_{11} \end{Bmatrix} \quad H_3 = \begin{Bmatrix} -a_{12} \\ -b_{12} \\ -c_{12} \\ -d_{12} \\ -e_{12} \\ -f_{12} \\ -g_{12} \\ -h_{12} \\ -i_{12} \end{Bmatrix} \quad 4.5.9c$$

$$\hat{v}_0''' = 1 \quad \hat{v}_0'' = 1 \quad \hat{\Omega}'_0 = 1 \quad 4.5.9d$$

$$H_4 = \begin{Bmatrix} 0 \\ 0 \\ 0 \\ 0 \\ 0 \\ 0 \\ -e_{13} \\ 0 \end{Bmatrix} \quad H_5 = \begin{Bmatrix} -a_{14} \\ -b_{14} \\ -c_{14} \\ -d_{14} \\ -e_{14} \\ -f_{14} \\ -g_{14} \\ -h_{14} \\ -i_{14} \end{Bmatrix} \quad H_6 = \begin{Bmatrix} -a_{15} \\ -b_{15} \\ -c_{15} \\ -d_{15} \\ -e_{15} \\ -f_{15} \\ -g_{15} \\ -h_{15} \\ -i_{15} \end{Bmatrix} \quad 4.5.9e$$

$$\hat{v}_{-2}''' = 1$$

$$\hat{v}_{-2}'' = 1$$

$$\hat{\Omega}_{-2}' = 1$$

4.5.9f

$$H_7 = \begin{Bmatrix} 0 \\ 0 \\ 0 \\ 0 \\ 0 \\ 0 \\ 0 \\ 0 \\ -e_{16} \end{Bmatrix} \quad H_8 = \begin{Bmatrix} -a_{17} \\ -b_{17} \\ -c_{17} \\ -d_{17} \\ -e_{17} \\ -f_{17} \\ -g_{17} \\ -h_{17} \\ -i_{17} \end{Bmatrix} \quad H_9 = \begin{Bmatrix} -a_{18} \\ -b_{18} \\ -c_{18} \\ -d_{18} \\ -e_{18} \\ -f_{18} \\ -g_{18} \\ -h_{18} \\ -i_{18} \end{Bmatrix} \quad 4.5.9g$$

Beginning with these vectors at the wall, we integrate across the boundary layer. Using the Gram-Schmidt orthonormalization as before, linear independent numerical vectors are maintained. Orthonormalization is performed whenever a vector exceeds a magnitude of 10^6 . A final orthonormalization is performed at the edge of the boundary layer before the solution vectors are matched with the asymptotic solutions (4.5.5). For a given primary instability, the secondary eigenvalue is altered until the matching condition is satisfied.

This completes our description of the numerical methods and the procedure for their implementation. In the next chapters, these methods will be tested and compared. Then results are presented for instabilities propagating over compliant and rigid walls.

CHAPTER 5

RESULTS OF THE PRIMARY INSTABILITY ANALYSIS

5.1 Rigid Wall Verification

In all of the cases considered for the solutions of primary and secondary instabilities, the freestream velocity (U_∞) is 20 m/s, the density (ρ) is 1000 kg/m³, and the kinematic viscosity (ν) is 1×10^{-6} m²/s. Before the compliant coatings are introduced, the spectral and shooting methods will be verified for predicting the spatial stability of primary waves over rigid walls.

The system of equations for a three-dimensional disturbance consists of the Orr-Sommerfeld and Squire's equations. A number of publications have listed the results from solving the Orr-Sommerfeld equation for a two-dimensional disturbance. The present methods are compared with Jordinson (1970) for a Reynolds number (R_{δ^+}) of 998 and a frequency (ω) of 0.1122. Spectral convergence records are given for the Linear Companion Matrix method, Bernoulli iteration, and Traub iteration methods in Tables 5.1-3 for the two-dimensional TSI wave. The Linear Companion Matrix method requires a $5(N + 1)$ matrix size where N is the order of the Chebyshev series for the disturbance normal velocity (\hat{v}_1). Table 5.1 indicates that a Chebyshev series of order 30 provides a sufficient number of terms for convergence on the eigenvalue. Results for the Bernoulli iteration method are shown in Table 5.2. The results from this method indicate that convergence is not only dependent on the order of the Chebyshev series but on the number of iterations performed. Although this approach requires less memory, the overall cpu time required for a sufficient convergence can exceed that of the Companion Matrix method. Results from the final global method considered are listed in Table 5.3. Similar to the Bernoulli method, results from Traub iteration depend on

the order of the Chebyshev series and the number of iterations. Only a few cases are listed in Table 5.3 to indicate that the cost exceeds the Companion Matrix method. For this Reynolds number and frequency Jordinson (1970) obtained the eigenvalue, $\alpha = 0.3086 - i0.0057$. From Lancaster's local refinement approach, $\alpha = 0.30859 - i0.005707$ is obtained using 30 polynomials. This required 5.5 cpu seconds. By using the shooting approach, $\alpha = 0.30859 - i0.005708$ results requiring only 4.1 cpu seconds. For the shooting approach, 175 steps were used to integrate across the boundary layer to $y_{max} = 9.0$. The results for Bernoulli and Traub methods indicate that an exact convergence is not shown. This is of little concern since the values that were obtained are sufficient to provide an initial guess for the local methods which are faster computationally.

Table 5.1: Spectral convergence of a TSI wavenumber over a rigid wall for $R_{\delta^*} = 998$ and $\omega = 0.1122$ by the Linear Companion Matrix method. (VAX 8550)

N	TSI	cpu(s)
10	$0.30779 - i0.0065175$	
15	$0.30719 - i0.0058083$	
20	$0.30862 - i0.0057190$	
25	$0.30859 - i0.0057114$	
30	$0.30859 - i0.0057071$	37.7
35	$0.30859 - i0.0057086$	64.1
40	$0.30859 - i0.0057084$	90.4

Table 5.2: Spectral convergence of a TSI wavenumber over a rigid wall for $R_{\delta^*} = 998$ and $\omega = 0.1122$ by Bernoulli Iteration. (VAX 8550)

N	TSI	cpu(s)	Iterations
25	0.30825 - $i0.0067739$	11.7	3
30	0.30897 - $i0.0059528$	19.2	3
30	0.30857 - $i0.0057637$	38.0	10
35	0.29898 - $i0.0055400$	29.5	3
35	0.30857 - $i0.0056873$	56.7	10
35	0.30899 - $i0.0055279$	78.4	15
40	0.30886 - $i0.0061454$	88.8	10
40	0.31068 - $i0.0032358$	115.0	15

Table 5.3: Spectral convergence of a TSI wavenumber over a rigid wall for $R_{\delta^*} = 998$ and $\omega = 0.1122$ by Traub Iteration (stage 1:stage 2). (VAX 8550)

N	TSI	cpu(s)	Iterations(1:2)
25	0.30859 - $i0.0056782$	17.7	2:3
30	0.30860 - $i0.0056457$	29.6	2:3
35	0.30863 - $i0.0057307$	45.2	2:3
35	0.30863 - $i0.0057400$	58.8	2:4

Eigenvectors may be obtained from either local method as outlined in the previous chapter. The resulting normalized \hat{v}_1 -eigenvector from both approaches is compared with Jordinson in Figure 5.1. Exact agreement occurs except at one location. A distortion occurs with Jordinson's data which is not found with the present results. Since no distortion of the eigenvector is shown in Figure 5 of Jordinson, it is apparent that a mistake was made in Jordinson's listing of the eigenvector values.

In the present study, we will make extensive use of points referenced to the curve of neutral stability. Although the numerical procedures agree with published information, one final comparison is made for the rigid wall case. This curve of neutral stability divides the regions in which a disturbance with an appropriate Reynolds number and frequency will either grow or decay. The neutral curve is shown in Figure 5.2. Agreement is found with the present results, the results of Jordinson (1970), and the results of van Stijn and van de Vooren (1980). The lower frequency portion of the curve is referred to as branch I and the high frequency portion is branch II. The curve itself corresponds to the frequency-wavenumber-Reynolds number combination for a wave with $\alpha_i = \omega_i = 0$. Either temporal or spatial instability calculations arrive at the same result. A disturbance with a given frequency enters the region of instability at branch I. As it propagates downstream it exponentially grows through the unstable region, then becomes damped after it crosses branch II.

In this section, we have shown that results obtained through the present spectral and shooting approaches agree with published results. In the next section various compliant walls will be introduced. The numerical approaches will be discussed followed by a further look at the idea of "neutral curve."

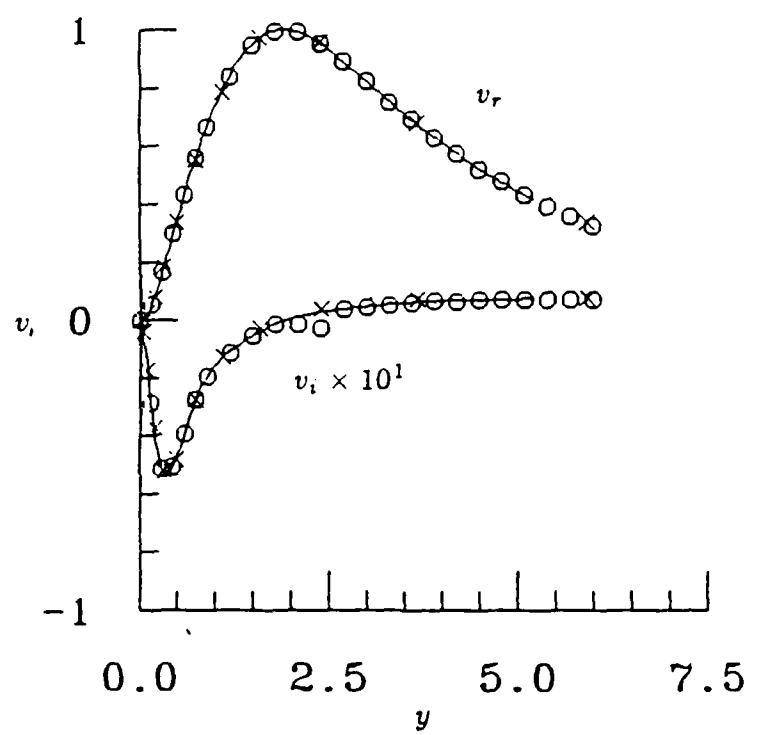


Figure 5.1 A comparison of the v_1 -eigenvector solution by the $- \times -$, spectral approach; $-$, shooting approach; with $-o-$, Jordinson (1970) for $Re_{\delta^*} = 998$, $\alpha = 0.3086 - i0.0057$ and $\omega = 0.1122$.

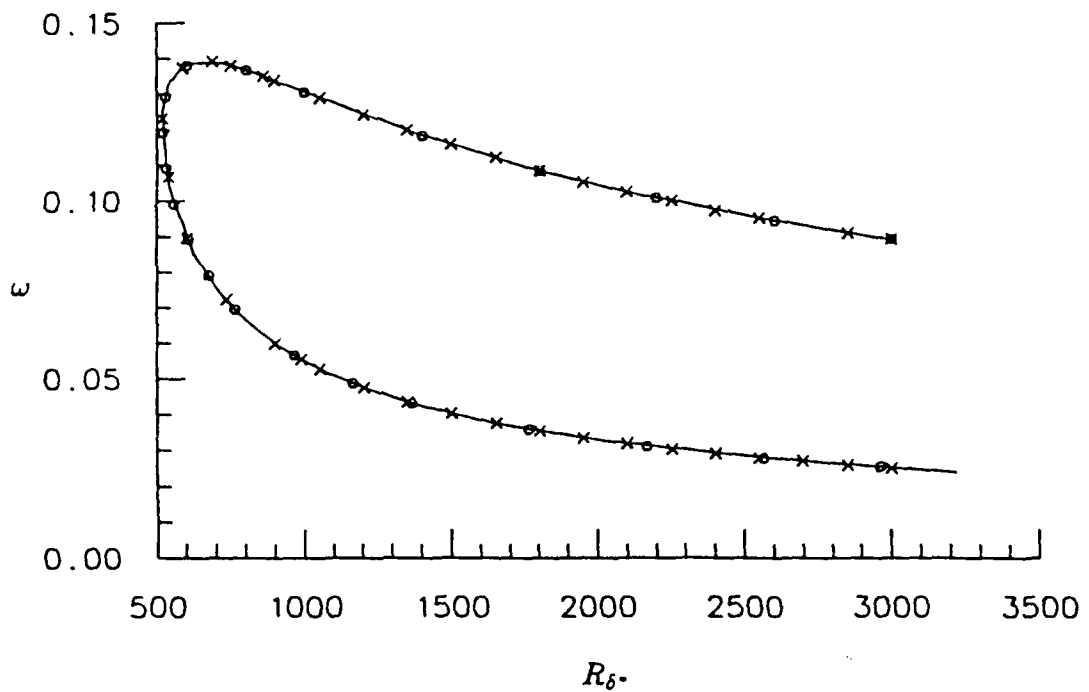


Figure 5.2 Curves of neutral stability for the rigid wall determined by —, present calculations; -o-, Jordinson (1970); and -×-, Van Stijn and Van de Vooren (1980).

5.2 Introduction of Wall Compliance

In this section, wall compliance is introduced. The properties are taken from Carpenter and Morris (1990) and are listed in Table 5.4. These wall properties are optimized to achieve a minimum growth rate of a two-dimensional TSI wave while keeping other modes that arise marginally stable. Two of the walls were optimized at $R_{\delta^*} = 2240$. A Reynolds number of 2240 was chosen because for the boundary layer over a rigid wall the disturbances with the critical frequency (in the e^n sense) reaches its maximum growth rate at close to this value of Reynolds number. Accordingly, this is a good choice of Reynolds number for optimizing the wall properties to achieve the lowest possible growth rate.

Table 5.4: Isotropic and non-isotropic compliant wall properties optimized at $R_{\delta^*} = 2240$ and $R_{\delta^*} = 5000$ with $\rho_m = 1000 \text{ kg/m}^3$ (Carpenter and Morris; 1990).

θ degrees	b mm	E_z N/mm^2	K N/mm^3
0°(2240)	0.7350	1.385	0.3540
60°(2240)	0.1110	0.509	0.0590
0°(5000)	1.1025	1.385	0.2360
60°(5000)	0.3340	0.507	0.0197

The Reynolds number of 5000 was chosen to show the effect of Reynolds number on the instability behavior. The results of the two-dimensional instability analysis over these coatings and the rigid wall are used for a comparison with the

present three-dimensional results. For the three-dimensional instability analysis, an isotropic plate ($E_x = E_z$) and an orthotropic plate ($E_z = 0$) are considered. An orthotropic plate with $E_z = 0$ is very compliant in the spanwise direction. This gives four coating combinations of interest. These are referred to as isotropic wall/isotropic plate, isotropic wall/orthotropic plate, non-isotropic wall/isotropic plate, non-isotropic wall/orthotropic plate. For the isotropic wall $\theta = 0^\circ$ and for the non-isotropic wall $\theta = 60^\circ$.

To simulate the rigid wall, $C_M \rightarrow \infty$ in the mechanical model. For $R_{\delta\cdot} = 2240$ and $\omega = 0.055$, spectral convergence is shown in Table 5.5 for the rigid wall simulation. Sufficient convergence is obtained with the same number of polynomials as the rigid wall problem (Table 5.1). Here we have switched to using the IBM to make comparisons with the three-dimensional problem. The VAX has insufficient virtual memory to solve the three-dimensional instability problem which requires approximately 8-10 Mbytes of memory. Additionally, cpu times are listed to give the reader an idea of the costs involved in these computations. Also, this gives an indication of the importance of supercomputers without which many of these calculations could not have been performed. This point is of more importance for the secondary calculations which will be discussed in the next chapter. To determine how many polynomials are required to converge on an eigenvalue of the TSI and TWF waves over the compliant wall, the $\theta = 60^\circ(2240)$ wall is introduced. The spectral convergence results are shown in Table 5.6 for the two-dimensional wave. For our purposes sufficient convergence is attained with 48 polynomials. With the increase in the required number of polynomials compared with the rigid wall a considerable increase in computational cost occurs. For the local spectral approach, convergence is shown in Table 5.7. As the results indicate, the local method is very efficient compared to the global methods.

Table 5.5: Spectral convergence of a TSI wavenumber over a rigid wall ($C_M \rightarrow \infty$) by the Linear Companion Matrix method. (IBM 3090-vectorized,V, and non-vectorized,NV)

N	TSI	cpu(s) NV	cpu(s) V
8	0.18097 - i 0.012688	0.63	0.15
12	0.18695 - i 0.010321	1.15	0.25
16	0.18623 - i 0.010308	2.16	0.42
20	0.18622 - i 0.010345	3.79	0.71
24	0.18620 - i 0.010347	6.03	1.05
28	0.18622 - i 0.010344	9.42	1.56
32	0.18622 - i 0.010342	13.38	2.22

Table 5.6: Spectral convergence of the two-dimensional TSI and TWF wavenumbers over a $\theta = 60^\circ$ (2240) wall by the Linear Companion Matrix method. (IBM 3090-vectorized,V, and non-vectorized,NV)

N	TSI	TWF	cpu(s) NV	cpu(s) V
36	.15800 - i 0.003341	.02158 + i 0.0006362	30.05	4.93
40	.15799 - i 0.003157	.02150 - i 0.0000134	40.88	8.11
44	.15783 - i 0.003062	.02135 + i 0.0001268	53.96	9.79
48	.15782 - i 0.003133	.02145 + i 0.0001462	69.21	11.38
52	.15781 - i 0.003127	.02139 + i 0.0000914	87.00	14.67
56	.15781 - i 0.003141	.02140 + i 0.0001086	111.15	19.86
60	.15781 - i 0.003141	.02139 + i 0.0000925	138.26	29.69
64	.15781 - i 0.003139	.02139 + i 0.0000938	169.62	35.68
68	.15781 - i 0.003139	.02139 + i 0.0000933	202.83	41.86

Table 5.7: Spectral convergence of the two-dimensional TSI and TWF wavenumbers over a $\theta = 60^\circ$ (2240) wall by Lancaster's method. (IBM 3090-vectorized,V, and non-vectorized,NV)

N	TSI	TWF	cpu(s) NV	cpu(s) V
36	.15800 - $i0.003341$.02158 + $i0.0006362$	0.51	0.12
40	.15799 - $i0.003157$.02150 - $i0.0000134$	0.58	0.15
44	.15783 - $i0.003062$.02135 + $i0.0001268$	0.89	0.19
48	.15782 - $i0.003133$.02145 + $i0.0001462$	0.96	0.23
52	.15781 - $i0.003128$.02139 + $i0.0000913$	1.41	0.29
56	.15781 - $i0.003141$.02140 + $i0.0001086$	1.74	0.35
60	.15781 - $i0.003141$.02139 + $i0.0000925$	1.79	0.41
64	.15781 - $i0.003139$.02139 + $i0.0000938$	2.55	0.50
68	.15781 - $i0.003139$.02139 + $i0.0000933$	3.05	0.59

A three-dimensional wave is introduced with a propagation angle of 10° . Convergence is shown for the global and local methods in Tables 5.8 and 5.9, respectively. Similar to the two-dimensional wave results, 48 polynomials are sufficient for convergence except the problem size has doubled since the disturbance velocity and vorticity must be solved for. For the same Reynolds number and frequency, the shooting approach yields the eigenvalue $\alpha = 0.15781 - i0.003138$ for the two-dimensional wave and $\alpha = 0.16017 - i0.003221$ for the oblique wave. So for the two- and three-dimensional instability waves propagating over compliant walls, the spectral and shooting codes agree.

Table 5.8: Spectral convergence of a three-dimensional TSI wavenumber over a $\theta = 60^\circ$ (2240) wall/isotropic plate by the Linear Companion Matrix method. (IBM 3090-vectorized,V, and non-vectorized,NV) (10° angle of wave propagation)

N	TSI	cpu(s) NV	cpu(s) V
40	.16035 - $i0.003240$	139.51	30.33
44	.16020 - $i0.003146$	179.59	35.85
48	.16018 - $i0.003214$	235.73	49.87
52	.16017 - $i0.003209$	301.42	65.60

Table 5.9: Spectral convergence of a three-dimensional TSI wavenumber over a $\theta = 60^\circ$ (2240) wall/istropic plate by Lancaster's method. (IBM 3090-vectorized,V, and non-vectorized,NV) (10° angle of wave propagation)

N	TSI	cpu(s) NV	cpu(s) V
36	.16035 - $i0.003419$	3.75	0.74
40	.16035 - $i0.003240$	4.30	0.94
44	.16020 - $i0.003146$	6.69	1.28
48	.16018 - $i0.003214$	7.22	1.60
52	.16017 - $i0.003209$	10.85	2.04
56	.16017 - $i0.003222$	13.41	2.54
60	.16017 - $i0.003223$	16.38	3.05
64	.16017 - $i0.003221$	19.83	3.66
68	.16017 - $i0.003221$	23.68	4.35

Before the results for the primary instability analysis are presented, one final advantage should be discussed for the global method in spite of the disadvantage of computational cost. This is drawn out in Figure 5.3 which is a plot of real versus imaginary phase velocity for the $\theta = 0^\circ$ (2240) wall. Four distinct, discrete eigenmodes are found. These were discussed by Carpenter, Joslin, and Morris (1990a). Mode 1 is for the slow moving TSI wave; mode 2 (not shown) is for the fast moving TWF; and mode 3 is (probably) a Static-Divergence instability. Mode 4 behaves more like a standing-wave and is of no concern for the present investigation. But mode 4 is dominant and caution should be taken for those using a local analysis, since this mode may mistakenly be used as the TSI mode. If one were to slowly add compliance from the rigid wall case, the eigenvalue tracked seemingly branches off to mode 4 and mode 1 (the TSI mode). Mode 4 arises from the compliant wall equation. Thus ignoring mode 4, we find from Figure 5.3 that the TSI eigenvalue is dominant. This is consistent with the optimization procedure.

In this section the compliant coatings were introduced and the numerical techniques were tested. In the next section, the focus of the discussion will be on comparing regions of stable and unstable instabilities for the compliant coatings and rigid wall. This is outlined by curves of neutral stability.

5.3 Curves of Neutral Stability

In this section, this concept of stable and unstable regions is considered further. These regions indicate where the instability wave grows or decays.

The first coatings considered were optimized at $R_{\delta^*} = 2240$. Illustrated in Figure 5.4 are the neutral curves for the rigid wall, $\theta = 0^\circ$ (2240) wall, and the $\theta = 60^\circ$ (2240) wall for the two-dimensional TSI. The $\theta = 60^\circ$ (2240) wall

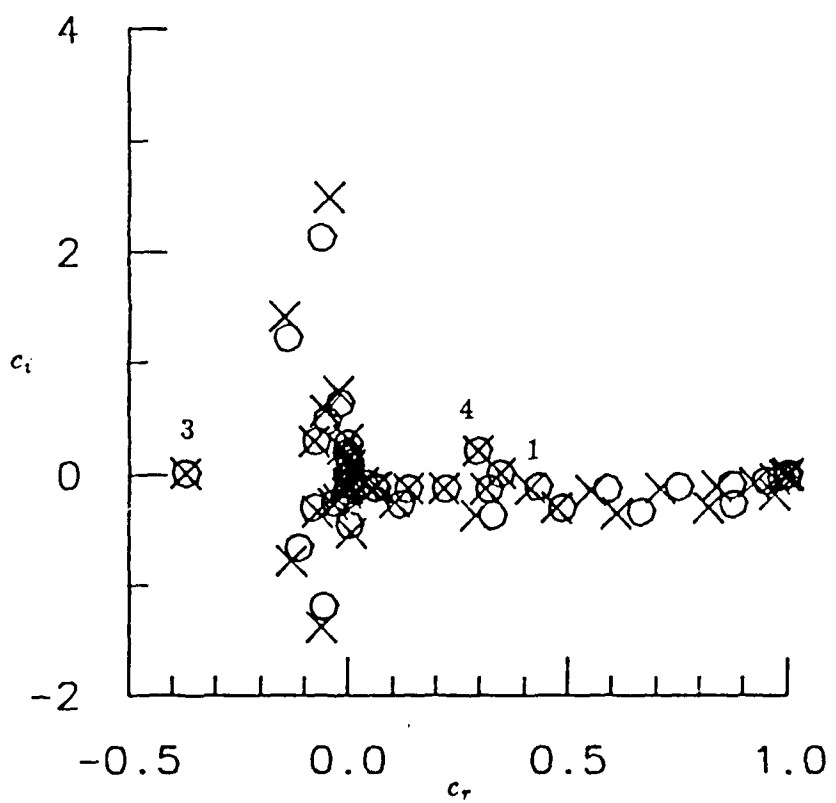


Figure 5.3 Real versus imaginary phase velocity for a two-dimensional TSI wave over a $\theta = 0^\circ$ (2240) compliant wall for $R_{\theta^\star} = 2240$ and $\omega = 0.065$. (o, $N=48$, x, $N=52$)

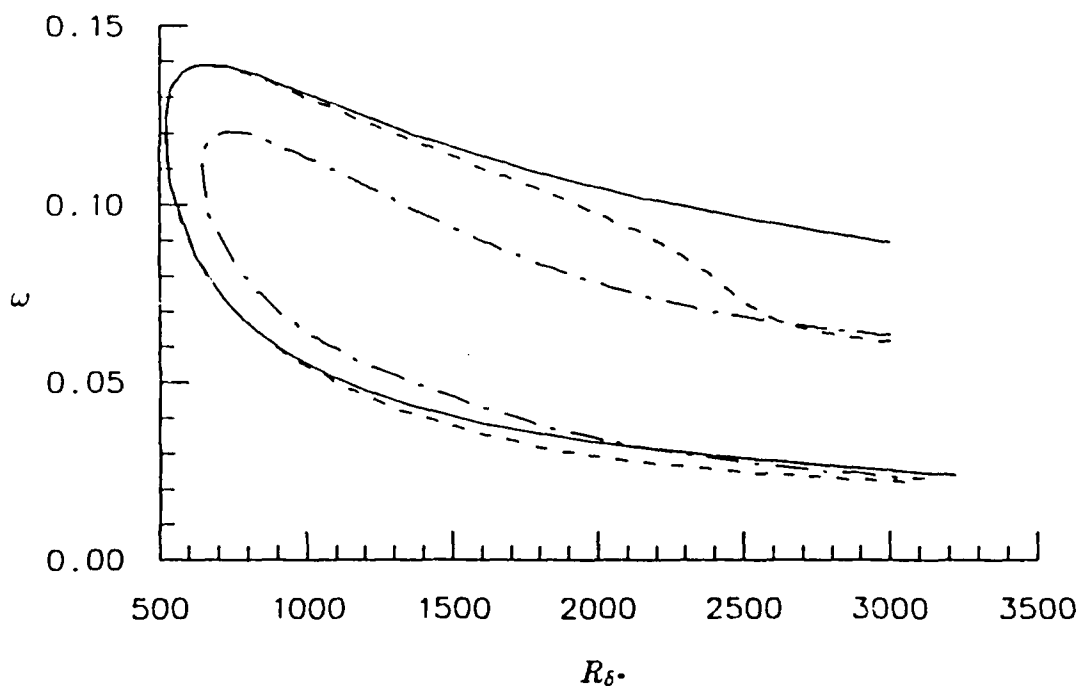


Figure 5.4 Curves of neutral stability over a —, rigid wall; - - -, $\theta = 0^\circ$ (2240); and - · -, $\theta = 60^\circ$ (2240) compliant walls.

has a smaller region of instability located within the rigid wall case. As the Reynolds number increases the lower branch approaches that of the rigid wall and the upper branch stretches midway between the rigid wall branches. The $\theta = 0^\circ$ (2240) wall produces a curve which coincides with the rigid wall curve at high wave frequencies. As the Reynolds number increases both branches approach the $\theta = 60^\circ$ (2240) branches. This in fact says nothing about the growth rates within the unstable region. Although the region of instability may be smaller for the compliant coatings, the growth rates may very well be greater than the rigid wall growth rates. This is not the case for the coatings under consideration. This will be shown in the next section.

The second set of coatings was optimized at $R_{\delta^*} = 5000$. Curves of neutral stability are shown in Figure 5.5. For these coatings, the neutral curve approaches the rigid wall curve for low Reynolds numbers and the curve of the $\theta = 60^\circ$ (2240) branches for high Reynolds numbers.

Some concern has been expressed with respect to the alignment of the ribs, or swivel-arm. It has been suggested that the same solutions would be expected irrespective of whether the ribs are aligned upstream or downstream. Although Carpenter and Morris (1985) have shown that ribs aligned downstream, or in the direction of the flow, lead to higher growth rates than coatings with ribs aligned upstream, we will briefly look at this comparison for the neutral curve. Curves of neutral stability for the rigid wall, $\theta = 60^\circ$ (2240) wall, and $\theta = -60^\circ$ (2240) wall are shown in Figure 5.6. These coatings have distinctly different curves where disturbances propagating over the $\theta = -60^\circ$ wall become unstable at lower frequencies and Reynolds numbers than those propagating over the rigid wall.

A final plot is introduced in this section. Curves of neutral stability for two-dimensional instabilities over the rigid wall and $\theta = 60^\circ$ (2240) wall are

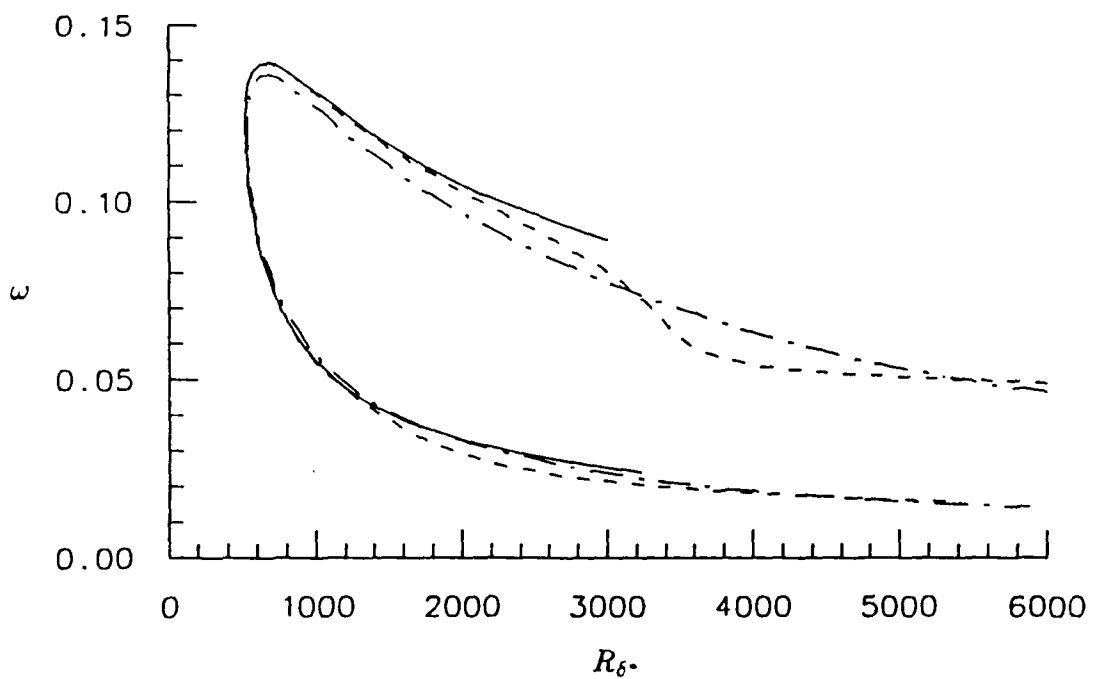


Figure 5.5 Curves of neutral stability over a —, rigid wall; - - -, $\theta = 0^\circ$ (5000); and - · -, $\theta = 60^\circ$ (5000) compliant walls.

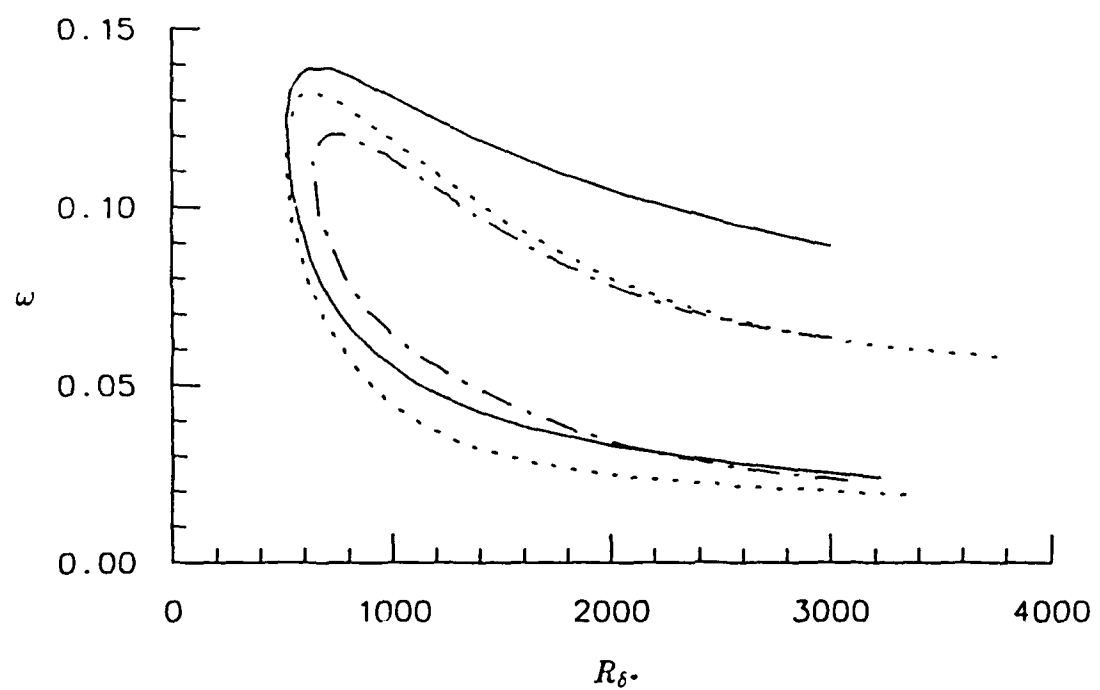


Figure 5.6 Curves of neutral stability over a —, rigid wall; - - -, $\theta = 60^\circ$ (2240); and · · ·, $\theta = -60^\circ$ (2240) compliant walls.

compared with three-dimensional instabilities propagating at an angle of 20° to the freestream direction over the $\theta = 60^\circ$ (2240) wall/isotropic plate. This is shown in Figure 5.7. The curve for the three-dimensional wave shrinks at the high frequency range and begins to slowly approach the rigid wall for branch I. As stated earlier, differences in the neutral curves give no indication of the growth rates within. Yet these curves are an important indication of how the region of instability is altered. When performing e^n type calculations for predicting transition, the results in Figure 5.7 indicate that three-dimensional waves become unstable sooner at the lower branch than the two-dimensional waves.

We will refer back to these curves of neutral stability from time to time in the remaining portion of this investigation. At this point we will proceed with the prediction of growth rates for two- and three-dimensional instabilities propagating over the compliant coatings.

5.4 Fixed Reynolds Number Results

As a first case we consider the two- and three-dimensional instabilities for a fixed Reynolds number of 2240. Figure 5.8 shows the growth rates of the two-dimensional waves for various frequencies for the compliant and rigid walls. For the $\theta = 60^\circ$ (2240) wall the maximum growth rate is about 25 percent of that for the rigid wall. The width of the unstable region in $\omega - R_f$ space is also reduced considerably for the compliant walls as compared to the rigid surface. Figures 5.9 and 5.10 show the growth rates as a function of frequency for various oblique waves propagating over the same two compliant walls. For both coatings, the maximum growth rates are found for three-dimensional waves travelling at oblique angles of $50-60^\circ$ to the flow direction. In the $\theta = 0^\circ$ (2240) case an approximately 60 percent increase in growth rate over the two-dimensional case is found.

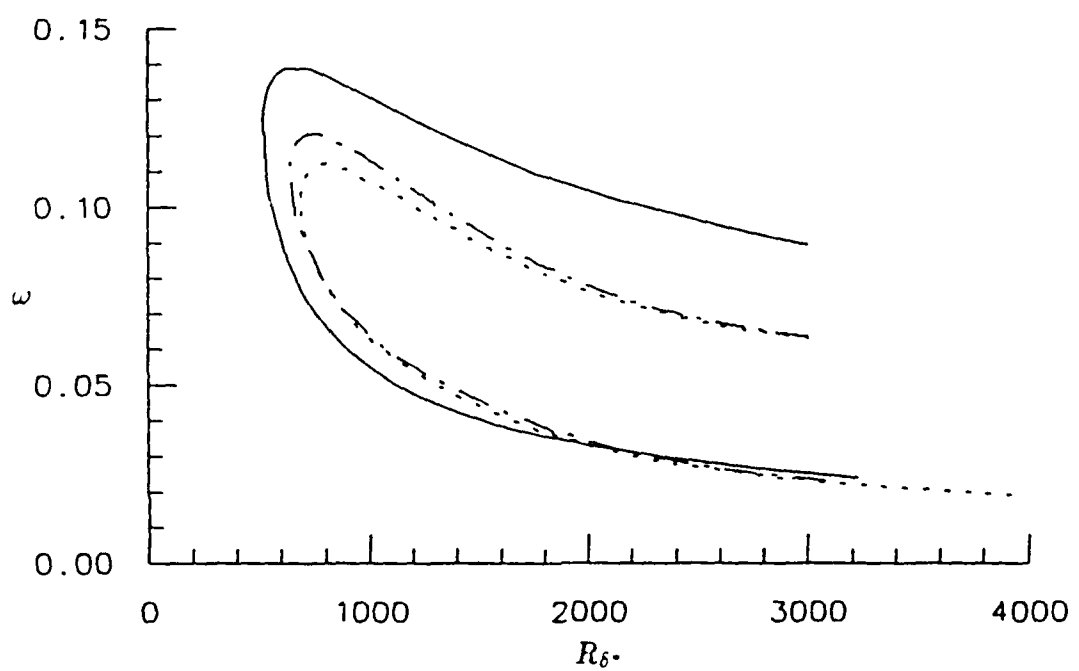


Figure 5.7 Curves of neutral stability over a —, rigid wall; - - -, 2D $\theta = 60^\circ$ (2240) wall; and · · ·, 3D $\theta = 60^\circ$ (2240) wall/isotropic plate at $\phi = 20^\circ$.

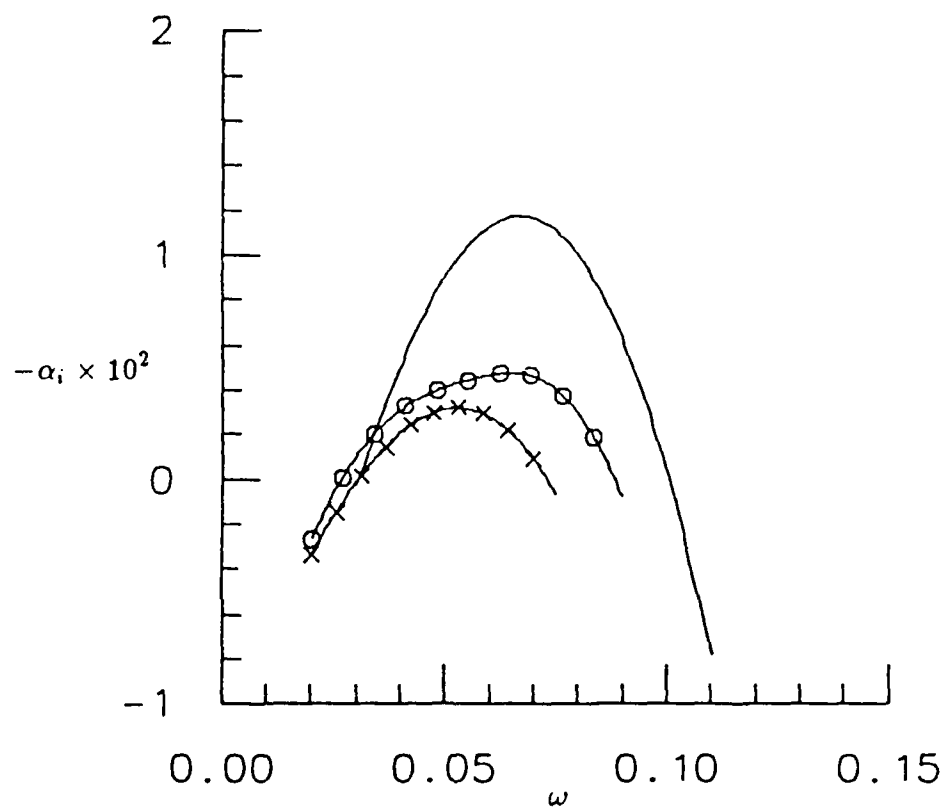


Figure 5.8 Two-dimensional growth rates as a function of frequency for TSI waves over a —, rigid wall; -o-, $\theta = 0^\circ$ (2240) wall; and -x-, $\theta = 60^\circ$ (2240) wall at $Re_{\theta} = 2240$.

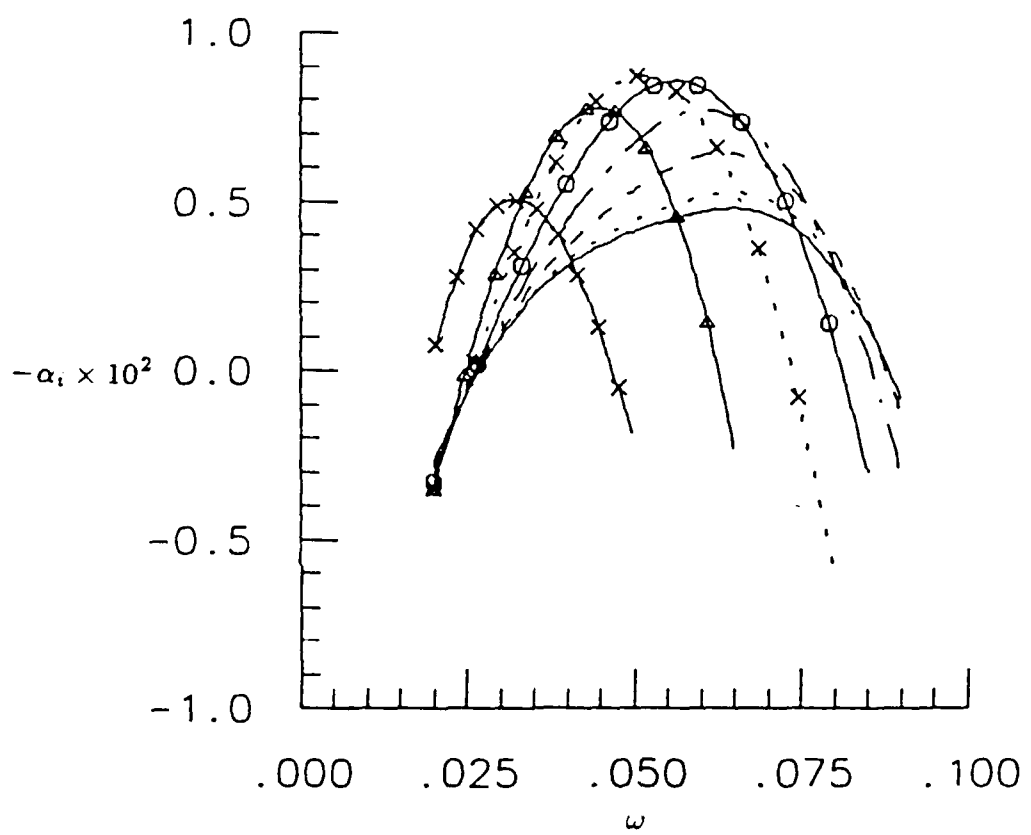


Figure 5.9 Growth rates as a function of frequency for TSI waves over a $\theta = 0^\circ$ (2240) wall/isotropic plate at $Re_s = 2240$ for oblique wave angles of —, 0° ; $\cdots, 10^\circ$; $--, 20^\circ$; $- \cdot -, 30^\circ$; $-o-, 40^\circ$; $\cdots \times \cdots, 50^\circ$; $-\Delta-, 60^\circ$; $-x-, 70^\circ$.

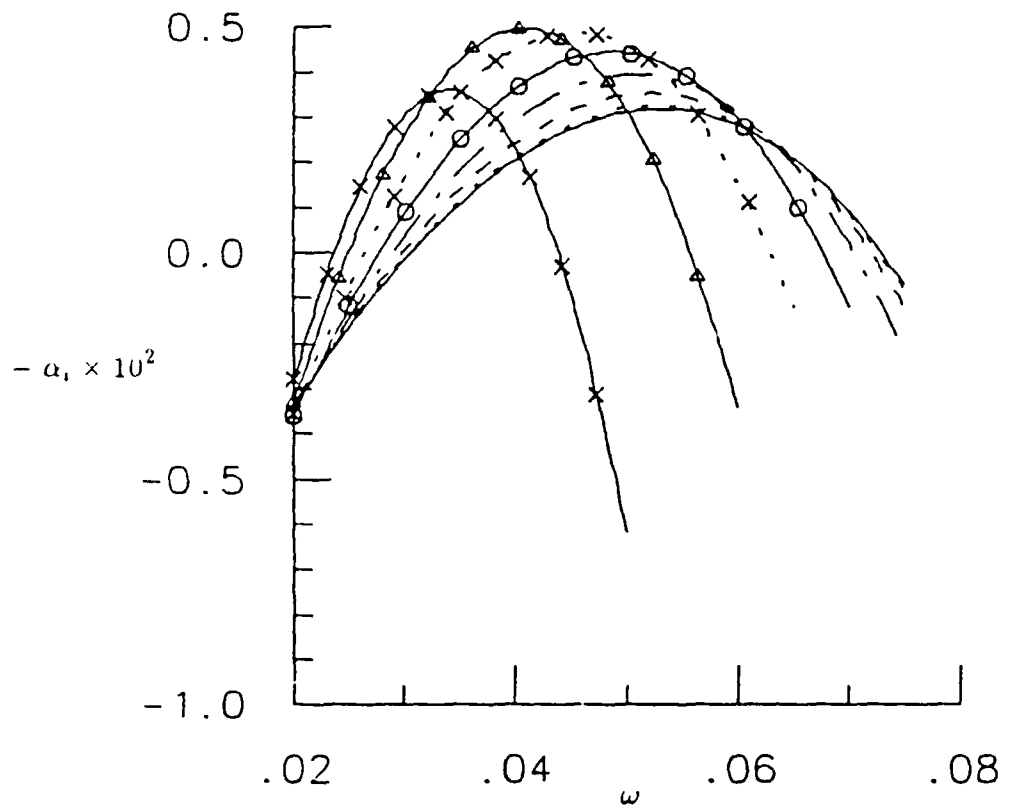


Figure 5.10 Growth rates as a function of frequency for TSI waves over a $\theta = 60^\circ$ (2240) wall/isotropic plate at $Re_{\delta^*} = 2240$ for oblique wave angles of —, 0° ; ···, 10° ; — —, 20° ; — · —, 30° ; —○—, 40° ; ···×···, 50° ; —△—, 60° ; —×—, 70° .

For the $\theta = 60^\circ$ (2240) wall the dominance of the three-dimensional waves is considerably reduced but still quite marked. The reduced sensitivity of the non-isotropic compliant wall to three-dimensional waves compared to the isotropic case can be attributed to the effects of irreversible energy exchange between the wall and the disturbance due to the work done by the fluctuating shear stress. Carpenter and Morris (1990) showed that this energy exchange has a relatively destabilizing effect on the Tollmien-Schlichting waves which grows as θ increases. This deleterious effect is reduced for oblique waves owing to the reduced magnitude of the fluctuating shear stress in the direction of wave propagation. Hence the relative improvement in terms of reductions in the three-dimensional growth rates and range of unstable frequencies for non-isotropic as compared to isotropic compliant walls.

The dominance of three-dimensional waves is caused by the reduced effective wall compliance for oblique waves. Accordingly, Yeo (1986) and Carpenter (1984b) have suggested that increasing the compliance in the spanwise direction by using an orthotropic plate may well reduce the growth rates of the oblique waves. It is apparent from Figure 5.11 that this strategy is successful for the $\theta = 0^\circ$ (2240) wall/orthotropic plate case. The three-dimensional waves are now no longer dominant. However, the orthotropic plate used has $E_z = 0$ which is the extreme case and may not be practical. For the $\theta = 60^\circ$ (2240) wall/orthotropic plate case illustrated in Figure 5.12 there is little change from the isotropic plate case shown in Figure 5.10. The reason for this is readily found from a consideration of the equation of motion for the wall (see 3.2.6). For the isotropic ($\theta = 0^\circ$) case all of the wavenumber dependent stiffness resides in the bending-stiffness terms ($B_z \partial^4 \eta / \partial x^4$ etc.). For non-isotropic compliant walls ($\theta > 0^\circ$), on the other hand, much of the wavenumber dependent stiffness is also contributed by the

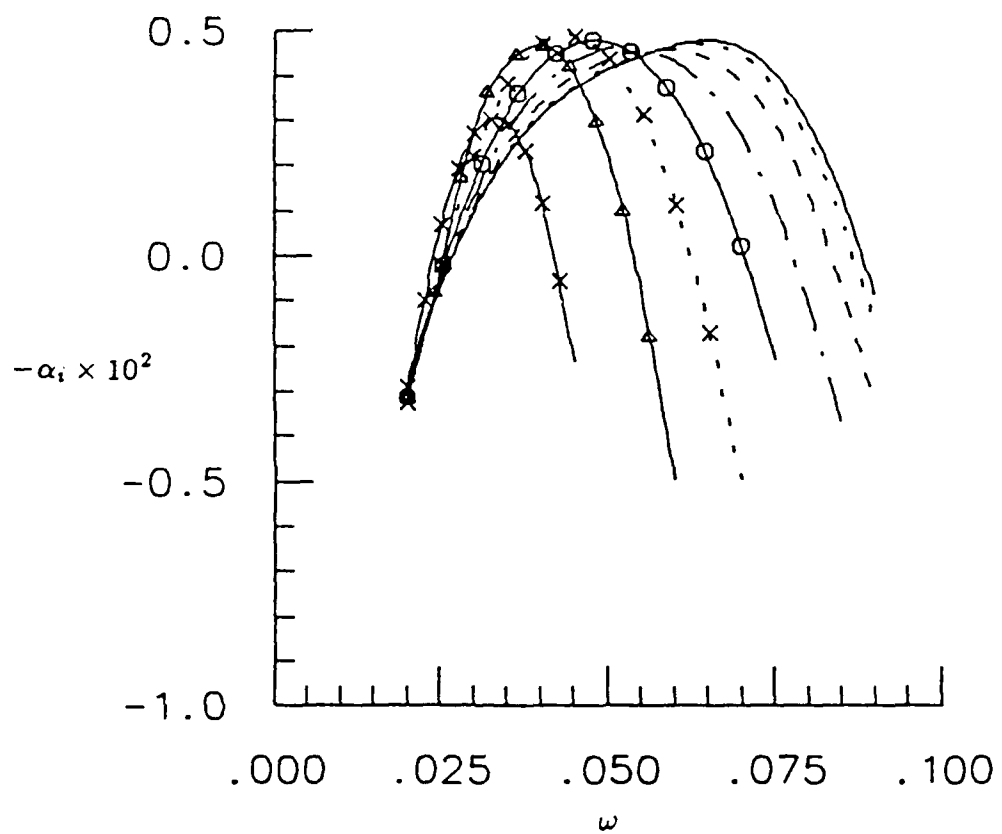


Figure 5.11 Growth rates as a function of frequency for TSI waves over a $\theta = 0^\circ$ (2240) wall/orthotropic plate at $Re_{\delta^*} = 2240$ for oblique wave angles of 0° ; 10° ; 20° ; 30° ; 40° ; 50° ; 60° ; 70° .

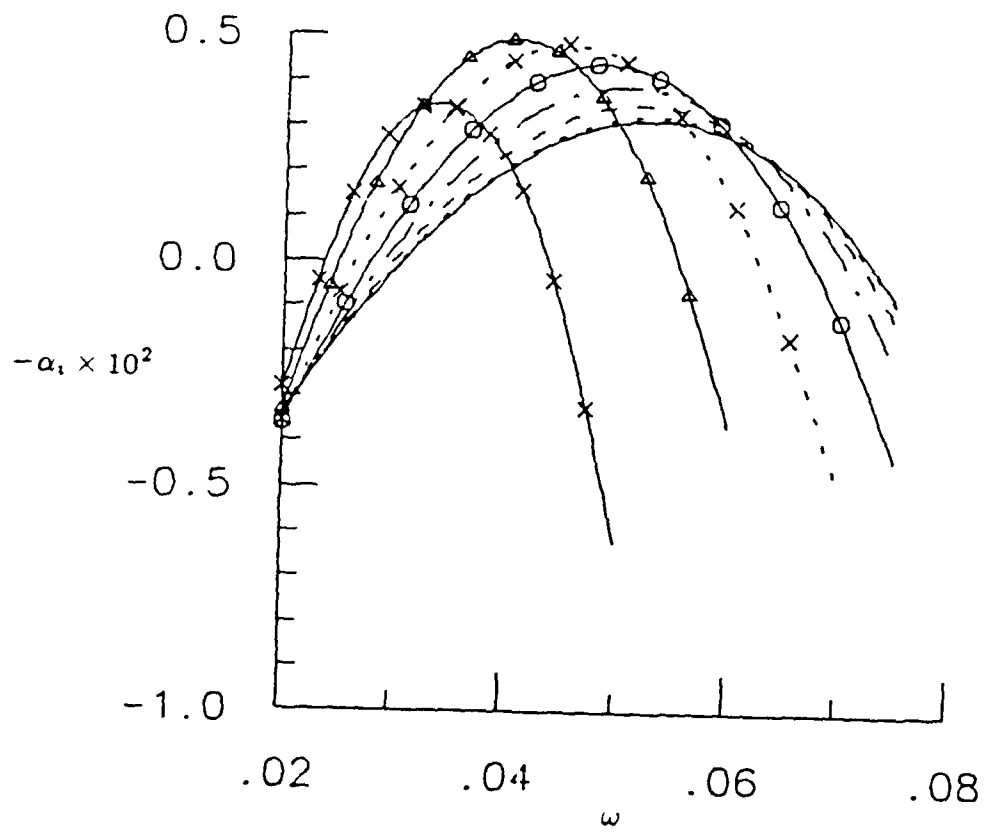


Figure 5.12 Growth rates as a function of frequency for TSI waves over a $\theta = 60^\circ$ (2240) wall/orthotropic plate at $Re_{\delta^*} = 2240$ for oblique wave angles of —, 0° ; ···, 10° ; — — —, 20° ; — ···, 30° ; —○—, 40° ; ···×···, 50° ; —△—, 60° ; —×—, 70° .

induced-tension term ($E_x \partial^2 \xi / \partial x^2 \sin \theta \cos \theta$). For $\theta = 60^\circ$ this second contribution to the stiffness is relatively large and is, of course, unaffected by the use of an orthotropic plate.

To show the effect of Reynolds number, the growth rates as a function of frequency at $R_{\delta^*} = 5000$ over the $\theta = 60^\circ$ (2240) wall are compared to $R_{\delta^*} = 2240$ results given before in Figures 5.10 and 5.12. Results for the isotropic and orthotropic plates are shown in Figures 5.13 and 5.14. The results for the isotropic and orthotropic plates yield similar growth rates. Similar behavior was observed at the lower Reynolds number. However, one difference does arise between the two different Reynolds number cases. At the low Reynolds number, maximum growth rates are reached for oblique waves propagating at approximately 55° . The present high Reynolds number results indicate that the dominant instability waves are highly three-dimensional. Instead of the growth rate reaching a maximum for some oblique wave angle, the growth rates continue to increase as the wave propagation angle increases. When comparing the curves of Figures 5.13 and 5.14 with those at the lower Reynolds number, Figures 5.10 and 5.12, it should be remembered that the length scale has changed by a factor of 1.5. Thus the maximum growth rates and the range of unstable frequencies are very similar in the two cases.

To show the effect of walls optimized for two-dimensional waves, at different Reynolds numbers, $\theta = 0^\circ(5000)$ and $\theta = 60^\circ(5000)$ compliant walls are used at $R_{\delta^*} = 5000$. Figure 5.15 shows the growth rates of the two-dimensional waves for various frequencies for the compliant and rigid walls. For the $\theta = 60^\circ(5000)$ wall, the maximum growth rate is about 30 percent of that for the rigid wall. The difference in the growth rates for the isotropic and non-isotropic walls is less pronounced than the lower Reynolds number walls of Figure 5.8. Figure 5.16

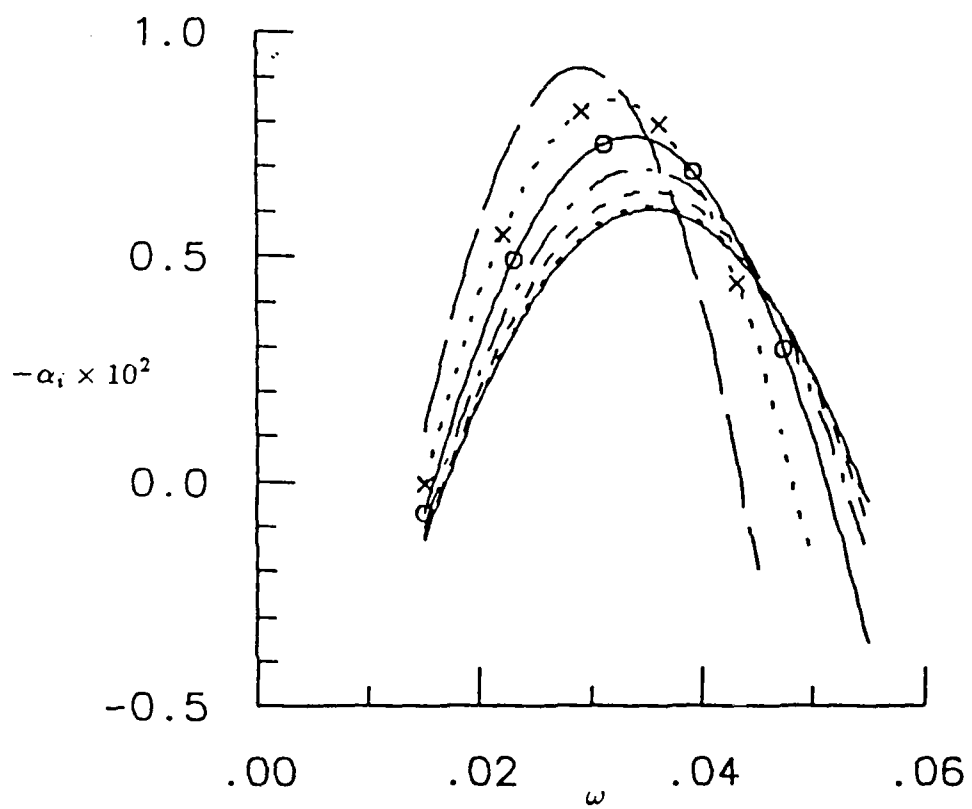


Figure 5.13 Growth rates as a function of frequency for TSI waves over a $\theta = 60^\circ$ (2240) wall/isotropic plate at $Re_f = 5000$ for oblique wave angles of —, 0° ; $\cdots, 10^\circ$; $\cdots, 20^\circ$; $\cdots, 30^\circ$; $-o-, 40^\circ$; $\cdots \times \cdots, 50^\circ$; — —, 60° .

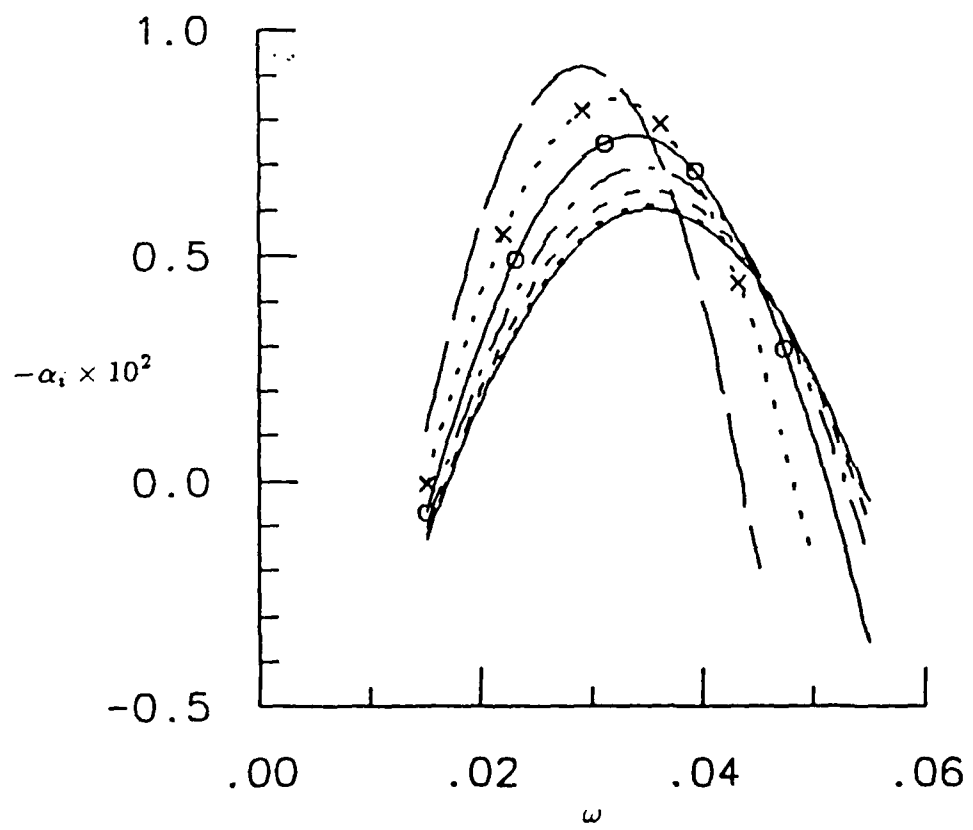


Figure 5.14 Growth rates as a function of frequency for TSI waves over a $\theta = 60^\circ$ (2240) wall/orthotropic plate at $Re_{\delta^*} = 5000$ for oblique wave angles of 0° ; $\dots, 10^\circ$; $\dots, 20^\circ$; $\dots, 30^\circ$; $\dots, 40^\circ$; $\dots \times \dots, 50^\circ$; $\dots \dots, 60^\circ$.

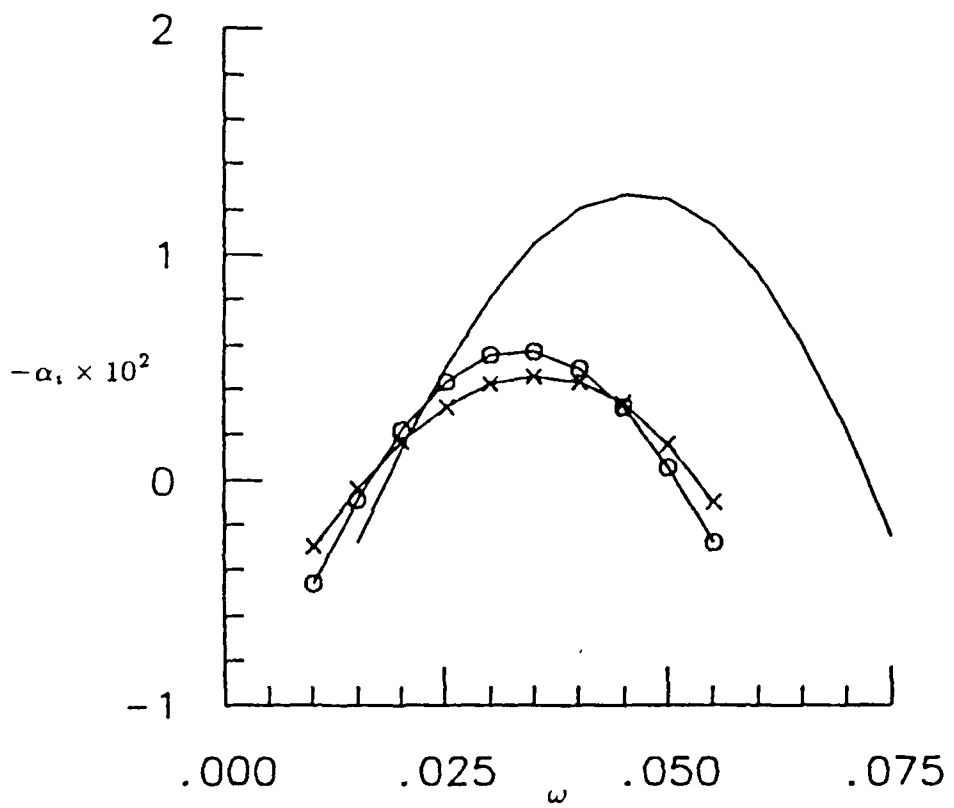


Figure 5.15 Two-dimensional growth rates as a function of frequency for TSI waves over a —, rigid wall; -o-, $\theta = 0^\circ$ (5000) wall; and -x-, $\theta = 60^\circ$ (5000) wall at $Re_{\delta^*} = 5000$.

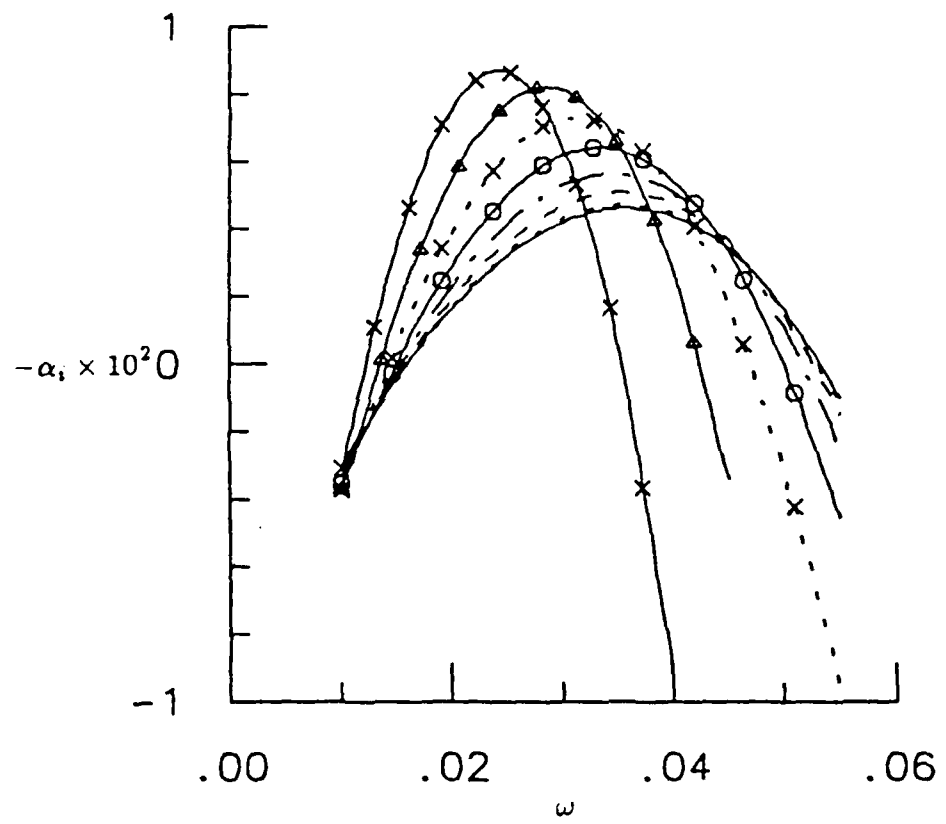


Figure 5.16 Growth rates as a function of frequency for TSI waves over a $\theta = 60^\circ$ (5000) wall/isotropic plate at $Re_{\theta^*} = 5000$ for oblique wave angles of —, 0° ; $\cdots, 10^\circ$; $--, 20^\circ$; $- \cdot -, 30^\circ$; $-o-, 40^\circ$; $\cdots \times \cdots, 50^\circ$; $-\Delta-, 60^\circ$; $- \times -, 70^\circ$.

shows the growth rates of oblique waves at various frequencies for the $\theta = 60^\circ(5000)$ wall/isotropic plate. The orthotropic plate shown in Figure 5.17 behaves in a similar manner. The results for these coatings agree with the coatings optimized at the lower Reynolds number. For this non-isotropic wall the orthotropic plate causes little change in the growth rates compared to the isotropic plate results. The growth rates for oblique waves at various frequencies for $\theta = 0^\circ(5000)$ wall/isotropic plate are shown in Figure 5.18. Growth rates over the orthotropic plate are shown in Figure 5.19. Unlike the results from the coatings optimized at the lower Reynolds number, the orthotropic plate has much less effect on reducing the growth rates for the oblique waves. For both plates three-dimensional instabilities are the dominant instability with the instabilities having similar growth rates. As with the comparison between isotropic and non-isotropic walls at the lower Reynolds number, the $\theta = 60^\circ(5000)$ wall has smaller growth rates than the $\theta = 0^\circ(5000)$ wall although there is less difference than the low Reynolds number coatings.

5.5 Travelling-Wave Flutter

To this point we have neglected any consideration of Travelling-Wave Flutter(TWF). The TWF instability was forced to be marginally stable in the choosing of the wall properties. Now consider TWF to determine the growth or decay characteristics of oblique modes compared with the two-dimensional case. Although spatial calculations may be performed using the spectral method, it is easier to carry out the temporal analysis using an asymptotic theory. The asymptotic theory developed by Carpenter and Gajjar (1990) provides a reasonable approximation for the TWF.

We consider first the coatings optimized at $R_{\delta^*} = 2240$. Figure 5.20 shows

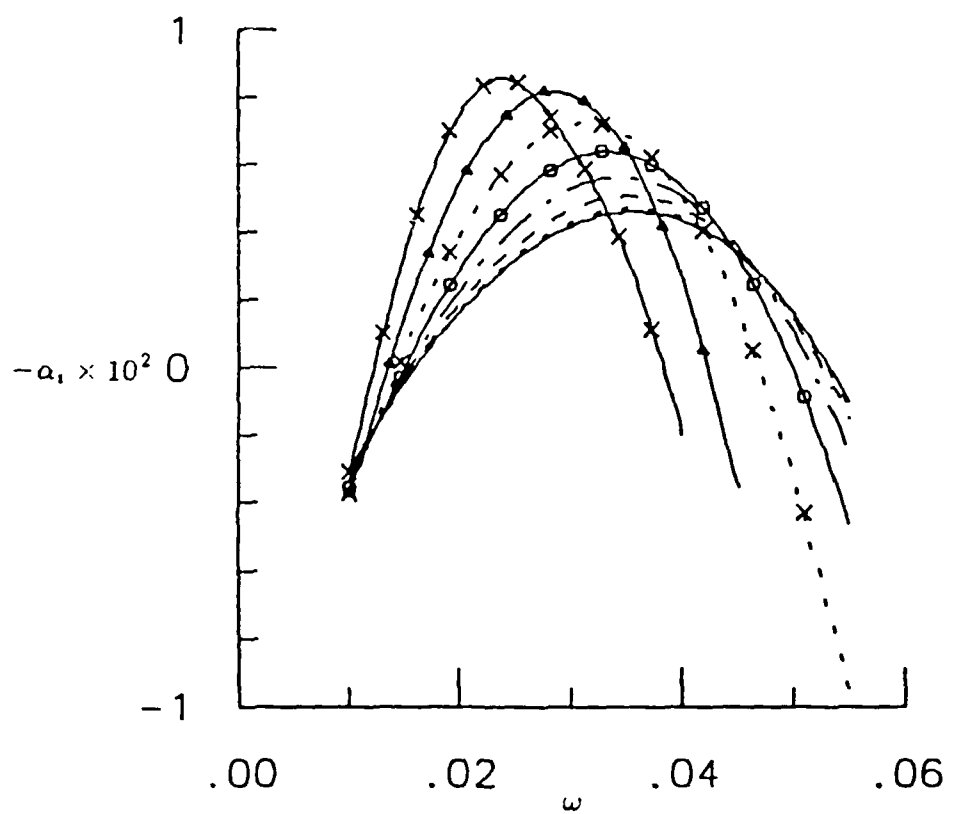


Figure 5.17 Growth rates as a function of frequency for TSI waves over a $\theta = 60^\circ$ (5000) wall/orthotropic plate at $Re_{\theta^*} = 5000$ for oblique wave angles of —, 0° ; $\cdots, 10^\circ$; $\cdots, 20^\circ$; $\cdots, 30^\circ$; $\cdots, 40^\circ$; $\cdots \times \cdots, 50^\circ$; $\cdots \triangle \cdots, 60^\circ$; $\cdots \times \cdots, 70^\circ$.

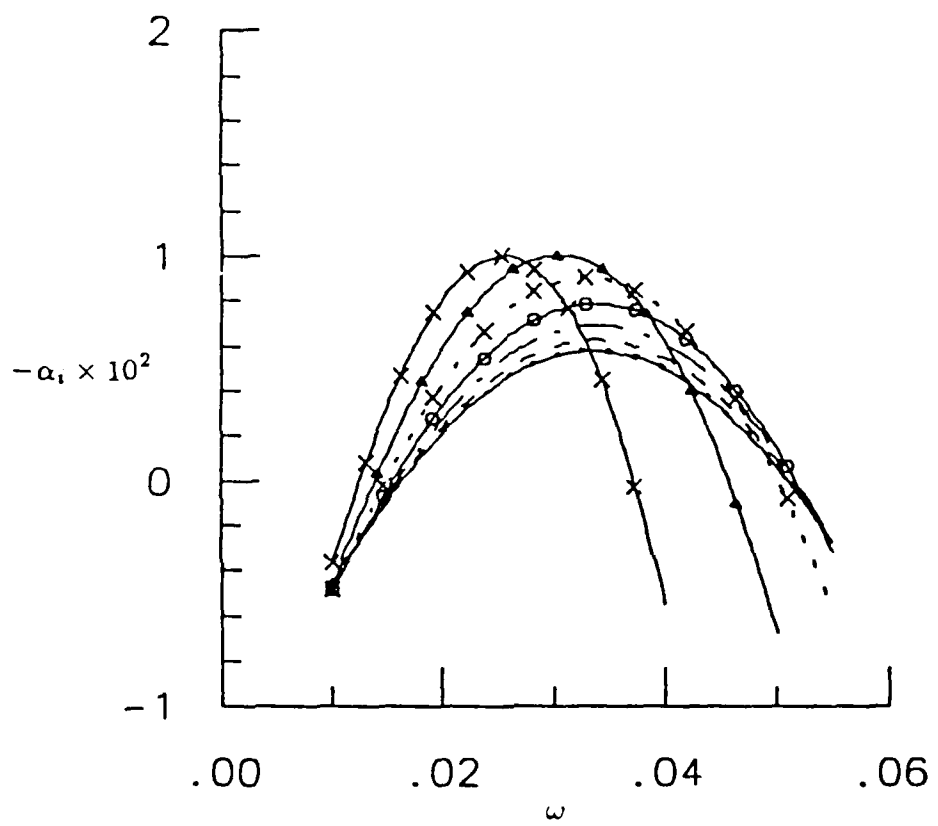


Figure 5.18 Growth rates as a function of frequency for TSI waves over a $\theta = 0^\circ$ (5000) wall/isotropic plate at $Re_\theta = 5000$ for oblique wave angles of —, 0° ; $\cdots, 10^\circ$; — —, 20° ; — · —, 30° ; — o —, 40° ; $\cdots \times \cdots, 50^\circ$; — Δ —, 60° ; — x —, 70° .

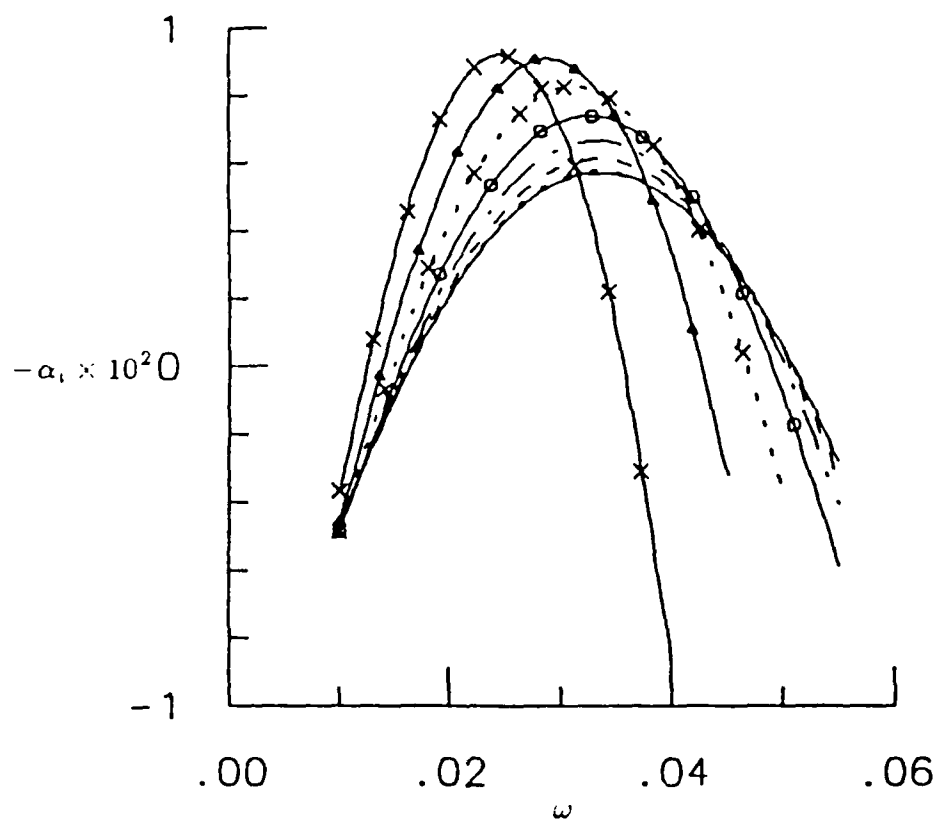


Figure 5.19 Growth rates as a function of frequency for TSI waves over a $\theta = 0^\circ$ (5000) wall/orthotropic plate at $Re_{\theta^*} = 5000$ for oblique wave angles of —, 0° ; ···, 10° ; — —, 20° ; — · —, 30° ; — o —, 40° ; ··· x ···, 50° ; — △ —, 60° ; — x —, 70° .

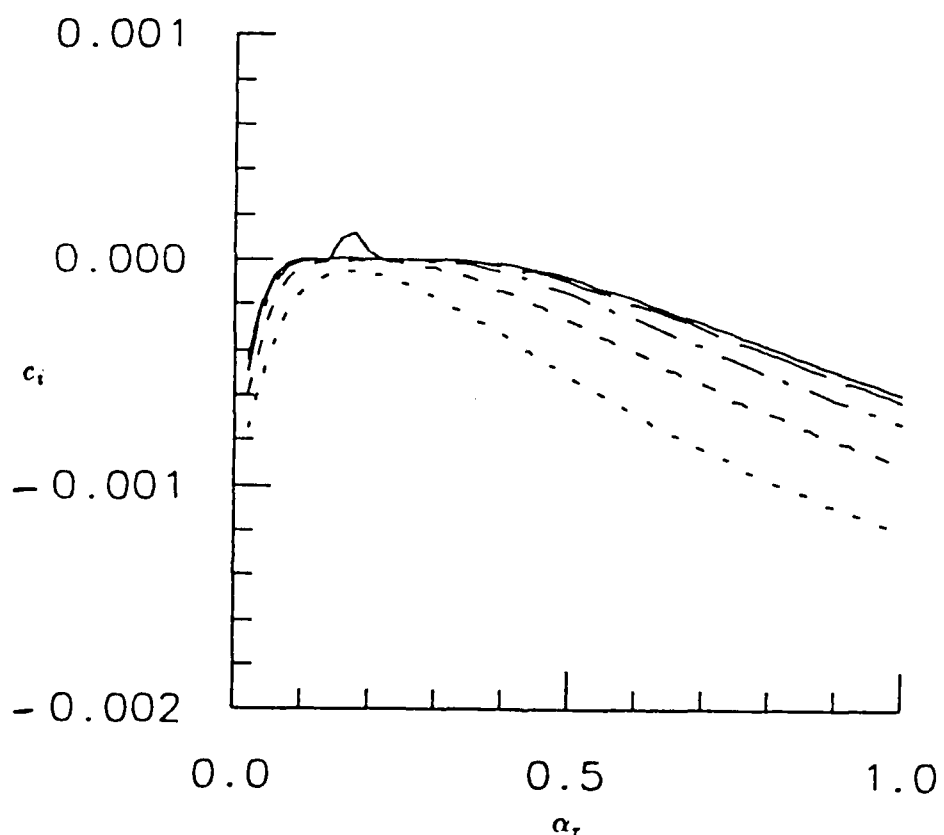


Figure 5.20 Temporal growth rates as a function of wavenumber for TWF over a $\theta = 0^\circ$ (2240) wall/isotropic plate at $Re_{\delta^*} = 2240$ for oblique wave angles of —, 0° ; — —, 15° ; - · -, 30° ; - - -, 45° ; · · ·, 60° . (Carpenter; 1990b).

the temporal growth rates of the TWF as a function of wavenumber for the $\theta = 0^\circ$ (2240) wall/isotropic plate at $R_{\delta^*} = 2240$. As is shown only a narrow band of weakly unstable wavenumbers is found. The oblique waves are more stable than the two-dimensional one. As was stated in the modal classification, mechanisms that destabilize Class A waves tend to stabilize Class B waves. In Figure 5.21, the isotropic plate is replaced with an orthotropic one. Figure 5.21 shows reduced stability for the oblique modes as compared to the two-dimensional waves at the higher wavenumbers. Nevertheless the effect is relatively small and the results suggest that there would be no concern with TWF if orthotropic plates were to be used. The $\theta = 0^\circ$ (2240) wall/isotropic plate is replaced with the $\theta = 60^\circ$ (2240) wall/isotropic plate. Figure 5.22 shows that the temporal growth rates increase with the angle of wave propagation, although the wall is stable with respect to TWF for all angles shown. In Figure 5.23, the isotropic plate is replaced with the orthotropic plate. Similar to the results for the isotropic plate, the temporal growth rates increase with the angle of wave propagation, and yet the wall is stable with respect to TWF for all angles shown. This similar result behavior for $\theta = 60^\circ$ (2240) wall/isotropic plate and $\theta = 60^\circ$ (2240) wall/orthotropic plate for TWF occurred earlier for TSI (Figures 5.10 and 5.12). These calculations were repeated for the walls at a Reynolds number of 5000. The TWF was again found to be stable for all angles.

The non-isotropic wall optimized at $R_{\delta^*} = 2240$ is replaced by the wall optimized at $R_{\delta^*} = 5000$. In this case the bending stiffness provides a larger contribution to the overall wall stiffness. We might expect that an orthotropic plate would be more effective in this case, but a comparison between the results for the isotropic plate in Figure 5.24 and orthotropic plate in Figure 5.25 reveals little change.

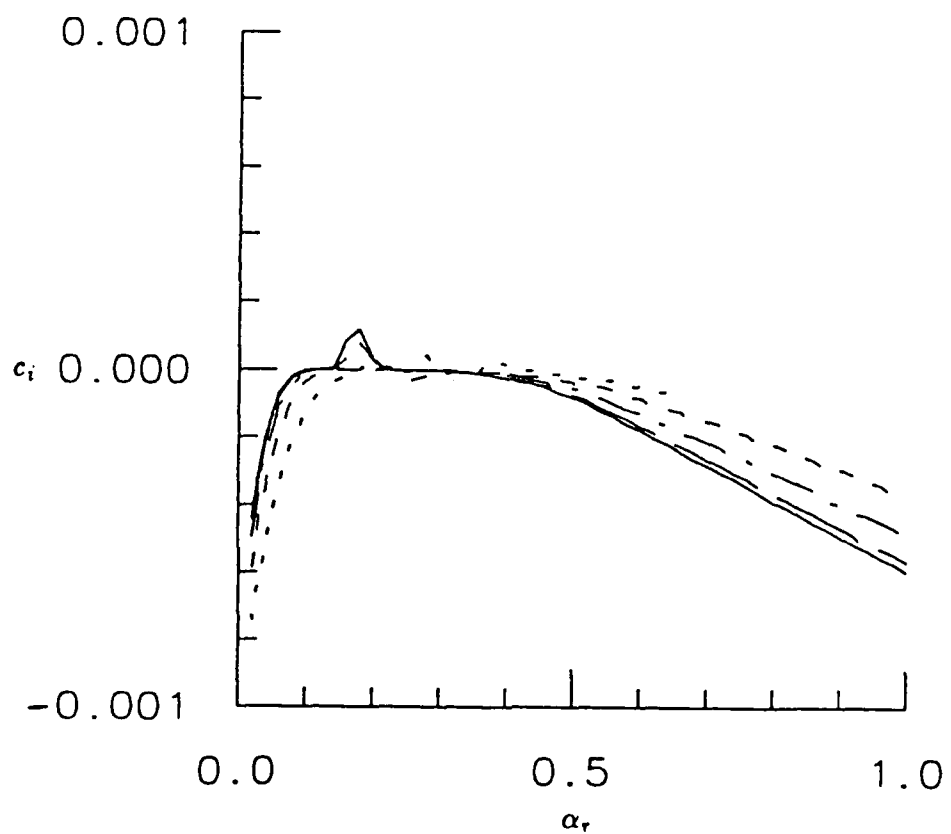


Figure 5.21 Temporal growth rates as a function of wavenumber for TWF over a $\theta = 0^\circ$ (2240) wall/orthotropic plate at $Re_{\delta^*} = 2240$ for oblique wave angles of —, 0° ; — —, 15° ; - · -, 30° ; - - -, 45° ; · · ·, 60° . (Carpenter; 1990b).

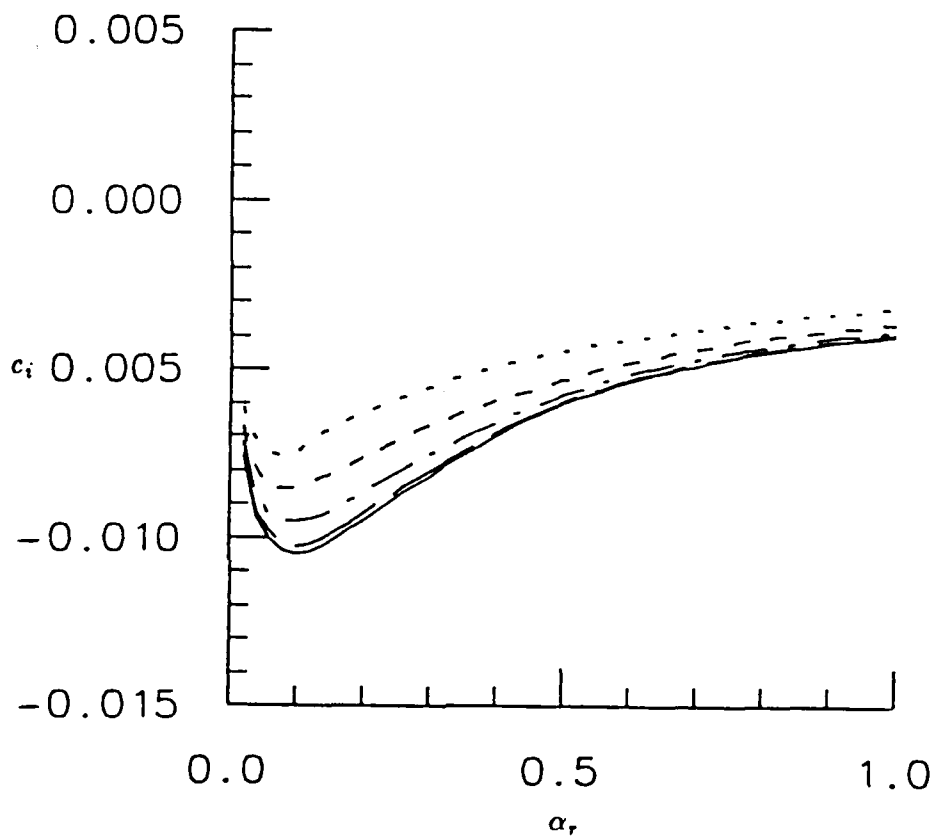


Figure 5.22 Temporal growth rates as a function of wavenumber for TWF over a $\theta = 60^\circ$ (2240) wall/isotropic plate at $Re_{\delta^+} = 2240$ for oblique wave angles of $0^\circ, 15^\circ, 30^\circ, 45^\circ, 60^\circ$. (Carpenter; 1990b).

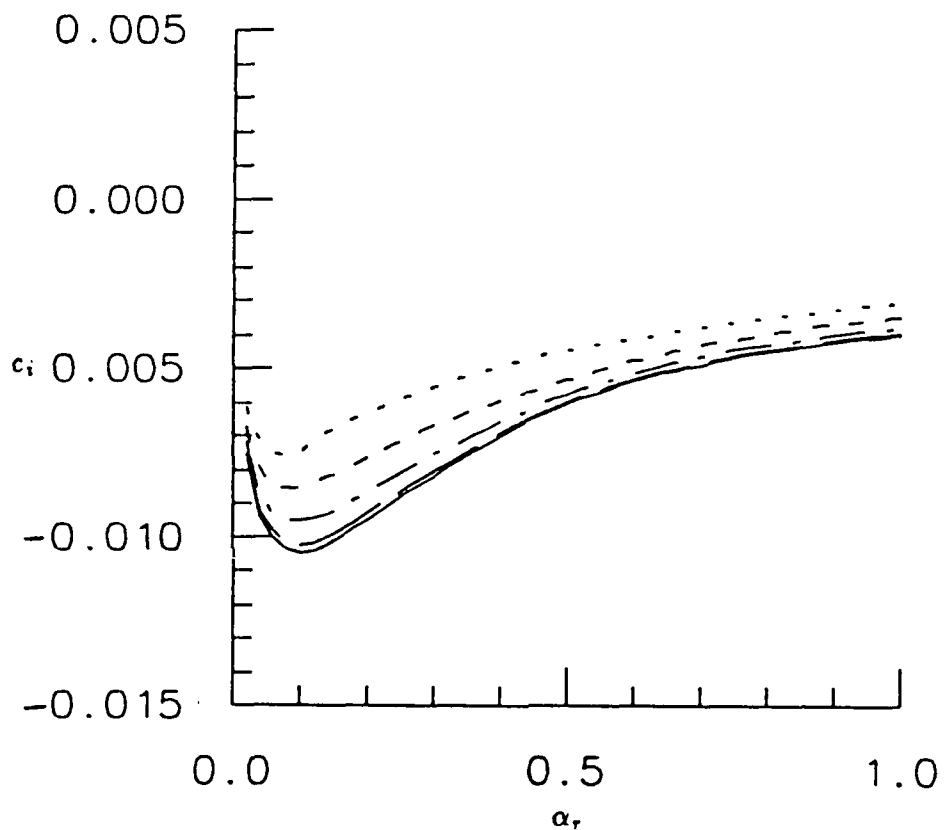


Figure 5.23 Temporal growth rates as a function of wavenumber for TWF over a $\theta = 60^\circ$ (2240) wall/orthotropic plate at $Re_{\theta^*} = 2240$ for oblique wave angles of 0° ; 15° ; 30° ; 45° ; 60° . (Carpenter; 1990b).

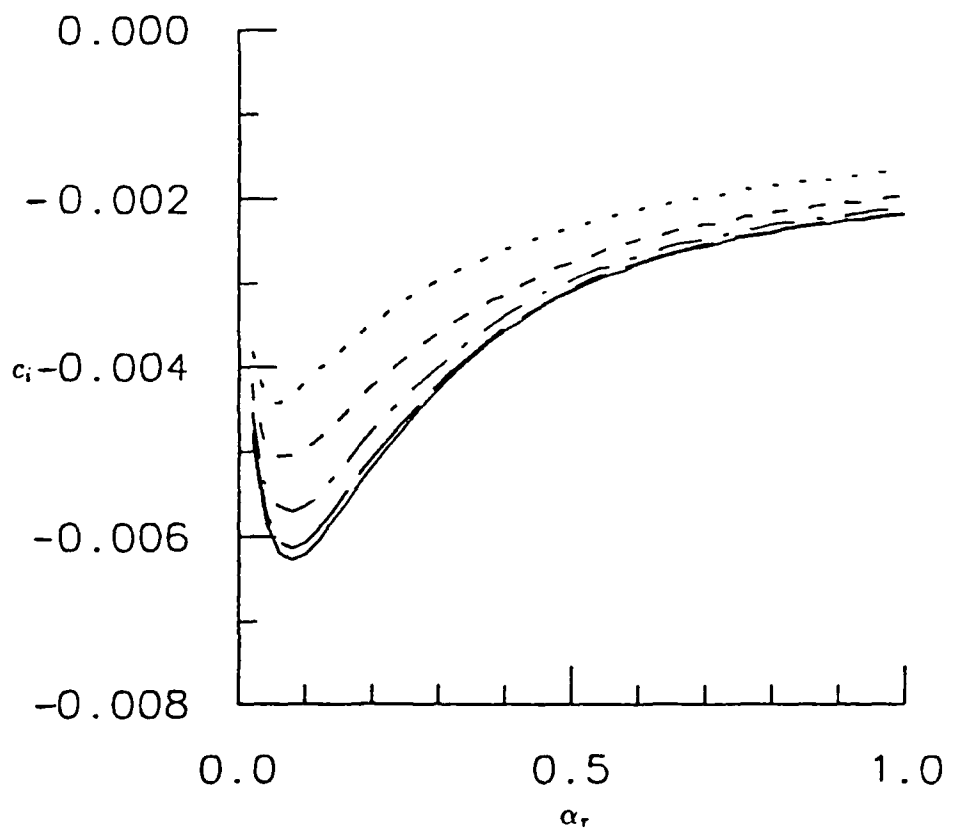


Figure 5.24 Temporal growth rates as a function of wavenumber for TWF over a $\theta = 60^\circ$ (5000) wall/isotropic plate at $Re_{\delta^*} = 5000$ for oblique wave angles of —, 0° ; — —, 15° ; - · -, 30° ; - - -, 45° ; · · ·, 60° . (Carpenter; 1990b).

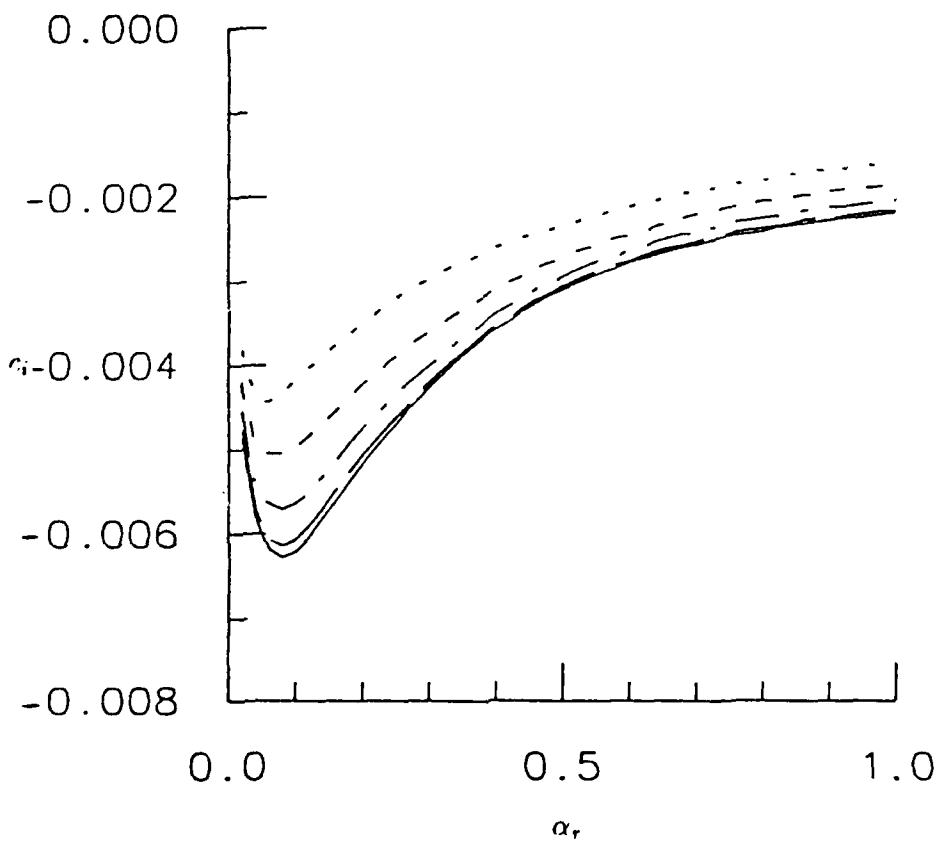


Figure 5.25 Temporal growth rates as a function of wavenumber for TWF over a $\theta = 60^\circ$ (5000) wall/orthotropic plate at $Re_60 = 5000$ for oblique wave angles of 0° ; 15° ; 30° ; 45° ; 60° . (Carpenter; 1990b).

The results for the TWF instabilities have been included to show a comparison between two- and three-dimensional modes. Made evident through the results presented, there would be no problem with TWF for the walls and plates that are used in the present investigation.

5.6 Static-Divergence

The Class A instability, TSI, and the Class B instability, TWF, have been discussed in the two previous sections. A third distinct class of instability which may arise due to wall compliance is Static-Divergence. Unlike the other instabilities, this is an absolute Class C instability dependent on the surface properties that when present alter the surface shape and render a linear analysis of the present kind invalid. An illustration of the instability was shown in Figure 1.5. With Static-Divergence present, any potential transition-delaying characteristics of the coating would be destroyed. Static-Divergence occurs when the freestream velocity exceeds the "Divergence velocity." Carpenter and Garrad (1985) gave a criteria for Divergence for an isotropic wall. Joslin and Morris (1989) extended their formula to account for non-isotropic walls. This is given as

$$U_d = \left[\frac{C_o}{C_a^{1/2}} \right] \quad 5.6.1$$

where

$$C_o = \{(B_z \alpha_d^2 + E_z b \tan^2 \theta + K_E (\alpha_d \cos \theta)^{-2}) / (b \rho_m / \cos^2 \theta)\}^{1/2}$$

$$C_a = \rho / (b \rho_m \alpha_d / \cos^2 \theta)$$

and

$$\alpha_d = [\sqrt{(E_z b \tan^2 \theta)^2 + 12 B_z K_E / \cos^2 \theta} - E_z b \tan^2 \theta] / (6 B_z)^{1/2}$$

For a given freestream velocity, the coating properties under consideration were optimized so that U_d remained above U_∞ , TWF became marginally stable, and

the TSI growth rate became minimal. This was performed for two-dimensional instabilities. In the previous sections, we have already discussed the effect of wall compliance on three-dimensional TWF and TSI instabilities. A question arises as to whether Static-Divergence may be of concern. This question can be answered with relative ease without any calculations. Static-Divergence occurs when the freestream velocity exceeds the Divergence velocity. For three-dimensional instabilities, the compliant wall experiences a reduced effective velocity ($U_\infty \cos \phi$) which is always less than the Divergence velocity. But to confirm this we look at the three-dimensional wall counterpart to (5.6.1). The following relation results

$$U_d = \left[\frac{B_o \gamma_d^3 \cos^2 \theta + E_x b \sin^2 \theta \cos^2 \phi \gamma_d + K_E \gamma_d^{-1}}{\rho_m \cos \phi \cos^2 \theta} \right]^{1/2} \quad 5.6.2$$

where

$$B_o = B_x \cos^4 \phi + 2B_{xz} \sin^2 \phi \cos^2 \phi + B_z \sin^4 \phi$$

and

$$\alpha_d = [\sqrt{(E_x b \sin^2 \theta \cos^2 \phi)^2 + 12B_o K_E \cos^2 \theta - E_x b \sin^2 \theta \cos^2 \phi} / (6B_x \cos^2 \theta)]^{1/2}$$

As an example, the Static-Divergence velocity is calculated for two- and three-dimensional waves over the $\theta = 60^\circ$ (2240) wall/isotropic plate. For the two-dimensional wave, $U_d = 20.003$ which agrees with Joslin and Morris (1989). For an oblique wave travelling with a 10° angle of wave propagation, $U_d = 20.018$. So similar to TWF, Divergence is more stable to three-dimensional instabilities and is of little concern when studying three-dimensional waves.

5.7 2D and 3D e^n -criteria Calculations

The problem of how to extend the e^n method to the case of three-dimensional disturbances has yet to be satisfactorily resolved even for rigid surfaces. Mathe-

matically the problem lies with the fact that for three-dimensional spatially growing disturbances there are, in general, two complex eigenvalues in the form of the complex wavenumbers, α^+ and β^+ . The Orr-Sommerfeld equation plus boundary conditions provides one condition and another needs to be supplied. The appropriate way to resolve this ambiguity would depend on the physical situation to be simulated. For example, a quite different approach would be required for simulating an experiment on Tollmien-Schlichting waves excited by a vibrating ribbon than for natural transition. For the latter case an appropriate initial-value problem would be that corresponding to the development of a wave-packet from a pulsed point source (see Gaster, 1983). A pulsed point source contains all frequencies and is perhaps a better model of the real disturbances leading to natural transition. This is by no means a simple problem and so various *ad hoc*, albeit plausible, assumptions have been advanced in an attempt to extend the e^n method to the case of three-dimensional instabilities. Some of these are discussed briefly below

Strokowski and Orszag (1977) circumvent the problem by calculating temporal three-dimensional instabilities which have only one complex eigenvalue, ω , for specified real wavenumbers, α^+ and β^+ . They then determine the combination of these wavenumbers giving the maximum growth rate at a given real frequency. They use the real part of the group velocity with the Gaster (1962) transformation to obtain approximations for the spatial growth rates in terms of the temporal ones. The real part of the group velocity is also used to define the ray along which the e^n -type integration is performed. Mack (1980) gives an illuminating discussion of the various possibilities. But for his spatial calculations he requires only α^+ to be complex, β^+ being solely real. Cebeci and Stewartson (1980) resolve the ambiguity by imposing the condition that $\partial\alpha^+/\partial\beta^+$ is real. This is equivalent to

the requirement that the wavenumber and growth-rate vectors be parallel. They then look for the direction of maximum growth and take this to define the path of integration for the e^n calculations.

In the present work, Cebeci and Stewartson's approach is closely followed. A recent study by Cebeci and Chen (1989) seems to show that it gives the best results of the methods discussed above when applied to transition prediction in various cases. Nevertheless it is undoubtedly only an approximation and not likely to be all that reliable when the direction of maximum growth is greatly different from that of the mainstream. For many of the cases studied by us the direction of maximum growth made an angle as great as 70° to the mainstream. Consequently, our transition results based on the Cebeci-Stewartson method must be viewed with some caution.

For simplicity we consider the growth of disturbances initiated at the lower branch of the two-dimensional neutral curve for each coating. This is a somewhat more conservative approach even compared to the approximate procedure used by Cebeci and Stewartson (1980) who begin their calculations on a sort of three-dimensional neutral curve which they termed the "Zarf." Since the growth rates, for both two- and three-dimensional instability waves, are small in this region it is not expected that the predicted transition Reynolds number will be significantly different. The instability is then allowed to seek the angle of wave propagation in which it has a maximum growth rate. The wave is then traced as it convects downstream and the growth rates are used to determine the amplification of the wave. The amplification is given by

$$\ln \frac{A}{A_0} = - \int_{(x_0, z_0)}^{(x, z)} \gamma_i(x) d(x, z) \quad 5.7.1$$

where A_0 is the initial amplitude of the disturbance at (x_0, z_0) . The e^n method is

based on the observation that when the amplification of the disturbance reaches some value- n which is equivalent to (5.7.1), transition occurs (or is imminent). As the waves travel downstream at fixed increments of the streamwise coordinate, x , values of the growth rate and the direction of wave propagation, ϕ , are retained. Although the spanwise incremental step is not known exactly, as it is a continuous function of x , a second order approximation is made with the known local values of ϕ and x . From this the spanwise increment is obtained. This gives a possible error of ± 1 degree in the propagation angle for integrations in the low frequency range.

To confirm these local observations e^n calculations have been performed. Figure 5.26 shows curves of maximum amplification for two-dimensional waves in the frequency range of interest for the compliant and rigid walls. The two-dimensional case agrees with Carpenter and Morris (1990). Figure 5.27 shows the same curves with the amplification of waves at a few frequencies. These curves for a given frequency, indicate the amplification of a wave as it grows from branch I downstream to branch II. Some controversy exists as to which value of n is the proper indication of transition. But if we choose a conservative value of $n = 7$ a delay of approximately 4-5 times the rigid wall transition Reynolds number is realized. However, for higher values of n the advantages of the wall compliance increase. Figure 5.28 shows similar calculations for the three-dimensional disturbances over the $\theta = 60^\circ(2240)$ wall. Instabilities travelling over isotropic and orthotropic plates for the $\theta = 60^\circ(2240)$ wall lead to similar maximum amplification curves. This is in agreement with the local calculations given above. A decrease from the two-dimensional transition delay occurs, but a transition delay remains compared to the rigid wall results. The same calculations for the $\theta = 0^\circ(2240)$ wall illustrated in Figure 5.29 show a notable difference between the

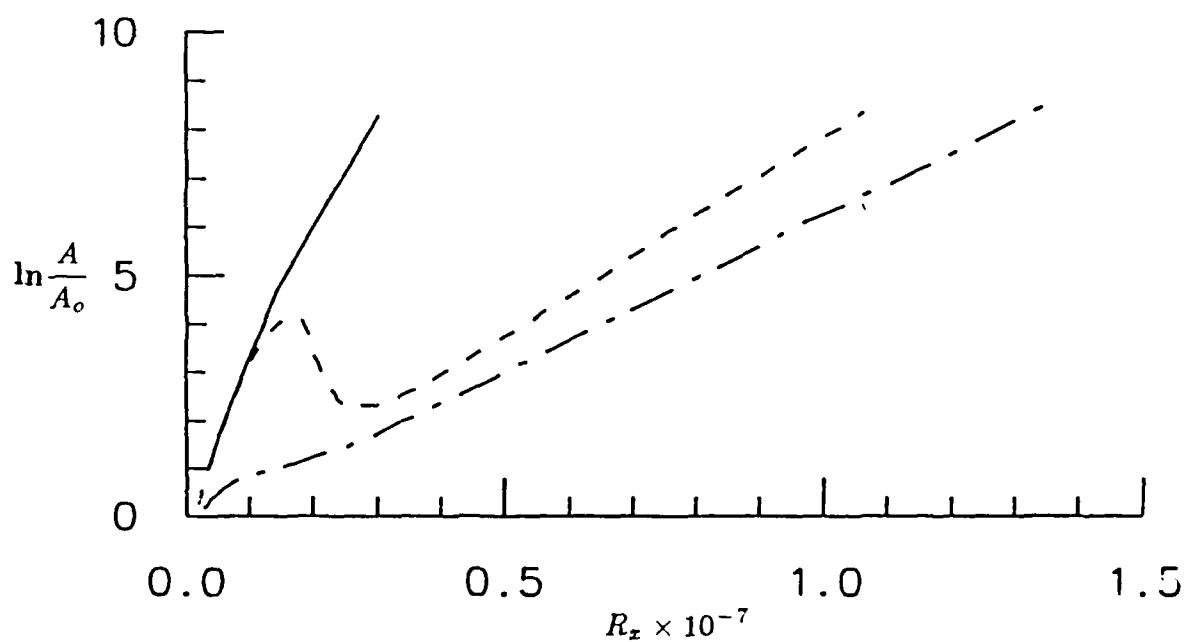


Figure 5.26 Two-dimensional curves of maximum amplification for TSI waves over a —, rigid wall; - - -, $\theta = 0^\circ$ (2240) wall; and - · -, $\theta = 60^\circ$ (2240) wall.

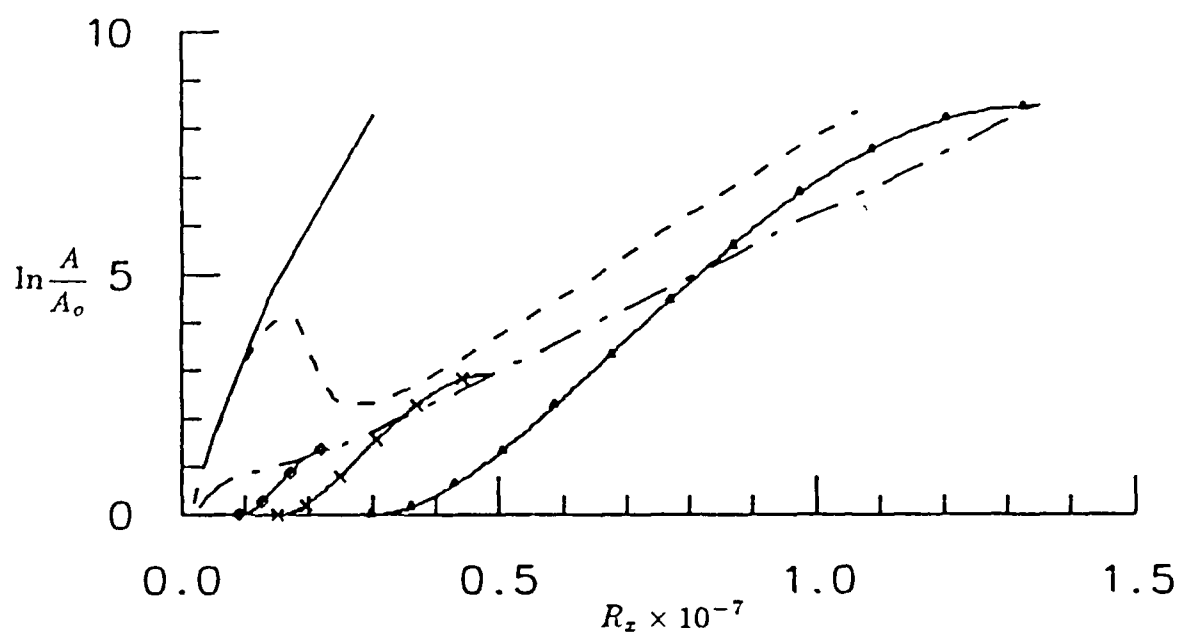


Figure 5.27 Two-dimensional curves of maximum amplification for TSI waves over a —, rigid wall; - - -, $\theta = 0^\circ$ (2240) wall; and - · -, $\theta = 60^\circ$ (2240) wall. Frequencies of: $Fr = -o-, 25.6$; $-x-, 15.4$; and $-\Delta-, 8.1$ over the $\theta = 60^\circ$ (2240) compliant wall.

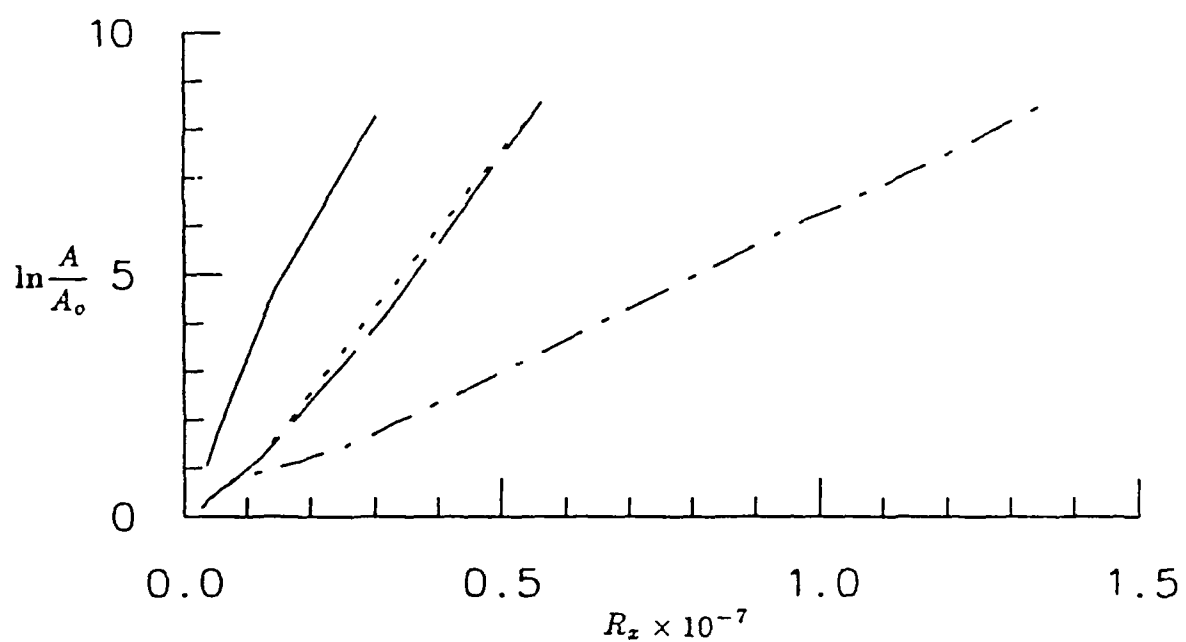


Figure 5.28 Two- and three-dimensional curves of maximum amplification for TSI waves over a —, 2D rigid wall; - · -, 2D $\theta = 60^\circ$ (2240) wall; — —, 3D $\theta = 60^\circ$ (2240) wall/orthotropic plate; and · · ·, 3D $\theta = 60^\circ$ (2240) wall/isotropic plate.

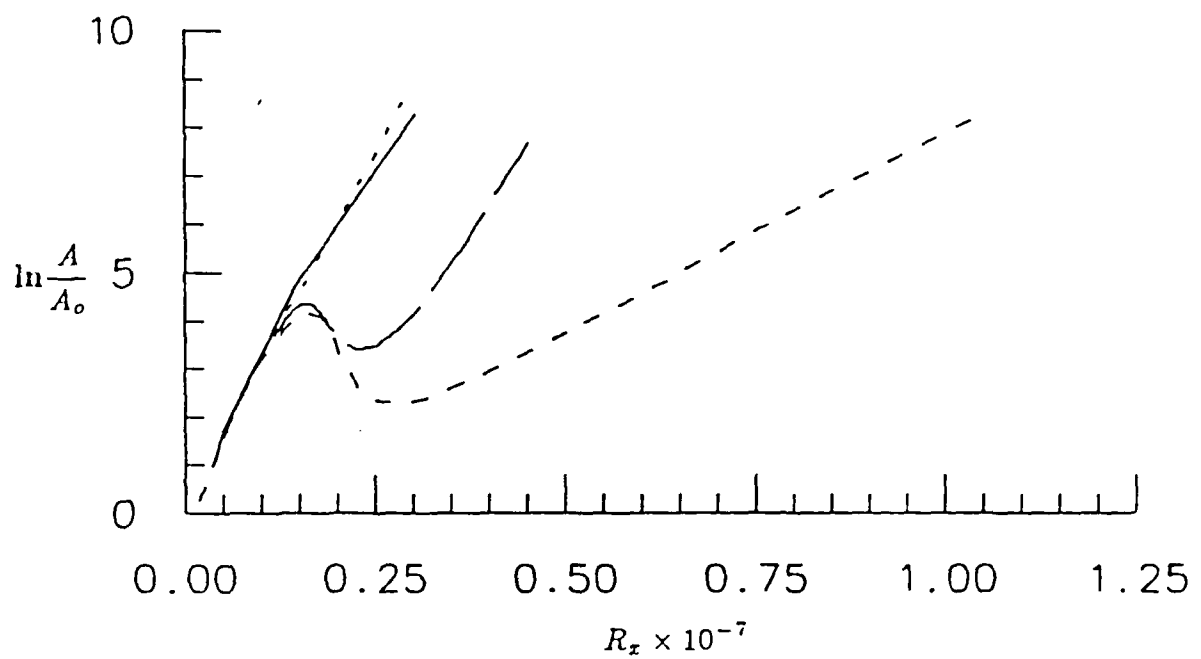


Figure 5.29 Two- and three-dimensional curves of maximum amplification for TSI waves over a —, 2D rigid wall; - - -, 2D $\theta = 0^\circ$ (2240) wall; — —, 3D $\theta = 0^\circ$ (2240) wall/orthotropic plate; and · · ·, 3D $\theta = 0^\circ$ (2240) wall/isotropic plate.

isotropic and orthotropic plate cases. In fact the results for the isotropic plate case approach the rigid wall results. No transition delay would be expected. The orthotropic plate shows a notable delay of transition and agrees with the proposed introduction of additional spanwise compliance as suggested by Yeo and Carpenter.

Two-dimensional e^n calculations have been performed for the $\theta = 0^\circ(5000)$ and $\theta = 60^\circ(5000)$ walls. Figure 5.30 shows the curves of maximum amplification for these walls. From the figure we find that the amplification of high frequency disturbances over the isotropic wall behave similar to those for the rigid wall. If the chosen $n = 7$ value indicates transition, then transition for this wall may occur at the same Reynolds number as the rigid wall. The reader must bear-in-mind that the value of n was chosen conservatively and a more realistic value might be $n = 8.5 - 9$. With this being the situation, both $\theta = 0^\circ(5000)$ and $\theta = 60^\circ(5000)$ walls would lead to considerable transition delay of 7-10 times the rigid wall transition Reynolds number. Similar to the walls optimized at the lower Reynolds number, the non-isotropic wall provides higher transition delays than the isotropic wall.

We now compare the isotropic and non-isotropic walls which are optimized at the different Reynolds numbers. Curves of maximum amplification are shown in Figure 5.31 for the isotropic walls and Figure 5.32 for the non-isotropic walls. For the isotropic walls, similar behavior is found for the amplification curves. The $\theta = 0^\circ(5000)$ wall provides a higher transition delay potential than the $\theta = 0^\circ(2240)$ wall. For the non-isotropic walls, the behavior of the results is much different for the two cases. The $\theta = 60^\circ(5000)$ wall provides a much greater transition delay than the $\theta = 60^\circ(2240)$ wall. The higher the choice of n the better the $\theta = 60^\circ(5000)$ wall is for obtaining transition delays. One might then expect

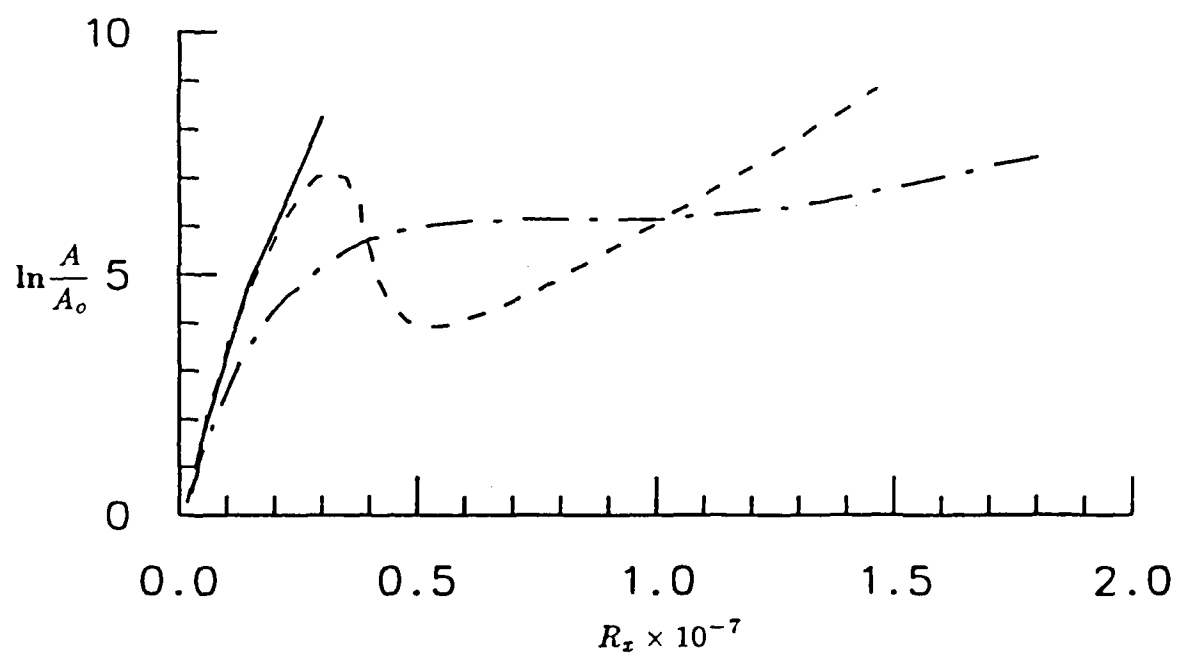


Figure 5.30 Two-dimensional curves of maximum amplification for TSI waves over a —, rigid wall; - - -, $\theta = 0^\circ$ (5000) wall; and - · -, $\theta = 60^\circ$ (5000) wall.

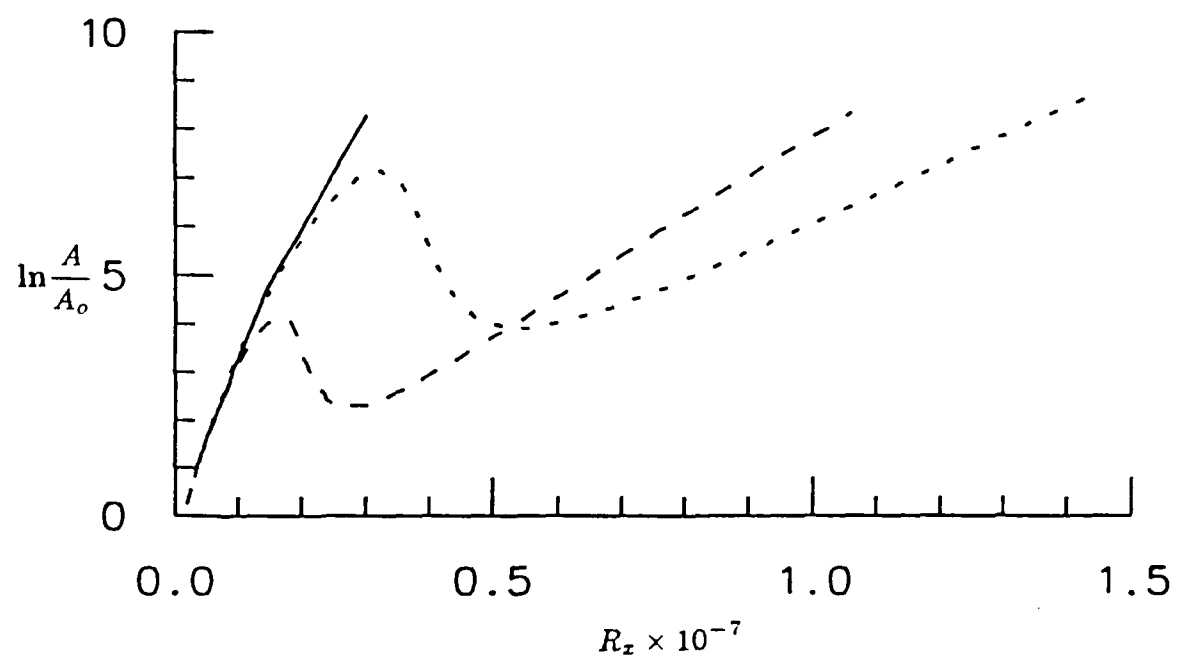


Figure 5.31 Two-dimensional curves of maximum amplification for TSI waves over a —, rigid wall; - - -, $\theta = 0^\circ$ (2240) wall; and · · ·, $\theta = 0^\circ$ (5000) wall.

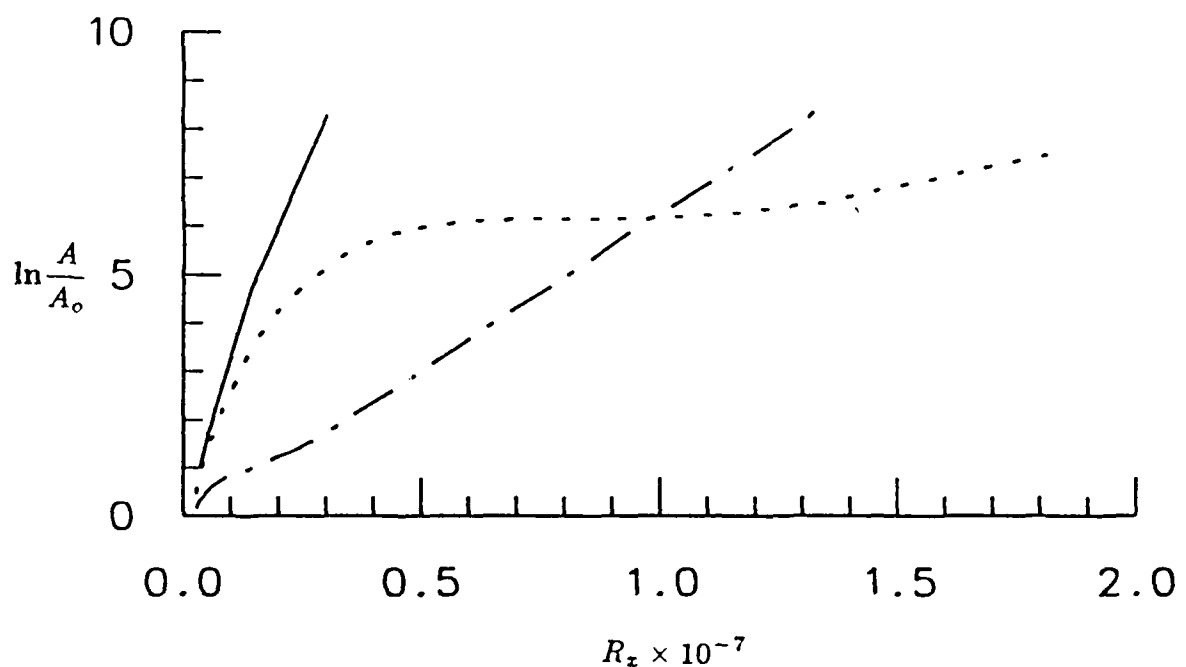


Figure 5.32 Two-dimensional curves of maximum amplification for TSI waves over a —, rigid wall; - · -, $\theta = 60^\circ$ (2240) wall; and · · ·, $\theta = 60^\circ$ (5000) wall.

that this wall would lead to significant transition delays even when three-dimensional instabilities are present.

Three-dimensional e^n calculations have been performed for the $\theta = 60^\circ(5000)$ wall and are shown in Figure 5.33. Only a few frequencies were considered in these calculations and these results are shown as circles in the figure. As before the oblique modes dominate transition. Except, with this wall, the delay of transition has decreased to only a factor of 1.4 over the rigid wall case. Additionally, the orthotropic plate is found to have no effect on reducing the amplification of the instabilities for the $\theta = 60^\circ(5000)$ wall which is similar to what was shown earlier for the $\theta = 60^\circ(2240)$ wall (Figure 5.28). Previous two-dimensional e^n results (Figure 5.30) indicated that this wall had a much stronger potential for transition delays as compared with the walls optimized at a Reynolds number of 2240. However, the present calculations reveal that this is not the case and with three-dimensional instabilities, the non-isotropic wall optimized at the lower Reynolds number leads to greater transition delays. It is evident for this wall that the three-dimensional growth rates are so large that the delay of transition potential for this wall is destroyed.

Shown in Figures 5.34 and 5.35 are the variation of the angle of wave propagation for maximum growth with downstream distance for waves of several frequencies propagating over the $\theta = 60^\circ(2240)$ wall/isotropic plate and $\theta = 60^\circ(2240)$ wall/orthotropic plate, respectively. Similar results are shown in Figures 5.36 and 5.37 for the $\theta = 0^\circ(2240)$ wall for the isotropic and orthotropic plates. The high frequency waves are predominantly two-dimensional. As the wave frequency decreases the waves propagate with increasing obliqueness. This begins at the lower branch of the neutral curve. As the waves travel downstream their angle of wave propagation becomes more two-dimensional. One might expect that for the

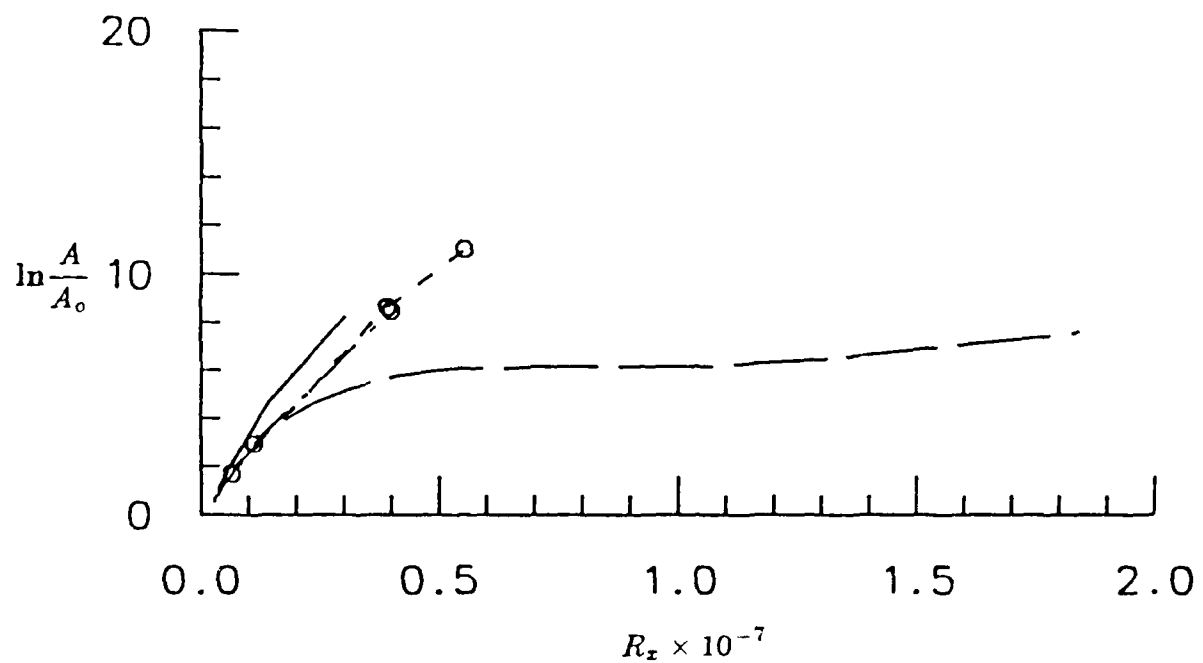


Figure 5.33 Two- and three-dimensional curves of maximum amplification for TSI waves over a —, 2D rigid wall; - - -, 2D $\theta = 60^\circ$ (5000) wall; — —, 3D $\theta = 60^\circ$ (5000) wall/orthotropic plate; and · · ·, 3D $\theta = 60^\circ$ (5000) wall/isotropic plate. (o-calculated values).

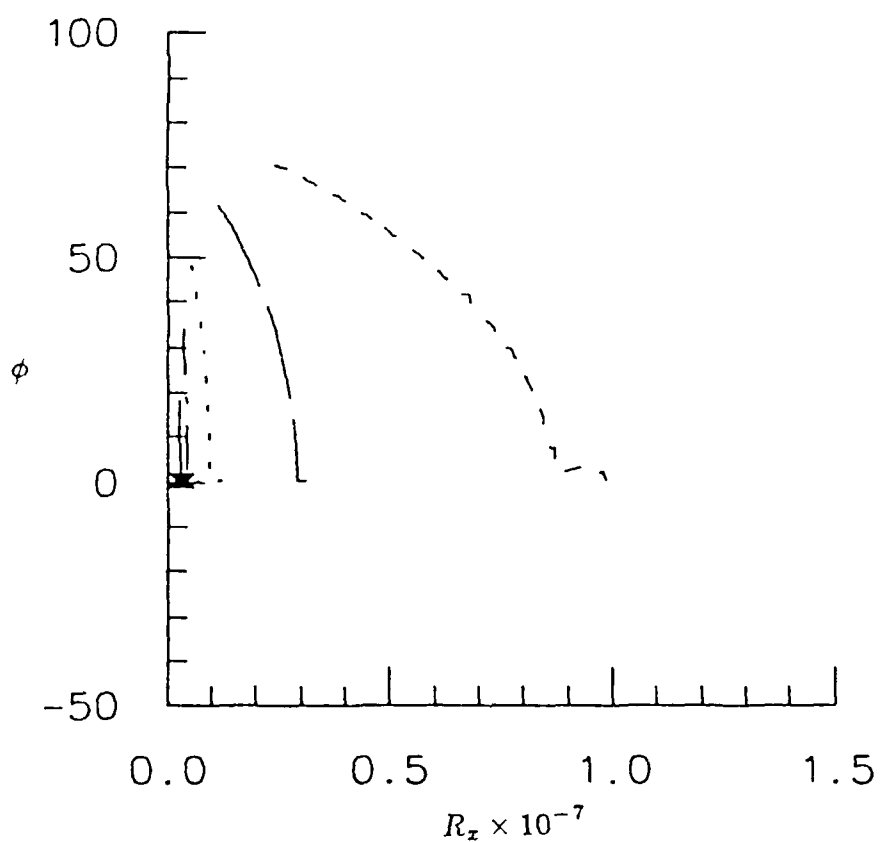


Figure 5.34 The angle of wave propagation as a function of Reynolds number for the most unstable TSI wave over a $\theta = 60^\circ$ (2240) wall/isotropic plate for frequencies of: $Fr = -\times-, 99.3$; $---$, 89.5; $--\cdot-$, 67.0; \cdots , 42.3; $-\cdots-$, 20.9; and $--\cdots-$, 9.8.

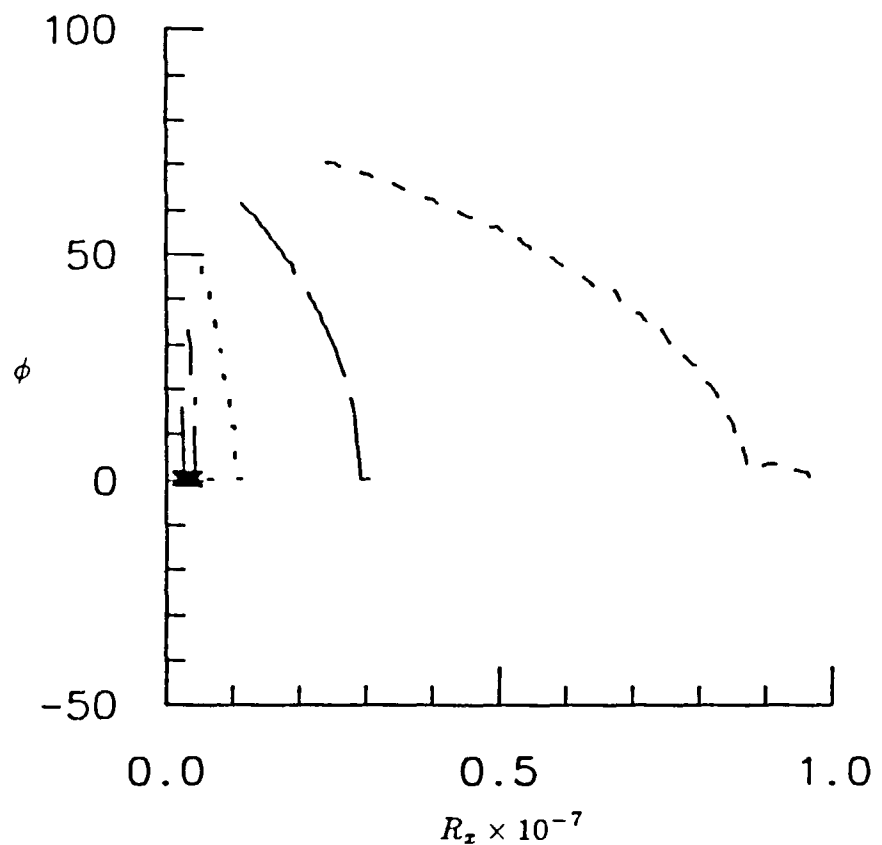


Figure 5.35 The angle of wave propagation as a function of Reynolds number for the most unstable TSI wave over a $\theta = 60^\circ$ (2240) wall/orthotropic plate for frequencies of: $Fr = - \times -$, 99.3; —, 89.5; - - -, 67.0; · · ·, 42.3; — —, 20.9; and - - -, 9.8.

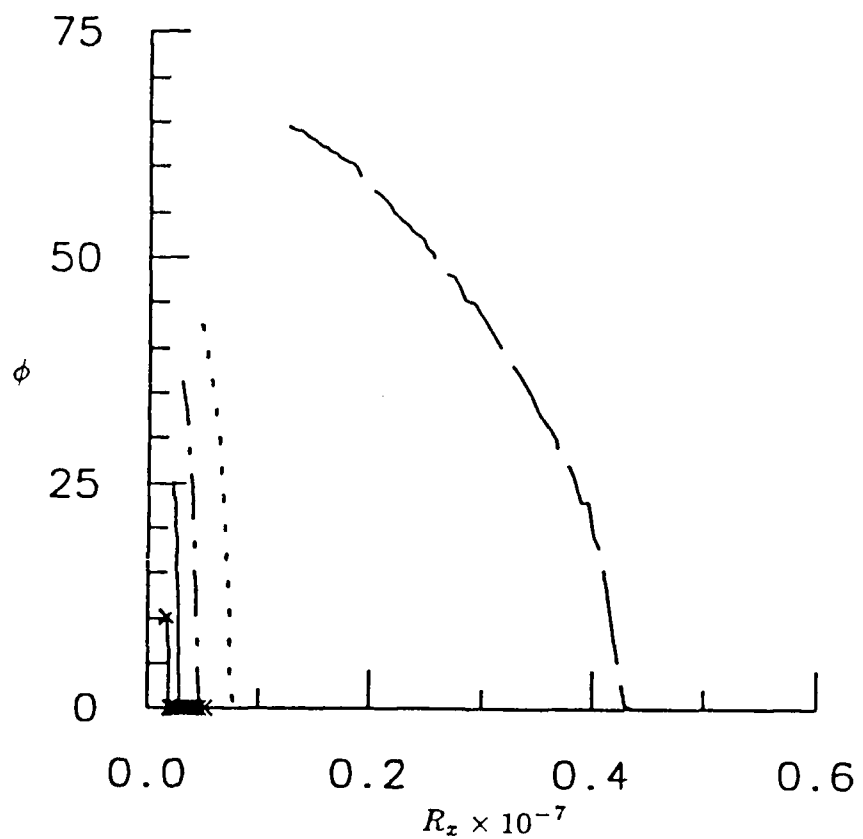


Figure 5.36 The angle of wave propagation as a function of Reynolds number for the most unstable TSI wave over a $\theta = 0^\circ$ (2240) wall/isotropic plate for frequencies of: $Fr = - \times -$, 99.7; —, 82.4; - · -, 62.0; · · ·, 41.1; and — —, 15.8.

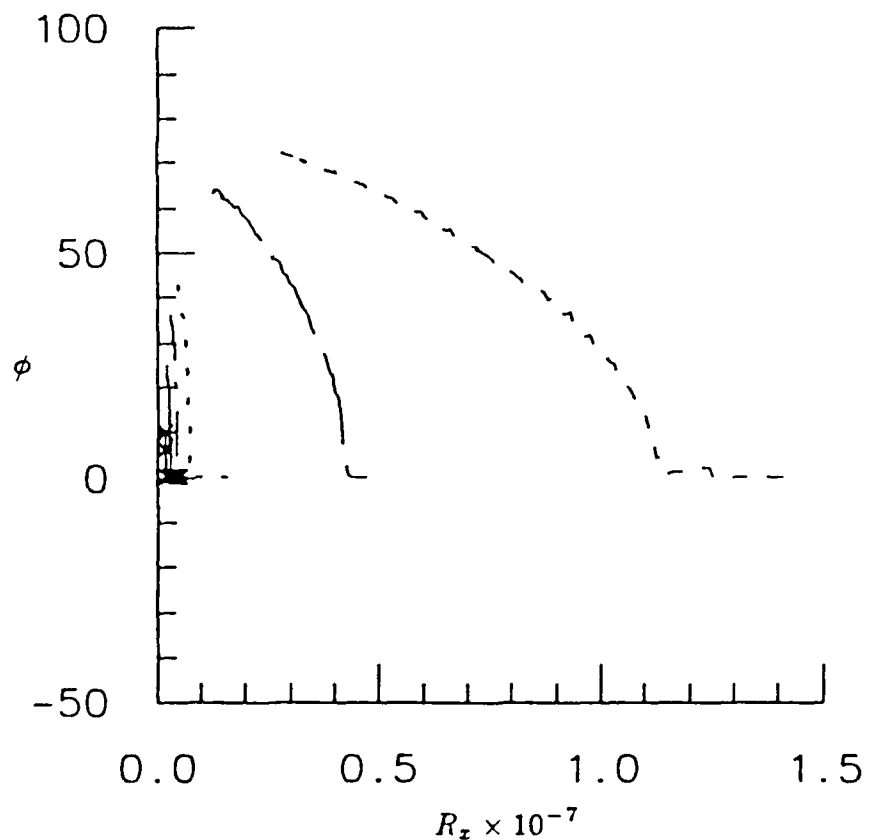


Figure 5.37 The angle of wave propagation as a function of Reynolds number for the most unstable TSI wave over a $\theta = 0^\circ$ (2240) wall/orthotropic plate for frequencies of: $Fr = - \times -$, 99.7; $Fr = -$, 82.4; $Fr = - \cdot -$, 62.0; $Fr = \cdots$, 41.1; $Fr = - - -$, 15.8; and $Fr = - - -$, 8.0.

plate-spring compliant wall model under consideration that for low R_z and high frequencies or for sufficiently high R_z and low frequencies the wall responds as a rigid wall and two-dimensional waves would dominate. For the $\theta = 60^\circ$ (2240) wall, waves propagating over the isotropic and orthotropic plates travel in similar trajectories. That is, at downstream distances, the dominant instability wave is propagating at the same (or nearly the same) angle of wave propagation. For the $\theta = 0^\circ$ (2240) wall, waves travel in a different manner over the isotropic and orthotropic plates. For the wave angles shown in Figure 5.36 for the isotropic plate, waves at a given frequency propagate at larger angles than the waves for the orthotropic plate shown in Figure 5.37.

This concludes our presentation of the primary instability results for the present study. From these results, we conclude that three-dimensional primary instabilities dominate transition over the compliant walls considered; yet, transition delays occur compared with the rigid wall case. More detailed conclusions will be made in Chapter 7. In the second part of the present study, the effect of compliant walls on secondary instabilities that result from two- and three-dimensional primary waves is determined. The results of this fluid/wall interaction study are given in the next chapter.

CHAPTER 6

RESULTS OF THE SECONDARY INSTABILITY ANALYSIS

6.1 Rigid Wall Verification

In the previous chapter, we showed that a delay of boundary layer transition could be attained through the use of compliant walls in an analysis considering the linear instability behavior only. In this chapter, the effect of wall compliance on the secondary instability mechanisms in transition is determined. Before the compliant wall is introduced, results from the spectral and shooting methods are verified for the rigid wall. In all of the cases considered for the solutions of secondary instabilities, the freestream velocity (U_∞) is 20 m/s, the density (ρ) is 1000 kg/m³, and the kinematic viscosity (ν) is 1×10^{-6} m²/s.

6.1.1 Subharmonic Disturbance

To be consistent with Herbert's terminology, hereafter the TSI wave is referred to as the primary instability. For the two-dimensional primary instability wave propagating over a rigid wall, results for the subharmonic mode of secondary instability are compared with Herbert (1985). Spectral convergence is shown in Table 6.10 for $R_\delta = 880$, $Fr = 58.8$, $\beta = 0.214$, and $A = 0.00695$. For our purposes 35 polynomials are sufficient for convergence on the dominant instability. From Lancaster's local refinement method and the shooting method, $\sigma = 0.00418$ is obtained. 35 collocation points are used for the primary wave; and the domain extends to $y_{max} = 15$. These results differ slightly from Herbert who obtained $\sigma = 0.00407$. This difference may be expected since the secondary instabilities are very sensitive to parameter changes. In Table 6.11, the effect of the secondary growth rate on the spanwise wavenumber variation is shown.

Table 6.10: Spectral convergence of temporal eigenvalues for the subharmonic mode of secondary instability for a two-dimensional primary wave over a rigid wall for $R_\delta = 880$, $Fr = 58.8$, $A = 0.00695$, $\beta = 0.214$ and $\alpha = 0.15488 - i0.005504$. (IBM 3090)

N	σ_1	$\sigma_{2,3}$	cpu(s)
15	0.0032924		2.99
20	0.0039769	0.0007067 \pm i0.010675	4.86
25	0.0041494	0.0011586 \pm i0.010510	7.91
30	0.0041667	0.0011565 \pm i0.010456	12.20
35	0.0041714	0.0011640 \pm i0.010448	18.11
40	0.0041713	0.0011628 \pm i0.010448	25.29
45	0.0041713	0.0011628 \pm i0.010448	35.05

Table 6.11: Variation of the spanwise wavenumber β for the subharmonic mode of secondary instability for a two-dimensional primary wave over a rigid wall for $R_\delta = 880$, $Fr = 58.8$, $A = 0.00695$, and $\alpha = 0.15488 - i0.005504$. (IBM 3090)

β	σ_1
0.214	0.004181
0.216	0.004150
0.218	0.004123
0.220	0.004095
0.222	0.004067

For small changes in the spanwise wavenumber, Herbert's results are obtained. Similar results may be obtained with small changes in the Reynolds number or primary wave amplitude. To further confirm that the approach is correct for the two-dimensional waves, Table 6.12 shows a comparison between the present results with Herbert (1983) for a very specific set of parameters. The present results agree with Herbert's.

Table 6.12: Comparison of the present results with Herbert (1983) for the unstable modes of the subharmonic mode of secondary instability for a two-dimensional primary wave over a rigid wall for $R_\delta = 826.36$, $Fr = 83$, $\beta = 0.18$ and $\alpha = 0.1949$. (IBM 3090)

Herbert	
$A = 0.02$	$A = 0.01$
0.01184	0.00860
$0.00558 \pm i0.01548$	$0.00331 \pm i0.01297$

present results	
$A = 0.02$	$A = 0.01$
0.011825	0.008565
$0.005588 \pm i0.01553$	$0.003308 \pm i0.01302$

The eigenfunctions may be obtained from either local method as outlined in Chapter 4. The velocity distribution is given by

$$u_3 = B \cos \beta z' [u_1 u_1^* + u_{-1} u_{-1}^*]^{1/2} \quad 6.1.1$$

The normalized u_3 -eigenvector is shown for the shooting and spectral methods

compared to the experimental results of Kachanov and Levchenko (1984) in Figure 6.1. Similar to what Herbert showed, this particular theory agrees quite well with the present experimental evidence.

In this section, we have shown that the present approach for subharmonic disturbances agree with published results for the rigid wall case.

6.1.2 Fundamental Disturbance

In a similar manner to the subharmonic mode, the present results are compared with Herbert (1985) for the rigid wall case. For $R_f = 880$, $Fr = 58.8$, $\beta = 0.214$ and $A = 0.00695$, the spectral convergence results are shown in Table 6.13. Reasonable convergence is attained with 35 polynomials. For these parameters, Herbert obtained $\sigma = 0.00084$. Again, a small difference between the present results and Herbert's exists. From Table 6.14, a small variation in the spanwise wavenumber yields comparable results.

The methods for determining the eigenfunctions are the same as were demonstrated for the subharmonic mode and the velocity distribution is determined by

$$u_3 = B \cos \beta z' [u_0 u_0^* + u_2 u_2^* + u_{-2} u_{-2}^*]^{1/2}. \quad 6.1.2$$

This completes the verification of the present theoretical approach for secondary instabilities over a rigid wall.

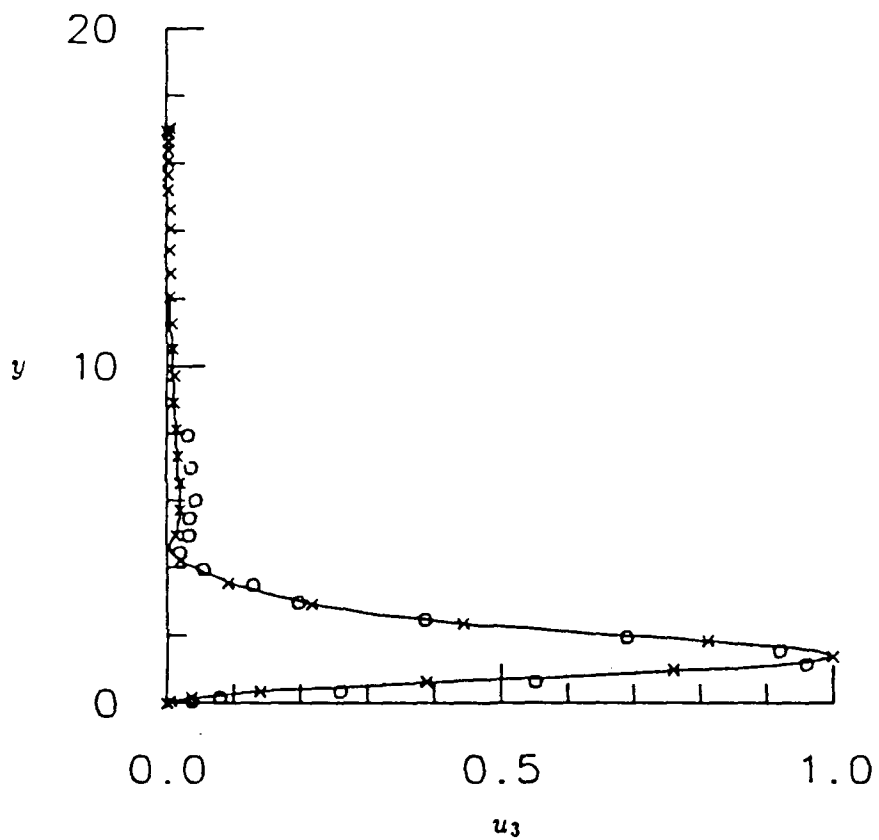


Figure 6.1 Comparison of the u_3 -distribution of a subharmonic disturbance at $R_\delta = 608$, $Fr = 124$, and $\bar{b} = 0.33$ for the —, shooting method; - \times -, spectral method; and o, Kachanov and Levchenko (1984).

Table 6.13: Spectral convergence of temporal eigenvalues for the fundamental mode of secondary instability for a two-dimensional primary wave over a rigid wall for $R_\delta = 880$, $Fr = 58.8$, $A = 0.00695$, $\beta = 0.214$ and $\alpha = 0.15488 - i0.005504$. (Cray Y/MP)

N	σ_1	cpu(s)
10	0.00013363	0.61
15	0.00028380	1.12
20	0.00091129	1.97
25	0.00087073	3.35
30	0.00090107	5.25
35	0.00091794	8.78
40	0.00091743	12.11
45	0.00091831	16.73

Table 6.14: Variation of the spanwise wavenumber β for the fundamental mode of secondary instability for a two-dimensional primary wave over a rigid wall for $R_\delta = 880$, $Fr = 58.8$, $A = 0.00695$, and $\alpha = 0.15488 - i0.005504$. (IBM 3090)

β	σ_1
0.214	0.000917
0.216	0.000908
0.218	0.000899
0.220	0.000890
0.222	0.000880

6.2 Introduction of Wall Compliance

In this section, compliant walls are introduced for the secondary instability analysis. Due to the computational cost involved with this type of study, we will only look at the $\theta = 0^\circ$ (2240) and $\theta = 60^\circ$ (2240) compliant walls with isotropic plates. Hereafter, these coatings are simply termed isotropic and non-isotropic compliant walls.

6.2.1 Subharmonic Disturbance

To simulate the rigid wall, $C_M \rightarrow \infty$ in the mechanical model. For $R_\delta = 880$, $Fr = 58.8$ and $A = 0.00695$, spectral convergence is shown in Table 6.15 for the rigid wall simulation. Sufficient convergence is obtained with the same number of polynomials as the rigid wall problem. Some of these calculations require in excess of 30Mbytes of virtual memory, so supercomputers are invaluable. To determine how many polynomials are required to converge to an eigenvalue for the compliant wall case, the isotropic wall is considered for the same Reynolds number and frequency. The spectral convergence results are shown in Table 6.16. For our purposes sufficient convergence is attained with 40 polynomials. The local spectral method requires as much cpu time as the global and achieves the same values. This cost arises in the local method since the matrix size is very large and matrix inversions are required for each iteration. These results are for a two-dimensional primary wave. The same cost and requirements occur for the three-dimensional primary wave, since the secondary instability analysis is three-dimensional for both cases.

Table 6.15: Spectral convergence of temporal eigenvalues for the subharmonic mode of secondary instability for a two-dimensional primary wave over a rigid wall ($C_M \rightarrow \infty$) for $R_\delta = 880$, $Fr = 58.8$, $A = 0.00695$, $\beta = 0.214$ and $\alpha = 0.15488 - i0.005504$ by the Bernoulli method with three iterations. (IBM 3090)

N	σ_1	$\sigma_{2,3}$	cpu(s)
30	0.0041430	$0.0011136 \pm i0.010461$	23.14
35	0.0041782	$0.0011780 \pm i0.010441$	34.68
40	0.0041698	$0.0011600 \pm i0.010452$	49.40

Table 6.16: Spectral convergence of temporal eigenvalues for the subharmonic mode of secondary instability for a two-dimensional primary wave over the $\theta = 0^\circ(2240)$ wall/isotropic plate for $R_\delta = 880$, $Fr = 58.8$, $A = 0.00695$, $\beta = 0.214$ and $\alpha = 0.15212 - i0.004853$ by the Bernoulli method with three iterations. (IBM 3090)

N	σ_1	$\sigma_{2,3}$	cpu(s)
20	0.0038300	$0.0007078 \pm i0.010295$	8.24
25	0.0039926	$0.0010218 \pm i0.010006$	14.35
30	0.0039835	$0.0009690 \pm i0.010048$	22.67
35	0.0039847	$0.0009714 \pm i0.010019$	33.74
40	0.0039865	$0.0009765 \pm i0.010025$	49.70
45	0.0039857	$0.0009744 \pm i0.010025$	67.71
50	0.0039859	$0.0009747 \pm i0.010025$	91.14

6.2.2 Fundamental Disturbance

For the fundamental mode with $R_\delta = 880$, $Fr = 58.8$ and $A = 0.00695$, spectral convergence is shown in Table 6.17 for the rigid wall simulation. Sufficient convergence is obtained with the same number of polynomials as the rigid wall problem. Some of these calculations require in excess of 60Mbytes of virtual memory which is a considerable computational demand. To determine how many polynomials are required to converge to an eigenvalue for the compliant wall case, the isotropic wall is introduced for the same Reynolds number and frequency. The spectral convergence results are shown in Table 6.18. For our purposes, reasonable convergence is attained with 40 polynomials similar to the subharmonic problem. The local spectral method requires as much cpu time as the global and achieves the same values.

Table 6.17: Spectral convergence of temporal eigenvalues for the fundamental mode of secondary instability for a two-dimensional primary wave over a rigid wall ($C_M \rightarrow \infty$) for $R_\delta = 880$, $Fr = 58.8$, $A = 0.00695$, $\beta = 0.214$ and $\alpha = 0.15488 - i0.005504$ by the Bernoulli method with three iterations.
(Cray Y/MP)

N	σ_1	cpu(s)
30	0.00085131	24.28
35	0.00093863	38.60
40	0.00090921	54.85
45	0.00092178	77.22

by the DNS of Spalart and Yang (1987). In the first part of this study we briefly examine both the subharmonic and fundamental modes over the compliant walls. Most emphasis is placed on the subharmonic mode since, as theory and computations indicate, subharmonic disturbances are more unstable than fundamental disturbances. We do include some fundamental disturbances to verify that these modes do not become more unstable over compliant walls.

For the secondary instability problem involving a two-dimensional primary wave, the dynamic equations for subharmonic and fundamental disturbances may be formed into real systems by appropriate addition and subtraction of the governing equations. From this we may expect to obtain real and complex conjugate eigenvalues. This is precisely what was found in the code verification of Tables 6.10-18. Additionally, the real eigenvalue is the most unstable. This implies that the secondary instability is travelling with the same phase speed as the primary wave. Hereafter, all illustrations are given with respect to the real eigenvalue which is the temporal growth rate of the secondary mode of instability unless otherwise noted.

An important aspect of this basic flow is its symmetry. The basic flow is two-dimensional flowing in the $x - y$ plane only, while the secondary instability is three-dimensional with spanwise wavenumber, β . With this basic flow, the result of the secondary instability for $+\beta$ and $-\beta$ is the same. With these considerations noted we proceed to a comparison of results for the rigid and compliant walls.

In a similar manner to the primary instability analysis, we consider results for a fixed Reynolds number of 2240. In this section, secondary instabilities which arise from two-dimensional primary waves are examined. The isotropic and non-isotropic compliant walls are used. We consider waves with frequencies for maximum growth rates. From Figure 5.8, we find that the maximum growth

rates occur at $\omega = 0.055$ ($Fr \approx 24.5$) for the non-isotropic wall and $\omega = 0.065$ ($Fr \approx 29.0$) for the isotropic wall. In Figure 6.2 the growth rates of the subharmonic and fundamental disturbances are shown versus the spanwise wavenumber for the rigid and isotropic walls. The figure illustrates that the growth rates over a compliant wall are reduced compared with the rigid wall results. Additionally, the subharmonic mode has larger growth rates than the fundamental. Due to this observation and the fact that a detailed study of both modes would be computationally expensive and for the most part unnecessary, only calculations for the dominant subharmonic disturbance will be made and presented.

In Figure 6.3, the growth rate of the subharmonic disturbance over the rigid and non-isotropic wall are shown. The non-isotropic wall leads to reduced secondary growth rates compared to the rigid wall results. Care must be taken in comparing Figures 6.2 and 6.3 since they are taken at different frequencies. The frequency of each is chosen for the maximum primary instability growth rate of the compliant wall. For the non-isotropic wall case, the growth rates of the secondary instabilities are reduced more than in the isotropic case. Yet the growth rates of secondary instabilities over the isotropic wall are less than those over the rigid wall.

At this point we examine aspects of the eigenvalue spectrum: both continuous and discrete modes. We found in our primary instability analysis that by using different numbers of polynomials (N) for the series approximation, discrete modes may be identified. Although we are only interested in the unstable, or growing, modes which are discrete, this approach will be used for the secondary problem to show any changes that may occur in the spectrum when compliant walls are used. Figure 6.4 shows the secondary eigenvalues for the rigid wall problem. For some modes it is difficult to determine which modes are of the discrete or continuous

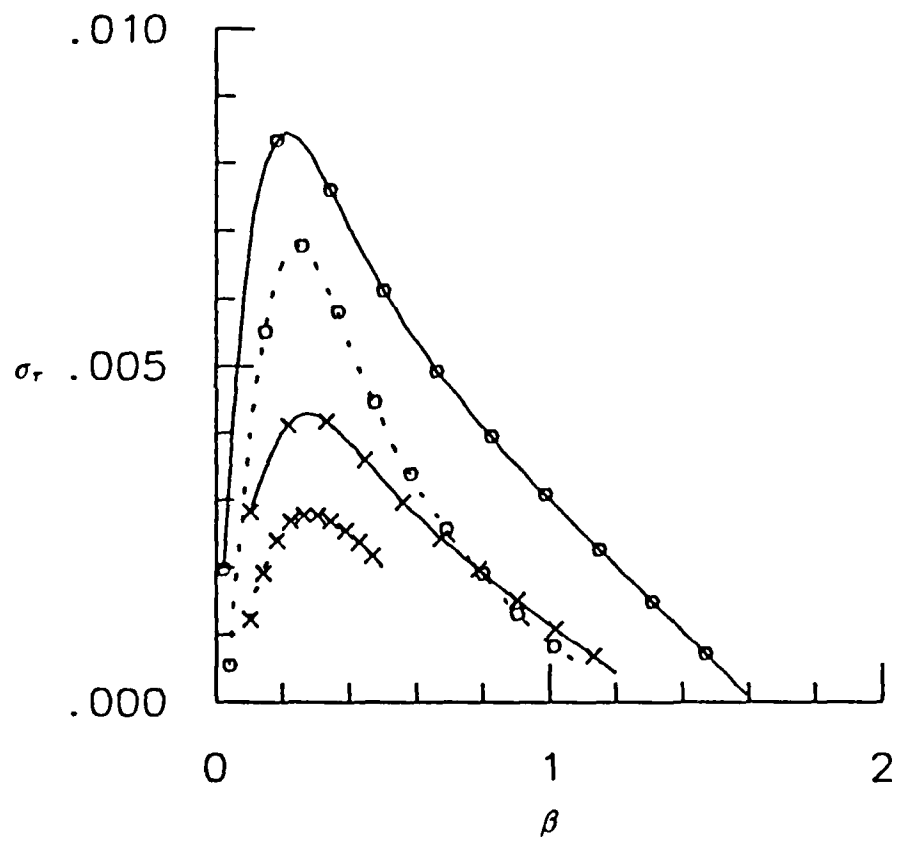


Figure 6.2 Growth rates of the secondary instabilities as a function of spanwise wavenumber for $R_\delta = 2240$, $Fr \simeq 29.0$, and $A = 0.01$. subharmonic: $-o-$, rigid wall; $\cdots o \cdots$, isotropic wall and fundamental: $-x-$, rigid wall; $\cdots x \cdots$, isotropic wall.

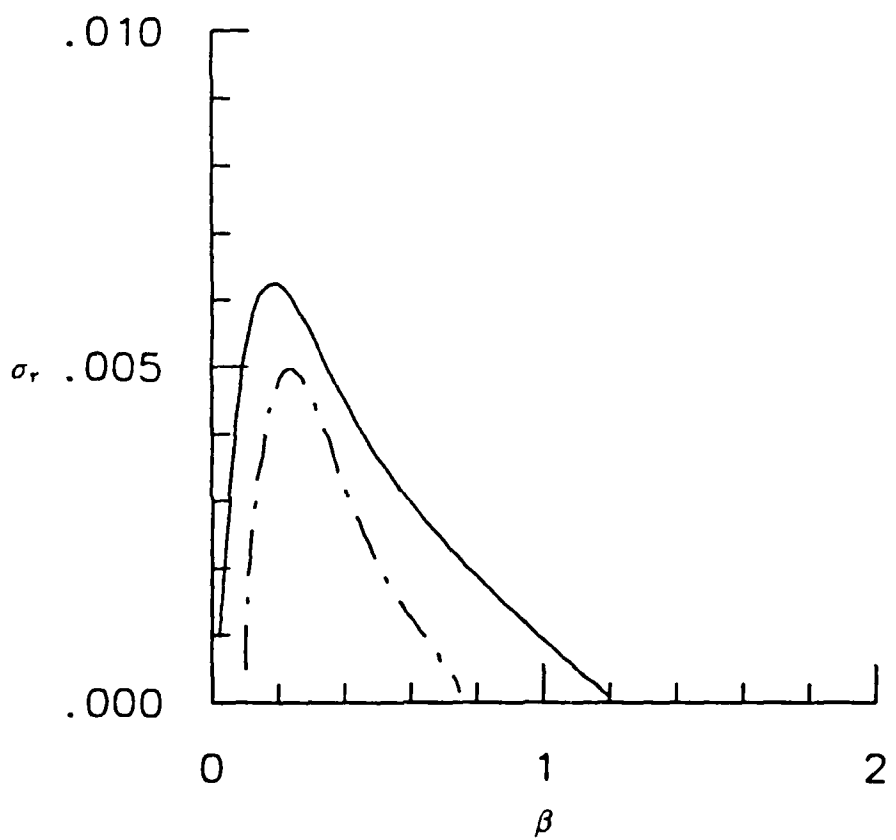


Figure 6.3 Growth rates of the subharmonic disturbance versus spanwise wavenumber for $R_\delta = 2240$, $Fr \approx 24.5$, and $A = 0.01$. —, rigid wall and - - -, non-isotropic wall.

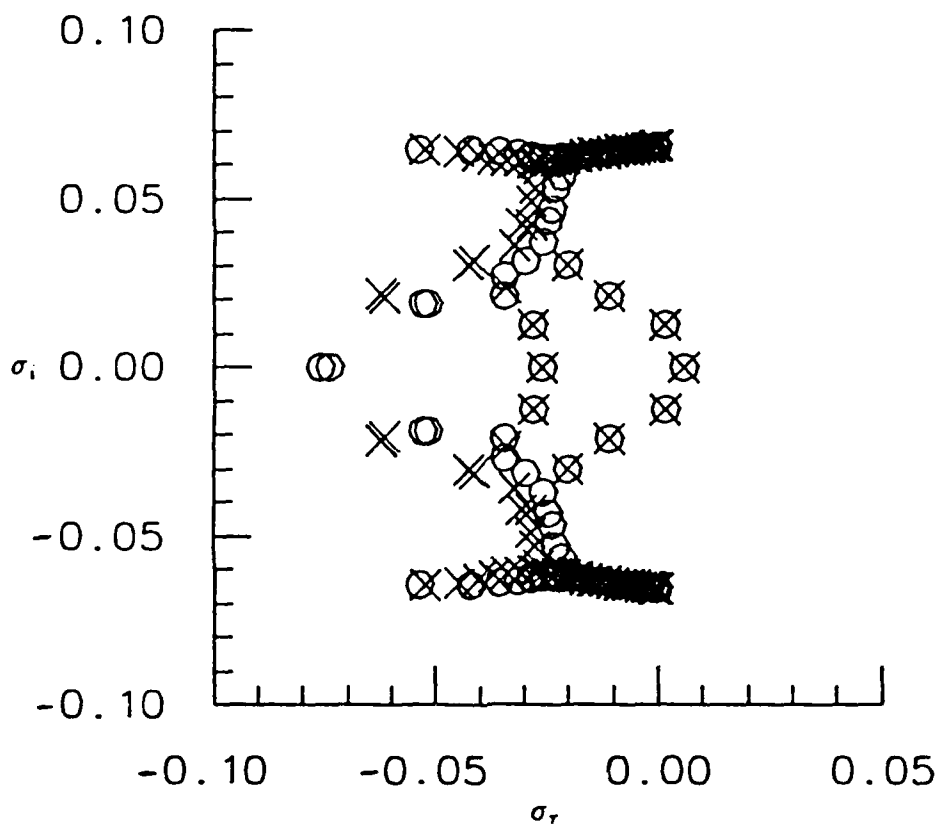


Figure 6.4 Real versus imaginary temporal eigenvalue of the subharmonic mode for a two-dimensional primary wave over a rigid wall with $R_{\delta^*} = 2240$, $Fr \approx 24.5$, $A = 0.01$, and $\beta = 0.2$. (o, $N=40$ and \times , $N=45$)

spectrum. It is apparent that a number of discrete growing and decaying modes exist near $\sigma_i = 0$. What is important for the instability analysis are the growing modes that have positive σ_r . The characteristic look of the spectrum is not too unlike that shown by Herbert (1983) for plane channel flow except for the asymmetry in the channel spectrum about σ_i . The present spectrum clusters at $-0.07 < \sigma_i < 0.07$ while the spectrum of the channel problem is clustered at $-0.4 < \sigma_i < 0.4$. Of course, this is indicative of two different physical situations with different flow parameters. This comparison is noted as an observation of the similarities and differences between the two class of flows. For the rigid wall, only three modes are growing-one real and a complex conjugate pair. The non-isotropic wall is introduced and the spectrum is shown in Figure 6.5. A similar pattern exists for the spectrum. A comparison of the non-isotropic eigenvalues(x) with the rigid wall case (o) is shown in Figure 6.6. The extent to which the spectrum extends in σ_i is slightly reduced for the compliant case. In Figure 6.7 only the growing modes are shown. For both the rigid and non-isotropic walls, the growing modes consist of a real and complex conjugate pair. This is what we might expect since the real and complex conjugate eigenvalues are a result of the symmetry in the basic flow which exists for both cases. The non-isotropic wall suppresses the growth rate of the subharmonic disturbance by 17% of a similar disturbance over the rigid wall. In Figure 6.8, the spectrum over the isotropic wall is shown. The results are comparable to the non-isotropic case. A comparison of the spectrum over the isotropic wall(x) is made with the rigid wall results(o) in Figure 6.9. A change in the spectrum occurs which is similar to the non-isotropic results. A smaller difference occurs between the isotropic and rigid walls. This is what we might expect since the basic flow over the isotropic wall is closer to the rigid wall case than the basic flow over the non-isotropic wall. In Figure 6.10, the

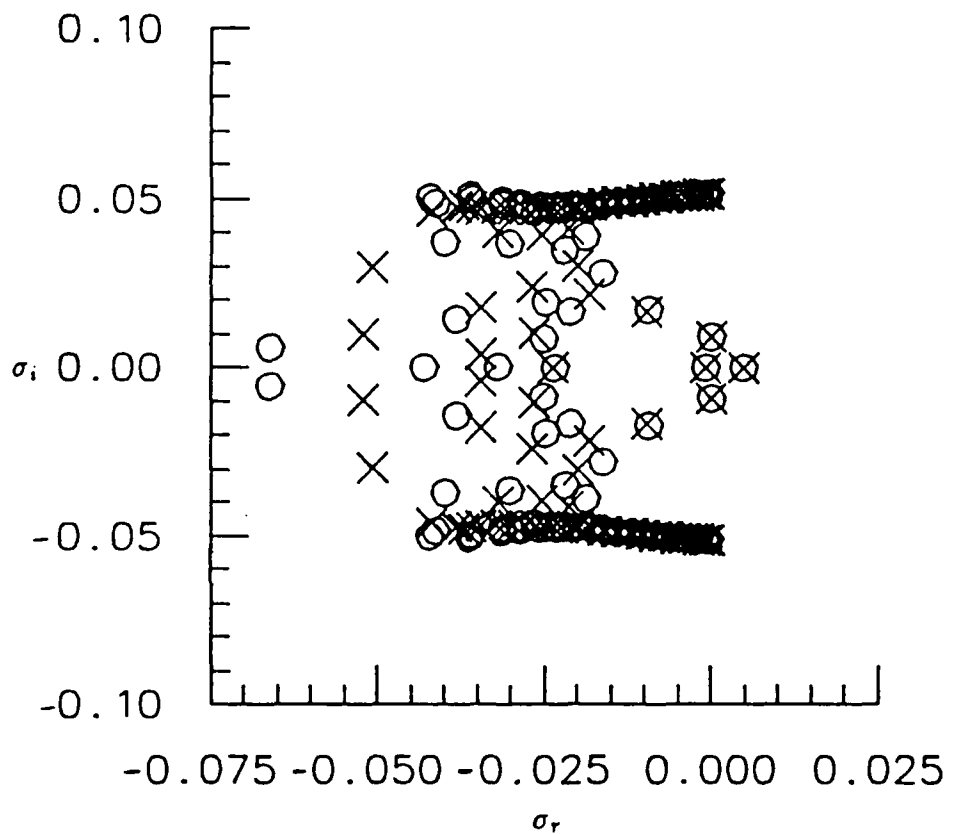


Figure 6.5 Real versus imaginary temporal eigenvalue of the subharmonic mode for a two-dimensional primary wave over a non-isotropic wall with $R_{\delta^*} = 2240$, $Fr \approx 24.5$, $A = 0.01$, and $\beta = 0.2$. (○, $N=40$ and ×, $N=45$)

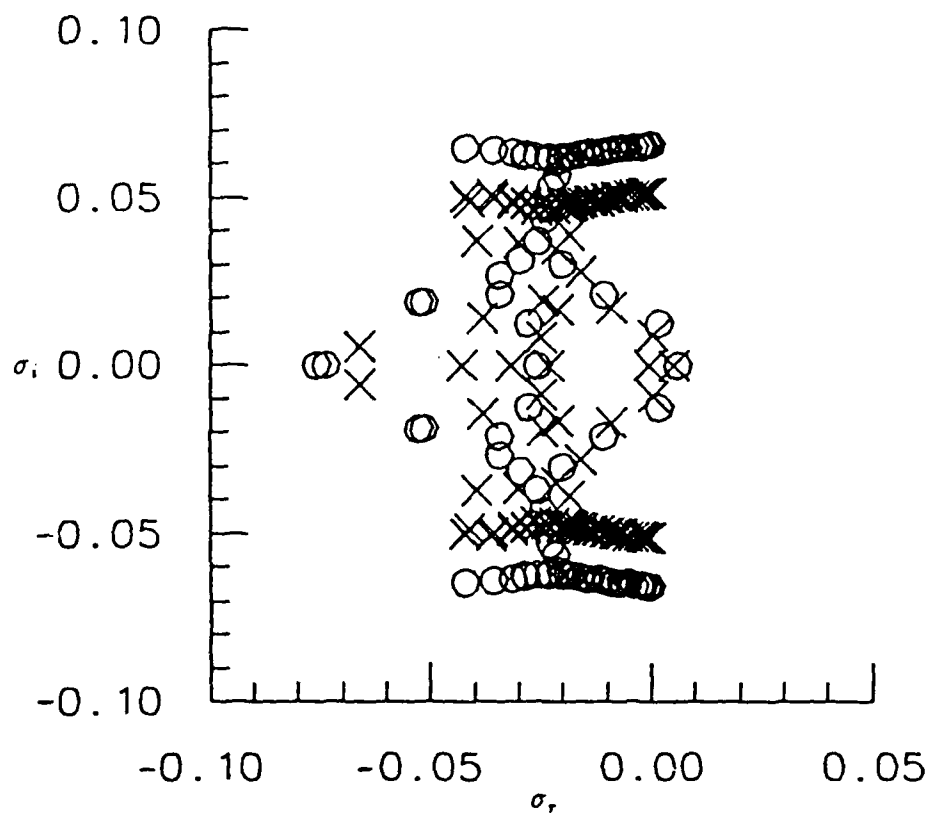


Figure 6.6 Real versus imaginary temporal eigenvalue of the subharmonic mode for a two-dimensional primary wave over a \circ , rigid wall and \times , non-isotropic wall with $R_{\delta^*} = 2240$, $Fr \simeq 24.5$, $A = 0.01$, and $\beta = 0.2$.

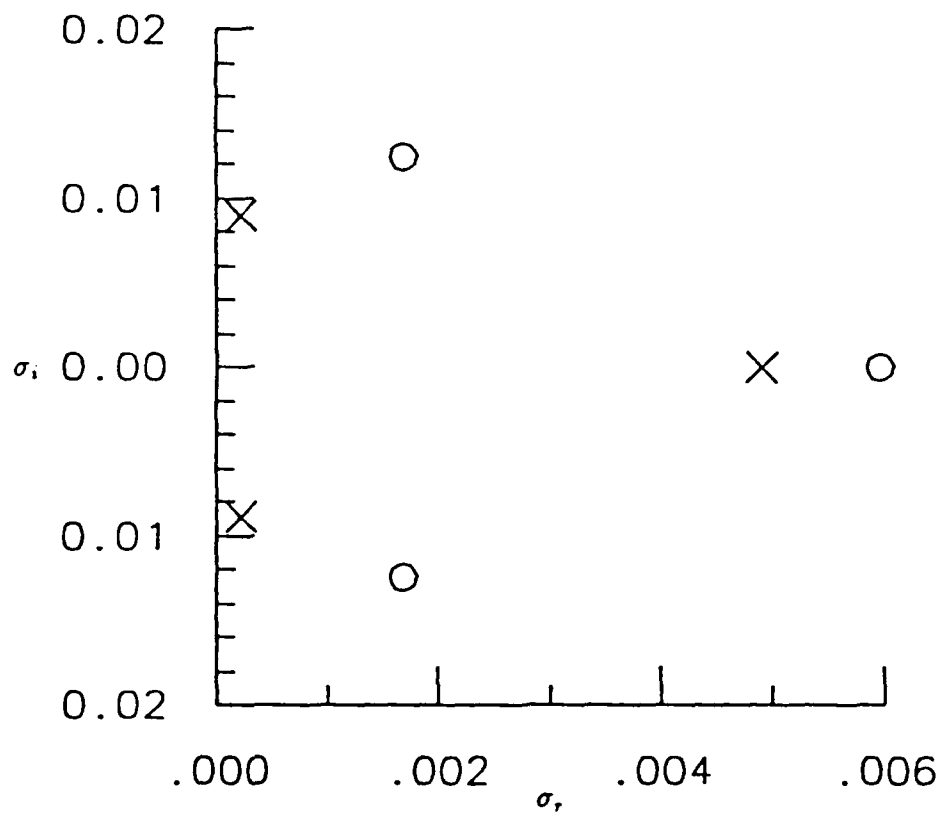


Figure 6.7 Real versus imaginary temporal eigenvalue for growing modes of the subharmonic mode for a two-dimensional primary wave over a o, rigid wall and x, non-isotropic wall with $R_{\delta^*} = 2240$, $Fr \approx 24.5$, $A = 0.01$, and $\beta = 0.2$.

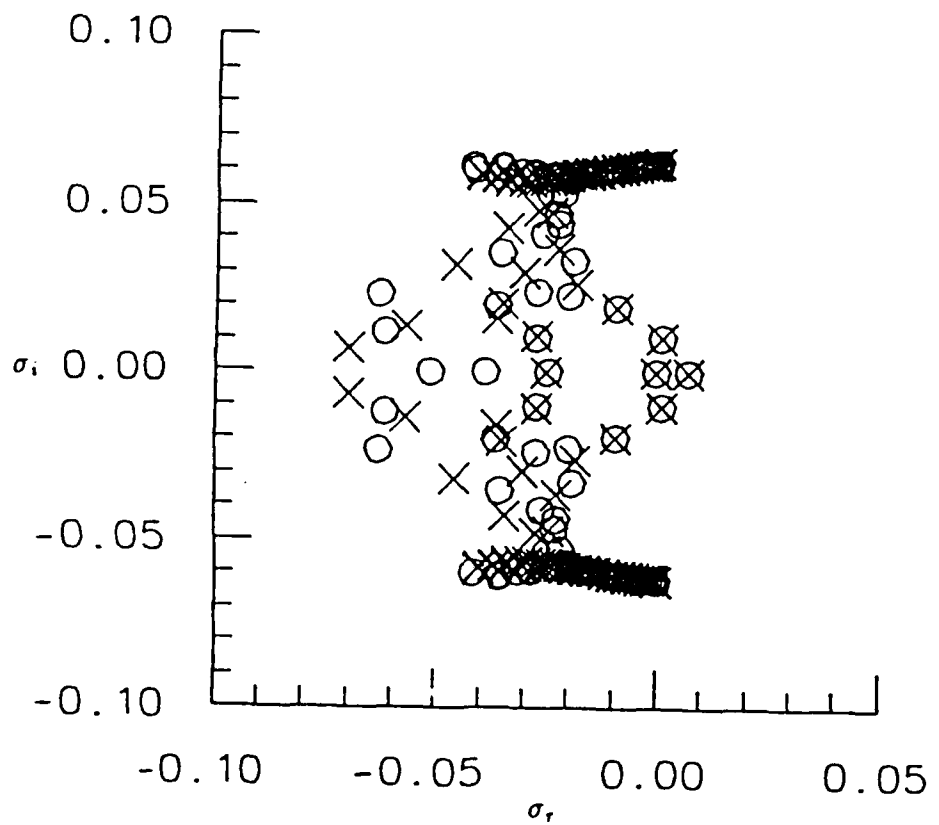


Figure 6.8 Real versus imaginary temporal eigenvalue of the subharmonic mode for a two-dimensional primary wave over a isotropic wall with $R_{\delta^*} = 2240$, $Fr \approx 24.5$, $A = 0.01$, and $\beta = 0.2$. (o, $N=40$ and \times , $N=45$)

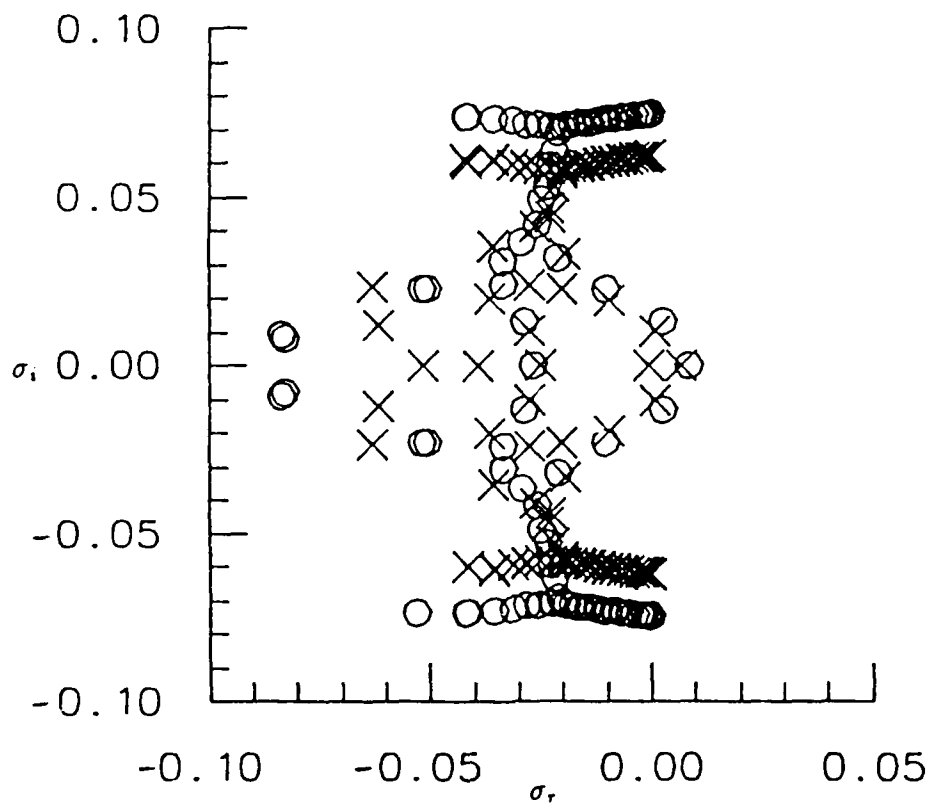


Figure 6.9 Real versus imaginary temporal eigenvalue of the subharmonic mode for a two-dimensional primary wave over a \circ , rigid wall and \times , isotropic wall with $R_{\delta^*} = 2240$, $Fr \simeq 29.0$, $A = 0.01$, and $\beta = 0.25$.

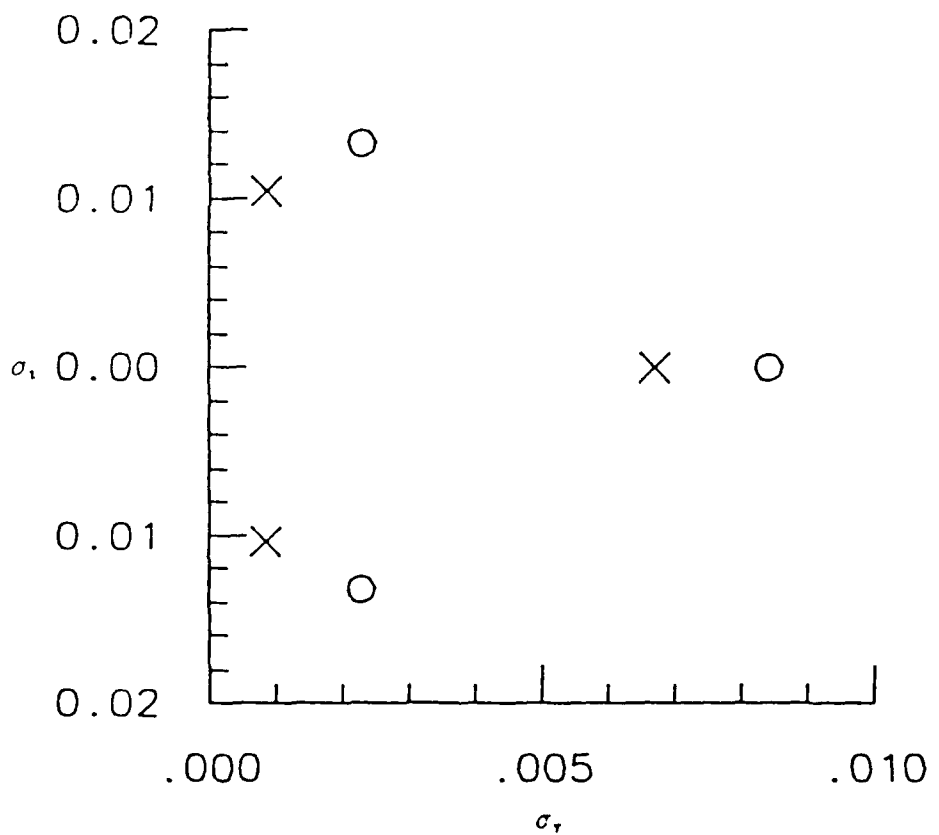


Figure 6.10 Real versus imaginary temporal eigenvalue for growing modes of the subharmonic mode for a two-dimensional primary wave over a o, rigid wall and x, isotropic wall with $R_{f\bullet} = 2240$, $Fr \approx 29.0$, $A = 0.01$, and $\beta = 0.25$.

growing modes for the isotropic wall(x) and rigid wall(o) are shown. A reduction of 20% in the growth rate of the subharmonic disturbance occurs due to the presence of the isotropic wall. For both compliant walls, a reduction in the growth rates of the secondary instability is found. Although it appears that the isotropic walls suppress the secondary instability growth rates more than the non-isotropic wall, a more extensive and complete comparison would be possible using a common frequency instability analysis.

The results that were just presented were for a fixed basic flow. A better measure of the degree to which compliant walls may suppress the development of the secondary instabilities is found by tracking waves as they grow and decay. The e^n -criterion proved an acceptable method in predicting the secondary growth compared with the experiments of Kachanov and Levchenko (1984) where the criterion for the secondary analysis is given by

$$\ln \frac{B}{B_o} = \int_{x_o}^x \frac{\sigma_r}{c_r} dx \quad 6.3.1$$

The comparison is shown in Figure 6.11. As discussed earlier, the reason for choosing Herbert's theory is the reasonably good agreement it has with available experiments.

An exhaustive parametric investigation is beyond the scope of this study, so a reasonable choice of cases must be decided to demonstrate the effects of compliant walls on the secondary instabilities. In order to compare secondary instabilities over the rigid and compliant walls in an e^n sense a relatively high frequency wave must be selected. In Figure 6.12, the maximum amplification of waves propagating over the rigid and compliant walls along with the amplification of waves at a frequency(Fr) of 53 is shown. We might expect at this frequency that the isotropic wall would be less effective in suppressing secondary

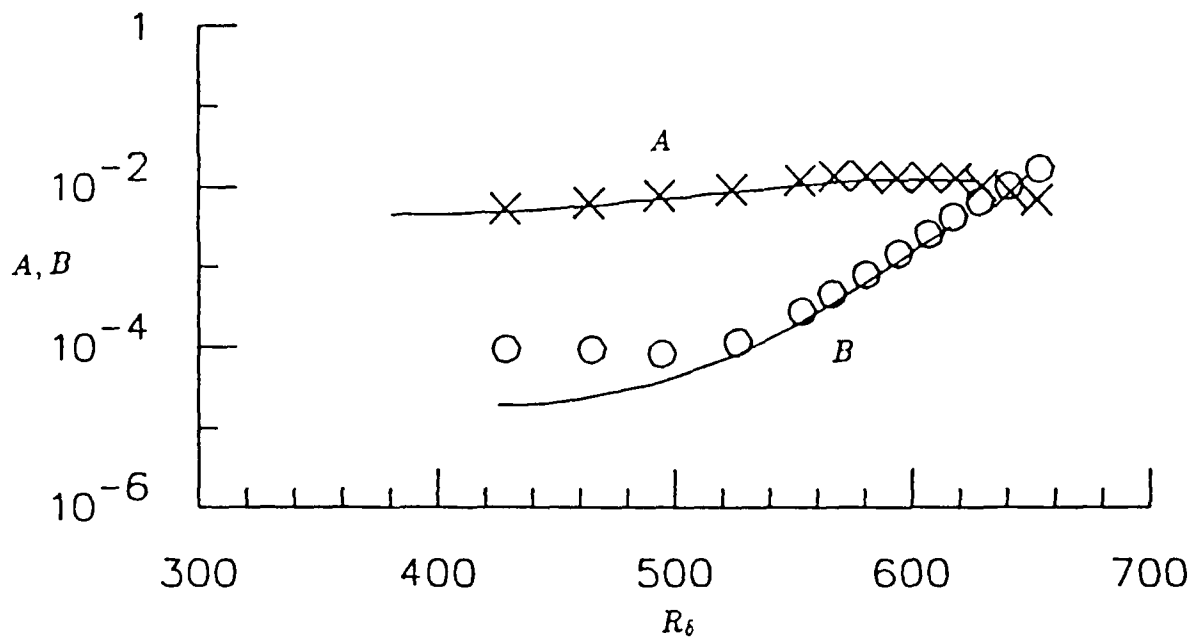


Figure 6.11 Amplitude growth with Reynolds number of the subharmonic mode (B) of a two-dimensional primary wave (A) over a rigid wall at $Fr = 124$, $A_o = 0.0044$, $B_o = 1.86 \times 10^{-5}$, and $\bar{b} = 0.33$. —, theory and (×,○), Kachanov and Levchenko (1984).

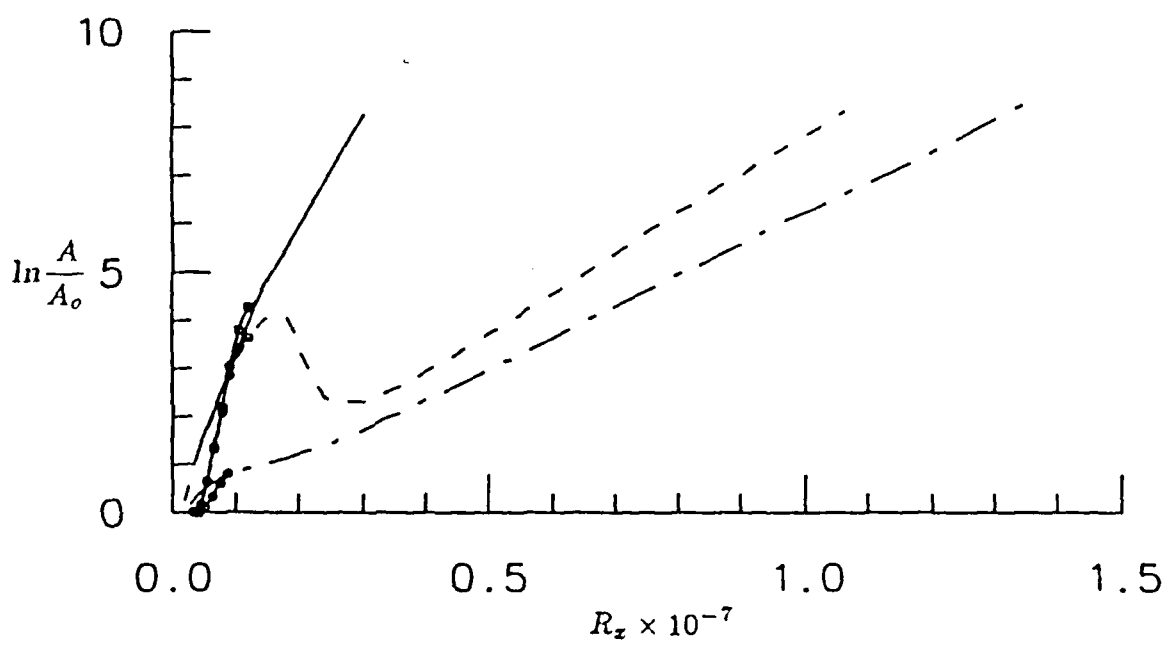


Figure 6.12 Two-dimensional curves of maximum amplification for TSI waves over a —, rigid wall; - - -, isotropic wall; and - · -, non-isotropic wall and --o--, waves of $Fr \approx 53$.

instabilities since the basic flow is comparable to the rigid wall case. The basic flow is quite different over the non-isotropic wall where the primary instability growth is suppressed significantly. Therefore we would expect the non-isotropic wall to be more effective in suppressing the secondary instabilities. Additionally, the effect of both compliant walls becomes more advantageous at lower frequencies. The e^n -criterion is used to track waves from branch I to branch II of the neutral curve for the rigid, isotropic, and non-isotropic walls. Figure 6.13 illustrates the amplitude growth of the primary instability (A) and secondary instability (B) for $A_o = 0.004$, $B_o = 1 \times 10^{-5}$, and $\bar{b} = 0.15$. The initial amplitudes are somewhat arbitrarily chosen. These were selected to be close to the parameters of Kachanov and Levchenko (1984). The spanwise wavenumber (b) was chosen near the maximum growth rate of the secondary instability at the branches of the neutral curve for the rigid wall case. The amplification of the instability over the isotropic and rigid walls are similar. The non-isotropic wall significantly suppresses both the primary and secondary instability growth.

Since the non-isotropic wall proved promising with the selected parameters we focus further on this case. In Figure 6.14 the amplification of the primary and secondary instabilities over the rigid wall with parameters unchanged is compared with the non-isotropic wall with various initial secondary amplitudes (B_o). Even though B_o has increased by a factor of 5, the secondary instability has not overtaken the primary growth. This increased amplitude of the secondary instability is still suppressed compared to the lower amplitude rigid wall case.

The behavior of the secondary instability is critically dependent on the parameters of the basic flow, for example, the amplitude of the primary instability. Figure 6.15 shows the amplification of the primary and secondary instabilities over the rigid wall with properties as

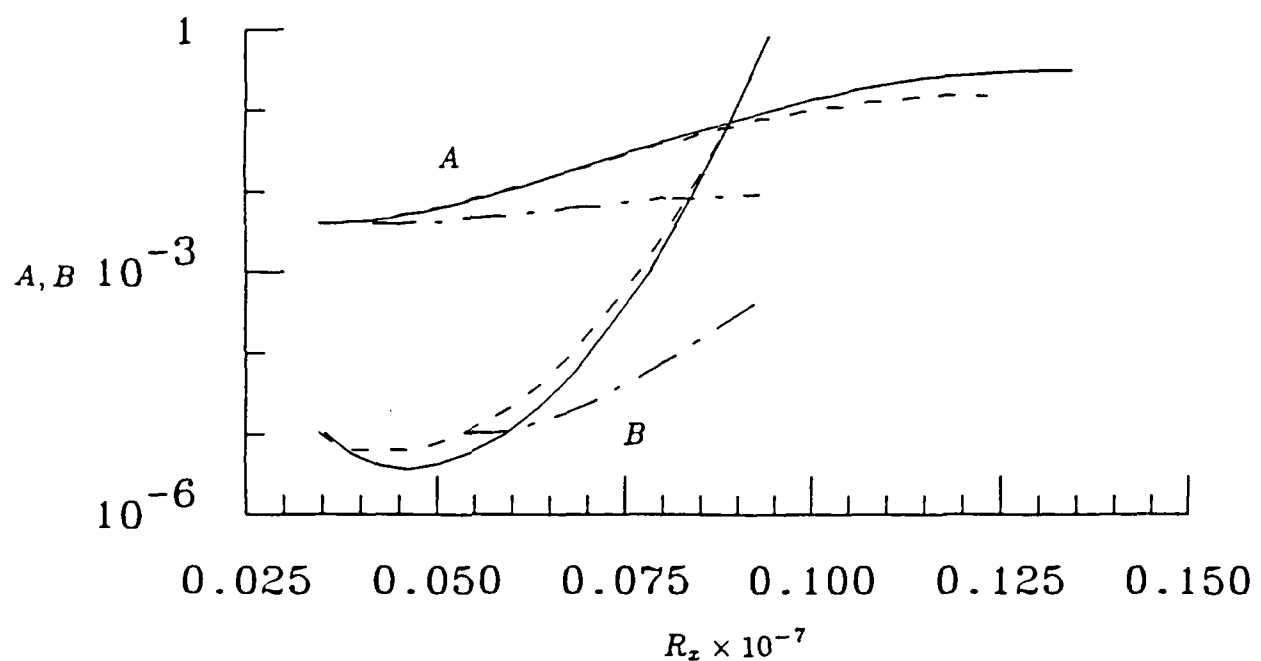


Figure 6.13 Amplitude growth with Reynolds number of the subharmonic mode (B) of a two-dimensional primary wave (A) at $Fr \simeq 53$, $A_o = 0.004$, $B_o = 1 \times 10^{-5}$, and $\bar{b} = 0.15$ over a —, rigid wall; — —, isotropic wall; and - · -, non-isotropic wall.

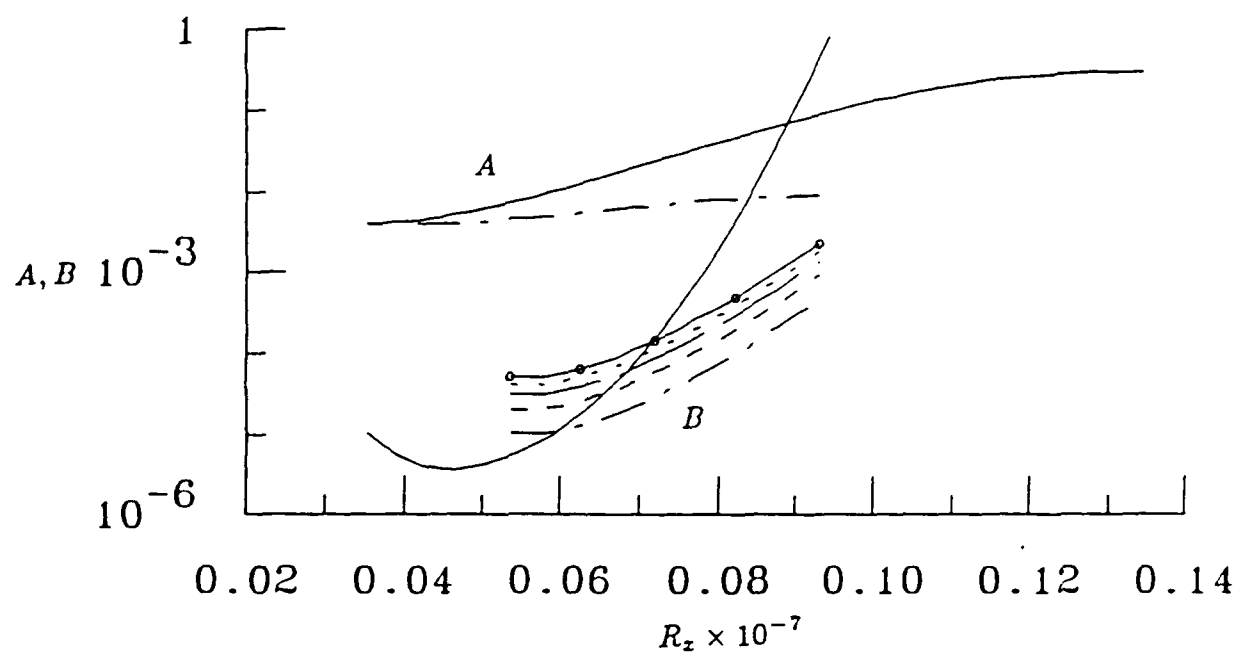


Figure 6.14 Amplitude growth with Reynolds number of the subharmonic mode (B) of a two-dimensional primary wave (A) at $Fr \approx 53$, $A_0 = 0.004$, and $\bar{b} = 0.15$ over a —, rigid wall and - - -, non-isotropic wall with B_0 : - - -, 1×10^{-5} ; - - -, 2×10^{-5} ; — —, 3×10^{-5} ; · · ·, 4×10^{-5} ; and - o -, 5×10^{-5} .

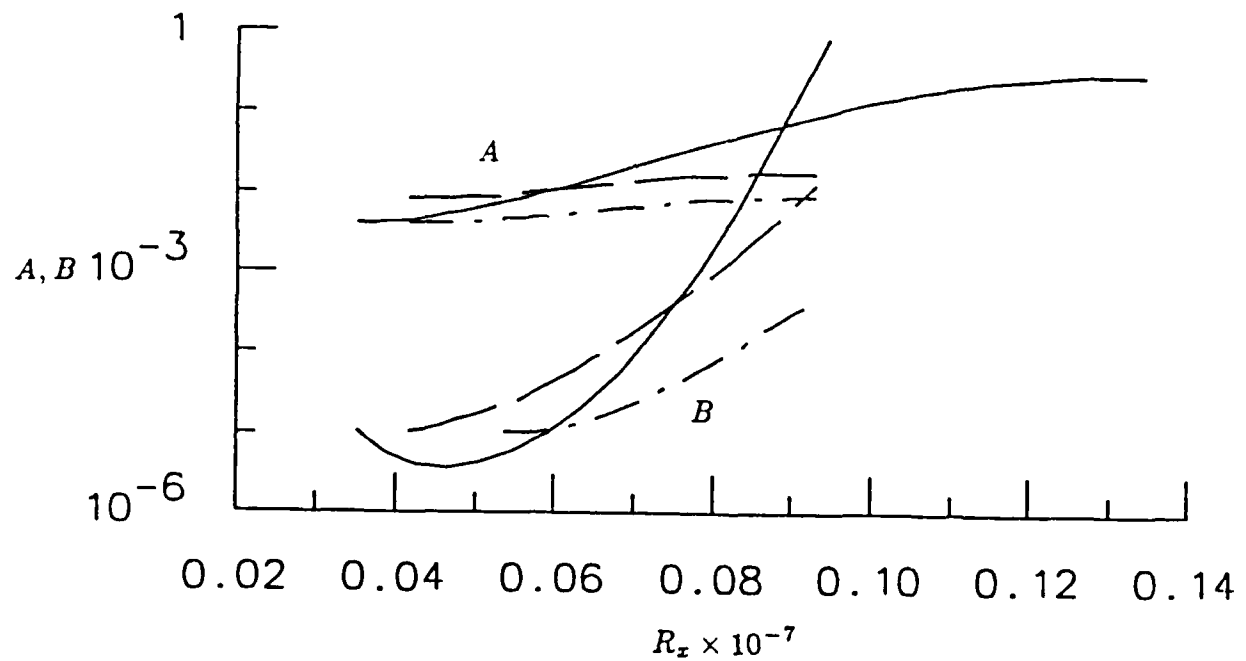


Figure 6.15 Amplitude growth with Reynolds number of the subharmonic mode (B) of a two-dimensional primary wave (A) at $Fr \approx 53$, $B_o = 1 \times 10^{-5}$, and $\bar{b} = 0.15$ over a —, rigid wall with $A_o = 0.004$; - · -, non-isotropic wall with $A_o = 0.004$; and — —, non-isotropic wall with $A_o = 0.008$.

before and the non-isotropic wall with $A_o = 0.004$ and $A_o = 0.008$. Even by doubling the amplitude of the disturbance over the non-isotropic wall, the growth of the secondary instabilities is considerably suppressed and has not exceeded the primary amplitude upon crossing branch II of the neutral curve.

It is difficult to visualize the nature of the three-dimensional secondary instability. An attempt has been made through the use of vector plots for the v_3, w_3 velocities and the u_3 velocity profiles in the spanwise plane. In Figures 6.16-17, velocities are shown for the rigid wall; in Figures 6.18-19, velocities are shown for the isotropic wall; and in Figures 6.20-21, velocities are shown for the non-isotropic wall. It would be very difficult to make exact parameter specifications for the respective walls at a fixed Reynolds number. Instead, emphasis is placed on showing the development of the secondary instability over each wall. The Reynolds numbers at the upper branch of the neutral curves are chosen with a normalized secondary instability that was derived from the e^n calculations. A second Reynolds number was chosen at an incremental step prior to branch II. Graphically, little difference occurs between the isotropic and rigid wall results as we might expect. At the lower Reynolds number the velocity magnitudes are extremely small compared with the downstream velocities. This is because of the strong convective growth of the secondary instability over only a few TSI wavelengths. The growth of the secondary disturbance over the non-isotropic wall is much slower which is evident in the e^n calculations and shown in Figures 6.20-21. In comparing the structure of the disturbance, regions of high speed up-flow and slower down-flow are found. This agrees with experimental observations.

Finally, we look briefly at the modal classification of the secondary instabilities. In the primary compliant wall problem, three general classes of instability can occur over, or as a result of, the compliant wall. The dominant mode which

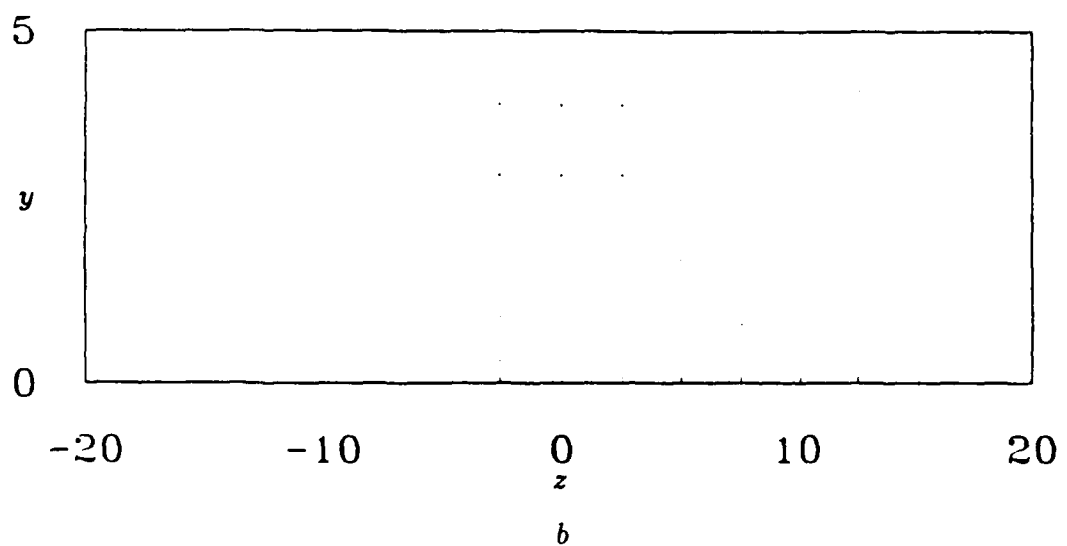
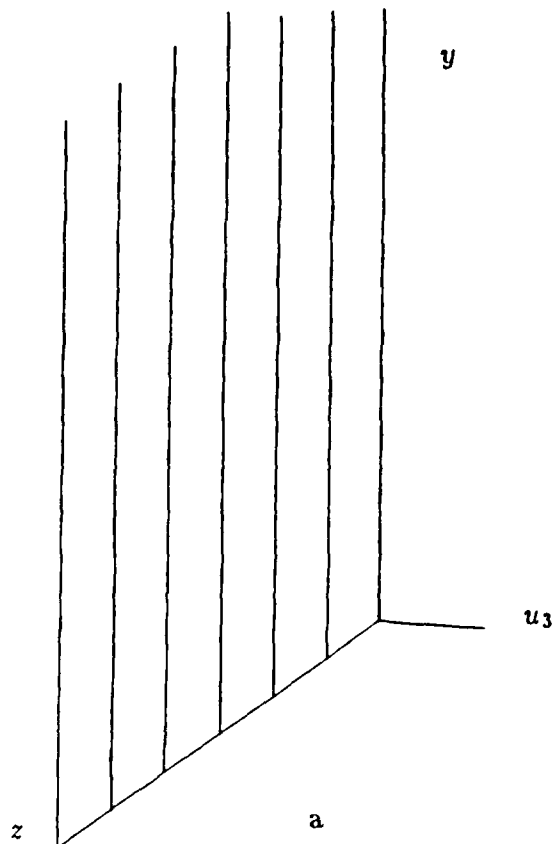


Figure 6.16 Velocity distribution of the subharmonic mode of a two-dimensional primary wave over a rigid wall at $R_{\delta^*} = 1771$, $A = 0.18$, $\bar{b} = 0.15$, and $B = 0.0015$ for a- u_3 velocity profiles and b- (v_3, w_3) velocity vectors versus spanwise position.

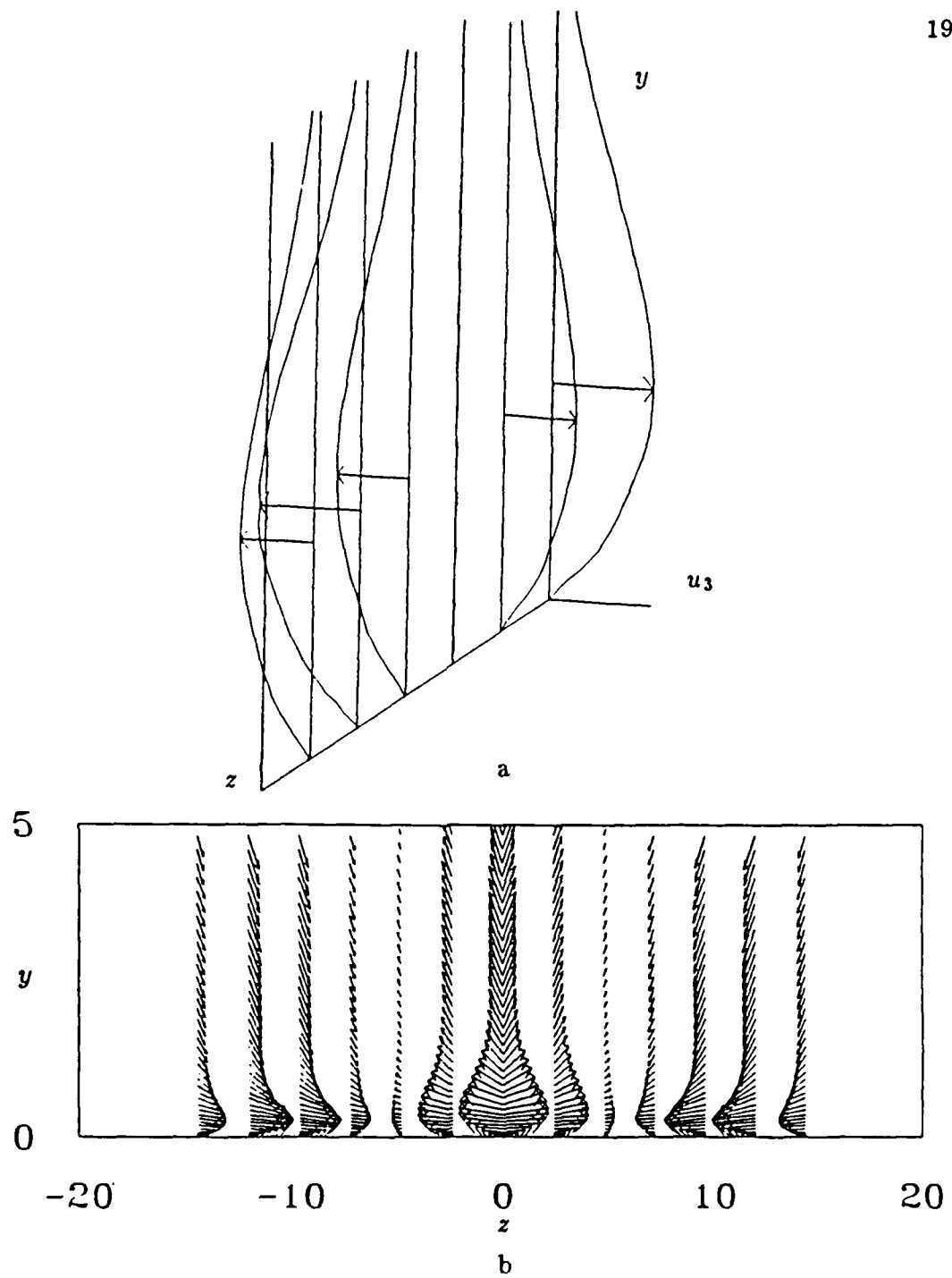


Figure 6.17 Velocity distribution of the subharmonic mode of a two-dimensional primary wave over a rigid wall at $R_{\delta^*} = 1871$, $A = 0.27$, $\bar{b} = 0.15$, and $B = 1.0$ for a- u_3 velocity profiles and b- (v_3, w_3) velocity vectors versus spanwise position.

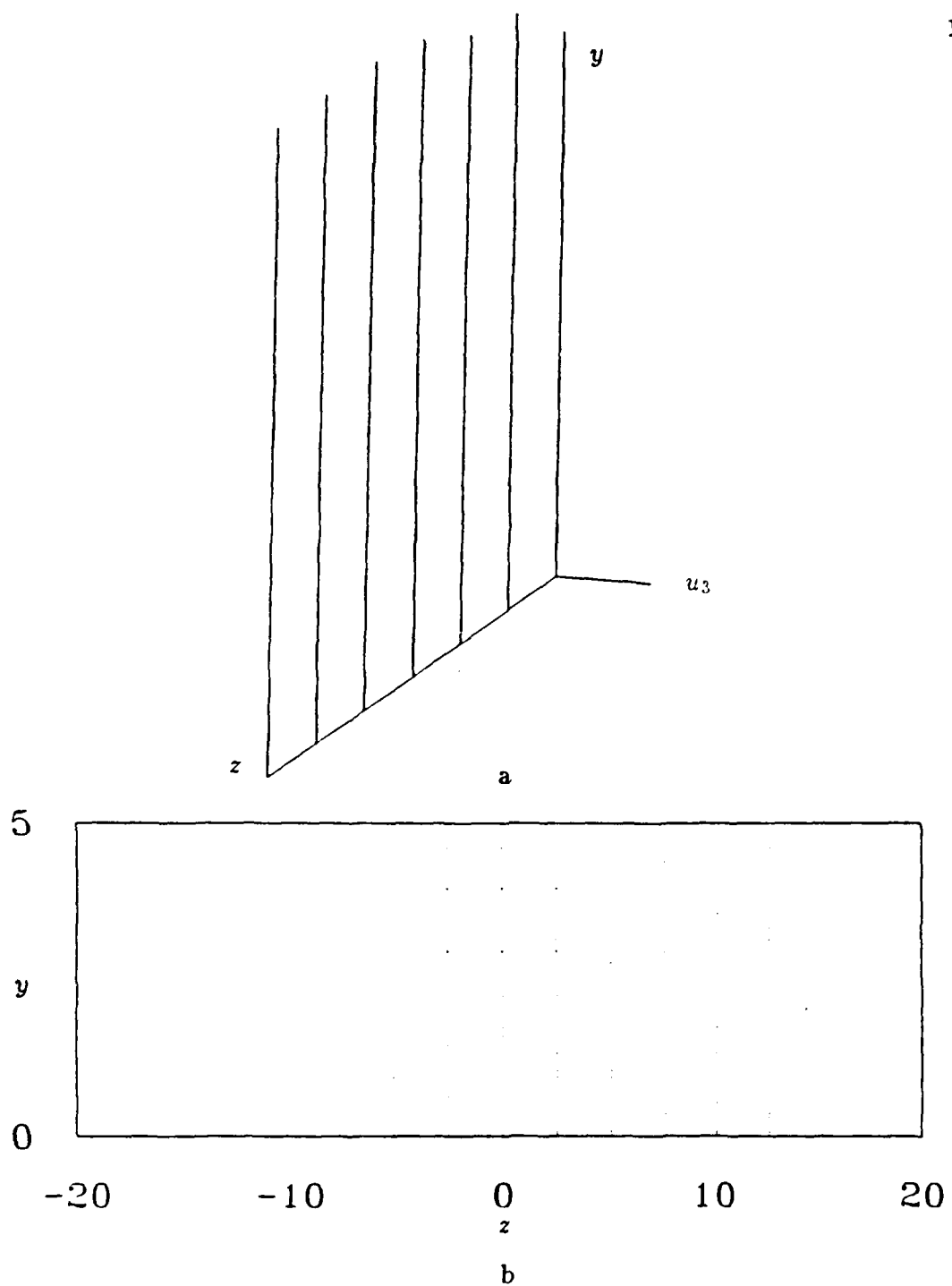


Figure 6.18 Velocity distribution of the subharmonic mode of a two-dimensional primary wave over a isotropic wall at $R_{\delta^*} = 1760$, $A = 0.12$, $\bar{b} = 0.15$, and $B = 0.0025$ for a- u_3 velocity profiles and b- (v_3, w_3) velocity vectors versus spanwise position.

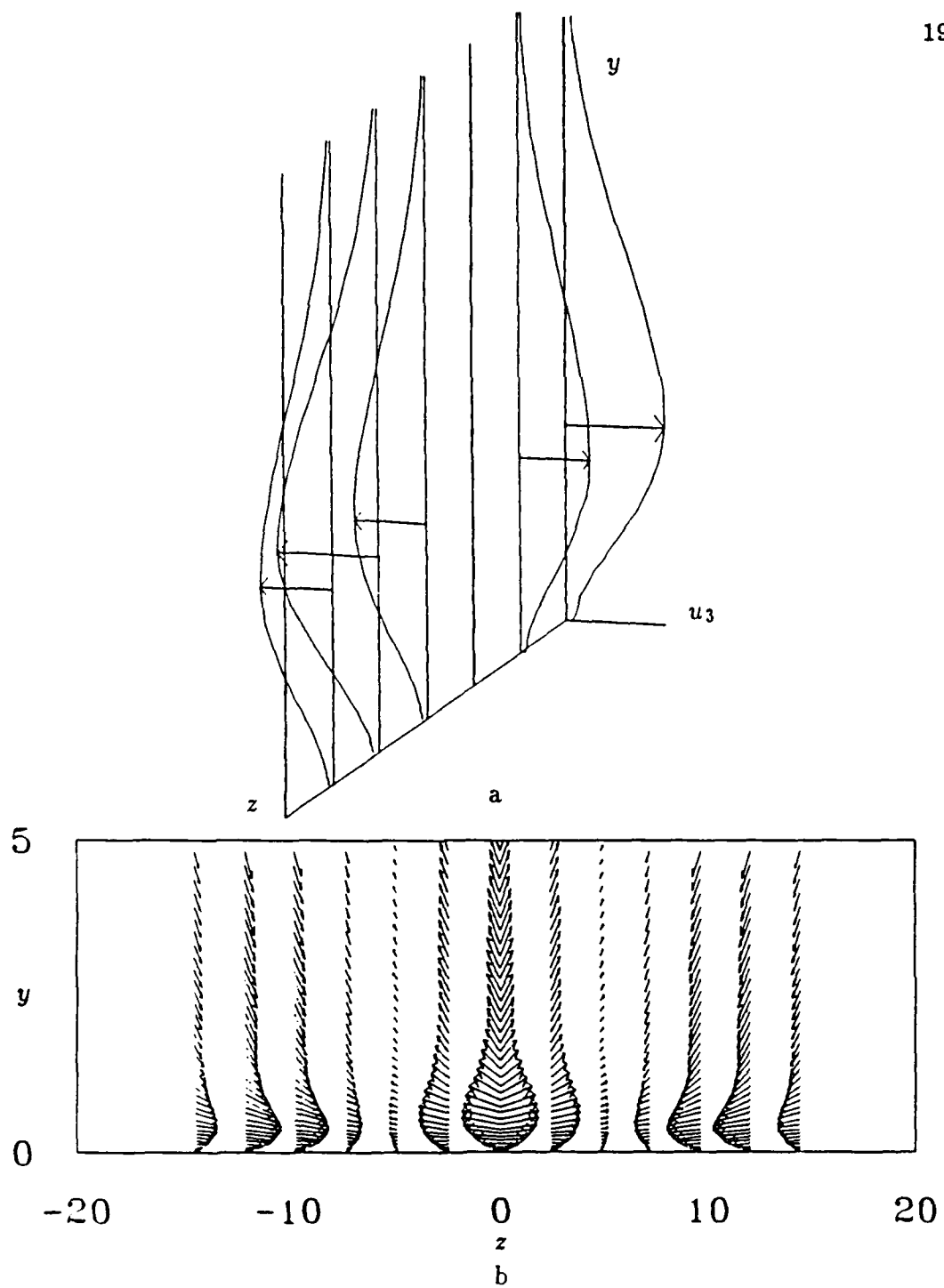


Figure 6.19 Velocity distribution of the subharmonic mode of a two-dimensional primary wave over a isotropic wall at $R_{\delta^*} = 1860$, $A = 0.15$, $\bar{b} = 0.15$, and $B = 1.0$ for a- u_3 velocity profiles and b- (v_3, w_3) velocity vectors versus spanwise position.

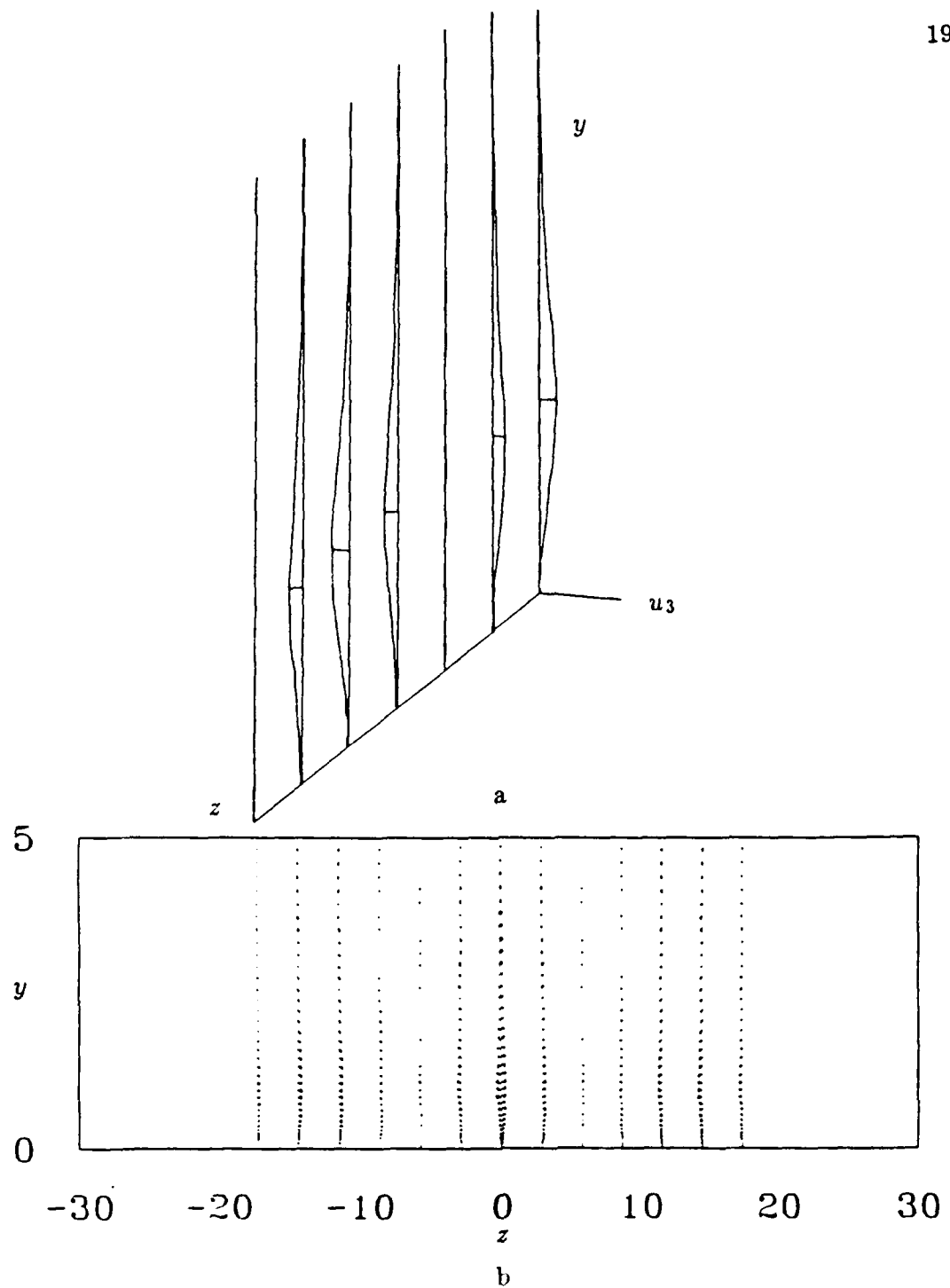


Figure 6.20 Velocity distribution of the subharmonic mode of a two-dimensional primary wave over a non-isotropic wall at $R_{\delta^*} = 1559$, $A = 0.08$, $\bar{b} = 0.15$, and $B = 0.21$ for a- u_3 velocity profiles and b- (v_3, w_3) velocity vectors versus spanwise position.

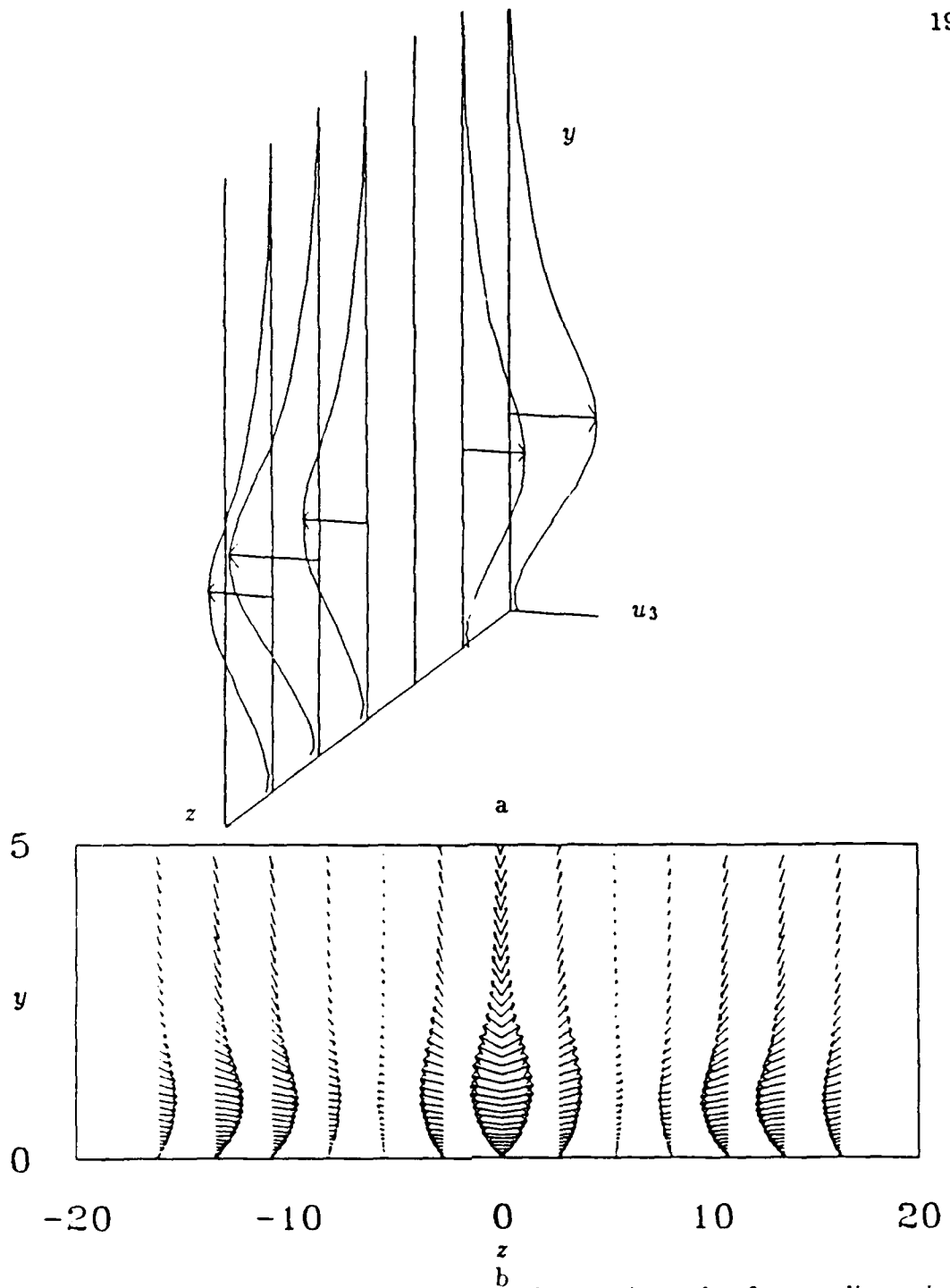


Figure 6.21 Velocity distribution of the subharmonic mode of a two-dimensional primary wave over a non-isotropic wall at $R_{\delta^*} = 1659$, $A = 0.09$, $\bar{b} = 0.15$, and $B = 1.0$ for a- u_3 velocity profiles and b- (v_3, w_3) velocity vectors versus spanwise position.

is used for the secondary instability analysis is the Class A-TSI wave. This class is destabilized by the introduction of damping in the wall. As an exercise to verify that the secondary instabilities behave in a similar fashion, wall damping is introduced and defined by

$$E = E(1 - i\eta_E) \quad 6.3.2$$

and

$$K = K(1 - i\eta_K) \quad 6.3.3$$

where η_E and η_K regulate the amount of damping. For the non-isotropic wall the primary and secondary instability growth rates are $\alpha_i = -0.003138$ and $\sigma_r = 0.00206$, respectively, for $R_{\delta^*} = 2240$, $A = 0.01$, $\beta = 0.5$, and $Fr \simeq 24.5$. Adding $\eta_E = \eta_K = 0.05$ as dissipation, the resulting growth rates become $\alpha_i = -0.004757$ and $\sigma_r = 0.00220$. The secondary instability is destabilized by wall damping. It appears that the secondary instabilities are less sensitive to wall damping compared to primary instabilities. It is interesting to note that the secondary instability does not sense the local growth rate of the primary instability. Yet, the secondary disturbance is destabilized by wall dissipation.

6.4 Results for 3D Primary Waves

We discovered in the previous chapter that oblique primary waves have larger growth rates than two-dimensional waves. In this section, we introduce the dominant three-dimensional primary wave to determine how the secondary instabilities react to the now three-dimensional basic flow.

The secondary instability problem is different for a three-dimensional basic flow. The symmetry of the problem is lost. This asymmetry occurs as a result of

terms arising from the spanwise basic flow. This occurs irrespective of whether we solve the system in the (x, z) or (x', z') coordinate reference frame. So we can place no expectations on the eigenvalues. In fact we expect not to obtain real and complex conjugate solutions. Additionally, since the basic flow is three-dimensional the results obtained for $+\beta$ should be different than those obtained for $-\beta$. We find that the eigenvalues obtained with $+\beta$ are complex conjugates of those obtained with $-\beta$.

In a similar manner to the two-dimensional primary instability case, aspects of the secondary eigenvalue spectrum for three-dimensional primary instabilities is examined. In Figure 6.22, the eigenvalue spectrum of a two-dimensional primary wave (o) is shown with a three-dimensional wave (x) propagating at a wave angle of $\phi = 10^\circ$. The spectrum of the three-dimensional wave has shifted in the positive σ_i direction as shown. Also the growth rate of the dominant mode is reduced slightly for the three-dimensional primary wave. The spectrum over the non-isotropic wall for three-dimensional primary waves is shown in Figure 6.23. Discrete modes are identified of which only three are unstable. In Figure 6.24, the spectrum from a two-dimensional primary wave(o) is compared with the three-dimensional primary wave(x) results. A similar shift occurs in the spectrum for three-dimensional waves over the compliant wall as was shown for the rigid wall. In Figure 6.25 the spectrum over the rigid wall is compared with the non-isotropic wall results. Similar to the two-dimensional instability comparison, the rigid wall yields the greater growth rates of the secondary disturbance compared to the compliant walls. In Figure 6.26 the non-isotropic wall is replaced with the isotropic wall. Figure 6.27 shows the comparison of the spectrum for two- and three-dimensional primary waves over an isotropic wall. A shift in the eigenvalue spectrum occurs as we might expect. Figure 6.28 is the comparison of rigid and

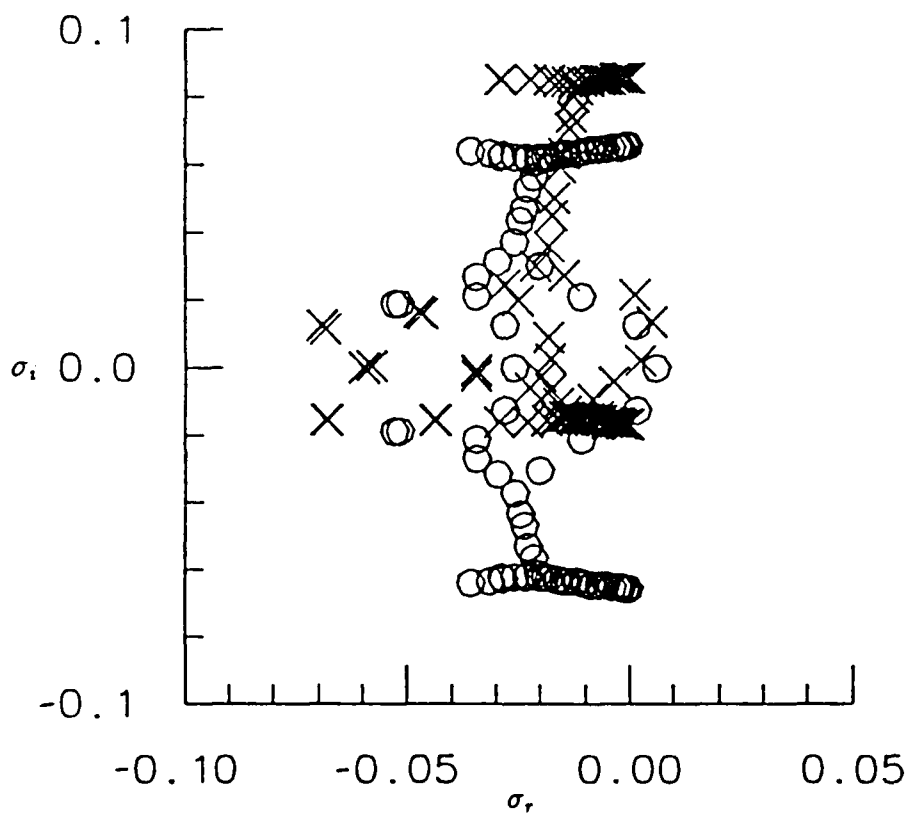


Figure 6.22 Real versus imaginary temporal eigenvalue of the subharmonic mode for two- and three-dimensional primary waves over a rigid wall with $R_{\delta^*} = 2240$, $Fr \approx 24.5$, $A = 0.01$, and $\beta = 0.2$. (o, 2D and x, 3D at $\phi = 10^\circ$)

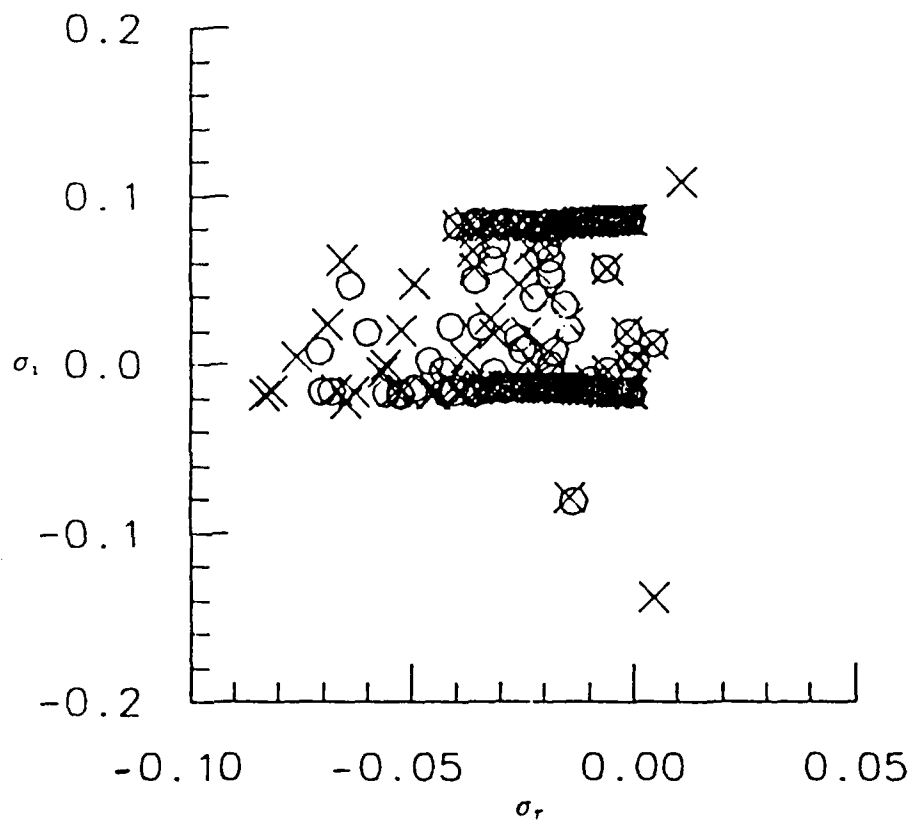


Figure 6.23 Real versus imaginary temporal eigenvalue of the subharmonic mode for a three-dimensional primary wave at $\phi = 10^\circ$ over a non-isotropic wall with $R_{f\bullet} = 2240$, $Fr \approx 24.5$, $A = 0.01$, and $\beta = 0.2$. (o, $N=40$ and x, $N=45$)

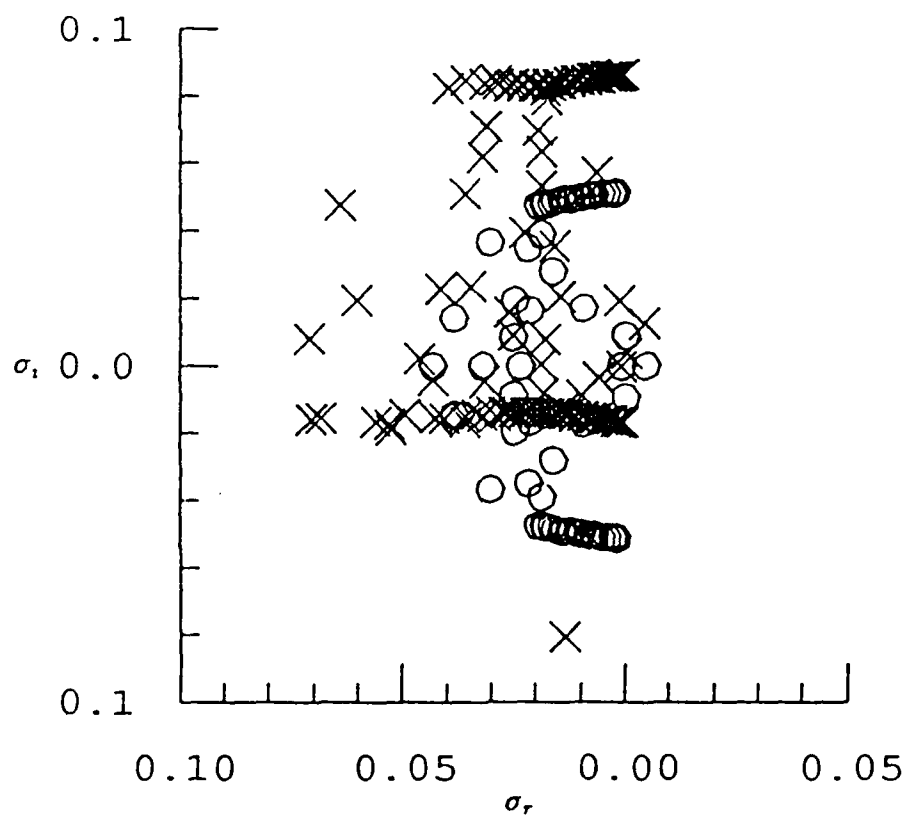


Figure 6.24 Real versus imaginary temporal eigenvalue of the subharmonic mode for two- and three-dimensional primary waves over a non-isotropic wall with $R_{\delta^*} = 2240$, $Fr \approx 24.5$, $A = 0.01$, and $\beta = 0.2$. (o, 2D and x, 3D at $\phi = 10^\circ$)

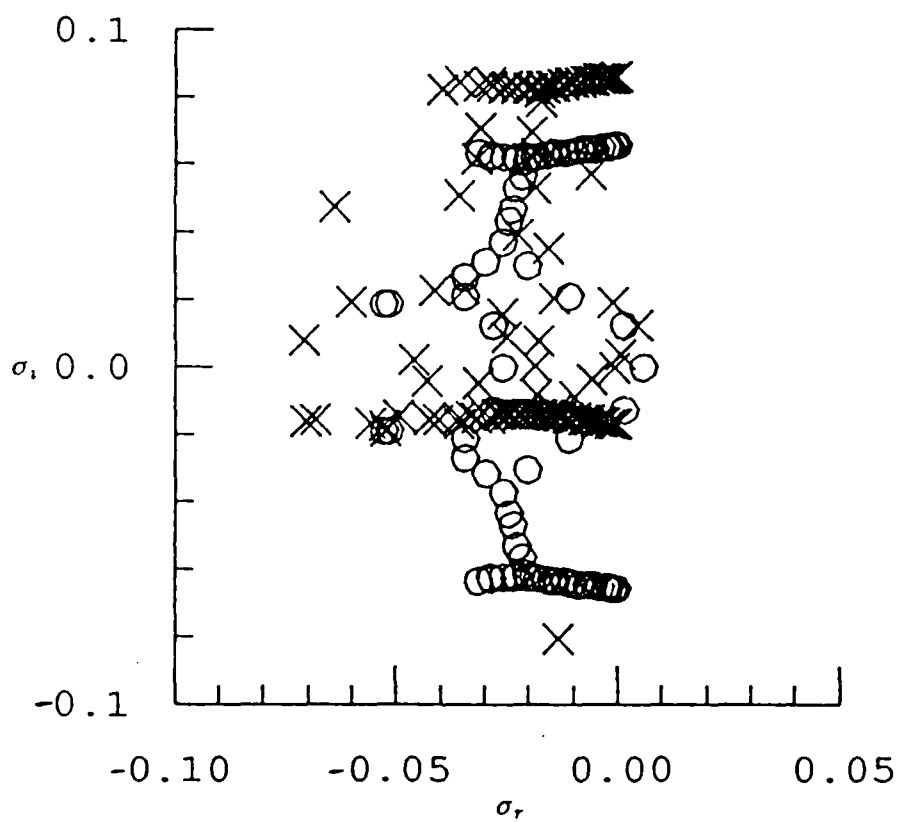


Figure 6.25 Real versus imaginary temporal eigenvalue of the subharmonic mode for a three-dimensional primary wave at $\phi = 10^\circ$ over a o, rigid wall and x, non-isotropic wall with $R_{\delta\bullet} = 2240$, $Fr \approx 24.5$, $A = 0.01$, and $\beta = 0.2$.

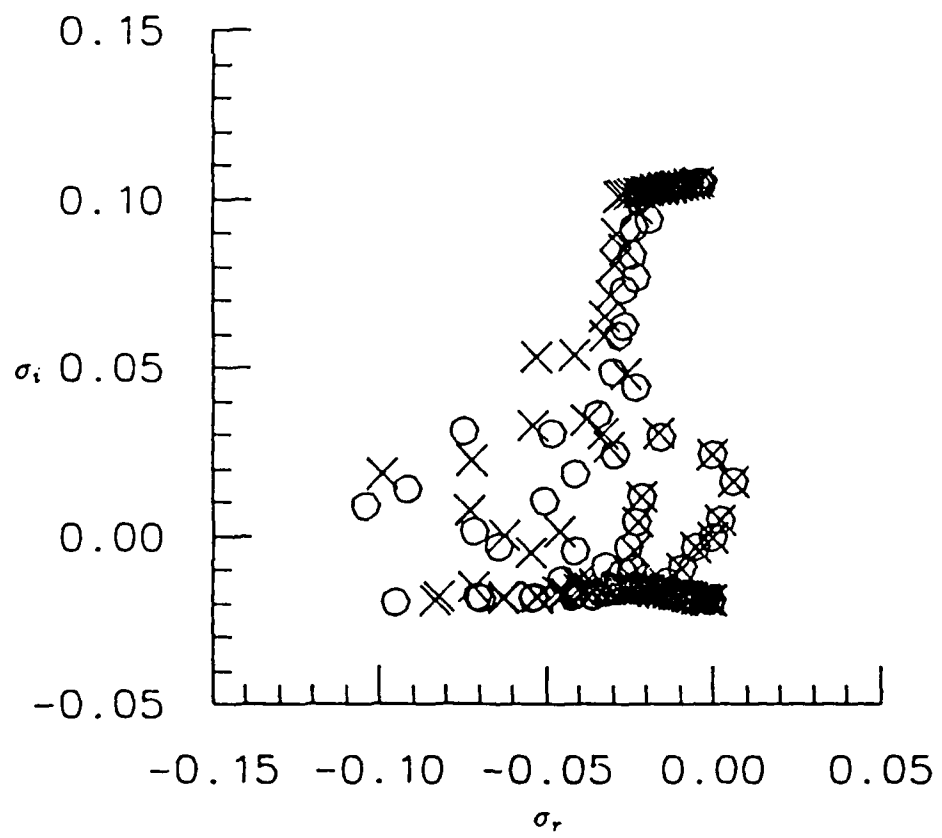


Figure 6.26 Real versus imaginary temporal eigenvalue of the subharmonic mode for a three-dimensional primary wave at $\phi = 10^\circ$ over a isotropic wall with $R_{\delta_*} = 2240$, $Fr \simeq 24.5$, $A = 0.01$, and $\beta = 0.25$. (o, $N=40$ and x, $N=45$)

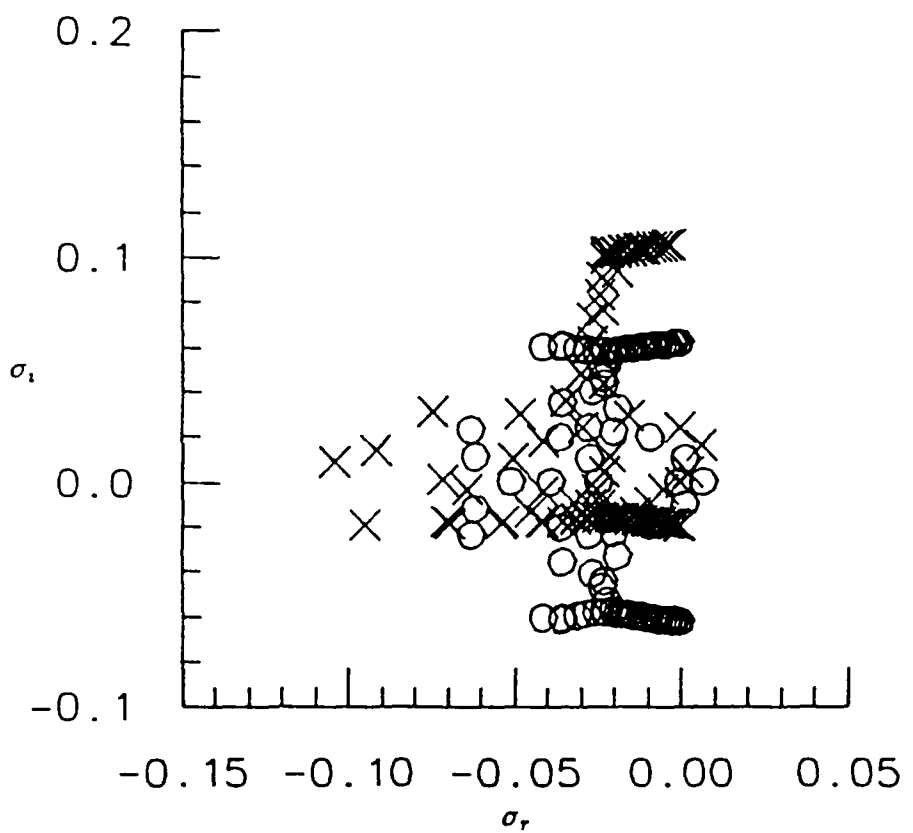


Figure 6.27 Real versus imaginary temporal eigenvalue of the subharmonic mode for two- and three-dimensional primary waves over a isotropic wall with $R_{\delta^*} = 2240$, $Fr \simeq 29.0$, $A = 0.01$, and $\beta = 0.25$. (o, 2D and x, 3D at $\phi = 10^\circ$)

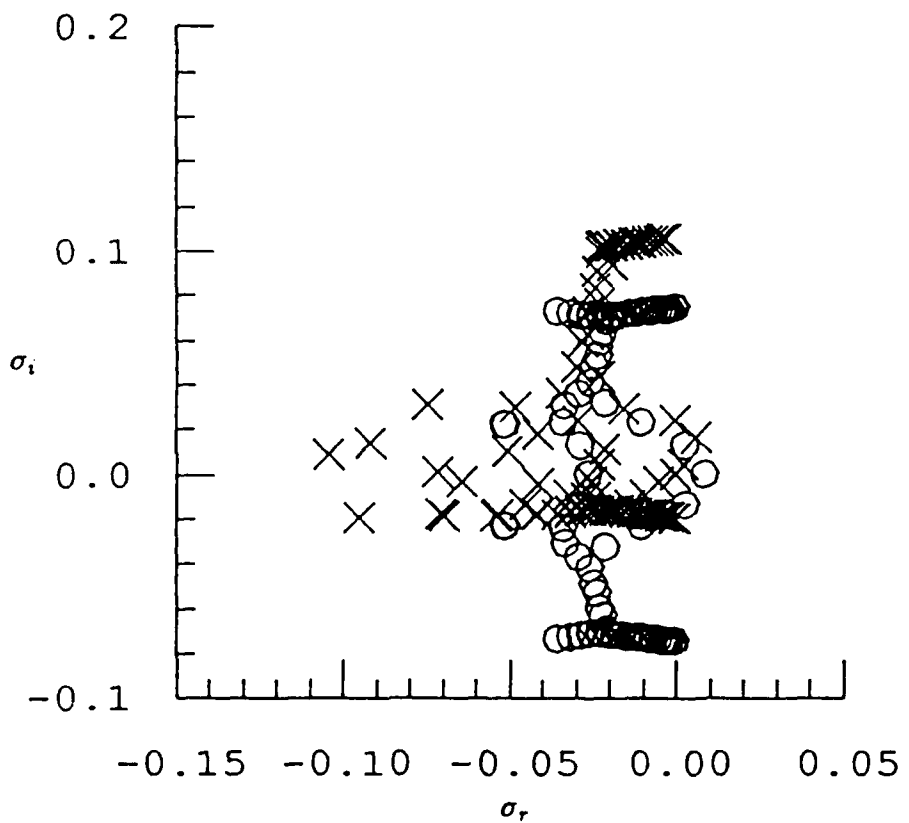


Figure 6.28 Real versus imaginary temporal eigenvalue of the subharmonic mode for a three-dimensional primary wave at $\phi = 10^\circ$ over a o, rigid wall and x, isotropic wall with $R_{\delta\bullet} = 2240$, $Fr \simeq 29.0$, $A = 0.01$, and $\beta = 0.25$.

isotropic wall results. Similar to the non-isotropic wall case, the rigid wall produces larger growth rates compared with the compliant wall results.

From Figure 5.9, the dominant growth rate for the isotropic wall occurs for a wave at a frequency of $\omega = 0.05$ ($Fr \approx 22.3$) and an angle of 50° . From Figure 5.10, the dominant growth rate for the non-isotropic wall is shown to occur for a wave with frequency $\omega = 0.04$ ($Fr \approx 17.9$) for an angle of 60° . To show further how the three-dimensional primary waves influence the growth rates of secondary disturbances, the growth rates of the subharmonic disturbance are shown for two- and three-dimensional primary waves versus spanwise wavenumber in Figure 6.29. For fixed properties, the subharmonic mode arising from the two-dimensional wave has the greatest growth rates. As the angle of wave propagation increases for three-dimensional waves, the growth rates continually decrease. For the three-dimensional waves, secondary disturbances no longer travel synchronously with the primary waves. This is drawn out by the frequency shift shown in Figure 6.30. We might postulate that this shift leads to a reduced efficiency of energy transfer from the basic flow to the secondary disturbance. In Figures 6.31-32, the non-isotropic wall is replaced by the isotropic wall. The two-dimensional wave has the dominant secondary growth rates. It appears from the frequency shift plots, that this shift is more a result of the three-dimensional nature of the basic flow instead of the influence of the compliant wall.

These two- and three-dimensional comparisons are somewhat misleading since the amplitude of the primary waves for a given Reynolds number should be different for each case. If the amplitudes that arise from the e^n calculations are used for the primary disturbance a better comparison is possible. This is shown in Figure 6.33 for the non-isotropic wall and Figure 6.34 for the isotropic wall. In both cases, the three-dimensional primary wave leads to much larger

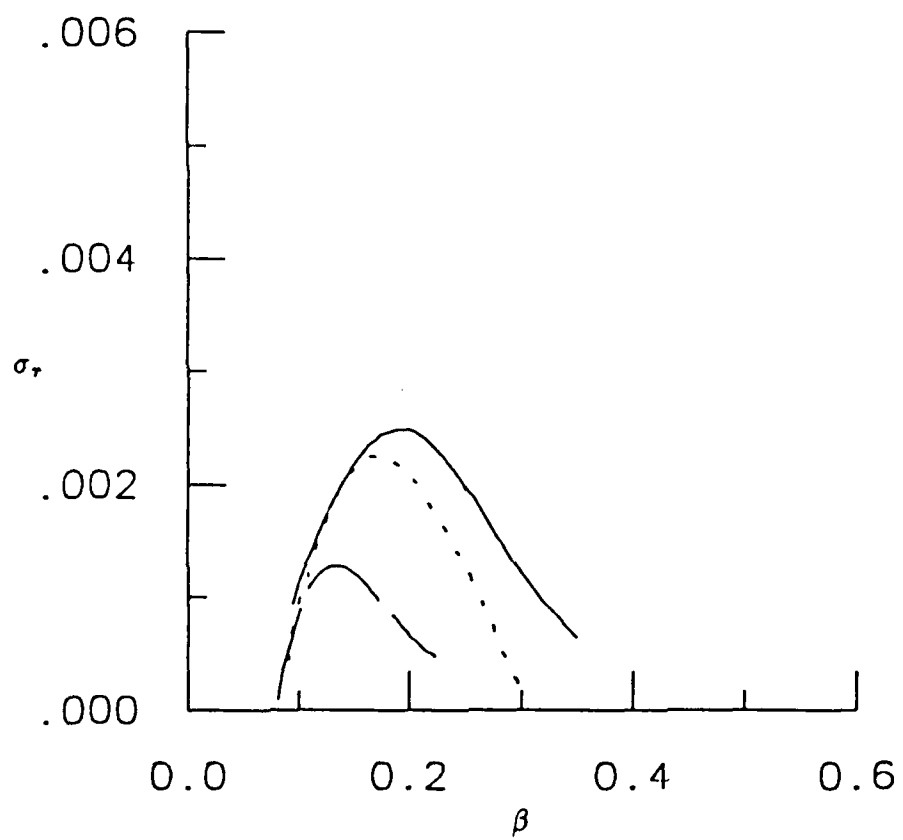


Figure 6.29 Growth rates of the subharmonic disturbance for two- and three-dimensional primary waves over the non-isotropic wall as a function of spanwise wavenumber for $R_{\delta^*} = 2240$, $Fr \simeq 17.9$, and $A = 0.01$. —, $\phi = 0^\circ$; ···, $\phi = 10^\circ$; and — —, $\phi = 20^\circ$.

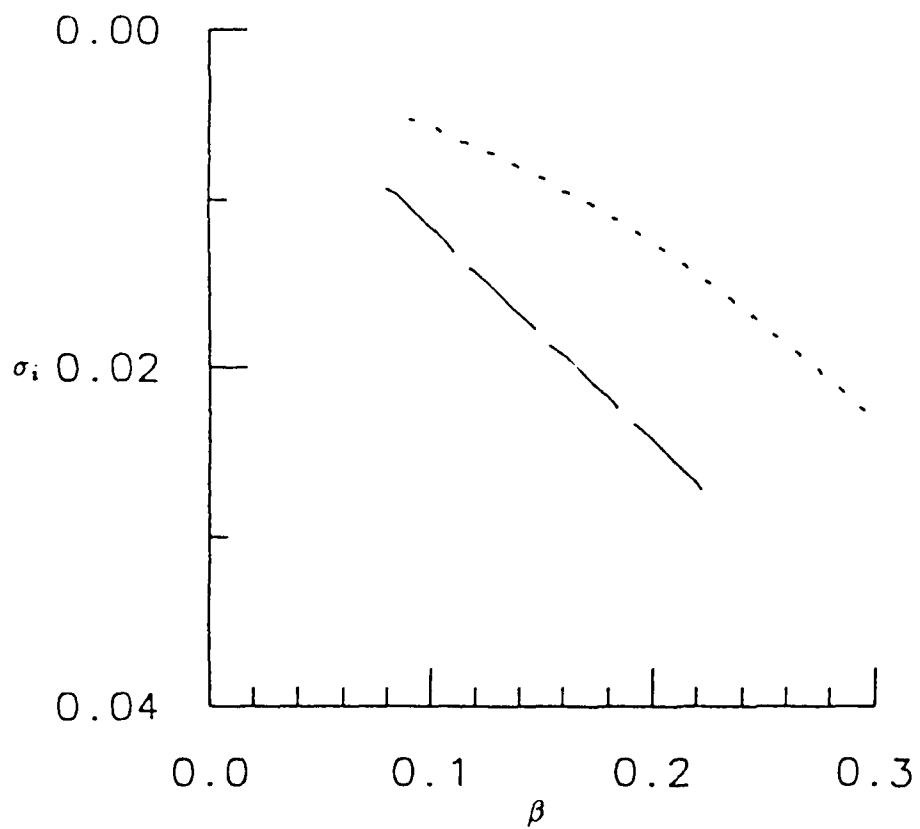


Figure 6.30 Frequency shift of the subharmonic disturbance for a three-dimensional primary wave over the non-isotropic wall as a function of spanwise wavenumber for $R_{\delta^*} = 2240$, $Fr \approx 17.9$, and $A = 0.01$. $\cdots, \phi = 10^\circ$ and $—$, $\phi = 20^\circ$.

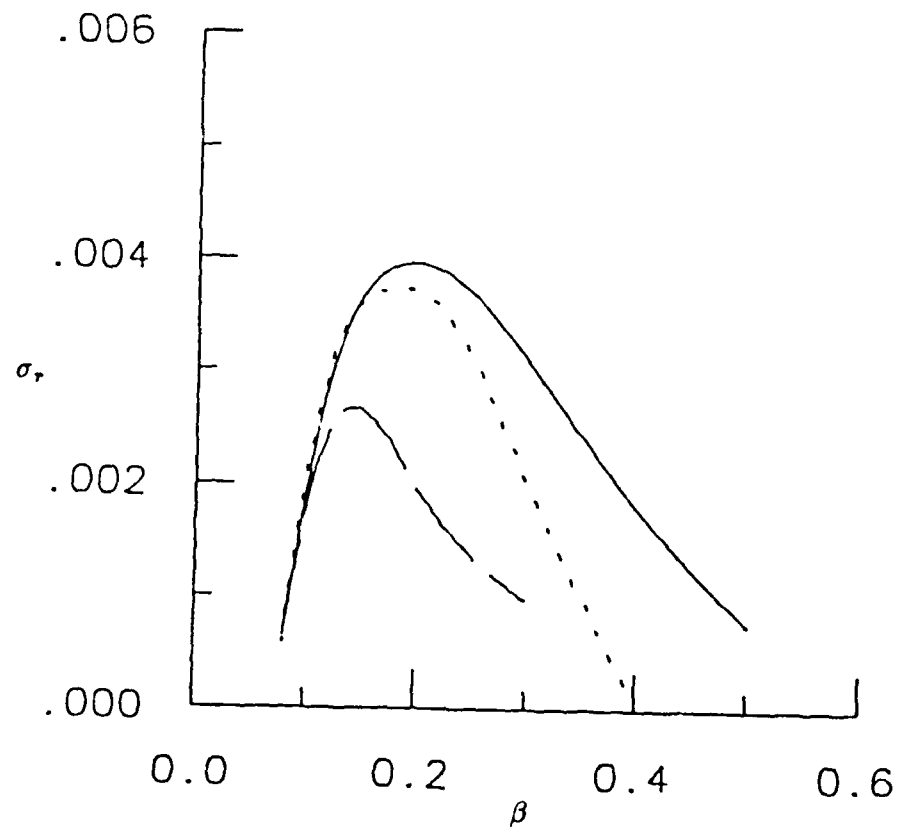


Figure 6.31 Growth rates of the subharmonic disturbance for two- and three-dimensional primary waves over the isotropic wall as a function of spanwise wavenumber for $R_{\delta^*} = 2240$, $Fr \approx 22.3$, and $A = 0.01$. —, $\phi = 0^\circ$; ···, $\phi = 10^\circ$; and — —, $\phi = 20^\circ$.

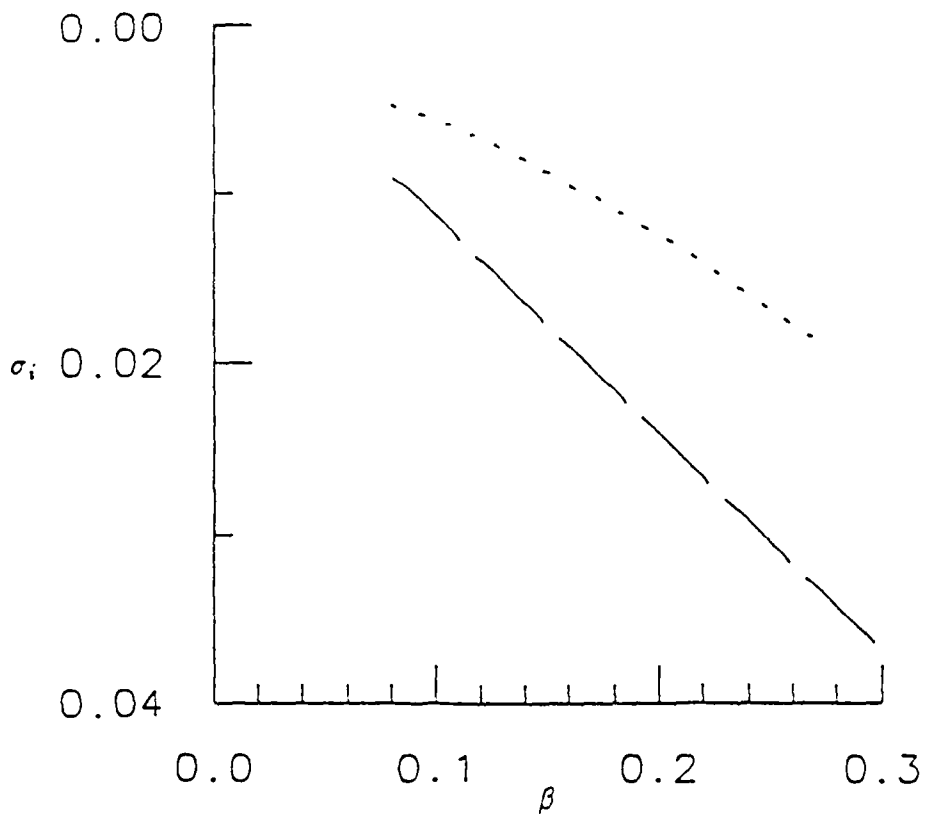


Figure 6.32 Frequency shift of the subharmonic disturbance for a three-dimensional primary wave over the isotropic wall as a function of spanwise wavenumber for $R_{\delta^*} = 2240$, $Fr \simeq 22.3$, and $A = 0.01$. $\cdots, \phi = 10^\circ$ and $-$, $\phi = 20^\circ$.

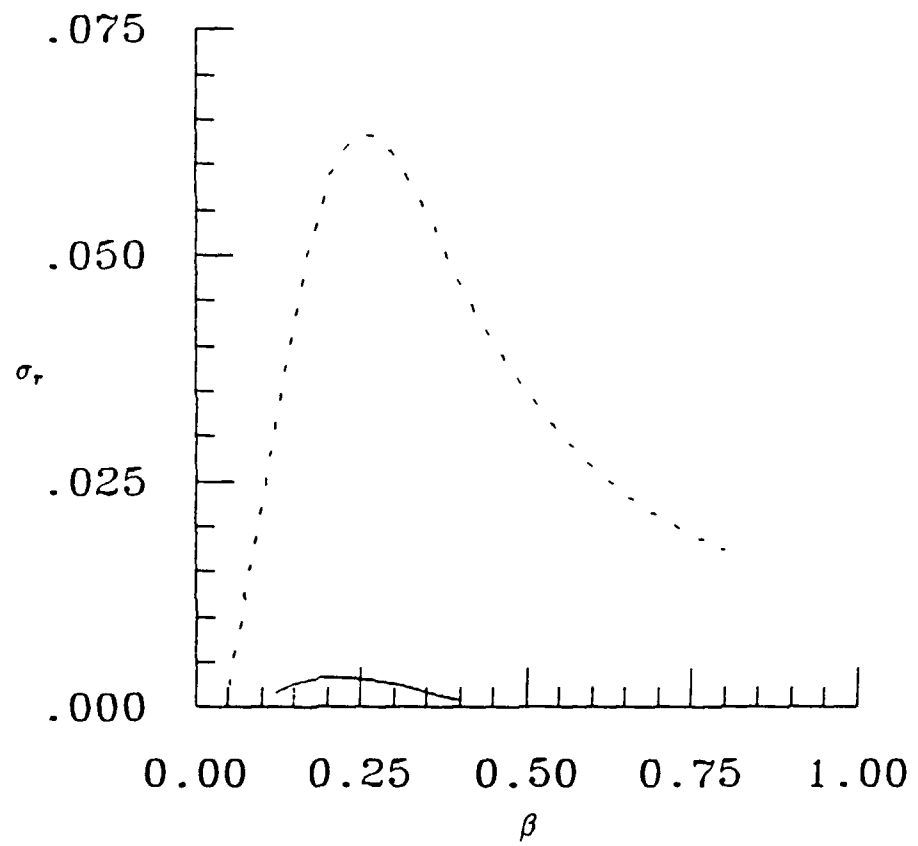


Figure 6.33 Growth rates of the subharmonic disturbance for two- and three-dimensional primary waves over the non-isotropic wall as a function of spanwise wavenumber for $R_{\delta^*} = 2288$ and $Fr \simeq 21.0$ for —, $\phi = 0^\circ$ with $A = 0.007$ and $\cdots, \phi = 50^\circ$ with $A = 0.045$.

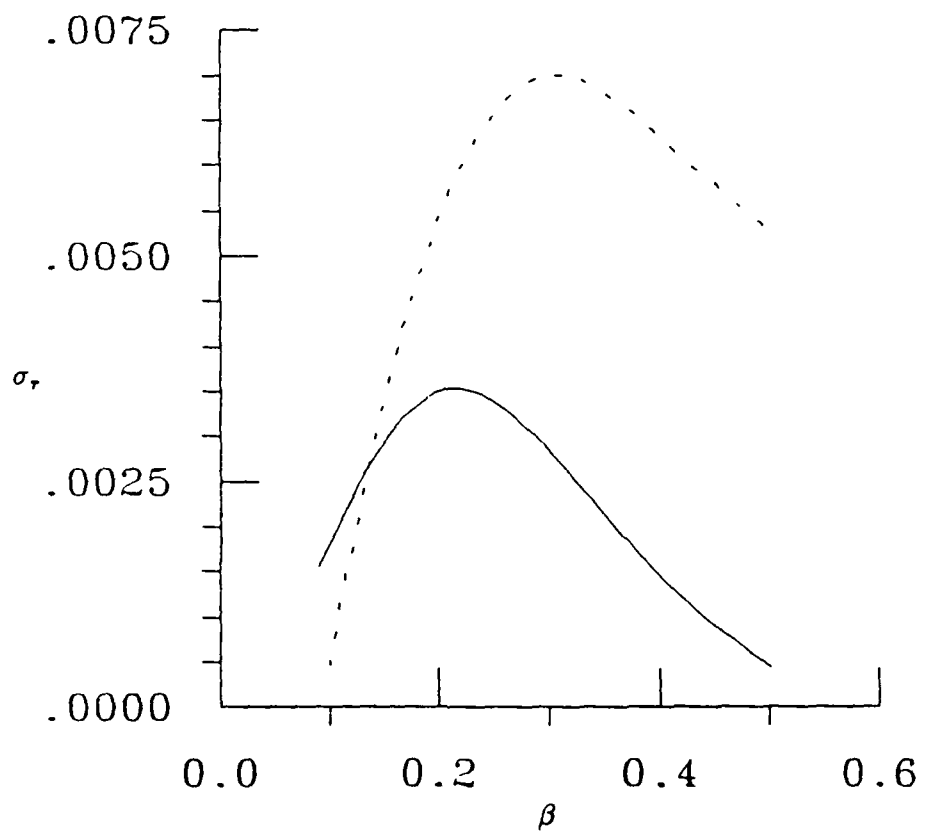


Figure 6.34 Growth rates of the subharmonic disturbance for two- and three-dimensional primary waves over the isotropic wall as a function of spanwise wavenumber for $R_{\delta^*} = 1760$ and $Fr \approx 30.2$ for —, $\phi = 0^\circ$ with $A = 0.010$ and ···, $\phi = 45^\circ$ with $A = 0.031$.

growth rates yet they are reduced significantly compared to the rigid wall case which is predicted to have already undergone transition.

From the e^n calculations in the primary instability analysis, it is clear that as the wave frequency decreases, the difference in amplitude between two- and three-dimensional TSI increases. Also, as this occurs, the dominant secondary instability arises from the three-dimensional primary wave as a result of its increased amplitude (A). Thus three-dimensional primary waves lead to the dominant secondary disturbance in spite of the loss of synchronization with the basic flow. But in order to identify the global effect of three-dimensional primary waves at higher frequencies, an e^n calculation has been carried out for a wave at $Fr \simeq 53$. Primary and secondary amplitudes versus Reynolds number are shown in Figure 6.35 for the rigid wall and non-isotropic wall. Only a relatively mild increase in amplitude occurs for both disturbances. As waves with lower frequencies are examined, the dominance of the three-dimensional instabilities becomes more pronounced. Yet, as we have already discussed, the rigid wall has already undergone transitioned.

This completes our presentation of results for the secondary instability analysis. It is found that three-dimensional primary waves lead to the dominant secondary instability over the compliant walls considered. This occurs only when the amplitude of the three-dimensional primary wave is much larger than the amplitude of the two-dimensional primary wave. The most important discovery of this study is that by using an appropriate compliant wall, the growth of the secondary instability can be suppressed. Further conclusions are drawn for both the primary and secondary analysis in the next, and final, chapter.

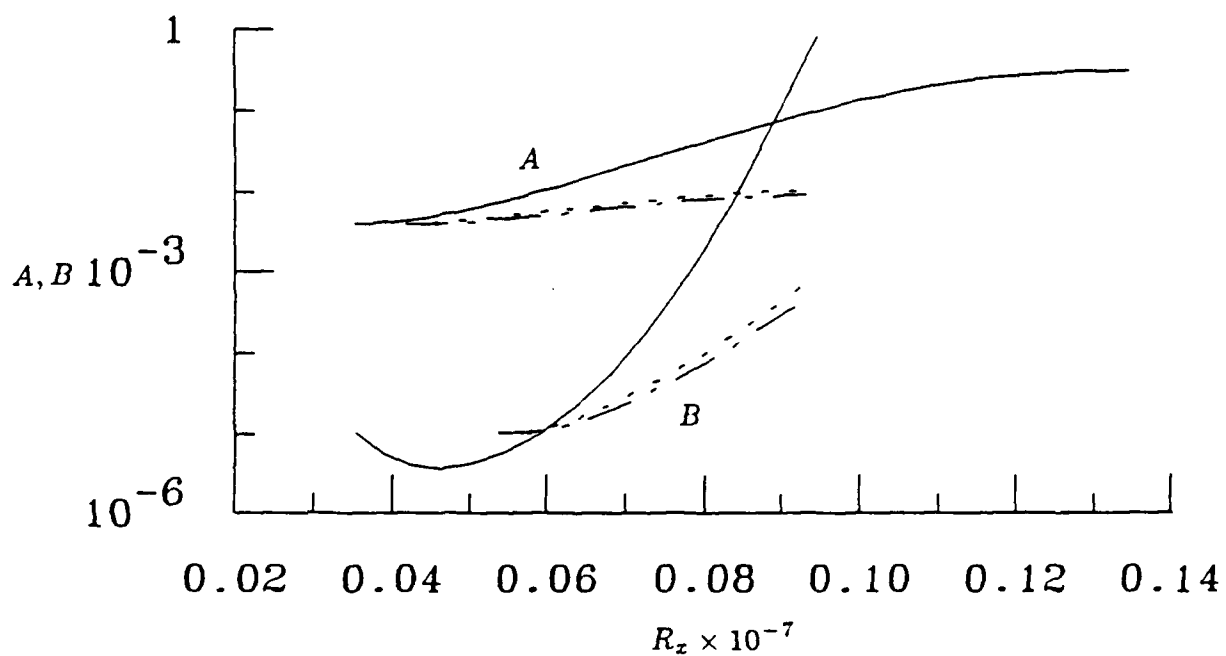


Figure 6.35 Amplitude growth with Reynolds number of the subharmonic mode (B) of a two- and three-dimensional primary wave (A) at $Fr \simeq 53$, $B_o = 1 \times 10^{-5}$, $A_o = 0.004$, and $\bar{b} = 0.15$ over a —, rigid wall — · —, 2D non-isotropic wall; and · · ·, 3D non-isotropic wall.

CHAPTER 7

CONCLUSIONS AND RECOMMENDATIONS

7.1 Conclusions

Previous studies involving compliant walls have focused on two-dimensional linear, or primary, instability analyses. The present thesis has considered the effect of compliant walls on three-dimensional primary instabilities in boundary layer transition. Additionally, the second stage of transition where secondary instabilities arise and lead to nonlinear breakdown to turbulence is examined. We have shown that three-dimensional primary instabilities dominate transition over the compliant walls considered; yet, transition delays occur compared to the rigid wall case. Further, it is demonstrated that the compliant walls can significantly suppress the growth of the secondary instabilities.

From the primary instability analysis, the three-dimensional Tollmien-Schlichting waves were shown to be dominant. The waves enter the unstable region at their most unstable three-dimensional state. As they travel downstream the angle of wave propagation becomes more two-dimensional. It has been shown that for the fixed Reynolds number at which the walls were optimized, the oblique modes dominate and reach maximum growth rates at angles of wave propagation of 40° - 60° from the streamwise direction.

The Cebeci-Stewartson method of extending e^n -type calculations to three-dimensional instabilities has been used in the present analysis. It is difficult to assess how good an approximation this is for three-dimensional disturbances over compliant walls. The local results show that the dominant disturbances often propagate at angles of up to 60° - 70° to the mainstream direction and that a narrower band of frequencies tend to be unstable for oblique waves. Consequently

the final value of n for a particular frequency is critically dependent on the precise path chosen for the e^n integration. Therefore, it is quite possible that the Cebeci-Stewartson method does not give good results in the present case. This matter will only be resolved by carrying out a study of the development of disturbances from a pulsed point source or some other appropriately formulated initial-value problem.

The non-isotropic wall optimized at $R_{\delta^*} = 5000$ indicated the greatest potential for transition delays for two-dimensional Tollmien-Schlichting waves. Yet, in considering three-dimensional modes, the transition delays were significantly reduced. This is somewhat puzzling. Two possible explanations come to mind. First, as we have just discussed, the e^n -criterion may not be accurate for three-dimensional modes. Thus anticipated benefits from a coating are not realized with this approach. Second, the optimization of each coating occurs through changing each property of the coating until a pre-determined criterion is reached. Thus, the walls that were used in the present study had very different property combinations. In comparing the results for the $\theta = 60^\circ(2240)$ wall with the $\theta = 60^\circ(5000)$ wall, we find that the wall optimized at the lower Reynolds number leads to a greater transition delay including three-dimensional instabilities. A possible explanation may be found in the resistance due to bending stiffness contributions. The $\theta = 60^\circ(2240)$ wall has lower bending stiffness than the $\theta = 60^\circ(5000)$ wall, so an increase in compliance may be felt by the three-dimensional modes leading to greater transition delays.

For the present study, the worst possible scenario was used in order to provide a conservative estimate of the compliant wall potential for transition delays for three-dimensional instabilities. However, the present calculations do indicate that three-dimensional instabilities are critically important in transition over compli-

ant walls. Finally, oblique Travelling-Wave Flutter and Static-Divergence instabilities were considered and were found to remain marginally stable for all walls studied. So, as with the previous two-dimensional investigations, the Tollmien-Schlichting instabilities dominate transition.

For the secondary instability analysis, a limited number of cases were considered for a set of parameters. To compare the rigid wall results with the compliant wall relatively high frequency cases had to be chosen. For two-dimensional primary instabilities at a fixed Reynolds number, both isotropic and non-isotropic walls lead to reduced secondary instability growth rates. Negligible changes occur in the spanwise wavenumber to capture the maximum growth rate of the three-dimensional secondary instability over the compliant walls. For e^n -criterion calculations, the non-isotropic wall suppressed the development and growth of the secondary instability while the isotropic wall yielded similar results to the rigid wall case. These calculations identified important features of the secondary instability behavior. For the frequency used in the calculations, the amplification of the primary wave over the isotropic wall was similar to the rigid wall results while the amplification of primary waves over the non-isotropic wall were significantly reduced. So as a preliminary study where one frequency is used, we may infer that a suppression of the primary instability leads to a resulting suppression of the three-dimensional secondary instability growth. This leads to a further delay of transition in the later stages of transition. Even by doubling the primary amplitude of the disturbance over the non-isotropic wall, reduced growth rates are observed compared with the results for the rigid wall. The illustrations of the three-dimensional instability show that the effect of the secondary instability become effective when the primary instability approaches branch II of the neutral curve. Results of this sort suggest that the isotropic wall would not be effective

in delaying transition. This is somewhat misleading since for the frequency used, the primary instability behavior over the isotropic wall is similar to the rigid wall case. As the primary instability analysis revealed, the advantages of the compliant walls become more pronounced at lower frequencies.

For the secondary instability arising from a three-dimensional primary wave, the physical phenomenon changes compared to the two-dimensional wave. For oblique waves, the basic flow is no longer symmetric and the spanwise induced flow causes a phase shifting of the secondary disturbance. The secondary disturbance no longer travels synchronously with the primary instability. As the angle of wave propagation increases, the frequency of the shift between the disturbances increases. Thus, the efficient energy exchange between two-dimensional primary and secondary disturbances is lost and a less efficient means is established for oblique waves. Locally, the two-dimensional primary waves lead to the largest growth rates for secondary instabilities. However, this comparison is misleading globally since the secondary theory neglects the local growth rate of the primary wave. From the initial primary stability analysis, we would expect that the two- and three-dimensional waves would not have the same wave amplitudes. When account is taken of the amplitude difference between the two- and three-dimensional waves, secondary instability growth rates arising from three-dimensional waves dominate for the compliant walls used. Yet for these comparisons, the rigid wall flow has undergone transition to turbulence.

In summary, we have the following unique results to contribute to the technology of compliant walls.

I. Primary instabilities (linear)

- (i) Three-dimensional instabilities dominate transition over compliant walls.

- (ii) Delays of transition to turbulence are theoretically predicted using compliant walls.
- (iii) Low frequency waves are highly three-dimensional while high frequency waves are predominantly two-dimensional.
- (iv) Orthotropic plates are less sensitive to three-dimensional disturbances compared with isotropic plates.
- (v) Non-isotropic walls are less sensitive to three-dimensional disturbances than isotropic walls.

II. Secondary instabilities

- (i) Compliant walls can lead to reduced growth rates of secondary instabilities compared with the rigid wall case.
- (ii) Three-dimensional primary waves lead to dominant secondary instabilities when the amplitude of the wave is larger than a similar two-dimensional primary wave.
- (iii) Suppression of primary instability growth leads to a resulting suppression of secondary instability growth.

7.2 Recommendations for Future Studies

The present analysis has considered three-dimensional primary and secondary instabilities over compliant walls. The results of this study provide a guideline for future studies involving transition over compliant walls. Namely, three-dimensional disturbances should be of concern. A number of future theoretical and experimental challenges present themselves. A brief list of suggestions follow.

- (i) No proven transition criterion for three-dimensional disturbances exist; therefore, work toward this end should progress.

- (ii) In the present study, a path for three-dimensional disturbances had to be assumed. A point source calculation would be useful to determine how disturbances propagate over compliant walls.
- (iii) Since three-dimensional disturbances were shown to dominate transition over compliant walls, wall properties should be chosen to achieve some predetermined optimal conditions for these modes.
- (iv) A study of how sensitive the secondary instability growth rates are to changes in the wall properties may be undertaken. This may be performed in a manner similar to the primary analysis by Joslin (1987).
- (v) A turbulent boundary layer may be studied to determine if the near-wall structure can be manipulated using compliant walls. The compliant wall properties can be optimized for some desired condition. A proposed formulation for the turbulent boundary layer problem is given in Appendix E.
- (vi) Experiments are needed to verify the present results and previous theoretical studies. The results of Willis (1986) indicate that theory and experiments agree in that reduced amplifications of disturbances can occur through the use of wall compliance. He used a foil-gage aft of the test section to measure disturbance response. Interference with the wall motion can arise through using surface mounted techniques. Future experiments could be performed using a non-intrusive means such as Laser Doppler Velocimetry. Tracking instability growth as it propagates downstream is of importance. Additionally, experiments similar to Kachanov et al. (1984) should be undertaken to compare results for secondary instabilities over rigid and compliant walls.
- (vii) In the past, difficulties have prevented the manufacturing of coatings with specified wall properties. This technology is currently maturing. Another problem exists with realizable coatings. Coating deterioration with time

has plagued these coatings making them unreliable. This concern should be addressed

There is a wealth of information that can be obtained from solving these problems. This list is far from complete, but I hope it provides a stimulus to the reader for further research in the use of compliant walls.

REFERENCES

Andreopoulos J., Durst F., Zaric Z., and Jovanovic J. 1984 "Influence of Reynolds number on characteristics of turbulent wall boundary layers," *Experiments in Fluids* 2, pp. 7-16.

Arscott F.M. 1964 Periodic Differential Equations, The Macmillan Co., New York.

Babenko V.V. and Surkina R.M. 1971a "Determining the oscillating mass parameter of the skin cover of some marine animals," *Bionika*, 5, pp. 94-98.

Babenko V.V. 1971b "Some mechanical characteristics of the skin cover of dolphins," *Bionika*, 5, pp. 76-81.

Babenko V.V. 1973a "Techniques for determining the mechanical properties of flexible coatings and a basis for the solution of their design," *Bionika*, 7, pp. 71-79.

Babenko V.V. 1973b "Experimental investigation of the hydrodynamic stability for simple flat membrane surfaces," [in Russian], *Gidromekhanika*, 24, pp. 3-11.

Babenko V.V. 1979 "Interaction of a stream with an elastic surface," In: *Stratified and Turbulent Currents*, Naukova Dumka Publishing House, Kiev, pp. 292-301.

Balasubramanian R. 1978 "Analytical and numerical investigations of structural response of compliant wall materials. Part I," NASA CR-2999.

Bayly B.J., Orszag S.A., and Herbert T. 1988 "Instability mechanisms in shear flow transition," *Annual Review of Fluid Mechanics*, 20, pp. 359-391.

Benjamin T.B. 1960 "Effects of a flexible boundary on hydrodynamic stability," *Journal of Fluid Mechanics*, 9, pp. 513-532.

Benjamin T.B. 1963 "The three-fold classification of unstable disturbances in flexible surfaces bounding inviscid flows," *Journal of Fluid Mechanics*, 16, pp. 436-450.

Benjamin T.B. 1964 "Fluid flow with flexible boundaries," *Proceedings of the 11th International Congress of Applied Mechanics*, Munich, pp. 109-128.

Benney D.J. and Lin C.C. 1960 "On the secondary motion induced by oscillations in a shear flow," *The Physics of Fluids*, 3(4), pp. 656-657.

Benney D.J. and Orszag S.A. 1977 "Stability analysis for laminar flow control. Part I.," NASA CR-2910.

Benney D.J. and Chow K. 1987 "Nonlinear theories for hydrodynamic instabilities," In: *Nonlinear wave Interactions in Fluids*, pp. 1-8.

Bertolotti F.P. 1985 "Temporal and spatial growth of subharmonic disturbances in Falkner-Skan flows," M.S. Thesis, Virginia Polytechnic Institute and State University.

Betchov R. 1959 "Simplified analysis of laminar boundary-layer oscillations," Douglas Aircraft Company Report No. ES-29174.

Blackwelder R.F. 1979 "Boundary-layer transition," *The Physics of Fluids*, 22, pp. 583-584.

Blasius H. 1908 "Grenzschichten in Flüssigkeiten mit kleiner Reibung, *Z. Math u Phys*, 56, pp. 1. (NACA Tech Mem 1256).

Boyd J.P. 1982 "The optimization of convergence for Chebyshev Polynomial methods in an unbounded domain," *Journal of Computational Physics*, 45, pp. 43-79.

Breuer K.S., Haritonidis J.H., and Landahl M.T. 1989 "The control of transient disturbances in a flat plate boundary layer through active wall motion," *The Physics of Fluids A*, 1(3), pp. 574-582.

Bridges T.J. 1984 "A mathematical analysis of the effect of freestream turbulence on the Blasius boundary layer," PhD Thesis, The Pennsylvania State University.

Bridges T.J. and Morris P.J. 1984a "Differential eigenvalue problems in which the parameter appears nonlinearly," *Journal of Computational Physics*, 55(3), pp. 437-460.

Bridges T.J. and Morris P.J. 1984b "Spectral calculations of the spatial stability of non-parallel boundary layers," *AIAA 22nd Aerospace Sciences Meeting*, January 9-12, 1984/Reno, Nevada. AIAA Paper No. 84-0437.

Burden R.L. and Faires J.D. 1985 Numerical Analysis, 3rd edition, Prindle, Weber and Schmidt.

Bushnell D.M., Hefner J.N., and Ash R.L. 1977 "Effect of compliant wall motion on turbulent boundary layers," *The Physics of Fluids A*, 20(10), pp. S31-S48.

Bushnell D.M. 1980 "Compliant surfaces introduction," In: *Viscous Flow Drag Reduction*, Progress in Aeronautics and Astronautics, **72**, pp. 387-390.

Bushnell D.M. 1984 "NASA research on viscous drag reduction II," In: *Laminar-Turbulent Boundary Layers*, **11**, pp. 93-98.

Canuto C., Hussaini M.Y., Quarteroni A., and Zang T.A. 1988 Spectral Methods in Fluid Dynamics, Springer-Verlag, New York.

Carpenter P.W. 1984a "The effect of damping on the hydrodynamic stability of flows over Kramer-type compliant surfaces," In: *Laminar-Turbulent Boundary Layers*, **11**, pp. 53-59.

Carpenter P.W. 1984b "A note on the hydroelastic instability of orthotropic panels," *Journal of Sound and Vibration*, **94**, pp. 553-554.

Carpenter P.W. and Morris P.J. 1985 "The hydrodynamic stability of flows over non-isotropic compliant surfaces-numerical solution of the differential eigenvalue problem," In: *Numerical Methods in Laminar and Turbulent Flow*, pp. 1613-1620.

Carpenter P.W. and Garrad A.D. 1985 "The hydrodynamic stability of flow over Kramer-type compliant surfaces: Part 1. Tollmien-Schlichting instabilities," *Journal of Fluid Mechanics*, **155**, pp. 465-510.

Carpenter P.W. and Garrad A.D. 1986 "The hydrodynamic stability of flow over Kramer-type compliant surfaces: Part 2. Flow-induced surface instabilities," *Journal of Fluid Mechanics*, **170**, pp. 199-232.

Carpenter P.W. "The optimization of compliant surfaces for transition delay," In: *Turbulence Management and Relaminarization*, IUTAM Symposium, January 19-23, 1987a/Bangalore, India.

Carpenter P.W. "The hydrodynamic stability of flows over simple non-isotropic compliant surfaces," *Proceedings of the International Conference on Fluid Mechanics*, July 1-4, 1987b/Beijing, China.

Carpenter P.W. and Gajjar J.S.B. 1990 "A general theory for two- and three-dimensional wall-mode instabilities in boundary layers over isotropic and anisotropic compliant walls," *Theoretical and Computational Fluid Dynamics*, **2**.

Carpenter P.W., Joslin R.D., and Morris P.J. 1990a "A note on the occurrence of an apparently anomalous spatially growing eigenmode for the coupled flow/compliant-wall eigenproblem," submitted to *Theoretical and Computational Fluid Dynamics*.

Carpenter P.W., Joslin R.D., and Morris P.J. 1990b "An energy analysis of compliant wall boundary layers," submitted to *Journal of Fluids and Structures*.

Carpenter P.W. and Morris P.J. 1990 "The effects of anisotropic wall compliance on boundary layer stability and transition," *Journal of Fluid Mechanics*.(to appear)

Carpenter P.W. 1990a "Status of transition delay using compliant walls," In: *Viscous Drag Reduction*, Progress in Aeronautics and Astronautics.(to appear)

Carpenter P.W. 1990b School of Engineering, University of Exeter, U.K. (personal communication)

Cebeci T. and Smith A.M.O. 1974 Analysis of Turbulent Boundary Layers, Academic Press, New York.

Cebeci T. and Stewartson K. 1980 "On stability and transition in three-dimensional flows," *AIAA Journal*, 18, pp. 398-405.

Cebeci T. and Chen H.H. 1989 "An evaluation of stability-based methods for transition of three-dimensional flows," In: *Laminar-Turbulent Transition*, IUTAM Symposium, Toulouse.

Coles D. 1956 "The law of the wake in the turbulent boundary layer," *Journal of Fluid Mechanics*, 1, pp. 191-226.

Conti S.D. 1966 "The numerical solution of linear boundary value problems , " *SIAM Review*, 8(3), pp. 309-321.

Coppel W.A. 1965 Stability and Asymptotic Behavior of Differential Equations, D.C. Heath & Co., Boston.

Corke T.C. and Mangano R.A. 1987 "Transition of a boundary layer: controlled fundamental-subharmonic interactions," In: *Turbulence Management and Relaminarization*, IUTAM Symposium, Bangalore, India.

Corke T.C. 1987 "Measurements of resonant phase locking in unstable axisymmetric jets and boundary layers," In: *Nonlinear wave Interactions in Fluids*, pp. 37-65.

Courant R. and Hilbert D. 1953 Methods of Mathematical Physics, Vol. I.

Craik A.D.D. 1971 "Non-linear resonant instability in boundary layers," *Journal of Fluid Mechanics*, 50(2), pp. 393-413.

Daniel A.P. 1984 "Boundary layer stability on compliant surfaces," Progress Report: Trials 2 and 3, BMT Report for MOD contract.

Daniel A.P. 1985 "Boundary layer stability on compliant surfaces," Progress Report: Trials 4 and 5, BMT Report for MOD contract.

Daniel A.P. 1986 "Boundary layer stability on compliant surfaces," Progress Report: Trials 6, BMT Report for MOD contract.

Dennis J.E. Jr., Traub J.F., and Weber R.P. 1978 "Algorithms for solvents of matrix polynomials," *SIAM Journal of Numerical Analysis*, 15(3), pp. 523-533.

Dowell E.H. 1985 "The effects of compliant walls on transition and turbulence," In: *Shear Flow-Structure Interaction Phenomena*, pp. 37-52.

Dryden H.L. 1955 "Fifty years of boundary-layer theory and experiment," *Science*, 121, pp. 375-380.

Duncan J.H., Waxman A.M., and Tulin M.P. 1985 "The dynamics of waves at the interface between a viscoelastic coating and a fluid flow," *Journal of Fluid Mechanics*, 158 pp. 177-197.

Evrensel C.A. and Kalnins A. 1985 "Response of a compliant slab to inviscid incompressible fluid flow," *Journal of the Acoustical Society of America*, 78(6), pp. 2034-2041.

Fasel H.F. 1974 "Numerical solution of the unsteady Navier-Stokes equations for the investigation of laminar boundary layer stability," *Proceedings of the 4th International Conference on Numerical Methods in Fluid Dynamics*, Berlin, pp. 151-160.

Fasel H.F. 1976 "Investigation of the stability of boundary layers by a finite-difference model of the Navier-Stokes equations," *Journal of Fluid Mechanics*, 78, pp. 355-383.

Fasel H.F., Rist U., and Konzelmann U. 1987 "Numerical investigation of the three-dimensional development in boundary layer transition," AIAA Paper No. 87-1203.

Fasel H.F. and Konzelmann U. 1990 "Nonparallel stability of a flat plate boundary layer using the complete Navier-Stokes equations," submitted to the *Journal of Fluid Mechanics*.

Floqué G. 1883 "Sur les équations différentielles linéaires à coefficients périodiques," *Ann. Sci. École Norm Sup.*, 2(12), pp. 47-89.

Fox L. and Parker I.B. 1968 Chebyshev Polynomials in Numerical Analysis, Oxford University Press, London.

Fraser L.A. and Carpenter P.W. 1985 "A numerical investigation of hydroelastic instabilities in laminar flows over compliant surfaces comprising of one or two-layers of viscoelastic materials," In: *Numerical Methods in Laminar and Turbulent Flows*, pp. 1171-1181.

Gad-el-Hak M., Blackwelder R.F., and Riley J.J. 1980 "Interaction of compliant surfaces with transitional and turbulent boundary layers," In: *Viscous Flow Drag Reduction*, Progress in Aeronautics and Astronautics, 72, pp. 20-29.

Gad-el-Hak M., Blackwelder R.F., and Riley J.J. 1984 "On the interaction of compliant coatings with boundary-layer flows," *Journal of Fluid Mechanics*, 140, pp. 257-280.

Gad-el-Hak M. 1987 "Compliant coatings research: A guide to the experimentalist," *Journal of Fluids and Structures*, 1, pp. 55-70.

Gad-el-Hak M. 1985 "Boundary layer interactions with compliant coatings: an overview," In: *Shear Flow-Structure Interaction Phenomena*, pp. 63-78.

Gaster M. 1962 "A note on the relation between temporally-growing and spatially-growing disturbances in hydrodynamic stability," *Journal of Fluid Mechanics*, 14, pp. 222-224.

Gaster M. 1974 "On the effects of boundary-layer growth on flow stability," *Journal of Fluid Mechanics*, 66, pp. 465-480.

Gaster M. 1983 "The development of a two-dimensional wavepacket in a growing boundary layer," *Proceedings of the Royal Society*, A384, pp. 317-332.

Gaster M. 1987 "Is the dolphin a red herring?" In: *Turbulence Management and Relaminarization*, IUTAM Symposium, Bangalore, India.

Gawn R.W.L. 1948 "Aspects of the locomotion of whales," *Nature*, 161, pp. 44-46.

Gear C.W. 1978 Applications and Algorithms in Science and Engineering, Science Research Associates, Inc.

Gohberg I., Lancaster P., and Rodman L. 1982 Matrix Polynomials, Academic Press.

Gottlieb D., Hussaini M.Y., and Orszag S.A. 1984 "Introduction: theory and applications of spectral methods," SIAM Spectral Methods for Partial Differential Equations, pp. 1-54.

Gottlieb D. and Orszag S.A. 1977 Numerical Analysis of Spectral Methods: Theory and Application, SIAM, 26.

Gray J. 1957 "How fishes swim," *Scientific American*, 197(2), pp. 48-54.

Gregory N. and Love E.M. 1961 "Progress report on an experiment on the effect of surface flexibility on the stability of laminar flow," ARC Report 23, 314.

Grosch C.E. and Orszag S.A. 1977 "Numerical solution of problems in unbounded regions: coordinate transforms," *Journal of Computational Physics*, 25, pp. 273-296.

Grosskreutz R. 1971 "Wechselwirkungen zwischen turbulenten Grenzschichten und Weichen wänden," MPI für Strömungsforschung und der AVA: (Proceedings of the Max Plank Institute of Flow Research and the Aerodynamic Experimental Station), Göttingen, Mitt. No. 53.

Grosskreutz R. 1975 "An attempt to control boundary layer turbulence with non-isotropic compliant walls," *University Science Journal*, (Dares es Salaam), 1(1), pp. 65-73.

Gyorgyfalvy D. 1967 "Possibilities of drag reduction by the use of flexible skin," *Journal of Aircraft*, 4(3), pp. 186-192.

Hall P. and Smith F.T. 1988 "Nonlinear Tollmien-Schlichting/vortex interaction in boundary layers," ICASE Report No. 88-46.

Hansen R.J., Hunston D.L., Ni C.C., Reischman M.M., and Hoyt J.W. 1979 "An experimental studies of flow-generated waves on a flexible surface," *Journal of Sound and Vibration*, 68, pp. 317.

Hansen R.J., Hunston D.L., Ni C.C., Reischman M.M., and Hoyt J.W. 1980 "Hydrodynamic drag and surface deformations generated by liquid flows over flexible surfaces," In: *Viscous Flow Drag Reduction*, Progress in Aeronautics and Astronautics, 72, pp. 439-453.

Hansen R.J. and Hunston D.L. 1983 "Fluid property effects on flow-generated waves on a compliant surface," *Journal of Fluid Mechanics*, 133, pp. 161-177.

Helmholtz H. 1868 "Über discontinuirliche Flüssigkeits-Bewegungen," *Akad. Wiss.*, Berlin, Monatsber 215.

Herbert T. 1976 "Periodic secondary motions in a plane channel," *Lecture Notes in Physics*, 59 pp. 235-240.

Herbert T. 1977 "Finite amplitude stability of plane parallel flows," AGARD-CP-224 pp. 3.1-3.10.

Herbert T. and Morkovin M.V. 1979 "Dialogue on bridging some gaps in stability and transition research," In: *Laminar-Turbulent Transition*, IUTAM Symposium, Stuttgart, Germany.

Herbert Th. 1981 "A secondary instability mechanism in plane Poiseuille flow," *Bulletin of the American Physical Society*, 26, p. 1257.

Herbert T. 1983 "Secondary instability of plane channel flow to subharmonic three-dimensional disturbances," *The Physics of Fluids*, 26(4), pp. 871-874.

Herbert T. 1984a "Nonlinear effects in hydrodynamic stability," AGARD-R-709.

Herbert T. 1984b "Secondary instability of shear flows," AGARD-R-709.

Herbert T. 1984c "Analysis of the subharmonic route to transition in boundary layers," *AIAA 22nd Aerospace Sciences Meeting*, January 9-12, 1984/Reno, Nevada. AIAA Paper No. 84-0009.

Herbert T. 1984d "Secondary instability of plane shear flows-theory and application," In: *Laminar-Turbulent Transition*, IUTAM Symposium, July 9-13, 1984/Novosibirsk, USSR. .

Herbert T. 1985a "Three-dimensional phenomena in the transitional flat-plate boundary layer," *AIAA 23rd Aerospace Sciences Meeting*. January 14-17, 1985/Reno, Nevada. AIAA Paper No. 85-0489.

Herbert T. 1985b "Vortical Mechanisms in shear flow transition," In: *Direct and Large Eddy Simulation of Turbulence*, Euromech Colloquium No. 199, September 30-October 2, 1985/München FRG., pp. 19-36.

Herbert T., Bertolotti F.P., and Santos G.R. 1985 "Floquet analysis of secondary instability in shear flows," In: *Stability of Time Dependent and Spatially Varying Flows*, August 19-23, 1985, pp. 43-57.

Herbert T. 1986 "Analysis of secondary instabilities in boundary layers," *Proceedings of the 10th US National Congress of Applied Mechanics*, June 16-20, 1986/The University of Texas at Austin, pp. 445-456.

Herbert T. 1988a "Onset of transition in boundary layers," *International Journal for Numerical Methods in Fluids*, 8, pp. 1151-1164.

Herbert T. 1988b "Secondary instability of boundary layers," *Annual Review of Fluid Mechanics*, 20, pp. 487-526.

Jordinson R. 1970 "The flat plate boundary layer. Part 1. Numerical integration of the Orr-Sommerfeld equation," *Journal of Fluid Mechanics*, 43(4), pp. 801-811.

Joslin R.D. 1987 "The sensitivity of boundary layer instability growth rates to compliant wall properties," M.S. Thesis, The Pennsylvania State University.

Joslin R.D. and Morris P.J. 1987 "The sensitivity of boundary layer instability growth rates to compliant wall properties," PSU/ARL Technical Report.

Joslin R.D. and Morris P.J. 1989 "The sensitivity of flow and surface instabilities to changes in compliant wall properties," *Journal of Fluids and Structures*, 3(4), pp. 423-437.

Kachanov Y.S., Kozlov V.V., and Levchenko V.Y. 1979 "Experiments on nonlinear interaction of waves in boundary layers," In: *Laminar-Turbulent Transition*, IUTAM Symposium, Stuttgart, Germany, pp. 135-152.

Kachanov Y.S. and Levchenko V.Y. 1984 "The resonant interaction of disturbances at laminar-turbulent transition in a boundary layer," *Journal of Fluid Mechanics*, 138, pp. 209-247.

Kaplan R.E. 1964 "The stability of laminar boundary layers in the presence of compliant boundaries," ScD Thesis, MIT.

Kelvin, Lord 1880 "On a disturbance in Lord Rayleigh's solution for waves in a plane vortex stratum," In: *Mathematical and Physical Papers*, 4, pp. 186-187.

Klebanoff P.S. and Tidstrom K.D. 1959 "Evaluation of amplified waves leading to transition in a boundary layer with zero pressure gradient," NASA TN D-195.

Klebanoff P.S., Tidstrom K.D., and Sargent L.M. 1962 "The three-dimensional nature of boundary-layer instability," *Journal of Fluid Mechanics*, 12, pp. 1-34.

Kozlov L.F., Korobov V.I., and Babenko V.V. 1983 "The effect of an elastic wall on a boundary layer," *Reports of the Ukrainian Academy of Sciences, Series A-Physical, Mathematical, and Technical Sciences*, pp. 45-47.

Kozlov L.F. and Banbenko V.V. 1978 "Experimental boundary layer studies," NAVSEA Translation No. 1759A, 1979.

Kramer M.O. 1957 "Boundary layer stabilization by distributed damping," *Journal of the Aeronautical Sciences*, 24(6), pp. 459-460.

Kramer M.O. 1960a "Boundary layer stabilization by distributed damping," *Journal of the American Society of Naval Engineers*, pp. 25-33.

Kramer M.O. 1960b "Boundary layer stabilization by distributed damping," Reader's Forum, *Journal of the American Society of Naval Engineers*, p. 69.

Kramer M.O. 1960c "The dolphins' secret," *The New Scientist*, 7 pp. 1118-1120.

Kramer M.O. 1965 "Hydrodynamics of the Dolphin," *Advances in Hydroscience*, 2, pp. 111-130.

Lancaster P. 1964 "Algorithms for lambda-matrices," *Numerische Mathematik*, 6, pp. 388-394.

Lanczos C. 1938 "Trigonometric interpolation of empirical and analytical functions," *Journal of Mathematics and Physics*, 17, pp. 123-199.

Landahl M.T. 1962 "On the stability of a laminar incompressible boundary layer over a flexible surface," *Journal of Fluid Mechanics*, 13, pp. 609-632.

Landahl M.T. and Kaplan R.E. 1965 "The effect of compliant walls on boundary layer stability and transition," AGARDograph 97 pp. 363-394.

Landahl M.T. 1967 "A wave-guide model for turbulent shear flow," *Journal of Fluid Mechanics*, 29, pp. 441-459.

Landahl M.T. 1972 "Wave mechanics of breakdown," *Journal of Fluid Mechanics*, 56(4), pp. 775-802.

Lang T.G. and Pryor K. 1966 "Hydrodynamic performance of porpoises (*Stenella attenuata*)," *Science*, 152, pp. 531-533.

Liepmann H.W. 1943 "Investigations on laminar boundary-layer stability and transition on curved boundaries," NACA Adv. Conf. Report 3H30.

Lighthill M.J. 1956 "A review of: The Structure of Turbulent Shear Flow," *Journal of Fluid Mechanics*, 1, pp. 554-560.

Lumley J. 1967 "Rational approach to relations between motions of differing scales in turbulent flows," *The Physics of Fluids*, 10, pp. 1405-1408.

Luther H.A. 1966 "Further explicit fifth-order Runge-Kutta formulas," *SIAM Review*, 8(3), pp. 374-380.

Mack L. 1980 "On the stability of three-dimensional boundary layers by suction and cooling," In: *Laminar-Turbulent Transition*, IUTAM Symposium, Stuttgart, Germany, pp. 223-238.

Maseev L.M. 1968 "Secondary instability of boundary layers," [in Russian] *Tr. Mosk. Inst. Inzh. Zheleznodorozh. Transp.*, Report No. 222

Maslowe S.A. 1981 "Shear flow instabilities and transition," *Topics in Applied Physics*, 45, pp. 181-225.

Morkovin M.V. 1983 "Understanding transition to turbulence in shear layers," AFOSR Final Report AD-A134796.

Morris P.J and Joslin R.D. "The optimization of compliant wall properties," *Euroomech 228 Colloquium*, September 21-25, 1987/University of Exeter, Devon, U.K.

Morris P.J. 1987 "Applications of matrix factorization in hydrodynamic stability," *4th Army Conference on Applied Mathematics and Computing*, Cornell, ARO Report 87-1.

Murdock J.W. and Taylor T.D. 1977 "Numerical investigation of nonlinear wave interaction in a two-dimensional boundary layer," AGARD- CP-224, pp. 4.1-4.8.

Murdock J.W. 1977 "A numerical study of nonlinear effects on boundary-layer stability," AIAA Paper No. 77-0127.

Nakao S.-I. 1985 "A numerical study of drag reduction by compliant walls," *Japan Society for Aeronautical and Space Sciences*, 27(78), pp. 195-205.

Nayfeh A.H. and Bozatli A.N. 1979 "Secondary instability in boundary-layer flows," *The Physics of Fluids*, 22, pp. 805-813.

Nayfeh A.H. and Padhye A. 1979 "Relation between temporal and spatial stability in three-dimensional flows," *AIAA Journal*, 17(10), pp. 1084-1090.

Nayfeh A.H. 1985 "On secondary instabilities in boundary layers," In: *Stability of Time Dependent and Spatially Varying Flows*, pp. 18-42.

Orr W.M.A. 1907 "The stability or instability of the steady motions of a perfect liquid and of a viscous liquid," *Proceedings of the Royal Irish Academy*, 27, pp. 9-138.

Orszag S.A. 1977 "Prediction of compliant wall drag reduction. part I," NASA CR-2911.

Orszag S.A. 1979 "Prediction of compliant wall drag reduction. part II," NASA CR-3071.

Orszag S.A. and Patera A.T. 1980 "Subcritical transition to turbulence in plane channel flows," *Physics Review Letter*, 45, pp. 989-993.

Orszag S.A. and Patera A.T. 1981 "Subcritical transition to turbulence in plane shear flows," In: *Transition and Turbulence*, pp. 127-146.

Press W.H., Flannery B.P., Teukolsky S.A., and Vetterling W.T. 1986 Numerical Recipes, Cambridge University Press.

Raetz G.S. 1959 "A new theory of the cause in fluid flows," NORAIR Report NOR-59-383.

Rayleigh, Lord 1878 "On the stability of jets," In: *Scientific Papers*, 1, pp. 361-371.

Rayleigh, Lord 1880 "On the stability or instability of certain fluid motions," In: *Scientific Papers*, 1, pp. 474-484.

Rayleigh, Lord 1887 "On the stability or instability of certain fluid motions II," In: *Scientific Papers*, 3, pp. 17-23.

Reed H.L. and Saric W.C. 1986 "Stability and transition of three-dimensional flows," *10th US National Congress on Applied Mechanics*, pp. 457-468.

Reichardt H. 1951 "Vollständige Darstellung der turbulenten Geschwindigkeitsverteilung in Glatten Leitungen," *Z. Angew. Math. Mech.*, 31, pp. 208.

Reischman M.M. 1984 "A review of compliant coating drag reduction research at ONR," In: *Laminar-Turbulent Boundary Layers*, 11, pp. 99-105.

Reshotko E. 1984 "Environment and Receptivity," AGARD-R-709.

Reshotko E. 1986 "Stability and transition, How much do we know," *Proceedings of the 10th US National Congress of Applied Mechanics*, June 16-20, 1986/The University of Texas at Austin, pp. 421-434.

Reynolds W.C. and Hussain A.K.M.F. 1972 "The mechanics of an organized wave in turbulent shear flows. Part 3. theoretical models and comparisons with experiments," *Journal of Fluid Mechanics*, 54, pp. 263-288.

Reynolds O. 1883 "An experimental investigation of the circumstances which determine whether the motion of water shall be direct or sinuous, and of the law of resistance in parallel channels," In: *Scientific Papers*, 2, pp. 51-105.

Riley J.J., Gad-el-Hak M., and Metcalfe R.W. 1988 "Compliant coatings," *Annual Review of Fluid Mechanics*, 20, pp. 393-420.

Rotenberry J.M. 1989 "Effect of compliant boundaries on weakly nonlinear shear waves in channel flow," PhD Thesis, California Institute of Technology.

Saric W.S. and Nayfeh A.H. 1977 "Nonparallel stability of boundary layers with pressure gradients and suction," In: *Laminar-Turbulent Transition*, AGARD-CP-224, pp. 6.1-21.

Saric W.S. and Reynolds G.A. 1979 "Experiments on the stability of nonlinear waves in a boundary layer," In: *Laminar-Turbulent Transition*, IUTAM Symposium, pp. 125-134.

Saric W.S., Kozlov V.V., and Levchenko V.Y. 1984 "Forced and unforced subharmonic resonance in boundary-layer transition," *AIAA 22nd Aerospace Sciences Meeting*, January 9-12, 1984/Reno, Nevada. AIAA Paper No. 84-0007.

Schlichting H. 1933 "Zur entstehung der turbulenz bei der plattenströmung," *Akademie des wissenschaften Göttingen* No. 38., pp. 181-208.

Schubauer G.B. and Skramstad H.K. 1947 "Laminar boundary layer oscillations and stability of laminar flow," *Journal of the Aeronautical Sciences*, 14(2), pp. 69-78.

Semenov B.N. 1971 "Interaction of an elastic boundary with a viscous sublayer of a turbulent boundary layer," *Journal of Applied Mechanics and Technical Physics*, 12(3), pp. 393-397; translated from *Zhurnal Prikladnai Mekhaniki i Tekhnicheskoi Fiziki* (3), 1971, pp. 58-62.

Sen P.K. and Arora D.S. 1988 "On the stability of laminar boundary-layer flow over a flat plate with a compliant surface," *Journal of Fluid Mechanics*, 197 pp. 201-240.

Sengupta T.K. and Lekoudis S.G. 1985 "Calculation of two-dimensional turbulent boundary layers over rigid and moving wavy surfaces," *AIAA Journal*, 23, pp. 530

Smith A.M.O. 1956 "Transition, pressure gradient, and stability theory," *Proceedings of the International Congress of Applied Mechanics*, Brussels, pp. 234-244.

Smith A.M.O. and Gamberoni N. 1956 "Transition, pressure gradient and stability theory," Douglas Aircraft Company Report No. ES-26388.

Smith F.T. 1988 "Nonlinear interaction of near-planar Tollmien-Schlichting waves and longitudinal vortices in boundary layer transition," ICASE Report No. 88-66.

Sommerfeld A. 1908 "Ein beitrag zur hydrodynamiscchen erklaerung ler turbulentaen fluessigkeitsbewegungen," *International Congress of Mathematics*, pp. 116-124.

Spalart P.R. and Yang K-S. 1987 "Numerical study of ribbon-induced transition in Blasius flow," *Journal of Fluid Mechanics*, 178, pp. 345-365.

Squire H.B. 1933 "On the stability of 3-D disturbances of viscous fluid flow between parallel walls," *Proceedings of the Royal Society of London Series(A)*, 142, pp.621-628.

Stewartson K. 1975 "Some aspects of nonlinear stability theory," *Polish Academy of Sciences*, 7, pp. 101-128.

Strokowski A.J. and Orszag S.A. 1977 "Mass flow requirements for LFC wing design," AIAA Paper No. 77-1222.

Stuart J.T. 1958 "On the non-linear mechanics of hydrodynamic stability," *Journal of Fluid Mechanics*, 4, pp. 1-21.

Stuart J.T. 1960 "On three-dimensional non-linear effects in the stability of parallel flows," In: *Advances in Aeronautical Sciences*, Proceedings of the 2nd International Congress in the Aeronautical Sciences, September 1960/Zürich, pp. 121-142.

Stuart J.T. 1962 "On three-dimensional nonlinear effects in the stability of parallel flows," *Advances in Aeronautical Science*, 3, pp. 121-142.

Tani I. 1977 "History of boundary layer theory," *Annual Review of Fluid Mechanics*, 9, pp. 87-111.

Thomas A.S.W. "Experiments on Secondary Instabilities in boundary layers," *Proceedings of the 10th US National Congress of Applied Mechanics*, June 16-20, 1986/The University of Texas at Austin, pp. 435-443.

Thomas M.D. and Craik A.D.D. 1988 "Three-wave resonance for free-surface flows over flexible boundaries," *Journal of Fluid and Structures*, 2, pp. 323-338.

Tollmien N. 1926 "Berechnung turbulenten ausbreitungs vorgänge," *Ztschr. F. angew Math und Mech.*, pp. 468-478.

Townsend A. 1956 The Structure of Turbulent Shear Flow, Cambridge University Press.

Traub J.F. 1966 "A class of globally convergent iteration functions for the solution of polynomial equations," *Mathematic Computing*, 20, pp. 113-138.

Van Ingen J.L. 1956 "A suggested semi-empirical method for the calculation of the boundary layer transition region," University of Delft, Department of Aerospace Engineering, Delft, The Netherlands, Report VTH-74.

Van Stijn Th.L and Van De Vooren A.I. 1980 "An accurate method for solving the Orr-Sommerfeld equation," *Journal of Engineering Mathematics*, 14, pp. 17-26.

Willis G.J.K. 1986 "Hydrodynamic stability of boundary layers over compliant surfaces," PhD Thesis, University of Exeter.

Wray A. and Hussaini M.Y. "Numerical experiments in boundary-layer stability," *AIAA 18th Aerospace Sciences Meeting*, January 14-16, 1980/Pasadena, California, AIAA Paper No. 80-0275.

Yeo K.S. 1986 "The stability of flow over flexible surfaces," PhD thesis, University of Cambridge.

Yeo K.S. and Dowling A.P. 1987 "The stability of inviscid flows over passive compliant walls," *Journal of Fluid Mechanics*, 183 pp. 265-292.

Yeo K.S. 1988 "The stability of boundary layer flow over single and multi-layer viscoelastic walls," *Journal of Fluid Mechanics*, 196 pp. 359-408.

Yurchenko N.F., Babenko V.V., and Kozlov L.F. 1984 "The control of the three-dimensional disturbances developement in the transitional Boundary Layer," In: *Laminar-Turbulent Transition*, IUTAM Symposium, Novosibirsk, USSR..

Zang T.A. and Hussaini M.Y. 1988 "Numerical experiments on the stability of controlled boundary layers," ICASE Report No. 88-20 (NASA CR-181649).

Zang T.A. and Hussaini M.Y. 1989 "Multiple paths to subharmonic laminar breakdown in a boundary layer," ICASE Report NO. 89-78. (NASA CR-181948).

APPENDIX A

SECONDARY INSTABILITY EQUATIONS

A.1 Introduction

In Chapter 2, the dynamic equations for secondary instabilities in a transitional boundary layer were derived but not listed. In this section the derivation is given again briefly along with the final listing of the equations for the subharmonic and fundamental modes of secondary instability.

A.2 Derivation of Equations

We consider an incompressible flow that is governed by the Navier-Stokes equations (2.2.1-2) with appropriate boundary conditions. We consider a Basic flow $\bar{v}_2 = (u_2, v_2, w_2)$ subject to three-dimensional disturbances $\bar{v}_3 = (u_3, v_3, w_3)$ which are termed secondary instabilities. The instantaneous velocity components are given as

$$u(\bar{x}, y, \bar{z}, t) = u_2(\bar{x}, y, \bar{z}, t) + B u_3(\bar{x}, y, \bar{z}, t) \quad A.1a$$

$$v(\bar{x}, y, \bar{z}, t) = v_2(\bar{x}, y, \bar{z}, t) + B v_3(\bar{x}, y, \bar{z}, t) \quad A.1b$$

$$w(\bar{x}, y, \bar{z}, t) = w_2(\bar{x}, y, \bar{z}, t) + B w_3(\bar{x}, y, \bar{z}, t) \quad A.1c$$

$$p(\bar{x}, y, \bar{z}, t) = p_2(\bar{x}, y, \bar{z}, t) + B p_3(\bar{x}, y, \bar{z}, t) \quad A.1d$$

and the basic flow is given as

$$u_2(\bar{x}, y, \bar{z}, t) = U_o(y) + A u_1(\bar{x}, y, \bar{z}, t) \quad A.2a$$

$$v_2(\bar{x}, y, \bar{z}, t) = A v_1(\bar{x}, y, \bar{z}, t) \quad A.2b$$

$$w_2(\bar{x}, y, \bar{z}, t) = W_o(y) + A w_1(\bar{x}, y, \bar{z}, t) \quad A.2c$$

$$p_2(\bar{x}, y, \bar{z}, t) = A p_1(\bar{x}, y, \bar{z}, t) \quad A.2d$$

The equations to determine the primary wave solution (u_1, v_1, w_1) are given in Chapter 2 and (U_0, W_0) is the Blasius velocity profile. If we transform to a coordinate reference frame moving with the wave, we have

$$\bar{v}_1(\bar{x}, y, \bar{z}) = \bar{v}_1(x, y, z) = \bar{v}_1(x + \lambda_z, y, z + \lambda_z) \quad A.3$$

where (\bar{x}, \bar{z}) is the fixed laboratory reference frame and (x, z) is the reference frame moving with the primary wave.

This theory assumes that the primary wave is governed by a linear system of equations. With the shape assumption, the normal velocity of the primary wave is given by

$$v_1(x, y, z) = v_1(y) e^{i\alpha_r(x \cos \phi + z \sin \phi)} + v_{-1}(y) e^{-i\alpha_r(x \cos \phi + z \sin \phi)} \quad A.4$$

where $v_1 = v_{-1}^*$ and $*$ denotes the complex conjugate. v_1 is an eigenfunction of the Orr-Sommerfeld and Squire's equations.

The instantaneous velocities are substituted into the Navier-Stokes equations and linearized on the secondary amplitude, B . This yields the nondimensional equations for v_3

$$\frac{\partial}{\partial t} \bar{v}_3 + (\bar{v}_2 \cdot \nabla) \bar{v}_3 + (\bar{v}_3 \cdot \nabla) \bar{v}_2 = -\Delta p_3 + \frac{1}{R_\delta} \nabla^2 \bar{v}_3 \quad A.5$$

The corresponding vorticity equations eliminate the pressure and are given by

$$\left[\frac{1}{R_\delta} \nabla^2 - \frac{\partial}{\partial t} \right] \bar{\Omega}_3 - (\bar{v}_2 \cdot \nabla) \bar{\Omega}_3 - (\bar{v}_3 \cdot \nabla) \bar{\Omega}_2 + (\bar{\Omega}_2 \cdot \nabla) \bar{v}_3 + (\bar{\Omega}_3 \cdot \nabla) \bar{v}_2 = 0 \quad A.6$$

Also the continuity equation is given by

$$\nabla \cdot \bar{v}_3 = 0 \quad A.7$$

As with the primary problem, we seek to form the equations in terms of the normal velocity and vorticity. The streamwise, normal, and spanwise vorticities are introduced.

$$\epsilon_v = \frac{\partial w}{\partial y} - \frac{\partial v}{\partial z} \quad \Omega = \frac{\partial u}{\partial z} - \frac{\partial w}{\partial x} \quad \rho_v = \frac{\partial v}{\partial x} - \frac{\partial u}{\partial y}$$

Only normal vorticity terms will remain when the analysis is complete.

We already have one equation by substituting the basic flow \bar{v}_2 into (A.6). This gives

$$\begin{aligned} & \left[\frac{1}{R} \nabla^2 - \frac{\partial}{\partial t} - (U_o - c_x) \frac{\partial}{\partial x} - (W_o - c_z) \frac{\partial}{\partial z} \right] \Omega_3 - \frac{dU_o}{dy} \frac{\partial v_3}{\partial z} + \frac{dW_o}{dy} \frac{\partial v_3}{\partial x} \\ & + A \left\{ -(\bar{v}_1 \cdot \nabla) \Omega_3 - (\bar{v}_3 \cdot \nabla) \Omega_1 + (\epsilon_1 + \frac{\partial v_1}{\partial z}) \frac{\partial v_3}{\partial x} \right. \\ & \left. + \Omega_1 \frac{\partial v_3}{\partial y} + (\rho_1 - \frac{\partial v_1}{\partial x}) \frac{\partial v_3}{\partial z} - \frac{\partial v_1}{\partial z} \frac{\partial u_3}{\partial y} + \frac{\partial v_1}{\partial x} \frac{\partial w_3}{\partial y} \right\} = 0 \end{aligned} \quad A.8$$

The other equation is found by taking $\partial/\partial z$ (streamwise vorticity)- $\partial/\partial x$ (spanwise vorticity). This results in the remaining equation describing the dynamical system.

$$\begin{aligned} & \left[\frac{1}{R} \nabla^2 - \frac{\partial}{\partial t} - (U_o - c_x) \frac{\partial}{\partial x} - (W_o - c_z) \frac{\partial}{\partial z} \right] \nabla^2 v_3 + \frac{d^2 U_o}{dy^2} \frac{\partial v_3}{\partial x} + \frac{d^2 W_o}{dy^2} \frac{\partial v_3}{\partial z} \\ & + A \left\{ \left[-(\bar{v}_1 \cdot \nabla) \nabla^2 - \frac{\partial}{\partial y} \nabla^2 v_1 - \left(\frac{\partial^2 u_1}{\partial x^2} + \frac{\partial^2 u_1}{\partial z^2} - \frac{\partial^2 u_1}{\partial y^2} + 2 \frac{\partial^2 v_1}{\partial x \partial y} \right) \frac{\partial}{\partial x} \right. \right. \\ & \left. + \left(\frac{\partial^2 v_1}{\partial z^2} - \frac{\partial^2 v_1}{\partial x^2} + \frac{\partial^2 v_1}{\partial y^2} + 2 \frac{\partial^2 u_1}{\partial x \partial y} \right) \frac{\partial}{\partial y} + \left(\frac{\partial^2 w_1}{\partial y^2} - \frac{\partial^2 w_1}{\partial x^2} + \frac{\partial^2 u_1}{\partial x \partial z} \right. \right. \\ & \left. - \frac{\partial^2 v_1}{\partial y \partial z} \right) \frac{\partial}{\partial z} + \left(\frac{\partial v_1}{\partial y} + 2 \frac{\partial u_1}{\partial x} \right) \left(\frac{\partial^2}{\partial z^2} - \frac{\partial^2}{\partial x^2} + \frac{\partial^2}{\partial y^2} \right) - 2 \frac{\partial v_1}{\partial x} \frac{\partial^2}{\partial x \partial y} - 2 \left(\frac{\partial u_1}{\partial z} \right. \\ & \left. + \frac{\partial w_1}{\partial x} \right) \frac{\partial^2}{\partial x \partial z} - \frac{\partial v_1}{\partial z} \frac{\partial^2}{\partial y \partial z} \right] v_3 \\ & + \left[-\frac{\partial}{\partial x} (\nabla^2 v_1) + 2 \left(\frac{\partial^2 v_1}{\partial z^2} - \frac{\partial^2 v_1}{\partial x^2} + \frac{\partial^2 v_1}{\partial y^2} + 2 \frac{\partial^2 u_1}{\partial x \partial y} \right) \frac{\partial}{\partial x} + 2 \left(\frac{\partial^2 w_1}{\partial x \partial y} \right. \right. \end{aligned}$$

$$\begin{aligned}
& -\frac{\partial^2 v_1}{\partial x \partial z} \frac{\partial}{\partial z} - \frac{\partial v_1}{\partial x} \left(\frac{\partial^2}{\partial x^2} + \frac{\partial^2}{\partial z^2} - \frac{\partial^2}{\partial y^2} \right) + 2 \left(\frac{\partial v_1}{\partial y} + 2 \frac{\partial u_1}{\partial x} \right) \frac{\partial^2}{\partial x \partial y} \\
& + 2 \frac{\partial w_1}{\partial x} \frac{\partial^2}{\partial y \partial z} + \frac{\partial v_1}{\partial z} \frac{\partial^2}{\partial x \partial z} \Big] u_3 \\
& + \left[-\frac{\partial}{\partial z} (\nabla^2 v_1) + 2 \left(\frac{\partial u_1}{\partial y \partial z} - \frac{\partial^2 v_1}{\partial x \partial z} \right) \frac{\partial}{\partial x} - \frac{\partial v_1}{\partial z} \left(\frac{\partial^2}{\partial x^2} - \frac{\partial^2}{\partial y^2} \right) \right. \\
& \left. + 2 \frac{\partial u_1}{\partial z} \frac{\partial^2}{\partial x \partial y} \right] w_3 \Big\} = 0 \tag{A.9}
\end{aligned}$$

To solve the secondary problem we seek an appropriate normal mode representation. As noted in Chapter 3, we wish to keep the form of solution general, so with respect to the secondary instability we define

$$\bar{\alpha}_n = \frac{\partial}{\partial x}, \quad \bar{\beta}_n = \frac{\partial}{\partial z}, \quad \Delta_n = \frac{\partial^2}{\partial x^2} + \frac{\partial^2}{\partial z^2} \tag{A.10a}$$

$$e^N = e^{i(n/2)\alpha, (x \cos \phi + z \sin \phi)} = e^{i(n/2)\alpha, z'} \tag{A.10b}$$

$$e^M = e^{im\alpha, (x \cos \phi + z \sin \phi)} = e^{im\alpha, z'} \tag{A.10c}$$

By substituting (A.5) where $m = \pm 1$ as the general exponential superscript and (A.10) into (A.8-9), the equations in normal modes result. These are given as

$$\begin{aligned}
& \left\{ \frac{1}{R} \hat{\Omega}_n'' + \left[\frac{1}{R} \Delta_n - \sigma - (U_o - c_x) \bar{\alpha}_n - (W_o - c_z) \bar{\beta}_n \right] \hat{\Omega}_n + (W_o' \bar{\alpha}_n - U_o' \bar{\beta}_n) \hat{v}_n \right\} e^N \\
& + A \left\{ \left[-1 - im\alpha \sin \phi \frac{\bar{\beta}_n}{\Delta_n} - im\alpha \cos \phi \frac{\bar{\alpha}_n}{\Delta_n} \right] v_m \hat{\Omega}_n' + \left[(-\bar{\alpha}_n \right. \right. \\
& \left. \left. + m^2 \alpha^2 \cos \phi \sin \phi \frac{\bar{\beta}_n}{\Delta_n} - m^2 \alpha^2 \frac{\bar{\alpha}_n}{\Delta_n}) u_m + (1 + im\alpha \cos \phi \frac{\bar{\alpha}_n}{\Delta_n}) v_m' \right. \\
& \left. \left. - (\bar{\beta}_n + m^2 \alpha^2 \cos^2 \phi \frac{\bar{\beta}_n}{\Delta_n}) w_m \right] \hat{\Omega}_n + \left[im\alpha \sin \phi \frac{\bar{\alpha}_n}{\Delta_n} \right. \right. \\
& \left. \left. - im\alpha \cos \phi \frac{\bar{\beta}_n}{\Delta_n} \right] v_m \hat{v}_n'' + \left[(-m^2 \alpha^2 \cos \phi \sin \phi \frac{\bar{\alpha}_n}{\Delta_n} - m^2 \alpha^2 \frac{\bar{\beta}_n}{\Delta_n} \right. \right. \\
& \left. \left. + im\alpha \sin \phi) u_m + im\alpha \cos \phi \frac{\bar{\beta}_n}{\Delta_n} v_m' + (m^2 \alpha^2 \cos^2 \phi \frac{\bar{\alpha}_n}{\Delta_n} \right. \right. \\
& \left. \left. - im\alpha \cos \phi) w_m \right] \hat{v}_n' - \left[im\alpha \sin \phi u_m' - im\alpha \cos \phi w_m' \right. \right. \\
& \left. \left. - \bar{\alpha}_n w_m' + \bar{\beta}_n u_m' \right] \hat{v}_n \right\} e^{M+N} = 0 \tag{A.11}
\end{aligned}$$

and

$$\begin{aligned}
& \left\{ \frac{1}{R} \hat{v}_n^{iv} + \left[\frac{2}{R} \Delta_n - \sigma - (U_o - c_x) \bar{\alpha}_n - (W_o - c_z) \bar{\beta}_n \right] \hat{v}_n'' + \left[\frac{1}{R} \Delta_n^2 - \sigma \Delta_n \right. \right. \\
& \quad \left. \left. - (U_o - c_x) \bar{\alpha}_n \Delta_n - (W_o - c_z) \bar{\beta}_n \Delta_n + U_o'' \bar{\alpha}_n + W_o'' \bar{\beta}_n \right] \hat{v}_n \right\} e^N \\
& + A \left\{ - \left[\frac{\bar{\alpha}_n}{\Delta_n} i m \alpha \cos \phi + 1 + \frac{\bar{\beta}_n}{\Delta_n} i m \alpha \sin \phi \right] v_m \hat{v}_n''' - \left[\left(\frac{\bar{\alpha}_n}{\Delta_n} 4 i m \alpha \cos \phi \bar{\alpha}_n \right. \right. \right. \\
& \quad \left. \left. + \bar{\alpha}_n - 2 i m \alpha \cos \phi + \frac{\bar{\beta}_n}{\Delta_n} 2 i m \alpha \sin \phi \bar{\alpha}_n \right) u_m + \left(\frac{\bar{\alpha}_n}{\Delta_n} 2 \bar{\alpha}_n - 1 \right) v_m' \right. \\
& \quad \left. \left. + \left(\frac{\bar{\alpha}_n}{\Delta_n} 2 i m \alpha \cos \phi \bar{\beta}_n + \bar{\beta}_n \right) w_m \right] \hat{v}_n'' + \left[- \frac{\bar{\alpha}_n}{\Delta_n} \{ (i m^3 \alpha^3 \cos \phi \right. \right. \\
& \quad \left. \left. + 2 m^2 \alpha^2 \cos 2 \phi \bar{\alpha}_n + 2 m^2 \alpha^2 \cos \phi \sin \phi \bar{\beta}_n - i m \alpha \cos \phi \Delta_n \right. \right. \\
& \quad \left. \left. + i m \alpha \sin \phi \bar{\alpha}_n \bar{\beta}_n \right) v_m - (i m \alpha \cos \phi - 2 \bar{\alpha}_n) v_m'' + 4 i m \alpha \cos \phi \bar{\alpha}_n u_m' \right. \\
& \quad \left. \left. + 2 i m \alpha \cos \phi \bar{\beta}_n w_m' \right\} - (\Delta_n - m^2 \alpha^2 \cos 2 \phi + 2 i m \alpha \cos \phi \bar{\alpha}_n \right. \\
& \quad \left. + i m \alpha \sin \phi \bar{\beta}_n) v_m + v_m'' + 2 i m \alpha \cos \phi u_m' - \frac{\bar{\beta}_n}{\Delta_n} \{ i m \alpha \sin \phi (m^2 \alpha^2 \right. \right. \\
& \quad \left. \left. - 2 i m \alpha \cos \phi \bar{\alpha}_n - \bar{\alpha}_n^2) v_m - i m \alpha \sin \phi v_m'' + 2 i m \alpha \sin \phi \bar{\alpha}_n u_m' \right\} \right] \hat{v}_n' \\
& \quad + \left[(-\bar{\alpha}_n \Delta_n + m^2 \alpha^2 \bar{\alpha}_n - m^2 \alpha^2 \sin \phi \cos \phi \bar{\beta}_n + 2 i m \alpha \cos \phi (\bar{\beta}_n^2 - \bar{\alpha}_n^2) \right. \\
& \quad \left. - 2 i m \alpha \sin \phi \bar{\alpha}_n \bar{\beta}_n) u_m + (m^2 \alpha^2 - 2 i m \alpha \cos \phi \bar{\alpha}_n - i m \alpha \sin \phi \bar{\beta}_n \right. \\
& \quad \left. + \bar{\beta}_n^2 - \bar{\alpha}_n^2) v_m' + \bar{\alpha}_n u_m'' - (\bar{\beta}_n \Delta_n - m^2 \alpha^2 \cos^2 \phi \bar{\beta}_n \right. \\
& \quad \left. + 2 i m \alpha \cos \phi \bar{\alpha}_n \bar{\beta}_n) w_m - v_m''' + \bar{\beta}_n w_m'' \right] \hat{v}_n + \left[\frac{\bar{\beta}_n}{\Delta_n} i m \alpha \cos \phi \right. \\
& \quad \left. - \frac{\bar{\alpha}_n}{\Delta_n} i m \alpha \sin \phi \right] v_m \hat{\Omega}_n'' + \left[\frac{\bar{\beta}_n}{\Delta_n} (2 \bar{\alpha}_n v_m' + 4 i m \alpha \cos \phi \bar{\alpha}_n u_m \right. \\
& \quad \left. + 2 i m \alpha \cos \phi \bar{\beta}_n w_m) - \frac{\bar{\alpha}_n}{\Delta_n} (2 i m \alpha \sin \phi \bar{\alpha}_n u_m) \right] \hat{\Omega}_n' + \left[\frac{\bar{\beta}_n}{\Delta_n} \{ (i m^3 \alpha^3 \cos \phi \right. \right. \\
& \quad \left. \left. + 2 m^2 \alpha^2 \cos 2 \phi \bar{\alpha}_n + 2 m^2 \alpha^2 \cos \phi \sin \phi \bar{\beta}_n - i m \alpha \cos \phi \Delta_n \right. \right. \\
& \quad \left. \left. + i m \alpha \sin \phi \bar{\alpha}_n \bar{\beta}_n \right) v_m - (i m \alpha \cos \phi - 2 \bar{\alpha}_n) v_m'' + 4 i m \alpha \cos \phi \bar{\alpha}_n u_m' \right. \\
& \quad \left. \left. + 2 i m \alpha \cos \phi \bar{\beta}_n w_m' \right\} - \frac{\bar{\alpha}_n}{\Delta_n} \{ i m \alpha \sin \phi (m^2 \alpha^2 - 2 i m \alpha \cos \phi \bar{\alpha}_n - \bar{\alpha}_n^2) v_m \right. \\
& \quad \left. \left. - i m \alpha \sin \phi v_m'' + 2 i m \alpha \sin \phi \bar{\alpha}_n u_m' \right\} \right] \hat{\Omega}_n \right\} e^{N+M} = 0 \quad A.12
\end{aligned}$$

This gives the form of equations for both the subharmonic and fundamental modes. Using only the first few terms or

$$\text{Subharmonic: } m = \pm 1, n = \pm 1$$

$$\text{Fundamental: } m = \pm 1, n = 0, \pm 2$$

This completes the formation of the equations of motion for the three-dimensional secondary instabilities in a transitional boundary layer. In the next sections, listings of the equations for the subharmonic and fundamental modes of secondary instabilities will be given with $W_o = W'_o = W''_o = 0$

A.3 Subharmonic Equations

The subharmonic mode is represented by $m = \pm 1$ and $n = \pm 1$. Substituting into (A.11-12) we find

Equation 1 and 2: normal vorticity, $n = \pm 1$

$$\begin{aligned} \frac{1}{R} \hat{\Omega}_{\pm 1}'' + \left[\frac{1}{R} \Delta_{\pm 1} - \sigma - (U_o - c_x) \bar{\alpha}_{\pm 1} + c_x \bar{\beta}_{\pm 1} \right] \hat{\Omega}_{\pm 1} - U'_o \bar{\beta}_{\pm 1} \hat{v}_{\pm 1} \\ + A \left\{ \left[-1 \mp i\alpha \sin \phi \frac{\bar{\beta}_{\mp 1}}{\Delta_{\mp 1}} \mp i\alpha \cos \phi \frac{\bar{\alpha}_{\mp 1}}{\Delta_{\mp 1}} \right] v_{\pm 1} \hat{\Omega}'_{\mp 1} + \left[(-\bar{\alpha}_{\mp 1} \right. \right. \\ \left. \left. + \alpha^2 \cos \phi \sin \phi \frac{\bar{\beta}_{\mp 1}}{\Delta_{\mp 1}} - \alpha^2 \frac{\bar{\alpha}_{\mp 1}}{\Delta_{\mp 1}} \right) u_{\pm 1} + (1 \pm i\alpha \cos \phi \frac{\bar{\alpha}_{\mp 1}}{\Delta_{\mp 1}}) v'_{\pm 1} \right. \\ \left. + (-\bar{\beta}_{\mp 1} - \alpha^2 \cos^2 \phi \frac{\bar{\beta}_{\mp 1}}{\Delta_{\mp 1}}) w_{\pm 1} \right] \hat{\Omega}_{\mp 1} \pm \left[i\alpha \sin \phi \frac{\bar{\alpha}_{\mp 1}}{\Delta_{\mp 1}} \right. \\ \left. - i\alpha \cos \phi \frac{\bar{\beta}_{\mp 1}}{\Delta_{\mp 1}} \right] v_{\pm 1} \hat{v}_{\mp 1}'' + \left[(-\alpha^2 \cos \phi \sin \phi \frac{\bar{\alpha}_{\mp 1}}{\Delta_{\mp 1}} - \alpha^2 \frac{\bar{\beta}_{\mp 1}}{\Delta_{\mp 1}} \right. \\ \left. \mp i\alpha \sin \phi) u_{\pm 1} \pm i\alpha \cos \phi \frac{\bar{\beta}_{\mp 1}}{\Delta_{\mp 1}} v'_{\pm 1} + (\alpha^2 \cos^2 \phi \frac{\bar{\alpha}_{\mp 1}}{\Delta_{\mp 1}} \right. \\ \left. \mp i\alpha \cos \phi) w_{\pm 1} \right] \hat{v}'_{\mp 1} + \left[\mp i\alpha \sin \phi u'_{\pm 1} \pm i\alpha \cos \phi w'_{\pm 1} \right. \\ \left. + \bar{\alpha}_{\mp 1} w'_{\pm 1} - \bar{\beta}_{\mp 1} u'_{\pm 1} \right] \hat{v}_{\mp 1} \} = 0 \end{aligned} \quad A.13 - 14$$

where equation (A.13) is given with the upper signs and equation (A.14)

with the lower signs. The same convention holds throughout, except for the zero mode equations where the upper and lower sign terms are summed.

Equation 3 and 4: normal velocity, $n = \pm 1$

$$\begin{aligned}
 & \frac{1}{R} \hat{v}_{\pm 1}^{iv} + \left[\frac{2}{R} \Delta_{\pm 1} - \sigma - (U_o - c_z) \bar{\alpha}_{\pm 1} + c_z \bar{\beta}_{\pm 1} \right] \hat{v}_{\pm 1}'' + \left[\frac{1}{R} \Delta_{\pm 1}^2 - \sigma \Delta_{\pm 1} \right. \\
 & \left. - (U_o - c_z) \bar{\alpha}_{\pm 1} \Delta_{\pm 1} + c_z \bar{\beta}_{\pm 1} \Delta_{\pm 1} + U_o'' \bar{\alpha}_{\pm 1} \right] \hat{v}_{\pm 1} \\
 & + A \left\{ \left[\mp \frac{\bar{\alpha}_{\mp 1}}{\Delta_{\mp 1}} i\alpha \cos \phi - 1 \mp \frac{\bar{\beta}_{\mp 1}}{\Delta_{\mp 1}} i\alpha \sin \phi \right] v_{\pm 1} \hat{v}_{\mp 1}''' \mp \left[\left(\frac{\bar{\alpha}_{\mp 1}}{\Delta_{\mp 1}} 4i\alpha \cos \phi \bar{\alpha}_{\mp 1} \right. \right. \right. \\
 & \left. \left. \left. \pm \bar{\alpha}_{\mp 1} - 2i\alpha \cos \phi + \frac{\bar{\beta}_{\mp 1}}{\Delta_{\mp 1}} 2i\alpha \sin \phi \bar{\alpha}_{\mp 1} \right) u_{\pm 1} \pm \left(\frac{\bar{\alpha}_{\mp 1}}{\Delta_{\mp 1}} 2\bar{\alpha}_{\mp 1} - 1 \right) v_{\pm 1}' \right. \\
 & \left. + \left(\frac{\bar{\alpha}_{\mp 1}}{\Delta_{\mp 1}} 2i\alpha \cos \phi \bar{\beta}_{\mp 1} \pm \bar{\beta}_{\mp 1} \right) w_{\pm 1} \right] \hat{v}_{\mp 1}'' + \left[- \frac{\bar{\alpha}_{\mp 1}}{\Delta_{\mp 1}} \{ (\pm i\alpha^3 \cos \phi \right. \right. \\
 & \left. \left. + 2\alpha^2 \cos 2\phi \bar{\alpha}_{\mp 1} + 2\alpha^2 \cos \phi \sin \phi \bar{\beta}_{\mp 1} \mp i\alpha \cos \phi \Delta_{\mp 1} \right. \right. \\
 & \left. \left. \pm i\alpha \sin \phi \bar{\alpha}_{\mp 1} \bar{\beta}_{\mp 1} \right) v_{\pm 1} \mp (i\alpha \cos \phi \mp 2\bar{\alpha}_{\mp 1}) v_{\pm 1}'' \pm 4i\alpha \cos \phi \bar{\alpha}_{\mp 1} u_{\pm 1}' \right. \\
 & \left. \pm 2i\alpha \cos \phi \bar{\beta}_{\mp 1} w_{\pm 1}' \} - (\Delta_{\mp 1} - \alpha^2 \cos 2\phi \mp 2i\alpha \cos \phi \bar{\alpha}_{\mp 1} \right. \\
 & \left. \pm i\alpha \sin \phi \bar{\beta}_{\mp 1}) v_{\pm 1} + v_{\pm 1}'' \pm 2i\alpha \cos \phi u_{\pm 1}' - \frac{\bar{\beta}_{\mp 1}}{\Delta_{\mp 1}} \{ \pm i\alpha \sin \phi (\alpha^2 \right. \right. \\
 & \left. \left. \mp 2i\alpha \cos \phi \bar{\alpha}_{\mp 1} - \bar{\alpha}_{\mp 1}^2 \right) v_{\pm 1} \mp i\alpha \sin \phi v_{\pm 1}'' \pm 2i\alpha \sin \phi \bar{\alpha}_{\mp 1} u_{\pm 1}' \} \right] \hat{v}_{\mp 1}' \\
 & + \left[(-\bar{\alpha}_{\mp 1} \Delta_{\mp 1} + \alpha^2 \bar{\alpha}_{\mp 1} - \alpha^2 \sin \phi \cos \phi \bar{\beta}_{\mp 1} \pm 2i\alpha \cos \phi (\bar{\beta}_{\mp 1}^2 - \bar{\alpha}_{\mp 1}^2) \right. \\
 & \left. \mp 2i\alpha \sin \phi \bar{\alpha}_{\mp 1} \bar{\beta}_{\mp 1}) u_{\pm 1} + (\alpha^2 \mp 2i\alpha \cos \phi \bar{\alpha}_{\mp 1} \mp i\alpha \sin \phi \bar{\beta}_{\mp 1} \right. \\
 & \left. + \bar{\beta}_{\mp 1}^2 - \bar{\alpha}_{\mp 1}^2) v_{\pm 1}' + \bar{\alpha}_{\mp 1} u_{\pm 1}'' - (\bar{\beta}_{\mp 1} \Delta_{\mp 1} - \alpha^2 \cos^2 \phi \bar{\beta}_{\mp 1} \right. \\
 & \left. \pm 2i\alpha \cos \phi \bar{\alpha}_{\mp 1} \bar{\beta}_{\mp 1}) w_{\pm 1} - v_{\pm 1}''' + \bar{\beta}_{\mp 1} w_{\pm 1}'' \right] \hat{v}_{\mp 1} \pm \left[\frac{\bar{\beta}_{\mp 1}}{\Delta_{\mp 1}} i\alpha \cos \phi \right. \\
 & \left. - \frac{\bar{\alpha}_{\mp 1}}{\Delta_{\mp 1}} i\alpha \sin \phi \right] v_{\pm 1} \hat{\Omega}_{\mp 1}'' + \left[\frac{\bar{\beta}_{\mp 1}}{\Delta_{\mp 1}} (2\bar{\alpha}_{\mp 1} v_{\pm 1}' \pm 4i\alpha \cos \phi \bar{\alpha}_{\mp 1} u_{\pm 1} \right. \\
 & \left. \pm 2i\alpha \cos \phi \bar{\beta}_{\mp 1} w_{\pm 1}) \mp \frac{\bar{\alpha}_{\mp 1}}{\Delta_{\mp 1}} (2i\alpha \sin \phi \bar{\alpha}_{\mp 1} u_{\pm 1}) \right] \hat{\Omega}_{\mp 1}' + \left[\frac{\bar{\beta}_{\mp 1}}{\Delta_{\mp 1}} \{ (\pm i\alpha^3 \cos \phi \right. \right. \\
 & \left. \left. + 2\alpha^2 \cos 2\phi \bar{\alpha}_{\mp 1} + 2\alpha^2 \cos \phi \sin \phi \bar{\beta}_{\mp 1} \mp i\alpha \cos \phi \Delta_{\mp 1} \right. \right. \\
 & \left. \left. \pm i\alpha \sin \phi \bar{\alpha}_{\mp 1} \bar{\beta}_{\mp 1} \right) v_{\pm 1} \mp (i\alpha \cos \phi \mp 2\bar{\alpha}_{\mp 1}) v_{\pm 1}'' \pm 4i\alpha \cos \phi \bar{\alpha}_{\mp 1} u_{\pm 1}' \right]
 \end{aligned}$$

$$\left. \left. \begin{aligned} & \pm 2i\alpha \cos \phi \bar{\beta}_{\mp 1} w'_{\pm 1} \} - \frac{\bar{\alpha}_{\mp 1}}{\Delta_{\mp 1}} \{ \pm i\alpha \sin \phi (\alpha^2 \mp 2i\alpha \cos \phi \bar{\alpha}_{\mp 1} - \bar{\alpha}_{\mp 1}^2) v_{\pm 1} \right. \\ & \left. \mp i\alpha \sin \phi v''_{\pm 1} \pm 2i\alpha \sin \phi \bar{\alpha}_{\mp 1} u'_{\pm 1} \} \right] \hat{\Omega}_{\mp 1} \} = 0 \end{aligned} \right\} \quad A.15 - 16$$

A.4 Fundamental Equations

The fundamental mode is represented by $m = \pm 1$ and $n = \pm 2, 0$. Substituting into (A.11-12) we find

Equation 1 and 2: normal vorticity, $n = \pm 2$

$$\begin{aligned} & \frac{1}{R} \hat{\Omega}_{\pm 2}'' + \left[\frac{1}{R} \Delta_{\pm 2} - \sigma - (U_o - c_z) \bar{\alpha}_{\pm 2} + c_z \bar{\beta}_{\pm 2} \right] \hat{\Omega}_{\pm 2} - U_o' \bar{\beta}_{\pm 2} \hat{v}_{\pm 2} \\ & + A \left\{ \left[-1 \mp i\alpha \sin \phi \frac{\bar{\beta}_o}{\Delta_o} \mp i\alpha \cos \phi \frac{\bar{\alpha}_o}{\Delta_o} \right] v_{\pm 1} \hat{\Omega}'_o + \left[(-\bar{\alpha}_o \right. \right. \\ & \left. \left. + \alpha^2 \cos \phi \sin \phi \frac{\bar{\beta}_o}{\Delta_o} - \alpha^2 \frac{\bar{\alpha}_o}{\Delta_o}) u_{\pm 1} + (1 \pm i\alpha \cos \phi \frac{\bar{\alpha}_o}{\Delta_o}) v'_{\pm 1} \right. \\ & \left. - (\bar{\beta}_o + \alpha^2 \cos^2 \phi \frac{\bar{\beta}_o}{\Delta_o}) w_{\pm 1} \right] \hat{\Omega}_o \pm \left[i\alpha \sin \phi \frac{\bar{\alpha}_o}{\Delta_o} \right. \\ & \left. - i\alpha \cos \phi \frac{\bar{\beta}_o}{\Delta_o} \right] v_{\pm 1} \hat{v}_o'' + \left[(-\alpha^2 \cos \phi \sin \phi \frac{\bar{\alpha}_o}{\Delta_o} - \alpha^2 \frac{\bar{\beta}_o}{\Delta_o} \right. \\ & \left. \pm i\alpha \sin \phi) u_{\pm 1} \pm i\alpha \cos \phi \frac{\bar{\beta}_o}{\Delta_o} v'_{\pm 1} + (\alpha^2 \cos^2 \phi \frac{\bar{\alpha}_o}{\Delta_o} \right. \\ & \left. \mp i\alpha \cos \phi) w_{\pm 1} \right] \hat{v}_o' + \left[\mp i\alpha \sin \phi u'_{\pm 1} \pm i\alpha \cos \phi w'_{\pm 1} \right. \\ & \left. + \bar{\alpha}_o w'_{\pm 1} - \bar{\beta}_o u'_{\pm 1} \right] \hat{v}_o \right\} = 0 \quad A.17 - 18 \end{aligned}$$

Equation 3: normal vorticity, n=0

$$\begin{aligned}
& \frac{1}{R} \hat{\Omega}_o'' + \left[\frac{1}{R} \Delta_o - \sigma - (U_o - c_z) \bar{\alpha}_o + c_z \bar{\beta}_o \right] \hat{\Omega}_o - U_o' \bar{\beta}_o \hat{v}_o \\
& + A \left\{ \left[-1 \mp i\alpha \sin \phi \frac{\bar{\beta}_{\mp 2}}{\Delta_{\mp 2}} \mp i\alpha \cos \phi \frac{\bar{\alpha}_{\mp 2}}{\Delta_{\mp 2}} \right] v_{\pm 1} \hat{\Omega}_{\mp 2}' + \left[(-\bar{\alpha}_{\mp 2} \right. \right. \\
& \left. \left. + \alpha^2 \cos \phi \sin \phi \frac{\bar{\beta}_{\mp 2}}{\Delta_{\mp 2}} - \alpha^2 \frac{\bar{\alpha}_{\mp 2}}{\Delta_{\mp 2}}) u_{\pm 1} + (1 \pm i\alpha \cos \phi \frac{\bar{\alpha}_{\mp 2}}{\Delta_{\mp 2}}) v_{\pm 1}' \right. \right. \\
& \left. \left. - (\bar{\beta}_{\mp 2} + \alpha^2 \cos^2 \phi \frac{\bar{\beta}_{\mp 2}}{\Delta_{\mp 2}}) w_{\pm 1} \right] \hat{\Omega}_{\mp 2} \pm \left[i\alpha \sin \phi \frac{\bar{\alpha}_{\mp 2}}{\Delta_{\mp 2}} \right. \right. \\
& \left. \left. - i\alpha \cos \phi \frac{\bar{\beta}_{\mp 2}}{\Delta_{\mp 2}} \right] v_{\pm 1} \hat{v}_{\mp 2}'' + \left[(-\alpha^2 \cos \phi \sin \phi \frac{\bar{\alpha}_{\mp 2}}{\Delta_{\mp 2}} - \alpha^2 \frac{\bar{\beta}_{\mp 2}}{\Delta_{\mp 2}} \right. \right. \\
& \left. \left. \pm i\alpha \sin \phi) u_{\pm 1} \pm i\alpha \cos \phi \frac{\bar{\beta}_{\mp 2}}{\Delta_{\mp 2}} v_{\pm 1}' + (\alpha^2 \cos^2 \phi \frac{\bar{\alpha}_{\mp 2}}{\Delta_{\mp 2}} \right. \right. \\
& \left. \left. \mp i\alpha \cos \phi) w_{\pm 1} \right] \hat{v}_{\mp 2}' + \left[\mp i\alpha \sin \phi u_{\pm 1}' \pm i\alpha \cos \phi w_{\pm 1}' \right. \right. \\
& \left. \left. + \bar{\alpha}_{\mp 2} w_{\pm 1}' - \bar{\beta}_{\mp 2} u_{\pm 1}' \right] \hat{v}_{\mp 2} \right\} = 0
\end{aligned} \tag{A.19}$$

Equation 4 and 5: normal velocity, $n = \pm 2$

$$\begin{aligned}
& \frac{1}{R} \hat{v}_{\pm 2}^{iv} + \left[\frac{2}{R} \Delta_{\pm 2} - \sigma - (U_o - c_z) \bar{\alpha}_{\pm 2} + c_z \bar{\beta}_{\pm 2} \right] \hat{v}_{\pm 2}'' + \left[\frac{1}{R} \Delta_{\pm 2}^2 - \sigma \Delta_{\pm 2} \right. \\
& \left. - (U_o - c_z) \bar{\alpha}_{\pm 2} \Delta_{\pm 2} + c_z \bar{\beta}_{\pm 2} \Delta_{\pm 2} + U_o'' \bar{\alpha}_{\pm 2} \right] \hat{v}_{\pm 2} \\
& + A \left\{ \left[\mp \frac{\bar{\alpha}_o}{\Delta_o} i\alpha \cos \phi - 1 \mp \frac{\bar{\beta}_o}{\Delta_o} i\alpha \sin \phi \right] v_{\pm 1} \hat{v}_o''' - \left[(\pm \frac{\bar{\alpha}_o}{\Delta_o} 4i\alpha \cos \phi \bar{\alpha}_o \right. \right. \\
& \left. + \bar{\alpha}_o \mp 2i\alpha \cos \phi \pm \frac{\bar{\beta}_o}{\Delta_o} 2i\alpha \sin \phi \bar{\alpha}_o) u_{\pm 1} + (\frac{\bar{\alpha}_o}{\Delta_o} 2\bar{\alpha}_o - 1) v_{\pm 1}' \right. \\
& \left. + (\pm \frac{\bar{\alpha}_o}{\Delta_o} 2i\alpha \cos \phi \bar{\beta}_o + \bar{\beta}_o) w_{\pm 1} \right] \hat{v}_o'' + \left[-\frac{\bar{\alpha}_o}{\Delta_o} \{ (\pm i\alpha^3 \cos \phi \right. \right. \\
& \left. + 2\alpha^2 \cos^2 \phi \bar{\alpha}_o + 2\alpha^2 \cos \phi \sin \phi \bar{\beta}_o \mp i\alpha \cos \phi \Delta_o \right. \\
& \left. \pm i\alpha \sin \phi \bar{\alpha}_o \bar{\beta}_o) v_{\pm 1} \mp (i\alpha \cos \phi \pm 2\bar{\alpha}_o) v_{\pm 1}'' \pm 4i\alpha \cos \phi \bar{\alpha}_o u_{\pm 1}' \right. \\
& \left. \pm 2i\alpha \cos \phi \bar{\beta}_o w_{\pm 1}' \} + (-\Delta_o + \alpha^2 \cos 2\phi \mp 2i\alpha \cos \phi \bar{\alpha}_o \right. \\
& \left. \mp i\alpha \sin \phi \bar{\beta}_o) v_{\pm 1} + v_{\pm 1}'' \pm 2i\alpha \cos \phi u_{\pm 1}' \mp \frac{\bar{\beta}_o}{\Delta_o} \{ i\alpha \sin \phi (\alpha^2 \right. \right. \\
& \left. \mp 2i\alpha \cos \phi \bar{\alpha}_o - \bar{\alpha}_o^2) v_{\pm 1} \mp i\alpha \sin \phi v_{\pm 1}'' \pm 2i\alpha \sin \phi \bar{\alpha}_o u_{\pm 1}' \} \right] \hat{v}_o' \\
& + \left[(-\bar{\alpha}_o \Delta_o + \alpha^2 \bar{\alpha}_o - \alpha^2 \sin \phi \cos \phi \bar{\beta}_o \pm 2i\alpha \cos \phi (\bar{\beta}_o^2 - \bar{\alpha}_o^2) \right. \\
& \left. \mp 2i\alpha \sin \phi \bar{\alpha}_o \bar{\beta}_o) u_{\pm 1} + (\alpha^2 \mp 2i\alpha \cos \phi \bar{\alpha}_o \mp i\alpha \sin \phi \bar{\beta}_o \right. \\
& \left. + \bar{\beta}_o^2 - \bar{\alpha}_o^2) v_{\pm 1}' + \bar{\alpha}_o u_{\pm 1}'' - (\bar{\beta}_o \Delta_o - \alpha^2 \cos^2 \phi \bar{\beta}_o \right. \\
& \left. \pm 2i\alpha \cos \phi \bar{\alpha}_o \bar{\beta}_o) w_{\pm 1} - v_{\pm 1}''' + \bar{\beta}_o w_{\pm 1}'' \right] \hat{v}_o \pm \left[\frac{\bar{\beta}_o}{\Delta_o} i\alpha \cos \phi \right. \\
& \left. - \frac{\bar{\alpha}_o}{\Delta_o} i\alpha \sin \phi \right] v_{\pm 1} \hat{\Omega}_o'' + \left[\frac{\bar{\beta}_o}{\Delta_o} (2\bar{\alpha}_o v_{\pm 1}' \pm 4i\alpha \cos \phi \bar{\alpha}_o u_{\pm 1} \right. \\
& \left. \mp 2i\alpha \cos \phi \bar{\beta}_o w_{\pm 1}) \mp \frac{\bar{\alpha}_o}{\Delta_o} 2i\alpha \sin \phi \bar{\alpha}_o u_{\pm 1} \right] \hat{\Omega}_o' + \left[\frac{\bar{\beta}_o}{\Delta_o} \{ (\pm i\alpha^3 \cos \phi \right. \right. \\
& \left. + 2\alpha^2 \cos 2\phi \bar{\alpha}_o + 2\alpha^2 \cos \phi \sin \phi \bar{\beta}_o \mp i\alpha \cos \phi \Delta_o \right. \\
& \left. \pm i\alpha \sin \phi \bar{\alpha}_o \bar{\beta}_o) v_{\pm 1} + (\mp i\alpha \cos \phi + 2\bar{\alpha}_o) v_{\pm 1}'' \pm 4i\alpha \cos \phi \bar{\alpha}_o u_{\pm 1}' \right. \\
& \left. \pm 2i\alpha \cos \phi \bar{\beta}_o w_{\pm 1}' \} - \frac{\bar{\alpha}_o}{\Delta_o} \{ \pm i\alpha \sin \phi (\alpha^2 \mp 2i\alpha \cos \phi \bar{\alpha}_o - \bar{\alpha}_o^2) v_{\pm 1} \right. \\
& \left. \mp i\alpha \sin \phi v_{\pm 1}'' \pm 2i\alpha \sin \phi \bar{\alpha}_o u_{\pm 1}' \} \right] \hat{\Omega}_o \} = 0
\end{aligned}$$

Equation 6: normal velocity, $n=0$

$$\begin{aligned}
& \frac{1}{R} \hat{v}_o^{i\mathbf{v}} + \left[\frac{2}{R} \Delta_o - \sigma - (U_o - c_x) \bar{\alpha}_o + c_z \bar{\beta}_o \right] \hat{v}_o'' + \left[\frac{1}{R} \Delta_o^2 - \sigma \Delta_o \right. \\
& \left. - (U_o - c_x) \bar{\alpha}_o \Delta_o + c_z \bar{\beta}_o \Delta_o + U_o'' \bar{\alpha}_o \right] \hat{v}_o \\
& + A \left\{ \left[\pm \frac{\bar{\alpha}_{\mp 2}}{\Delta_{\mp 2}} i\alpha \cos \phi - 1 \mp \frac{\bar{\beta}_{\mp 2}}{\Delta_{\mp 2}} i\alpha \sin \phi \right] v_{\pm 1} \hat{v}_{\mp 2}''' - \left[(\pm \frac{\bar{\alpha}_{\mp 2}}{\Delta_{\mp 2}} 4i\alpha \cos \phi \bar{\alpha}_{\mp 2} \right. \right. \\
& \left. + \bar{\alpha}_{\mp} \mp 2i\alpha \cos \phi \pm \frac{\bar{\beta}_{\mp 2}}{\Delta_{\mp 2}} 2i\alpha \sin \phi \bar{\alpha}_{\mp 2}) u_{\pm 1} + (\frac{\bar{\alpha}_{\mp 2}}{\Delta_{\mp 2}} 2\bar{\alpha}_{\mp 2} - 1) v_{\pm 1}' \right. \\
& \left. + (\pm \frac{\bar{\alpha}_{\mp 2}}{\Delta_{\mp 2}} 2i\alpha \cos \phi \bar{\beta}_{\mp 2} + \bar{\beta}_{\mp 2}) w_{\pm 1} \right] \hat{v}_{\mp 2}'' + \left[-\frac{\bar{\alpha}_{\mp 2}}{\Delta_{\mp 2}} \{ (\pm i\alpha^3 \cos \phi \right. \right. \\
& \left. + 2\alpha^2 \cos 2\phi \bar{\alpha}_{\mp 2} + 2\alpha^2 \cos \phi \sin \phi \bar{\beta}_{\mp 2} \mp i\alpha \cos \phi \Delta_{\mp 2} \right. \\
& \left. \pm i\alpha \sin \phi \bar{\alpha}_{\mp 2} \bar{\beta}_{\mp 2}) v_{\pm 1} \mp (i\alpha \cos \phi \pm 2\bar{\alpha}_{\mp 2}) v_{\pm 1}'' \pm 4i\alpha \cos \phi \bar{\alpha}_{\mp 2} u_{\pm 1}' \right. \\
& \left. \pm 2i\alpha \cos \phi \bar{\beta}_{\mp 2} w_{\pm 1}' \} + (-\Delta_{\mp 2} + \alpha^2 \cos 2\phi \mp 2i\alpha \cos \phi \bar{\alpha}_{\mp 2} \right. \\
& \left. \mp i\alpha \sin \phi \bar{\beta}_{\mp 2}) v_{\pm 1} + v_{\pm 1}'' \pm 2i\alpha \cos \phi u_{\pm 1}' \mp \frac{\bar{\beta}_{\mp 2}}{\Delta_{\mp 2}} \{ i\alpha \sin \phi (\alpha^2 \right. \right. \\
& \left. \mp 2i\alpha \cos \phi \bar{\alpha}_{\mp 2} - \bar{\alpha}_{\mp 2}^2) v_{\pm 1} \mp i\alpha \sin \phi v_{\pm 1}'' \pm 2i\alpha \sin \phi \bar{\alpha}_{\mp 2} u_{\pm 1}' \} \right] \hat{v}_{\mp 2}' \\
& + \left[(-\bar{\alpha}_{\mp 2} \Delta_{\mp 2} + \alpha^2 \bar{\alpha}_{\mp 2} - \alpha^2 \sin \phi \cos \phi \bar{\beta}_{\mp 2} \pm 2i\alpha \cos \phi (\bar{\beta}_{\mp 2}^2 - \bar{\alpha}_{\mp 2}^2) \right. \\
& \left. \mp 2i\alpha \sin \phi \bar{\alpha}_{\mp 2} \bar{\beta}_{\mp 2}) u_{\pm 1} + (\alpha^2 \mp 2i\alpha \cos \phi \bar{\alpha}_{\mp 2} \mp i\alpha \sin \phi \bar{\beta}_{\mp 1} \right. \\
& \left. + \bar{\beta}_{\mp 2}^2 - \bar{\alpha}_{\mp 2}^2) v_{\pm 1}' + \bar{\alpha}_{\mp 2} u_{\pm 1}'' - (\bar{\beta}_{\mp 2} \Delta_{\mp 2} - \alpha^2 \cos^2 \phi \bar{\beta}_{\mp 2} \right. \\
& \left. \pm 2i\alpha \cos \phi \bar{\alpha}_{\mp 2} \bar{\beta}_{\mp 2}) w_{\pm 1} - v_{\pm 1}''' + \bar{\beta}_{\mp 2} w_{\pm 1}'' \right] \hat{v}_{\mp 2} \pm \left[\frac{\bar{\beta}_{\mp 2}}{\Delta_{\mp 2}} i\alpha \cos \phi \right. \\
& \left. - \frac{\bar{\alpha}_{\mp 2}}{\Delta_{\mp 2}} i\alpha \sin \phi \right] v_{\pm 1} \hat{\Omega}_{\mp 2}'' + \left[\frac{\bar{\beta}_{\mp 2}}{\Delta_{\mp 2}} (2\bar{\alpha}_{\mp 2} v_{\pm 1}' \pm 4i\alpha \cos \phi \bar{\alpha}_{\mp 2} u_{\pm 1} \right. \\
& \left. \pm 2i\alpha \cos \phi \bar{\beta}_{\mp 2} w_{\pm 1}) \mp \frac{\bar{\alpha}_{\mp 2}}{\Delta_{\mp 2}} 2i\alpha \sin \phi \bar{\alpha}_{\mp 2} u_{\pm 1} \right] \hat{\Omega}_{\mp 2}' + \left[\frac{\bar{\beta}_{\mp 2}}{\Delta_{\mp 2}} \{ (\pm i\alpha^3 \cos \phi \right. \right. \\
& \left. + 2\alpha^2 \cos 2\phi \bar{\alpha}_{\mp 2} + 2i\alpha^2 \cos \phi \sin \phi \bar{\beta}_{\mp 2} \mp i\alpha \cos \phi \Delta_{\mp 2} \right. \\
& \left. \pm i\alpha \sin \phi \bar{\alpha}_{\mp 2} \bar{\beta}_{\mp 2}) v_{\pm 1} + (\mp i\alpha \cos \phi + 2\bar{\alpha}_{\mp 2}) v_{\pm 1}'' \pm 4i\alpha \cos \phi \bar{\alpha}_{\mp 2} u_{\pm 1}' \right. \\
& \left. \pm 2i\alpha \cos \phi \bar{\beta}_{\mp 2} w_{\pm 1}' \} - \frac{\bar{\alpha}_{\mp 2}}{\Delta_{\mp 2}} \{ \pm i\alpha \sin \phi (\alpha^2 \mp 2i\alpha \cos \phi \bar{\alpha}_{\mp 2} - \bar{\alpha}_{\mp 2}^2) v_{\pm 1} \right. \\
& \left. \mp i\alpha \sin \phi v_{\pm 1}'' \pm 2i\alpha \sin \phi \bar{\alpha}_{\mp 2} u_{\pm 1}' \} \right] \hat{\Omega}_{\mp 2} \} = 0
\end{aligned} \tag{A.22}$$

APPENDIX B

SECONDARY COMPLIANT WALL EQUATIONS

B.1 Introduction

In Chapter 3 the compliant wall model was introduced and the corresponding boundary conditions were derived for the primary and the secondary instability problems. A thorough derivation was presented for the primary wall model with a final listing of the resulting boundary equations. For the secondary instability, a few of the equations and the final form of the wall equations was neglected due to the size of the equations. In this section a complete derivation and listing of the final equations is given.

B.2 Secondary Wall Equations

We begin with the continuity of fluid and wall motion.

$$\frac{\partial \xi}{\partial t} = u(x, y, z, t) \quad B.1a$$

$$\frac{\partial \eta}{\partial t} = v(x, y, z, t) \quad B.1b$$

$$\frac{\partial \zeta}{\partial t} = w(x, y, z, t) \quad B.1c$$

The instantaneous velocity and surface displacements are

$$\xi = \xi_0 + A\xi_1 + B\xi_3 \quad \text{and} \quad u = U_0 + Au_1 + Bu_3 \quad B.2a$$

$$\eta = \eta_0 + A\eta_1 + B\eta_3 \quad \text{and} \quad v = Av_1 + Bv_3 \quad B.2b$$

$$\zeta = \zeta_0 + A\zeta_1 + B\zeta_3 \quad \text{and} \quad w = W_0 + Aw_1 + Bw_3 \quad B.2c$$

These are substituted into (B.1) and linearized on the secondary amplitude B . We find

$$\frac{\partial \xi_3}{\partial t} = u_3 + \eta_3 U'_o + A \left\{ \xi_1 \frac{\partial u_3}{\partial x} + \eta_1 \frac{\partial u_3}{\partial y} + \zeta_1 \frac{\partial u_3}{\partial z} + \xi_3 \frac{\partial u_1}{\partial x} + \eta_3 \frac{\partial u_1}{\partial y} + \zeta_3 \frac{\partial u_1}{\partial z} \right\} \quad B.3a$$

$$\frac{\partial \eta_3}{\partial t} = v_3 + A \left\{ \xi_1 \frac{\partial v_3}{\partial x} + \eta_1 \frac{\partial v_3}{\partial y} + \zeta_1 \frac{\partial v_3}{\partial z} + \xi_3 \frac{\partial v_1}{\partial x} + \eta_3 \frac{\partial v_1}{\partial y} + \zeta_3 \frac{\partial v_1}{\partial z} \right\} \quad B.3b$$

$$\frac{\partial \zeta_3}{\partial t} = w_3 + \eta_3 W'_o + A \left\{ \xi_1 \frac{\partial w_3}{\partial x} + \eta_1 \frac{\partial w_3}{\partial y} + \zeta_1 \frac{\partial w_3}{\partial z} + \xi_3 \frac{\partial w_1}{\partial x} + \eta_3 \frac{\partial w_1}{\partial y} + \zeta_3 \frac{\partial w_1}{\partial z} \right\} \quad B.3c$$

The primary and secondary normal modes for velocities and surface displacements are given respectively as,

$$v_1 = \sum_{m=-\infty}^{\infty} v_m e^{im\alpha(z \cos \phi + z \sin \phi)} \quad B.4$$

for $m = \pm 1$ and

$$v_3 = e^{\sigma t + i\beta(z \cos \phi - z \sin \phi) + \gamma(z \cos \phi + z \sin \phi)} \sum_{n=-\infty}^{\infty} v_n e^{i(n/2)\alpha(z \cos \phi + z \sin \phi)} \quad B.5$$

The relation for the streamwise and normal surface displacement is given as

$$\xi = \eta \tan \theta \quad B.6$$

The continuity-vorticity relations for u and w are given as

$$\hat{u}_n = \left(\frac{\bar{\beta}_n}{\Delta_n} \hat{\Omega}_n - \frac{\bar{\alpha}_n}{\Delta_n} \hat{v}'_n \right) \quad B.7a$$

and

$$\hat{w}_n = - \left(\frac{\bar{\alpha}_n}{\Delta_n} \hat{\Omega}_n + \frac{\bar{\beta}_n}{\Delta_n} \hat{v}'_n \right) \quad B.7b$$

The relations (B.4-7) are substituted into (B.3) giving

$$\begin{aligned}
 (\sigma \tan \theta - U'_o) \hat{\eta}_n e^N &= \left(\frac{\bar{\beta}_n}{\Delta_n} \hat{\Omega}_n - \frac{\bar{\alpha}_n}{\Delta_n} \hat{v}'_n \right) e^N \\
 &+ A \left\{ (\eta_m \tan \theta \bar{\alpha}_n + \zeta_m \bar{\beta}_n) \left(\frac{\bar{\beta}_n}{\Delta_n} \hat{\Omega}_n - \frac{\bar{\alpha}_n}{\Delta_n} \hat{v}'_n \right) \right. \\
 &+ \eta_m \left(\frac{\bar{\beta}_n}{\Delta_n} \hat{\Omega}'_n - \frac{\bar{\alpha}_n}{\Delta_n} \hat{v}''_n \right) + (\tan \theta i m \alpha \cos \phi u_m + u'_m) \hat{\eta}_n \\
 &\left. + i m \alpha \sin \phi u_m \hat{\zeta}_n \right\} e^{N+M} \quad B.8a
 \end{aligned}$$

$$\begin{aligned}
 \sigma \hat{\eta}_n e^N &= \hat{v}_n e^N + A \left\{ (\eta_m \tan \theta \bar{\alpha}_n + \zeta_m \bar{\beta}_n) \hat{v}_n + \eta_m \hat{v}'_n \right. \\
 &\left. + (\tan \theta i m \alpha \cos \phi v_m + v'_m) \hat{\eta}_n + i m \alpha \sin \phi v_m \hat{\zeta}_n \right\} e^{N+M} \quad B.8b
 \end{aligned}$$

$$\begin{aligned}
 \sigma \hat{\zeta}_n e^N &= - \left(\frac{\bar{\alpha}_n}{\Delta_n} \hat{\Omega}_n + \frac{\bar{\beta}_n}{\Delta_n} \hat{v}'_n \right) e^N + W'_o \hat{\eta}_n e^N \\
 &- A \left\{ (\eta_m \tan \theta \bar{\alpha}_n + \zeta_m \bar{\beta}_n) \left(\frac{\bar{\alpha}_n}{\Delta_n} \hat{\Omega}_n + \frac{\bar{\beta}_n}{\Delta_n} \hat{v}'_n \right) \right. \\
 &+ \eta_m \left(\frac{\bar{\alpha}_n}{\Delta_n} \hat{\Omega}'_n + \frac{\bar{\beta}_n}{\Delta_n} \hat{v}''_n \right) - (\tan \theta i m \alpha \cos \phi w_m + w'_m) \hat{\eta}_n \\
 &\left. - i m \alpha \sin \phi w_m \hat{\zeta}_n \right\} e^{N+M} \quad B.8c
 \end{aligned}$$

To remove the spanwise surface displacement variable, an equation for a balance of forces in the spanwise direction is introduced

$$\rho_m b \frac{\partial^2 \zeta}{\partial t^2} + K_s \zeta - E_z b \frac{\partial^2 \zeta}{\partial z^2} = \tau_{yz} \quad B.9$$

From the stress tensor we find

$$\tau_{yz} = \frac{1}{R} \left(\frac{\partial v_3}{\partial z} + \frac{\partial w_3}{\partial y} \right) \quad B.10a$$

or in normal modes

$$\hat{\tau}_{yz} = \frac{1}{R} (\bar{\beta}_n \hat{v}_n + \hat{w}'_n) e^N \quad B.10b$$

Substituting (B.7b) gives

$$\hat{\tau}_{yz} = \frac{1}{R} (\bar{\beta}_n \hat{v}_n - \frac{\bar{\alpha}_n}{\Delta_n} \hat{\Omega}'_n - \frac{\bar{\beta}_n}{\Delta_n} \hat{v}''_n) e^N \quad B.10c$$

Equation (B.9) is nondimensionalized and the stress relation (B.10) is substituted giving

$$\hat{\zeta}_n = \frac{1}{R} (\bar{\beta}_n \hat{v}_n - \frac{\bar{\alpha}_n}{\Delta_n} \hat{\Omega}'_n - \frac{\bar{\beta}_n}{\Delta_n} \hat{v}''_n) / (C_M \sigma^2 + C_{Ks} - C_{Tz} \bar{\beta}_n^2) e^N \quad B.11$$

This is substituted into (B.8) to give

$$\begin{aligned} & [\frac{\bar{\alpha}_n}{\Delta_n} \hat{v}'_n - \frac{\bar{\beta}_n}{\Delta_n} \hat{\Omega}_n + (\sigma \tan \theta - U'_o) \hat{\eta}_n] e^N \\ &= A \left\{ (\eta_m \tan \theta \bar{\alpha}_n + \zeta_m \bar{\beta}_n) (\frac{\bar{\beta}_n}{\Delta_n} \hat{\Omega}_n - \frac{\bar{\alpha}_n}{\Delta_n} \hat{v}'_n) \right. \\ &+ \eta_m (\frac{\bar{\beta}_n}{\Delta_n} \hat{\Omega}'_n - \frac{\bar{\alpha}_n}{\Delta_n} \hat{v}''_n) + (\tan \theta i m \alpha \cos \phi u_m + u'_m) \hat{\eta}_n \\ &+ \left. \frac{i m \alpha \sin \phi u_m}{R(C_M \sigma^2 + C_{Ks} - C_{Tz} \bar{\beta}_n^2)} (\bar{\beta}_n \hat{v}_n - \frac{\bar{\alpha}_n}{\Delta_n} \hat{\Omega}'_n - \frac{\bar{\beta}_n}{\Delta_n} \hat{v}''_n) \right\} e^{N+M} \quad B.12a \end{aligned}$$

$$\begin{aligned} (\sigma \hat{\eta}_n - \hat{v}_n) e^N &= A \left\{ (\eta_m \tan \theta \bar{\alpha}_n + \zeta_m \bar{\beta}_n) \hat{v}_n + \eta_m \hat{v}'_n \right. \\ &+ (\tan \theta i m \alpha \cos \phi v_m + v'_m) \hat{\eta}_n \\ &+ \left. \frac{i m \alpha \sin \phi v_m}{R(C_M \sigma^2 + C_{Ks} - C_{Tz} \bar{\beta}_n^2)} (\bar{\beta}_n \hat{v}_n - \frac{\bar{\alpha}_n}{\Delta_n} \hat{\Omega}'_n - \frac{\bar{\beta}_n}{\Delta_n} \hat{v}''_n) \right\} e^{N+M} \quad B.12b \end{aligned}$$

$$\begin{aligned}
& \left[\frac{\sigma}{R} (\bar{\beta}_n \hat{v}_n - \frac{\bar{\alpha}_n}{\Delta_n} \hat{\Omega}'_n - \frac{\bar{\beta}_n}{\Delta_n} \hat{v}''_n) + (C_M \sigma^2 + C_{Ks} - C_{Tz} \bar{\beta}_n^2) (\frac{\bar{\alpha}_n}{\Delta_n} \hat{\Omega}_n + \frac{\bar{\beta}_n}{\Delta_n} \hat{v}'_n) \right] e^N \\
& + W'_o \hat{\eta}_n e^N = -A (C_M \sigma^2 + C_{Ks} - C_{Tz} \bar{\beta}_n^2) \left\{ (\eta_m \tan \theta \bar{\alpha}_n + \zeta_m \bar{\beta}_n) (\frac{\bar{\alpha}_n}{\Delta_n} \hat{\Omega}_n + \frac{\bar{\beta}_n}{\Delta_n} \hat{v}'_n) \right. \\
& + \eta_m (\frac{\bar{\alpha}_n}{\Delta_n} \hat{\Omega}'_n + \frac{\bar{\beta}_n}{\Delta_n} \hat{v}''_n) - (\tan \theta i m \alpha \cos \phi w_m + w'_m) \hat{\eta}_n \\
& \left. - \frac{i m \alpha \sin \phi w_m}{R (C_M \sigma^2 + C_{Ks} - C_{Tz} \bar{\beta}_n^2)} (\bar{\beta}_n \hat{v}_n - \frac{\bar{\alpha}_n}{\Delta_n} \hat{\Omega}'_n - \frac{\bar{\beta}_n}{\Delta_n} \hat{v}''_n) \right\} e^{N+M} \quad B.12c
\end{aligned}$$

The equations are in terms of normal velocity, vorticity, and surface displacement.

The final equation is introduced to remove the normal surface displacement variable. This is a balance of forces in the streamwise direction

$$\begin{aligned}
& \left[\rho_m b \frac{\partial^2}{\partial t^2} + (B_z \frac{\partial^4}{\partial x^4} + 2B_{xz} \frac{\partial^4}{\partial x^2 \partial z^2} + B_z \frac{\partial^4}{\partial z^4}) \cos^2 \theta + K_E \right. \\
& \left. - E_z b \frac{\partial^2}{\partial x^2} \sin^2 \theta \right] \eta_3 = -p \cos^2 \theta + \tau_{yy} \cos^2 \theta + \tau_{yz} \sin \theta \cos \theta \quad B.13
\end{aligned}$$

or nondimensionally

$$\begin{aligned}
& \left[C_M \frac{\partial^2}{\partial t^2} + (C_{Bz} \frac{\partial^4}{\partial x^4} + 2C_{Bxz} \frac{\partial^4}{\partial x^2 \partial z^2} + C_{Bz} \frac{\partial^4}{\partial z^4}) \cos^2 \theta + C_K \right. \\
& \left. - C_{Tz} \frac{\partial^2}{\partial x^2} \sin^2 \theta \right] \eta_3 = -\hat{p} \cos^2 \theta + \hat{\tau}_{yy} \cos^2 \theta + \hat{\tau}_{yz} \sin \theta \cos \theta \quad B.14
\end{aligned}$$

The normal stress is given as

$$\hat{\tau}_{yy} = \frac{2}{R} \frac{\partial v}{\partial y} \quad B.15a$$

or

$$\hat{\tau}_{yy} = \frac{2}{R} \hat{v}'_n e^N \quad B.15b$$

The streamwise shear stress is given by

$$\hat{\tau}_{yz} = \frac{1}{R} \left(\frac{\partial v}{\partial x} + \frac{\partial u}{\partial y} \right) \quad B.16a$$

In normal modes and replacing u by the appropriate velocity-vorticity relation (B.9a) we find

$$\hat{\tau}_{yz} = \frac{1}{R} (\bar{\alpha}_n \hat{v}_n - \frac{\bar{\alpha}_n}{\Delta_n} \hat{v}_n'' + \frac{\bar{\beta}_n}{\Delta_n} \hat{\Omega}'_n) e^N \quad B.16b$$

The pressure fluctuations at the wall are found from the linearized streamwise and spanwise momentum equations. This results in the following pressure, in normal modes

$$\begin{aligned} \Delta_n \hat{p} = & \left\{ -[\frac{1}{R} \Delta_n - \sigma + c_x \bar{\alpha}_n + c_z \bar{\beta}_n] \hat{v}'_n - \frac{1}{R} \hat{v}'''_n - (U'_o \bar{\alpha}_n + W'_o \bar{\beta}_n) \hat{v}_n \right\} e^N \\ & + A \left\{ (u_m \bar{\alpha}_n + w_m \bar{\beta}_n) \hat{v}'_n + v_m \hat{v}''_n - (u'_m \bar{\alpha}_n + w'_m \bar{\beta}_n) \hat{v}_n \right. \\ & \left. + im\alpha \cos \phi (u_m \bar{\alpha}_n + w_m \bar{\beta}_n) (\frac{\bar{\alpha}_n}{\Delta_n} \hat{v}'_n - \frac{\bar{\beta}_n}{\Delta_n} \hat{\Omega}_n) \right. \\ & \left. + im\alpha \sin \phi (u_m \bar{\alpha}_n + w_m \bar{\beta}_n) (\frac{\bar{\beta}_n}{\Delta_n} \hat{v}'_n + \frac{\bar{\alpha}_n}{\Delta_n} \hat{\Omega}_n) \right\} e^{N+M} \end{aligned} \quad B.17$$

Substituting the normal mode relations into (B.14) along with the stress and pressure relations (B.15-17), we arrive at the final necessary equation to complete the boundary conditions. This gives

$$\begin{aligned} & [C_M \sigma^2 + (C_{Bz} \bar{\alpha}_n^4 + 2C_{Bzz} \bar{\alpha}_n^2 \bar{\beta}_n^2 + C_{Bz} \bar{\beta}_n^4) \cos^2 \theta + C_K \\ & - C_{Tz} \bar{\alpha}_n^2 \sin^2 \theta] \hat{\eta}_n \Delta_n e^N \\ & - \left\{ [\frac{3}{R} \Delta_n - \sigma + c_x \bar{\alpha}_n + c_z \bar{\beta}_n] \hat{v}'_n + \frac{1}{R} \hat{v}'''_n + (U'_o \bar{\alpha}_n + W'_o \bar{\beta}_n) \hat{v}_n \right. \\ & \left. - \frac{\Delta_n \tan \theta}{R} (\frac{\bar{\alpha}_n}{\Delta_n} \hat{v}''_n - \bar{\alpha}_n \hat{v}_n - \frac{\bar{\beta}_n}{\Delta_n} \hat{\Omega}'_n) \right\} \cos^2 \theta e^N \\ & + A \left\{ (u_m \bar{\alpha}_n + w_m \bar{\beta}_n) \hat{v}'_n + v_m \hat{v}''_n - (u'_m \bar{\alpha}_n + w'_m \bar{\beta}_n) \hat{v}_n \right. \\ & \left. + im\alpha \cos \phi (u_m \bar{\alpha}_n + w_m \bar{\beta}_n) (\frac{\bar{\alpha}_n}{\Delta_n} \hat{v}'_n - \frac{\bar{\beta}_n}{\Delta_n} \hat{\Omega}_n) \right. \\ & \left. + im\alpha \sin \phi (u_m \bar{\alpha}_n + w_m \bar{\beta}_n) (\frac{\bar{\beta}_n}{\Delta_n} \hat{v}'_n + \frac{\bar{\alpha}_n}{\Delta_n} \hat{\Omega}_n) \right\} \cos^2 \theta e^{N+M} \end{aligned} \quad B.18$$

The complete boundary conditions are the system of equations given by (B.12, 18). This can be reduced to three equations in terms of the normal velocity and normal vorticity as are the fluid equations of motion. For the reference frame with the solution given by (2.3.14), $W_o = W'_o = W''_o = 0$. The remaining equations in this reference frame are determined below.

B.3 Subharmonic Mode

To remove the normal surface displacement variable we make use of the normal continuity equation. For the two Fourier modes representing the subharmonic secondary instability, we find

$$\begin{aligned} \sigma \hat{\eta}_1 - \hat{v}_1 = A & \left\{ (\eta_1 \tan \theta \bar{\alpha}_{-1} + \zeta_1 \bar{\beta}_{-1}) \hat{v}_{-1} + \eta_1 \hat{v}'_{-1} + (\tan \theta i \alpha \cos \phi v_1 + v'_1) \hat{\eta}_{-1} \right. \\ & \left. + \frac{i \alpha \sin \phi v_1}{R(C_M \sigma^2 + C_{Ks} - C_{Tz} \bar{\beta}_{-1}^2)} (\bar{\beta}_{-1} \hat{v}_{-1} - \frac{\bar{\alpha}_{-1}}{\Delta_{-1}} \hat{\Omega}'_{-1} - \frac{\bar{\beta}_{-1}}{\Delta_{-1}} \hat{v}''_{-1}) \right\} \quad B.19a \end{aligned}$$

and

$$\begin{aligned} \sigma \hat{\eta}_{-1} - \hat{v}_{-1} = A & \left\{ (\eta_{-1} \tan \theta \bar{\alpha}_1 + \zeta_{-1} \bar{\beta}_1) \hat{v}_1 + \eta_{-1} \hat{v}'_1 - (\tan \theta i \alpha \cos \phi v_{-1} - v'_{-1}) \hat{\eta}_1 \right. \\ & \left. - \frac{i \alpha \sin \phi v_{-1}}{R(C_M \sigma^2 + C_{Ks} - C_{Tz} \bar{\beta}_1^2)} (\bar{\beta}_1 \hat{v}_1 - \frac{\bar{\alpha}_1}{\Delta_1} \hat{\Omega}'_1 - \frac{\bar{\beta}_1}{\Delta_1} \hat{v}''_1) \right\} \quad B.19b \end{aligned}$$

This gives two equations with two unknowns $(\hat{\eta}_1, \hat{\eta}_{-1})$. These are solved simultaneously to give

$$\begin{aligned}
 & \left[\sigma^2 + A^2 (\tan \theta i \alpha \cos \phi v_1 + v'_1) (\tan \theta i \alpha \cos \phi v_{-1} - v'_{-1}) \right] \hat{\eta}_1 = \sigma \hat{v}_1 \\
 & + A \sigma \left\{ (\eta_1 \tan \theta \bar{\alpha}_{-1} + \zeta_1 \bar{\beta}_{-1}) \hat{v}_{-1} + \eta_1 \hat{v}'_{-1} \right. \\
 & + \frac{i \alpha \sin \phi v_1}{R(C_M \sigma^2 + C_{Ks} - C_{Ts} \bar{\beta}_{-1}^2)} (\bar{\beta}_{-1} \hat{v}_{-1} - \frac{\bar{\alpha}_{-1}}{\Delta_{-1}} \hat{\Omega}'_{-1} - \frac{\bar{\beta}_{-1}}{\Delta_{-1}} \hat{v}''_{-1}) \Big\} \\
 & + A (\tan \theta i \alpha \cos \phi v_1 + v'_1) \hat{v}_{-1} + A^2 (\tan \theta i \alpha \cos \phi v_1 + v'_1) \left\{ (\eta_{-1} \tan \theta \bar{\alpha}_1 \right. \\
 & + \zeta_{-1} \bar{\beta}_1) \hat{v}_1 + \eta_{-1} \hat{v}'_1 \\
 & \left. - \frac{i \alpha \sin \phi v_{-1}}{R(C_M \sigma^2 + C_{Ks} - C_{Ts} \bar{\beta}_1^2)} (\bar{\beta}_1 \hat{v}_1 - \frac{\bar{\alpha}_1}{\Delta_1} \hat{\Omega}'_1 - \frac{\bar{\beta}_1}{\Delta_1} \hat{v}''_1) \right\} \quad B.20a
 \end{aligned}$$

and

$$\begin{aligned}
 & \left[\sigma^2 + A^2 (\tan \theta i \alpha \cos \phi v_1 + v'_1) (\tan \theta i \alpha \cos \phi v_{-1} - v'_{-1}) \right] \hat{\eta}_{-1} = \sigma \hat{v}_{-1} \\
 & + A \sigma \left\{ (\eta_{-1} \tan \theta \bar{\alpha}_1 + \zeta_{-1} \bar{\beta}_1) \hat{v}_1 + \eta_{-1} \hat{v}'_1 \right. \\
 & - \frac{i \alpha \sin \phi v_{-1}}{R(C_M \sigma^2 + C_{Ks} - C_{Ts} \bar{\beta}_1^2)} (\bar{\beta}_1 \hat{v}_1 - \frac{\bar{\alpha}_1}{\Delta_1} \hat{\Omega}'_1 - \frac{\bar{\beta}_1}{\Delta_1} \hat{v}''_1) \Big\} \\
 & - A (\tan \theta i \alpha \cos \phi v_{-1} - v'_{-1}) \hat{v}_1 - A^2 (\tan \theta i \alpha \cos \phi v_{-1} - v'_{-1}) \left\{ (\eta_1 \tan \theta \bar{\alpha}_{-1} \right. \\
 & + \zeta_1 \bar{\beta}_{-1}) \hat{v}_{-1} + \eta_1 \hat{v}'_{-1} \\
 & \left. + \frac{i \alpha \sin \phi v_1}{R(C_M \sigma^2 + C_{Ks} - C_{Ts} \bar{\beta}_{-1}^2)} (\bar{\beta}_{-1} \hat{v}_{-1} - \frac{\bar{\alpha}_{-1}}{\Delta_{-1}} \hat{\Omega}'_{-1} - \frac{\bar{\beta}_{-1}}{\Delta_{-1}} \hat{v}''_{-1}) \right\} \quad B.20b
 \end{aligned}$$

This gives explicit relations for $(\hat{\eta}_1, \hat{\eta}_{-1})$. These are then substituted into (B.12a, 12c and 18) to give six equations representing compliant wall boundary conditions for the Subharmonic mode. These are given as.

B.C. 1 and 2: streamwise continuity, $n = \pm 1$

$$\begin{aligned}
 & \left[\sigma^2 + A^2 (\tan \theta i \alpha \cos \phi v_1 + v'_1) (\tan \theta i \alpha \cos \phi v_{-1} - v'_{-1}) \right] \left(\frac{\bar{\alpha}_{\pm 1}}{\Delta_{\pm 1}} \hat{v}'_{\pm 1} - \frac{\bar{\beta}_{\pm 1}}{\Delta_{\pm 1}} \hat{\Omega}'_{\pm 1} \right) \\
 & + (\sigma \tan \theta - U'_o) \left[\sigma \hat{v}_{\pm 1} + A \sigma \left\{ (\eta_{\pm 1} \tan \theta \bar{\alpha}_{\mp 1} + \zeta_{\pm 1} \bar{\beta}_{\mp 1}) \hat{v}_{\mp 1} + \eta_{\pm 1} \hat{v}'_{\mp 1} \right. \right. \\
 & \pm \frac{i \alpha \sin \phi v_{\pm 1}}{R(C_M \sigma^2 + C_{Ks} - C_{Tz} \bar{\beta}_{\mp 1}^2)} (\bar{\beta}_{\mp 1} \hat{v}_{\mp 1} - \frac{\bar{\alpha}_{\mp 1}}{\Delta_{\mp 1}} \hat{\Omega}'_{\mp 1} - \frac{\bar{\beta}_{\mp 1}}{\Delta_{\mp 1}} \hat{v}''_{\mp 1}) \left. \right\} \\
 & \pm A (\tan \theta i \alpha \cos \phi v_{\pm 1} \pm v'_{\pm 1}) \hat{v}_{\mp 1} \pm A^2 (\tan \theta i \alpha \cos \phi v_{\pm 1} \pm v'_{\pm 1}) \left\{ (\eta_{\mp 1} \tan \theta \bar{\alpha}_{\pm 1} \right. \\
 & \left. \left. + \zeta_{\mp 1} \bar{\beta}_{\pm 1}) \hat{v}_{\pm 1} + \eta_{\mp 1} \hat{v}'_{\pm 1} \right. \right. \\
 & \mp \frac{i \alpha \sin \phi v_{\mp 1}}{R(C_M \sigma^2 + C_{Ks} - C_{Tz} \bar{\beta}_{\pm 1}^2)} (\bar{\beta}_{\pm 1} \hat{v}_{\pm 1} - \frac{\bar{\alpha}_{\pm 1}}{\Delta_{\pm 1}} \hat{\Omega}'_{\pm 1} - \frac{\bar{\beta}_{\pm 1}}{\Delta_{\pm 1}} \hat{v}''_{\pm 1}) \left. \right\} \\
 & - A \left[\sigma^2 + A^2 (\tan \theta i \alpha \cos \phi v_1 + v'_1) (\tan \theta i \alpha \cos \phi v_{-1} - v'_{-1}) \right] \left[(\eta_{\pm 1} \tan \theta \bar{\alpha}_{\mp 1} \right. \\
 & \left. + \zeta_{\pm 1} \bar{\beta}_{\mp 1}) (\frac{\bar{\beta}_{\mp 1}}{\Delta_{\mp 1}} \hat{\Omega}_{\mp 1} - \frac{\bar{\alpha}_{\mp 1}}{\Delta_{\mp 1}} \hat{v}'_{\mp 1}) + \eta_{\pm 1} (\frac{\bar{\beta}_{\mp 1}}{\Delta_{\mp 1}} \hat{\Omega}'_{\mp 1} - \frac{\bar{\alpha}_{\mp 1}}{\Delta_{\mp 1}} \hat{v}''_{\mp 1}) \right. \\
 & \pm \frac{i \alpha \sin \phi u_{\pm 1}}{R(C_M \sigma^2 + C_{Ks} - C_{Tz} \bar{\beta}_{\mp 1}^2)} (\bar{\beta}_{\mp 1} \hat{v}_{\mp 1} - \frac{\bar{\alpha}_{\mp 1}}{\Delta_{\mp 1}} \hat{\Omega}'_{\mp 1} - \frac{\bar{\beta}_{\mp 1}}{\Delta_{\mp 1}} \hat{v}''_{\mp 1}) \left. \right] \\
 & \mp A (\tan \theta i \alpha \cos \phi u_{\pm 1} \pm u'_{\pm 1}) \left[\sigma \hat{v}_{\mp 1} + A \sigma \left\{ (\eta_{\mp 1} \tan \theta \bar{\alpha}_{\pm 1} + \zeta_{\mp 1} \bar{\beta}_{\pm 1}) \hat{v}_{\pm 1} + \eta_{\mp 1} \hat{v}'_{\pm 1} \right. \right. \\
 & \mp \frac{i \alpha \sin \phi v_{\mp 1}}{R(C_M \sigma^2 + C_{Ks} - C_{Tz} \bar{\beta}_{\pm 1}^2)} (\bar{\beta}_{\pm 1} \hat{v}_{\pm 1} - \frac{\bar{\alpha}_{\pm 1}}{\Delta_{\pm 1}} \hat{\Omega}'_{\pm 1} - \frac{\bar{\beta}_{\pm 1}}{\Delta_{\pm 1}} \hat{v}''_{\pm 1}) \left. \right\} \\
 & \mp A (\tan \theta i \alpha \cos \phi v_{\mp 1} \mp v'_{\mp 1}) \hat{v}_{\pm 1} \mp A^2 (\tan \theta i \alpha \cos \phi v_{\mp 1} \mp v'_{\mp 1}) \left\{ (\eta_{\pm 1} \tan \theta \bar{\alpha}_{\mp 1} \right. \\
 & \left. + \zeta_{\pm 1} \bar{\beta}_{\mp 1}) \hat{v}_{\mp 1} + \eta_{\pm 1} \hat{v}'_{\mp 1} \pm \frac{i \alpha \sin \phi v_{\pm 1}}{R(C_M \sigma^2 + C_{Ks} - C_{Tz} \bar{\beta}_{\mp 1}^2)} (\bar{\beta}_{\mp 1} \hat{v}_{\mp 1} \right. \\
 & \left. - \frac{\bar{\alpha}_{\mp 1}}{\Delta_{\mp 1}} \hat{\Omega}'_{\mp 1} - \frac{\bar{\beta}_{\mp 1}}{\Delta_{\mp 1}} \hat{v}''_{\mp 1}) \right\} = 0
 \end{aligned}$$

B.C. 3 and 4: spanwise continuity, $n = \pm 1$

$$\begin{aligned}
& \left[\sigma^2 + A^2 (\tan \theta i \alpha \cos \phi v_1 + v'_1) (\tan \theta i \alpha \cos \phi v_{-1} - v'_{-1}) \right] \left[\frac{\sigma}{R(C_M \sigma^2 + C_{Ks} - C_{Tz} \bar{\beta}_{\pm 1})} \right. \\
& \cdot (\bar{\beta}_{\pm 1} \hat{v}_{\pm 1} - \frac{\bar{\alpha}_{\pm 1}}{\Delta_{\pm 1}} \hat{\Omega}'_{\pm 1} - \frac{\bar{\beta}_{\pm 1}}{\Delta_{\pm 1}} \hat{v}''_{\pm 1}) + \frac{\bar{\alpha}_{\pm 1}}{\Delta_{\pm 1}} \hat{\Omega}_{\pm 1} + \frac{\bar{\beta}_{\pm 1}}{\Delta_{\pm 1}} \hat{v}'_{\pm 1} \\
& + A \left\{ (\eta_{\pm 1} \tan \theta \bar{\alpha}_{\mp 1} - \zeta_{\pm 1} \bar{\beta}_{\mp 1}) (\frac{\bar{\alpha}_{\mp 1}}{\Delta_{\mp 1}} \hat{\Omega}_{\mp 1} + \frac{\bar{\beta}_{\mp 1}}{\Delta_{\mp 1}} \hat{v}'_{\mp 1}) + \eta_{\pm 1} (\frac{\bar{\alpha}_{\mp 1}}{\Delta_{\mp 1}} \hat{\Omega}'_{\mp 1} + \frac{\bar{\beta}_{\mp 1}}{\Delta_{\mp 1}} \hat{v}''_{\mp 1}) \right. \\
& \mp \frac{i \alpha \sin \phi w_{\pm 1}}{R(C_M \sigma^2 + C_{Ks} - C_{Tz} \bar{\beta}_{\mp 1}^2)} (\bar{\beta}_{\mp 1} \hat{v}_{\mp 1} - \frac{\bar{\alpha}_{\mp 1}}{\Delta_{\mp 1}} \hat{\Omega}'_{\mp 1} - \frac{\bar{\beta}_{\mp 1}}{\Delta_{\mp 1}} \hat{v}''_{\mp 1}) \Big\} \\
& \mp A (\tan \theta i \alpha \cos \phi w_{\pm 1} \pm w'_{\pm 1}) \left[\sigma \hat{v}_{\mp 1} + A \sigma \left\{ (\eta_{\mp 1} \tan \theta \bar{\alpha}_{\pm 1} + \zeta_{\mp 1} \bar{\beta}_{\pm 1}) \hat{v}_{\pm 1} + \eta_{\mp 1} \hat{v}'_{\pm 1} \right. \right. \\
& \mp \frac{i \alpha \sin \phi v_{\mp 1}}{R(C_M \sigma^2 + C_{Ks} - C_{Tz} \bar{\beta}_{\pm 1}^2)} (\bar{\beta}_{\pm 1} \hat{v}_{\pm 1} - \frac{\bar{\alpha}_{\pm 1}}{\Delta_{\pm 1}} \hat{\Omega}'_{\pm 1} - \frac{\bar{\beta}_{\pm 1}}{\Delta_{\pm 1}} \hat{v}''_{\pm 1}) \Big\} \\
& \mp A (\tan \theta i \alpha \cos \phi v_{\mp 1} \mp v'_{\mp 1}) \hat{v}_{\pm 1} \mp A^2 (\tan \theta i \alpha \cos \phi v_{\mp 1} \mp v'_{\mp 1}) \left\{ (\eta_{\pm 1} \tan \theta \bar{\alpha}_{\mp 1} \right. \\
& \left. + \zeta_{\pm 1} \bar{\beta}_{\mp 1}) \hat{v}_{\mp 1} + \eta_{\pm 1} \hat{v}'_{\mp 1} \pm \frac{i \alpha \sin \phi v_{\pm 1}}{R(C_M \sigma^2 + C_{Ks} - C_{Tz} \bar{\beta}_{\mp 1}^2)} (\bar{\beta}_{\mp 1} \hat{v}_{\mp 1} \right. \\
& \left. - \frac{\bar{\alpha}_{\mp 1}}{\Delta_{\mp 1}} \hat{\Omega}'_{\mp 1} - \frac{\bar{\beta}_{\mp 1}}{\Delta_{\mp 1}} \hat{v}''_{\mp 1}) \right\} = 0
\end{aligned}$$

B.23 - 24

B.C. 5 and 6: Force balance, $n = \pm 1$

$$\begin{aligned}
& \left[C_M \sigma^2 + (C_{Bx} \bar{\alpha}_{\pm 1}^4 + 2C_{Bzz} \bar{\alpha}_{\pm 1}^2 \bar{\beta}_{\pm 1}^2 + C_{Bz} \bar{\beta}_{\pm 1}^4) \cos^2 \theta + C_K \right. \\
& \quad \left. - C_{Tx} \bar{\alpha}_{\pm 1}^2 \sin^2 \theta \right] \Delta_{\pm 1} \left[\sigma \hat{v}_{\pm 1} + A \sigma \left\{ (\eta_{\pm 1} \tan \theta \bar{\alpha}_{\mp 1} + \zeta_{\pm 1} \bar{\beta}_{\mp 1}) \hat{v}_{\mp 1} + \eta_{\pm 1} \hat{v}'_{\mp 1} \right. \right. \\
& \quad \pm \frac{i \alpha \sin \phi v_{\pm 1}}{R(C_M \sigma^2 + C_K - C_{Tx} \bar{\beta}_{\mp 1}^2)} (\bar{\beta}_{\mp 1} \hat{v}_{\mp 1} - \frac{\bar{\alpha}_{\mp 1}}{\Delta_{\mp 1}} \hat{\Omega}'_{\mp 1} - \frac{\bar{\beta}_{\mp 1}}{\Delta_{\mp 1}} \hat{v}''_{\mp 1}) \left. \right\} \\
& \quad \pm A (\tan \theta i \alpha \cos \phi v_{\pm 1} \pm v'_{\pm 1}) \hat{v}_{\mp 1} \pm A^2 (\tan \theta i \alpha \cos \phi v_{\pm 1} \pm v'_{\pm 1}) \left\{ (\eta_{\mp 1} \tan \theta \bar{\alpha}_{\pm 1} \right. \\
& \quad \left. + \zeta_{\mp 1} \bar{\beta}_{\pm 1}) \hat{v}_{\pm 1} + \eta_{\mp 1} \hat{v}'_{\pm 1} \right. \\
& \quad \left. \mp \frac{i \alpha \sin \phi v_{\mp 1}}{R(C_M \sigma^2 + C_K - C_{Tx} \bar{\beta}_{\pm 1}^2)} (\bar{\beta}_{\pm 1} \hat{v}_{\pm 1} - \frac{\bar{\alpha}_{\pm 1}}{\Delta_{\pm 1}} \hat{\Omega}'_{\pm 1} - \frac{\bar{\beta}_{\pm 1}}{\Delta_{\pm 1}} \hat{v}''_{\pm 1}) \right\} \left. \right] \\
& \quad - \left[\sigma^2 + A^2 (\tan \theta i \alpha \cos \phi v_1 + v'_1) (\tan \theta i \alpha \cos \phi v_{-1} - v'_{-1}) \right] \\
& \quad \left[\left[\frac{3}{R} \Delta_{\pm 1} - \sigma + c_x \bar{\alpha}_{\pm 1} + c_z \bar{\beta}_{\pm 1} \right] \hat{v}'_{\pm 1} + \frac{1}{R} \hat{v}'''_{\pm 1} + U'_o \bar{\alpha}_{\pm 1} \hat{v}_{\pm 1} \right. \\
& \quad - \frac{\Delta_{\pm 1} \tan \theta}{R} \left(\frac{\bar{\alpha}_{\pm 1}}{\Delta_{\pm 1}} \hat{v}''_{\pm 1} - \bar{\alpha}_{\pm 1} \hat{v}_{\pm 1} - \frac{\bar{\beta}_{\pm 1}}{\Delta_{\pm 1}} \hat{\Omega}'_{\pm 1} \right) - A \left\{ (u_{\pm 1} \bar{\alpha}_{\mp 1} + w_{\pm 1} \bar{\beta}_{\mp 1}) \hat{v}'_1 \right. \\
& \quad + v_{\pm 1} \hat{v}''_{\mp 1} - (u'_{\pm 1} \bar{\alpha}_{\mp 1} + w'_{\pm 1} \bar{\beta}_{\mp 1}) \hat{v}_{\mp 1} \\
& \quad \pm i \alpha \cos \phi (u_{\pm 1} \bar{\alpha}_{\mp 1} + w_{\pm 1} \bar{\beta}_{\mp 1}) \left(\frac{\bar{\alpha}_{\mp 1}}{\Delta_{\mp 1}} \hat{v}'_{\mp 1} - \frac{\bar{\beta}_{\mp 1}}{\Delta_{\mp 1}} \hat{\Omega}_{\mp 1} \right) \\
& \quad \left. \pm i \alpha \sin \phi (u_{\pm 1} \bar{\alpha}_{\mp 1} + w_{\pm 1} \bar{\beta}_{\mp 1}) \left(\frac{\bar{\beta}_{\mp 1}}{\Delta_{\mp 1}} \hat{v}'_{\mp 1} + \frac{\bar{\alpha}_{\mp 1}}{\Delta_{\mp 1}} \hat{\Omega}_{\mp 1} \right) \right\} \right] \cos^2 \theta = 0B.25 - 26
\end{aligned}$$

B.4 Fundamental Mode

The same procedure is performed for the fundamental mode as was done for the subharmonic. To remove the normal surface displacement variable we make use of the normal continuity equation. For the three Fourier modes representing the fundamental mode we find

$$\sigma\hat{\eta}_2 - \hat{v}_2 = A \left\{ (\eta_1 \tan\theta \bar{\alpha}_o + \zeta_1 \bar{\beta}_o) \hat{v}_o + \eta_1 \hat{v}'_o + (\tan\theta i\alpha \cos\phi v_1 + v'_1) \hat{\eta}_o + \frac{i\alpha \sin\phi v_1}{R(C_M \sigma^2 + C_{K_o} - C_{T_z} \bar{\beta}_o^2)} (\bar{\beta}_o \hat{v}_o - \frac{\bar{\alpha}_o}{\Delta_o} \hat{\Omega}'_o - \frac{\bar{\beta}_o}{\Delta_o} \hat{v}''_o) \right\} \quad B.27a$$

$$\begin{aligned} \sigma\hat{\eta}_o - \hat{v}_o = A & \left\{ (\eta_1 \tan\theta \bar{\alpha}_{-2} + \zeta_1 \bar{\beta}_{-2}) \hat{v}_{-2} + \eta_1 \hat{v}'_{-2} + (\tan\theta i\alpha \cos\phi v_1 + v'_1) \hat{\eta}_{-2} \right. \\ & + \frac{i\alpha \sin\phi v_1}{R(C_M \sigma^2 + C_{K_o} - C_{T_z} \bar{\beta}_{-2}^2)} (\bar{\beta}_{-2} \hat{v}_{-2} - \frac{\bar{\alpha}_{-2}}{\Delta_{-2}} \hat{\Omega}'_{-2} - \frac{\bar{\beta}_{-2}}{\Delta_{-2}} \hat{v}''_{-2}) \\ & (\eta_{-1} \tan\theta \bar{\alpha}_2 + \zeta_{-1} \bar{\beta}_2) \hat{v}_2 + \eta_{-1} \hat{v}'_2 - (\tan\theta i\alpha \cos\phi v_{-1} - v'_{-1}) \hat{\eta}_2 \\ & \left. - \frac{i\alpha \sin\phi v_{-1}}{R(C_M \sigma^2 + C_{K_o} - C_{T_z} \bar{\beta}_2^2)} (\bar{\beta}_2 \hat{v}_2 - \frac{\bar{\alpha}_2}{\Delta_2} \hat{\Omega}'_2 - \frac{\bar{\beta}_2}{\Delta_2} \hat{v}''_2) \right\} \quad B.27b \end{aligned}$$

$$\begin{aligned} \sigma\hat{\eta}_{-2} - \hat{v}_{-2} = A & \left\{ (\eta_{-1} \tan\theta \bar{\alpha}_o + \zeta_{-1} \bar{\beta}_o) \hat{v}_o + \eta_{-1} \hat{v}'_o - (\tan\theta i\alpha \cos\phi v_{-1} - v'_{-1}) \hat{\eta}_o \right. \\ & \left. - \frac{i\alpha \sin\phi v_{-1}}{R(C_M \sigma^2 + C_{K_o} - C_{T_z} \bar{\beta}_o^2)} (\bar{\beta}_o \hat{v}_o - \frac{\bar{\alpha}_o}{\Delta_o} \hat{\Omega}'_o - \frac{\bar{\beta}_o}{\Delta_o} \hat{v}''_o) \right\} \quad B.27c \end{aligned}$$

This gives three equations with three unknowns $(\hat{\eta}_o, \hat{\eta}_{\pm 2})$. These are solved simultaneously to give

$$\begin{aligned}
 & \sigma \left[\sigma^2 + 2A^2 (\tan \theta i \alpha \cos \phi v_1 + v'_1) (\tan \theta i \alpha \cos \phi v_{-1} - v'_{-1}) \right] \hat{\eta}_2 \\
 &= \left[\sigma^2 + 2A^2 (\tan \theta i \alpha \cos \phi v_1 + v'_1) (\tan \theta i \alpha \cos \phi v_{-1} - v'_{-1}) \right] \left[\hat{v}_2 \right. \\
 &+ A \left\{ (\eta_1 \tan \theta \bar{\alpha}_o + \zeta_1 \bar{\beta}_o) \hat{v}_o + \eta_1 \hat{v}'_o \right. \\
 &+ \left. \left. + \frac{i \alpha \sin \phi v_1}{R(C_M \sigma^2 + C_{K_o} - C_{T_z} \bar{\beta}_o^2)} (\bar{\beta}_o \hat{v}_o - \frac{\bar{\alpha}_o}{\Delta_o} \hat{\Omega}'_o - \frac{\bar{\beta}_o}{\Delta_o} \hat{v}''_o) \right\} \right] \\
 &+ A (\tan \theta i \alpha \cos \phi v_1 + v'_1) \left[\sigma \hat{v}_o + A \sigma \left\{ (\eta_1 \tan \theta \bar{\alpha}_{-2} + \zeta_1 \bar{\beta}_{-2}) \hat{v}_{-2} \right. \right. \\
 &+ \eta_1 \hat{v}'_{-2} + \frac{i \alpha \sin \phi v_1}{R(C_M \sigma^2 + C_{K_o} - C_{T_z} \bar{\beta}_{-2}^2)} (\bar{\beta}_{-2} \hat{v}_{-2} - \frac{\bar{\alpha}_{-2}}{\Delta_{-2}} \hat{\Omega}'_{-2} - \frac{\bar{\beta}_{-2}}{\Delta_{-2}} \hat{v}''_{-2}) \\
 &(\eta_{-1} \tan \theta \bar{\alpha}_2 + \zeta_{-1} \bar{\beta}_2) \hat{v}_2 + \eta_{-1} \hat{v}'_2 \\
 &- \left. \left. \frac{i \alpha \sin \phi v_{-1}}{R(C_M \sigma^2 + C_{K_o} - C_{T_z} \bar{\beta}_2^2)} (\bar{\beta}_2 \hat{v}_2 - \frac{\bar{\alpha}_2}{\Delta_2} \hat{\Omega}'_2 - \frac{\bar{\beta}_2}{\Delta_2} \hat{v}''_2) \right\} \right] \\
 &+ A (\tan \theta i \alpha \cos \phi v_1 + v'_1) \hat{v}_{-2} + A^2 (\tan \theta i \alpha \cos \phi v_1 + v'_1) \left\{ (\eta_{-1} \tan \theta \bar{\alpha}_o \right. \\
 &+ \zeta_{-1} \bar{\beta}_o) \hat{v}_o + \eta_{-1} \hat{v}'_o \\
 &- \left. \left. \frac{i \alpha \sin \phi v_{-1}}{R(C_M \sigma^2 + C_{K_o} - C_{T_z} \bar{\beta}_o^2)} (\bar{\beta}_o \hat{v}_o - \frac{\bar{\alpha}_o}{\Delta_o} \hat{\Omega}'_o - \frac{\bar{\beta}_o}{\Delta_o} \hat{v}''_o) \right\} \right. \\
 &- A (\tan \theta i \alpha \cos \phi v_{-1} - v'_{-1}) \hat{v}_2 \\
 &- A^2 (\tan \theta i \alpha \cos \phi v_{-1} - v'_{-1}) \left\{ (\eta_1 \tan \theta \bar{\alpha}_o + \zeta_1 \bar{\beta}_o) \hat{v}_o + \eta_1 \hat{v}'_o \right. \\
 &+ \left. \left. \frac{i \alpha \sin \phi v_1}{R(C_M \sigma^2 + C_{K_o} - C_{T_z} \bar{\beta}_o^2)} (\bar{\beta}_o \hat{v}_o - \frac{\bar{\alpha}_o}{\Delta_o} \hat{\Omega}'_o - \frac{\bar{\beta}_o}{\Delta_o} \hat{v}''_o) \right\} \right] \quad B.28a
 \end{aligned}$$

and

$$\begin{aligned}
& \left[\sigma^2 + 2A^2(\tan\theta i\alpha \cos\phi v_1 + v'_1)(\tan\theta i\alpha \cos\phi v_{-1} - v'_{-1}) \right] \hat{\eta}_o = \sigma \hat{v}_o \\
& + A\sigma \left\{ (\eta_1 \tan\theta \bar{\alpha}_{-2} + \zeta_1 \bar{\beta}_{-2}) \hat{v}_{-2} + \eta_1 \hat{v}'_{-2} \right. \\
& + \frac{i\alpha \sin\phi v_1}{R(C_M \sigma^2 + C_{K_o} - C_{T_z} \bar{\beta}_{-2}^2)} (\bar{\beta}_{-2} \hat{v}_{-2} - \frac{\bar{\alpha}_{-2}}{\Delta_{-2}} \hat{\Omega}'_{-2} - \frac{\bar{\beta}_{-2}}{\Delta_{-2}} \hat{v}''_{-2}) \\
& (\eta_{-1} \tan\theta \bar{\alpha}_2 + \zeta_{-1} \bar{\beta}_2) \hat{v}_2 + \eta_{-1} \hat{v}'_2 \\
& \left. - \frac{i\alpha \sin\phi v_{-1}}{R(C_M \sigma^2 + C_{K_o} - C_{T_z} \bar{\beta}_2^2)} (\bar{\beta}_2 \hat{v}_2 - \frac{\bar{\alpha}_2}{\Delta_2} \hat{\Omega}'_2 - \frac{\bar{\beta}_2}{\Delta_2} \hat{v}''_2) \right\} \\
& + A(\tan\theta i\alpha \cos\phi v_1 + v'_1) \left[\hat{v}_{-2} + A \left\{ (\eta_{-1} \tan\theta \bar{\alpha}_o \right. \right. \\
& + \zeta_{-1} \bar{\beta}_o) \hat{v}_o + \eta_{-1} \hat{v}'_o \\
& \left. \left. - \frac{i\alpha \sin\phi v_{-1}}{R(C_M \sigma^2 + C_{K_o} - C_{T_z} \bar{\beta}_o^2)} (\bar{\beta}_o \hat{v}_o - \frac{\bar{\alpha}_o}{\Delta_o} \hat{\Omega}'_o - \frac{\bar{\beta}_o}{\Delta_o} \hat{v}''_o) \right\} \right] \\
& - A(\tan\theta i\alpha \cos\phi v_{-1} - v'_{-1}) \left[\hat{v}_{+2} + A \left\{ (\eta_1 \tan\theta \bar{\alpha}_o \right. \right. \\
& + \zeta_1 \bar{\beta}_o) \hat{v}_o + \eta_1 \hat{v}'_o \\
& \left. \left. + \frac{i\alpha \sin\phi v_1}{R(C_M \sigma^2 + C_{K_o} - C_{T_z} \bar{\beta}_o^2)} (\bar{\beta}_o \hat{v}_o - \frac{\bar{\alpha}_o}{\Delta_o} \hat{\Omega}'_o - \frac{\bar{\beta}_o}{\Delta_o} \hat{v}''_o) \right\} \right] \quad B.28b
\end{aligned}$$

and

$$\begin{aligned}
& \sigma \left[\sigma^2 + 2A^2 (\tan \theta i \alpha \cos \phi v_1 + v'_1) (\tan \theta i \alpha \cos \phi v_{-1} - v'_{-1}) \right] \hat{\eta}_{-2} \\
&= \left[\sigma^2 + 2A^2 (\tan \theta i \alpha \cos \phi v_1 + v'_1) (\tan \theta i \alpha \cos \phi v_{-1} - v'_{-1}) \right] \left[\hat{v}_{-2} \right. \\
&+ A \left\{ (\eta_{-1} \tan \theta \bar{\alpha}_o + \zeta_{-1} \bar{\beta}_o) \hat{v}_o + \eta_{-1} \hat{v}'_o \right. \\
&- \frac{i \alpha \sin \phi v_{-1}}{R(C_M \sigma^2 + C_{K_s} - C_{Tz} \bar{\beta}_o^2)} (\bar{\beta}_o \hat{v}_o - \frac{\bar{\alpha}_o}{\Delta_o} \hat{\Omega}'_o - \frac{\bar{\beta}_o}{\Delta_o} \hat{v}''_o) \left. \right\} \\
&- A (\tan \theta i \alpha \cos \phi v_{-1} - v'_{-1}) \left[\sigma \hat{v}_o + A \sigma \left\{ (\eta_1 \tan \theta \bar{\alpha}_{-2} + \zeta_1 \bar{\beta}_{-2}) \hat{v}_{-2} + \eta_1 \hat{v}'_{-2} \right. \right. \\
&+ \frac{i \alpha \sin \phi v_1}{R(C_M \sigma^2 + C_{K_s} - C_{Tz} \bar{\beta}_{-2}^2)} (\bar{\beta}_{-2} \hat{v}_{-2} - \frac{\bar{\alpha}_{-2}}{\Delta_{-2}} \hat{\Omega}'_{-2} - \frac{\bar{\beta}_{-2}}{\Delta_{-2}} \hat{v}''_{-2}) \\
&(\eta_{-1} \tan \theta \bar{\alpha}_2 + \zeta_{-1} \bar{\beta}_2) \hat{v}_2 + \eta_{-1} \hat{v}'_2 \\
&- \frac{i \alpha \sin \phi v_{-1}}{R(C_M \sigma^2 + C_{K_s} - C_{Tz} \bar{\beta}_2^2)} (\bar{\beta}_2 \hat{v}_2 - \frac{\bar{\alpha}_2}{\Delta_2} \hat{\Omega}'_2 - \frac{\bar{\beta}_2}{\Delta_2} \hat{v}''_2) \left. \right\} \\
&+ A (\tan \theta i \alpha \cos \phi v_1 + v'_1) \hat{v}_{-2} + A^2 (\tan \theta i \alpha \cos \phi v_1 + v'_1) \left\{ (\eta_{-1} \tan \theta \bar{\alpha}_o \right. \\
&+ \zeta_{-1} \bar{\beta}_o) \hat{v}_o + \eta_{-1} \hat{v}'_o \\
&- \frac{i \alpha \sin \phi v_{-1}}{R(C_M \sigma^2 + C_{K_s} - C_{Tz} \bar{\beta}_o^2)} (\bar{\beta}_o \hat{v}_o - \frac{\bar{\alpha}_o}{\Delta_o} \hat{\Omega}'_o - \frac{\bar{\beta}_o}{\Delta_o} \hat{v}''_o) \left. \right\} \\
&- A (\tan \theta i \alpha \cos \phi v_{-1} - v'_{-1}) \hat{v}_2 - A^2 (\tan \theta i \alpha \cos \phi v_{-1} - v'_{-1}) \left\{ (\eta_1 \tan \theta \bar{\alpha}_o \right. \\
&+ \zeta_1 \bar{\beta}_o) \hat{v}_o + \eta_1 \hat{v}'_o \\
&+ \frac{i \alpha \sin \phi v_1}{R(C_M \sigma^2 + C_{K_s} - C_{Tz} \bar{\beta}_o^2)} (\bar{\beta}_o \hat{v}_o - \frac{\bar{\alpha}_o}{\Delta_o} \hat{\Omega}'_o - \frac{\bar{\beta}_o}{\Delta_o} \hat{v}''_o) \left. \right\} \quad B.28c
\end{aligned}$$

This gives explicit relations for $(\hat{\eta}_o, \hat{\eta}_{\pm 2})$. These are then substituted into (B.12a, 12c and 18) to give nine equations representing a compliant wall boundary conditions for the fundamental mode. Since the above relations for $\hat{\eta}$ are quite large, we will give the boundary conditions prior to substitution of $\hat{\eta}$. These are

B.C. 1 and 2: streamwise continuity, $n = \pm 2$

$$\begin{aligned} \frac{\bar{\alpha}_{\pm 2}}{\Delta_{\pm 2}} \hat{v}'_{\pm 2} - \frac{\bar{\beta}_{\pm 2}}{\Delta_{\pm 2}} \hat{\Omega}_{\pm 2} + (\sigma \tan \theta - U'_o) \hat{\eta}_{\pm 2} - A \left\{ (\eta_{\pm 1} \tan \theta \bar{\alpha}_o + \zeta_{\pm 1} \bar{\beta}_o) \left(\frac{\bar{\beta}_o}{\Delta_o} \hat{\Omega}_o \right. \right. \\ \left. \left. - \frac{\bar{\alpha}_o}{\Delta_o} \hat{v}'_o \right) + \eta_{\pm 1} \left(\frac{\bar{\beta}_o}{\Delta_o} \hat{\Omega}'_o - \frac{\bar{\alpha}_o}{\Delta_o} \hat{v}''_o \right) \pm (\tan \theta i \alpha \cos \phi u_{\pm 1} \pm u'_{\pm 1}) \hat{\eta}_o \right. \\ \left. \pm \frac{i \alpha \sin \phi u_{\pm 1}}{R(C_M \sigma^2 + C_{Ks} - C_{Tz} \bar{\beta}_o^2)} \left(\bar{\beta}_o \hat{v}_o - \frac{\bar{\alpha}_o}{\Delta_o} \hat{\Omega}'_o - \frac{\bar{\beta}_o}{\Delta_o} \hat{v}''_o \right) \right\} = 0 \quad B.29 - 30 \end{aligned}$$

B.C. 3: streamwise continuity, $n=0$

$$\begin{aligned} \frac{\bar{\alpha}_o}{\Delta_o} \hat{v}'_o - \frac{\bar{\beta}_o}{\Delta_o} \hat{\Omega}_o + (\sigma \tan \theta - U'_o) \hat{\eta}_o \\ - A \left\{ (\eta_1 \tan \theta \bar{\alpha}_{-2} + \zeta_1 \bar{\beta}_{-2}) \left(\frac{\bar{\beta}_{-2}}{\Delta_{-2}} \hat{\Omega}_{-2} - \frac{\bar{\alpha}_{-2}}{\Delta_{-2}} \hat{v}'_{-2} \right) \right. \\ \left. + \eta_1 \left(\frac{\bar{\beta}_{-2}}{\Delta_{-2}} \hat{\Omega}'_{-2} - \frac{\bar{\alpha}_{-2}}{\Delta_{-2}} \hat{v}''_{-2} \right) + (\tan \theta i \alpha \cos \phi u_1 + u'_1) \hat{\eta}_{-2} \right. \\ \left. + \frac{i \alpha \sin \phi u_1}{R(C_M \sigma^2 + C_{Ks} - C_{Tz} \bar{\beta}_{-2}^2)} \left(\bar{\beta}_{-2} \hat{v}_{-2} - \frac{\bar{\alpha}_{-2}}{\Delta_{-2}} \hat{\Omega}'_{-2} - \frac{\bar{\beta}_{-2}}{\Delta_{-2}} \hat{v}''_{-2} \right) \right. \\ \left. + (\eta_{-1} \tan \theta \bar{\alpha}_2 + \zeta_{-1} \bar{\beta}_2) \left(\frac{\bar{\beta}_2}{\Delta_2} \hat{\Omega}_2 - \frac{\bar{\alpha}_2}{\Delta_2} \hat{v}'_2 \right) \right. \\ \left. + \eta_{-1} \left(\frac{\bar{\beta}_2}{\Delta_2} \hat{\Omega}'_2 - \frac{\bar{\alpha}_2}{\Delta_2} \hat{v}''_2 \right) - (\tan \theta i \alpha \cos \phi u_{-1} - u'_{-1}) \hat{\eta}_2 \right. \\ \left. - \frac{i \alpha \sin \phi u_{-1}}{R(C_M \sigma^2 + C_{Ks} - C_{Tz} \bar{\beta}_2^2)} \left(\bar{\beta}_2 \hat{v}_2 - \frac{\bar{\alpha}_2}{\Delta_2} \hat{\Omega}'_2 - \frac{\bar{\beta}_2}{\Delta_2} \hat{v}''_2 \right) \right\} = 0 \quad B.31 \end{aligned}$$

B.C. 4 and 5: spanwise continuity, $n = \pm 2$

$$\begin{aligned}
& \frac{\sigma}{R} (\bar{\beta}_{\pm 2} \hat{v}_{\pm 2} - \frac{\bar{\alpha}_{\pm 2}}{\Delta_{\pm 2}} \hat{\Omega}'_{\pm 2} - \frac{\bar{\beta}_{\pm 2}}{\Delta_{\pm 2}} \hat{v}''_{\pm 2}) + (C_M \sigma^2 + C_{K_s} - C_{T_z} \bar{\beta}_{\pm 2}^2) \left(\frac{\bar{\alpha}_{\pm 2}}{\Delta_{\pm 2}} \hat{\Omega}_{\pm 2} \right. \\
& + \frac{\bar{\beta}_{\pm 2}}{\Delta_{\pm 2}} \hat{v}'_{\pm 2} \left. \right) + A (C_M \sigma^2 + C_{K_s} - C_{T_z} \bar{\beta}_{\pm 2}^2) \left\{ (\eta_{\pm 1} \tan \theta \bar{\alpha}_o + \zeta_{\pm 1} \bar{\beta}_o) \left(\frac{\bar{\alpha}_o}{\Delta_o} \hat{\Omega}_o \right. \right. \\
& + \frac{\bar{\beta}_o}{\Delta_o} \hat{v}'_o \left. \right) + \eta_{\pm 1} \left(\frac{\bar{\alpha}_o}{\Delta_o} \hat{\Omega}'_o + \frac{\bar{\beta}_o}{\Delta_o} \hat{v}''_o \right) \mp (\tan \theta i \alpha \cos \phi w_{\pm 1} \pm w'_{\pm 1}) \hat{\eta}_o \\
& \left. \mp \frac{i \alpha \sin \phi w_{\pm 1}}{R (C_M \sigma^2 + C_{K_s} - C_{T_z} \bar{\beta}_o^2)} (\bar{\beta}_o \hat{v}_o - \frac{\bar{\alpha}_o}{\Delta_o} \hat{\Omega}'_o - \frac{\bar{\beta}_o}{\Delta_o} \hat{v}''_o) \right\} = 0 \quad B.32 - 33
\end{aligned}$$

B.C. 6: spanwise continuity, $n=0$

$$\begin{aligned}
& \frac{\sigma}{R} (\bar{\beta}_o \hat{v}_o - \frac{\bar{\alpha}_o}{\Delta_o} \hat{\Omega}'_o - \frac{\bar{\beta}_o}{\Delta_o} \hat{v}''_o) + (C_M \sigma^2 + C_{K_s} - C_{T_z} \bar{\beta}_o^2) \left(\frac{\bar{\alpha}_o}{\Delta_o} \hat{\Omega}_o + \frac{\bar{\beta}_o}{\Delta_o} \hat{v}'_o \right) \\
& + A (C_M \sigma^2 + C_{K_s} - C_{T_z} \bar{\beta}_o^2) \left\{ (\eta_1 \tan \theta \bar{\alpha}_{-2} + \zeta_1 \bar{\beta}_{-2}) \left(\frac{\bar{\alpha}_{-2}}{\Delta_{-2}} \hat{\Omega}_{-2} + \frac{\bar{\beta}_{-2}}{\Delta_{-2}} \hat{v}'_{-2} \right) \right. \\
& + \eta_1 \left(\frac{\bar{\alpha}_{-2}}{\Delta_{-2}} \hat{\Omega}'_{-2} + \frac{\bar{\beta}_{-2}}{\Delta_{-2}} \hat{v}''_{-2} \right) - (\tan \theta i \alpha \cos \phi w_1 + w'_1) \hat{\eta}_{-2} \\
& - \frac{i \alpha \sin \phi w_1}{R (C_M \sigma^2 + C_{K_s} - C_{T_z} \bar{\beta}_{-2}^2)} (\bar{\beta}_{-2} \hat{v}_{-2} - \frac{\bar{\alpha}_{-2}}{\Delta_{-2}} \hat{\Omega}'_{-2} - \frac{\bar{\beta}_{-2}}{\Delta_{-2}} \hat{v}''_{-2}) \\
& + (\eta_{-1} \tan \theta \bar{\alpha}_2 + \zeta_{-1} \bar{\beta}_2) \left(\frac{\bar{\alpha}_2}{\Delta_2} \hat{\Omega}_2 + \frac{\bar{\beta}_2}{\Delta_2} \hat{v}'_2 \right) \\
& + \eta_{-1} \left(\frac{\bar{\alpha}_2}{\Delta_2} \hat{\Omega}'_2 + \frac{\bar{\beta}_2}{\Delta_2} \hat{v}''_2 \right) + (\tan \theta i \alpha \cos \phi w_{-1} - w'_{-1}) \hat{\eta}_2 \\
& \left. + \frac{i \alpha \sin \phi w_{-1}}{R (C_M \sigma^2 + C_{K_s} - C_{T_z} \bar{\beta}_2^2)} (\bar{\beta}_2 \hat{v}_2 - \frac{\bar{\alpha}_2}{\Delta_2} \hat{\Omega}'_2 - \frac{\bar{\beta}_2}{\Delta_2} \hat{v}''_2) \right\} = 0 \quad B.34
\end{aligned}$$

B.C. 7 and 8: force balance, $n = \pm 2$

$$\begin{aligned}
& [C_M \sigma^2 + (C_{Bz} \bar{\alpha}_{\pm 2}^4 + 2C_{Bzz} \bar{\alpha}_{\pm 2}^2 \bar{\beta}_{\pm 2}^2 + C_{Bz} \bar{\beta}_{\pm 2}^4) \cos^2 \theta + C_K \\
& - C_{Tz} \bar{\alpha}_{\pm 2}^2 \sin^2 \theta] \hat{\eta}_{\pm 2} \Delta_{\pm 2} \\
& - \left\{ \left[\frac{3}{R} \Delta_{\pm 2} - \sigma + c_z \bar{\alpha}_{\pm 2} + c_z \bar{\beta}_{\pm 2} \right] \hat{v}'_{\pm 2} + \frac{1}{R} \hat{v}'''_{\pm 2} + U'_o \bar{\alpha}_{\pm 2} \hat{v}_{\pm 2} \right. \\
& \left. - \frac{\Delta_{\pm 2} \tan \theta}{R} \left(\frac{\bar{\alpha}_{\pm 2}}{\Delta_{\pm 2}} \hat{v}''_{\pm 2} - \bar{\alpha}_{\pm 2} \hat{v}_{\pm 2} - \frac{\bar{\beta}_{\pm 2}}{\Delta_{\pm 2}} \hat{\Omega}'_{\pm 2} \right) \right\} \cos^2 \theta \\
& + A \left\{ (u_{\pm 1} \bar{\alpha}_o + w_{\pm 1} \bar{\beta}_o) \hat{v}'_o + v_{\pm 1} \hat{v}''_o - (u'_{\pm 1} \bar{\alpha}_o + w'_{\pm 1} \bar{\beta}_o) \hat{v}_o \right. \\
& \pm i\alpha \cos \phi (u_{\pm 1} \bar{\alpha}_o + w_{\pm 1} \bar{\beta}_o) \left(\frac{\bar{\alpha}_o}{\Delta_o} \hat{v}'_o - \frac{\bar{\beta}_o}{\Delta_o} \hat{\Omega}_o \right) \\
& \left. \pm i\alpha \sin \phi (u_{\pm 1} \bar{\alpha}_o + w_{\pm 1} \bar{\beta}_o) \left(\frac{\bar{\beta}_o}{\Delta_o} \hat{v}'_o + \frac{\bar{\alpha}_o}{\Delta_o} \hat{\Omega}_o \right) \right\} \cos^2 \theta = 0 \quad B.35 - 36
\end{aligned}$$

B.C. 4 and 5: spanwise continuity, $n = \pm 2$

$$\begin{aligned}
& \frac{\sigma}{R} (\bar{\beta}_{\pm 2} \hat{v}_{\pm 2} - \frac{\bar{\alpha}_{\pm 2}}{\Delta_{\pm 2}} \hat{\Omega}'_{\pm 2} - \frac{\bar{\beta}_{\pm 2}}{\Delta_{\pm 2}} \hat{v}''_{\pm 2}) + (C_M \sigma^2 + C_{K_s} - C_{T_z} \bar{\beta}_{\pm 2}^2) \left(\frac{\bar{\alpha}_{\pm 2}}{\Delta_{\pm 2}} \hat{\Omega}_{\pm 2} \right. \\
& + \frac{\bar{\beta}_{\pm 2}}{\Delta_{\pm 2}} \hat{v}'_{\pm 2})] + A (C_M \sigma^2 + C_{K_s} - C_{T_z} \bar{\beta}_{\pm 2}^2) \left\{ (\eta_{\pm 1} \tan \theta \bar{\alpha}_o + \zeta_{\pm 1} \bar{\beta}_o) \left(\frac{\bar{\alpha}_o}{\Delta_o} \hat{\Omega}_o \right. \right. \\
& + \frac{\bar{\beta}_o}{\Delta_o} \hat{v}'_o) + \eta_{\pm 1} \left(\frac{\bar{\alpha}_o}{\Delta_o} \hat{\Omega}'_o + \frac{\bar{\beta}_o}{\Delta_o} \hat{v}''_o \right) \mp (\tan \theta i \alpha \cos \phi w_{\pm 1} \pm w'_{\pm 1}) \hat{\eta}_o \\
& \left. \left. \mp \frac{i \alpha \sin \phi w_{\pm 1}}{R (C_M \sigma^2 + C_{K_s} - C_{T_z} \bar{\beta}_o)} (\bar{\beta}_o \hat{v}_o - \frac{\bar{\alpha}_o}{\Delta_o} \hat{\Omega}'_o - \frac{\bar{\beta}_o}{\Delta_o} \hat{v}''_o) \right\} = 0 \quad B.32 - 33
\end{aligned}$$

B.C. 6: spanwise continuity, $n=0$

$$\begin{aligned}
& \frac{\sigma}{R} (\bar{\beta}_o \hat{v}_o - \frac{\bar{\alpha}_o}{\Delta_o} \hat{\Omega}'_o - \frac{\bar{\beta}_o}{\Delta_o} \hat{v}''_o) + (C_M \sigma^2 + C_{K_s} - C_{T_z} \bar{\beta}_o^2) \left(\frac{\bar{\alpha}_o}{\Delta_o} \hat{\Omega}_o + \frac{\bar{\beta}_o}{\Delta_o} \hat{v}'_o \right) \\
& + A (C_M \sigma^2 + C_{K_s} - C_{T_z} \bar{\beta}_o^2) \left\{ (\eta_1 \tan \theta \bar{\alpha}_{-2} + \zeta_1 \bar{\beta}_{-2}) \left(\frac{\bar{\alpha}_{-2}}{\Delta_{-2}} \hat{\Omega}_{-2} + \frac{\bar{\beta}_{-2}}{\Delta_{-2}} \hat{v}'_{-2} \right) \right. \\
& + \eta_1 \left(\frac{\bar{\alpha}_{-2}}{\Delta_{-2}} \hat{\Omega}'_{-2} + \frac{\bar{\beta}_{-2}}{\Delta_{-2}} \hat{v}''_{-2} \right) - (\tan \theta i \alpha \cos \phi w_1 + w'_1) \hat{\eta}_{-2} \\
& - \frac{i \alpha \sin \phi w_1}{R (C_M \sigma^2 + C_{K_s} - C_{T_z} \bar{\beta}_{-2}^2)} (\bar{\beta}_{-2} \hat{v}_{-2} - \frac{\bar{\alpha}_{-2}}{\Delta_{-2}} \hat{\Omega}'_{-2} - \frac{\bar{\beta}_{-2}}{\Delta_{-2}} \hat{v}''_{-2}) \\
& + (\eta_{-1} \tan \theta \bar{\alpha}_2 + \zeta_{-1} \bar{\beta}_2) \left(\frac{\bar{\alpha}_2}{\Delta_2} \hat{\Omega}_2 + \frac{\bar{\beta}_2}{\Delta_2} \hat{v}'_2 \right) \\
& + \eta_{-1} \left(\frac{\bar{\alpha}_2}{\Delta_2} \hat{\Omega}'_2 + \frac{\bar{\beta}_2}{\Delta_2} \hat{v}''_2 \right) + (\tan \theta i \alpha \cos \phi w_{-1} - w'_{-1}) \hat{\eta}_2 \\
& \left. \left. + \frac{i \alpha \sin \phi w_{-1}}{R (C_M \sigma^2 + C_{K_s} - C_{T_z} \bar{\beta}_2^2)} (\bar{\beta}_2 \hat{v}_2 - \frac{\bar{\alpha}_2}{\Delta_2} \hat{\Omega}'_2 - \frac{\bar{\beta}_2}{\Delta_2} \hat{v}''_2) \right\} = 0 \quad B.34
\end{aligned}$$

B.C. 9: force balance, n=0

$$\begin{aligned}
& [C_M \sigma^2 + (C_{Bz} \bar{\alpha}_o^4 + 2C_{Bzz} \bar{\alpha}_o^2 \bar{\beta}_o^2 + C_{Bz} \bar{\beta}_o^4) \cos^2 \theta + C_K \\
& - C_{Tz} \bar{\alpha}_o^2 \sin^2 \theta] \hat{\eta}_o \Delta_o \\
& - \left\{ \left[\frac{3}{R} \Delta_o - \sigma + c_z \bar{\alpha}_o + c_z \bar{\beta}_o \right] \hat{v}'_o + \frac{1}{R} \hat{v}'''_o + U'_o \bar{\alpha}_o \hat{v}_o \right. \\
& - \frac{\Delta_o \tan \theta}{R} \left(\frac{\bar{\alpha}_o}{\Delta_o} \hat{v}''_o - \bar{\alpha}_o \hat{v}_o - \frac{\bar{\beta}_o}{\Delta_o} \hat{\Omega}'_o \right) \left. \right\} \cos^2 \theta \\
& + A \left\{ (u_1 \bar{\alpha}_{-2} + w_1 \bar{\beta}_{-2}) \hat{v}'_{-2} + v_1 \hat{v}''_{-2} - (u'_1 \bar{\alpha}_{-2} + w'_1 \bar{\beta}_{-2}) \hat{v}_{-2} \right. \\
& + i\alpha \cos \phi (u_1 \bar{\alpha}_{-2} + w_1 \bar{\beta}_{-2}) \left(\frac{\bar{\alpha}_{-2}}{\Delta_{-2}} \hat{v}'_{-2} - \frac{\bar{\beta}_{-2}}{\Delta_{-2}} \hat{\Omega}_{-2} \right) \\
& + i\alpha \sin \phi (u_1 \bar{\alpha}_{-2} + w_1 \bar{\beta}_{-2}) \left(\frac{\bar{\beta}_{-2}}{\Delta_{-2}} \hat{v}'_{-2} + \frac{\bar{\alpha}_{-2}}{\Delta_{-2}} \hat{\Omega}_{-2} \right) \\
& + (u_{-1} \bar{\alpha}_2 + w_{-1} \bar{\beta}_2) \hat{v}'_2 + v_{-1} \hat{v}''_2 - (u'_{-1} \bar{\alpha}_2 + w'_{-1} \bar{\beta}_2) \hat{v}_2 \\
& - i\alpha \cos \phi (u_{-1} \bar{\alpha}_2 + w_{-1} \bar{\beta}_2) \left(\frac{\bar{\alpha}_2}{\Delta_2} \hat{v}'_2 - \frac{\bar{\beta}_2}{\Delta_2} \hat{\Omega}_2 \right) \\
& \left. - i\alpha \sin \phi (u_{-1} \bar{\alpha}_2 + w_{-1} \bar{\beta}_2) \left(\frac{\bar{\beta}_2}{\Delta_2} \hat{v}'_2 + \frac{\bar{\alpha}_2}{\Delta_2} \hat{\Omega}_2 \right) \right\} \cos^2 \theta = 0 \quad B.37
\end{aligned}$$

APPENDIX C

CHEBYSHEV SERIES FORMULAS

C.1 Introduction

In this section a listing of the formulae that were necessary for this thesis is given. The first section gives the definition and listing of the Chebyshev polynomials. The second section gives an example of how to represent a known function by a Chebyshev series.

C.2 The Chebyshev Series

The Chebyshev polynomials, $T_n(x)$, are defined on the interval $x \in [-1, +1]$ and are derived from and related to the cosine function by

$$T_n(\cos \theta) = \cos n\theta \quad C.1$$

with the initial few polynomials appearing as

$$\begin{aligned}
 T_0(x) &= 1 \\
 T_1(x) &= x \\
 T_2(x) &= 2x^2 - 1 \\
 T_3(x) &= 4x^3 - 3x \\
 \text{etc} & \quad (C.2)
 \end{aligned}$$

The following trigonometric identity can be obtained.

$$\cos(n + 1)\theta = 2 \cos \theta \cdot \cos n\theta - \cos(n - 1)\theta \quad C.2$$

This results in a Chebyshev recurrence formula for higher order polynomials.

$$T_{n+1}(x) = 2xT_n(x) - T_{n-1}(x) \quad C.3$$

The product formula is

$$T_n(x)T_m(x) = \frac{1}{2} [T_{n+m}(x) + T_{|n-m|}(x)] \quad C.4$$

and the indefinite integral relation is

$$\int T_n(x)dx = \begin{cases} T_1(x) & n = 0 \\ \frac{1}{4}(T_0(x) + T_2(x)) & n = 1 \\ \frac{1}{2} \left[\frac{T_{n+1}(x)}{n+1} - \frac{T_{n-1}(x)}{n-1} \right] & n \geq 2. \end{cases} \quad C.5$$

The series boundary conditions for a polynomial of order n are

$$T_n(\pm 1) = (\pm 1)^n \quad C.6$$

and the differential relation for Chebyshev polynomials at the boundaries is

$$\frac{d^p}{dx^p} T_n(\pm 1) = (\pm 1)^{n+p} \prod_{k=0}^{p-1} (n^2 - k^2)/(2k+1). \quad C.7$$

Another efficient relation useful when performing the summation of a Chebyshev series to determine a functional value of x is given by

$$f(x) = \sum_{n=0}^N 'a_n T_n(x) = \frac{1}{2} [b_0(x) - b_2(x)], \quad C.8$$

where the prime signifies that the leading term is to be halved. The recurrence system required to evaluate (C.8) is

$$b_n(x) = 2x b_{n+1}(x) - b_{n+2}(x) + a_n \quad C.9$$

$$b_{N+1}(x) = b_{N+2}(x) = 0.$$

A Chebyshev formula useful in approximating a known function in a Chebyshev series can be defined as

$$\Phi(x) = \sum_{n=0}^N {}' \phi_n T_n(x), \quad C.10a$$

where $\Phi(x)$ is a known function. The coefficients, ϕ_n , are given by

$$\phi_n = \frac{2}{N} \sum_{k=0}^N {}'' \Phi(x_k) T_n(x_k) \quad C.10b$$

with

$$x_k = \cos \frac{k\pi}{N} \quad \text{for } k = 0, 1, 2, \dots, N. \quad C.10c$$

The double prime on the summation signifies that the leading and trailing coefficients are to be halved. This approximation of a known function is required for the Blasius profile and the primary eigenfunctions. As an example, the Blasius profile will be represented by the series after listing the remaining general formulae.

The final Chebyshev property that will be given prior to listing practical integral formulae is the approximation of the differential of a known function in Chebyshev series. The derivative is given by

$$\phi'(x) = \sum_{n=0}^{\infty} b_n T_n(x) \quad C.11a$$

where

$$b_n = \frac{2}{c_n} \sum_{\substack{p=n+1 \\ p+odd}}^{\infty} p a_p \quad C.11b$$

and

$$c_n = \begin{cases} 2 & n = 0 \\ 1 & n > 0. \end{cases} \quad C.11c$$

The coefficients, a_n , are obtained from the series approximation to the known function, $\phi(x)$.

To obtain the solution of a differential equation by a Chebyshev series approximation, it is convenient, although not necessary, to convert the differential equation to an integral form. As such, a function is represented by the following finite, Chebyshev series.

$$\phi(x) = \sum_{n=0}^N a_n T_n(x) \quad C.12$$

By applying the integral relation (C.5) appropriately and repeatedly, the following relations are obtained.

$$1. \quad \int \phi(x) dx = \sum_{n=0}^{N+1} b_n T_n(x) \quad C.13a$$

where

$$b_n = \frac{1}{2n} (a_{n-1} - a_{n+1}) \quad \text{for } n \geq 1 \quad C.13b$$

$$2. \int \int \phi(x) dx^2 = \sum_{n=0}^{N+2} {}' b_n T_n(x) \quad C.14a$$

where

$$b_n = \left[\frac{a_{n-2}}{4n(n-1)} - \frac{a_n}{2(n^2-1)} + \frac{a_{n+2}}{4n(n+1)} \right] \quad \text{for } n \geq 2 \quad C.14b$$

$$3. \int \int \int \phi(x) dx^3 = \sum_{n=0}^{N+3} {}' b_n T_n(x) \quad C.15a$$

where

$$b_n = \frac{a_{n-3}}{8n(n-1)(n-2)} - \frac{3a_{n-1}}{8n(n-2)(n+1)} + \frac{3a_{n+1}}{8n(n-1)(n+2)} - \frac{a_{n+3}}{8n(n+1)(n+2)} \quad \text{for } n \geq 3 \quad C.15b$$

$$4. \int \int \int \int \phi(x) dx^4 = \sum_{n=0}^{N+4} {}' b_n T_n(x) \quad C.16a$$

where

$$b_n = \frac{a_{n-4}}{16n(n-1)(n-2)(n-3)} - \frac{a_{n-2}}{4n(n^2-1)(n-3)} + \frac{3a_n}{8(n^2-1)(n^2-4)} - \frac{a_{n+2}}{4n(n^2-1)(n+3)} + \frac{a_{n+4}}{16n(n+1)(n+2)(n+3)} \quad \text{for } n \geq 4 \quad C.16b$$

When the coefficients in the differential equations are non-constant, the Chebyshev product formula (C.4) is needed. Introducing a function, $u(x)$, representing the non-constant coefficient, the following is obtained.

$$u(x)\phi(x) = \sum_{n=0}^{\infty} {}' d_n T_n(x) \quad C.17a$$

with

$$u(x) = \sum_{n=0}^{\infty} {}' u_n T_n(x) \quad C.17b$$

and

$$d_n = \frac{1}{2} u_n a_o + \frac{1}{2} \sum_{m=1}^N (u_{|m-n|} + u_{m+n}) a_m \quad \text{for } n \geq 0 \quad C.17c$$

Integrations are performed in a straight forward manner using the integral relation (C.5). The following integral relations prove useful for the problem presented in this thesis.

$$1. \quad \int u(x) \phi(x) dx = \sum_{n=0}^{N+1} {}' d_n T_n(x) \quad C.18a$$

where

$$d_n = \frac{1}{4n} (u_{n-1} - u_{n+1}) a_o + \frac{1}{4n} \sum_{m=1}^N (u_{|m-n+1|} - u_{|m-n-1|} + u_{m+n-1} - u_{m+n+1}) a_m \quad \text{for } n \geq 1 \quad C.18b$$

$$2. \quad \int \int u(x) \phi(x) dx^2 = \sum_{n=0}^{N+2} {}' d_n T_n(x) \quad C.19a$$

where

$$d_n = \left[\frac{u_{n-2}}{8n(n-1)} - \frac{u_n}{4(n^2-1)} + \frac{u_{n+2}}{8n(n+1)} \right] a_o + \sum_{m=1}^N \left[\frac{u_{|m-n+2|} + u_{m+n-2}}{8n(n-1)} - \frac{u_{m+n} + u_{|m-n|}}{4(n^2-1)} + \frac{u_{|m-n-2|} + u_{m+n+2}}{8n(n+1)} \right] a_m \quad \text{for } n \geq 2 \quad C.19a$$

$$3. \int \int \int u(x)\phi(x)dx^3 = \sum_{n=0}^{N+3} d_n T_n(x) \quad C.20a$$

where

$$d_n = \left[\frac{u_{n-3}}{16n(n-1)(n-2)} - \frac{3u_{n-1}}{16n(n+1)(n-2)} + \frac{3u_{n+1}}{16n(n-1)(n+2)} \right. \\ \left. - \frac{u_{n+3}}{16n(n+1)(n+2)} \right] a_0 \\ + \sum_{m=1}^N \left[\frac{u_{|m-n+3|} + u_{m+n-3}}{16n(n-1)(n-2)} - \frac{3(u_{|m-n+1|} + u_{m+n-1})}{16n(n+1)(n-2)} \right. \\ \left. + \frac{3(u_{|m-n-1|} + u_{m+n+1})}{16n(n-1)(n+2)} - \frac{u_{|m-n-3|} + u_{m+n+3}}{16n(n+1)(n+2)} \right] a_m \quad \text{for } n \geq 3 \quad C.20b$$

$$4. \int \int \int \int u(x)\phi(x)dx^4 = \sum_{n=0}^{N+4} d_n T_n(x) \quad C.21a$$

where

$$d_n = \left[\frac{u_{n-4}}{32n(n-1)(n-2)(n-3)} - \frac{u_{n-2}}{8n(n^2-1)(n-3)} + \frac{3u_n}{16(n^2-1)(n^2-4)} \right. \\ \left. - \frac{u_{n+2}}{8n(n^2-1)(n+3)} + \frac{u_{n+4}}{32n(n+1)(n+2)(n+3)} \right] a_0 \\ + \sum_{m=1}^N \left[\frac{u_{|m-n+4|} + u_{m+n-4}}{32n(n-1)(n-2)(n-3)} - \frac{u_{|m-n+2|} + u_{m+n-2}}{8n(n^2-1)(n-3)} + \frac{3(u_{|m-n|} + u_{m+n})}{16(n^2-1)(n^2-4)} \right. \\ \left. - \frac{u_{|m-n-2|} + u_{m+n+2}}{8n(n^2-1)(n-3)} + \frac{u_{|m-n-4|} + u_{m+n+4}}{32n(n+1)(n+2)(n+3)} \right] a_m \quad \text{for } n \geq 4 \quad C.21b$$

These relations replace the appropriate terms in an integral equation in order to obtain a solution. The integral formulae require the order of the Chebyshev terms to begin with the order of the integral equation. The proof of this will not be given here, but can be found in Gottlieb and Orszag (1977).

C.3 Approximation of the Blasius Profile

In this thesis, the solution to the Blasius equation is necessary and is represented by a Chebyshev series. To attain this, an accurate means of obtaining a numerical solution is first necessary. In the similarity variables the governing equation is an ordinary differential equation of the form

$$f''' + \frac{1}{2}ff'' = 0 \quad C.22$$

where $(\)' = \frac{d}{dy}$ and the appropriate boundary conditions are

$$f(0) = f'(0) = 0 \quad , \quad \lim_{y \rightarrow \infty} f'(y) \rightarrow 1, \quad C.23$$

where the derivative of $f(y)$ is the streamwise velocity. Using a shooting-type method with a Runge-Kutta integration scheme, the initial condition satisfying the streamwise velocity limit can be found. This results in

$$f''(0) = 0.3320573362185815 . \quad C.24$$

The discrete points desired in the Chebyshev domain, $z \in [-1, +1]$, are transformed to the Blasius variable, $y \in [0, \infty)$, via the algebraic transformation

$$y = L \cdot (1 + \hat{y})/(\hat{y}) \quad C.25$$

with

$$\hat{y} = \bar{y} Re_x^{-\frac{1}{2}} \quad C.26$$

where \bar{y} is the physical coordinate with domain $[0, \infty)$. The solution obtained at the desired points are then transformed back to the computational domain using the inverse of (C.25). Taking the solution of a function(i.e., the Blasius solution), $F(z)$, given at all points in $z \in [-1, +1]$, a Chebyshev expansion of such is sought.

$$F(z) = \sum_{n=0}^N {}'f_n T_n(z) \quad C.27$$

The prime signifies that the leading term of the series is to be halved. An exact solution is obtained for $N \rightarrow \infty$. For a series expansion, the function must be evaluated at the Chebyshev points

$$z_i = \cos(\pi i / N) \quad i = 0, 1, 2, \dots, N. \quad C.28$$

The series at these points is

$$F(z_i) = \sum_{n=0}^N {}'f_n T_n(z_i). \quad C.29$$

Using the relationship between the Chebyshev polynomial and the cosine function, a curve-fitting formula can be obtained. Thus, the coefficients can be computed using

$$f_n = \frac{2}{N} \sum_{i=0}^N {}''f(z_i) T_n(z_i) \quad C.30$$

where the double prime signifies that the leading and trailing terms of the series are to be halved. With the identity

$$T_n(z_i) = \cos(\pi n i / N) \quad C.31$$

the desired form of the curve-fitting formula is obtained. Making a substitution of (C.31) into (C.30), the following results

$$f_n = \frac{2}{N} \sum_{i=0}^N f(z_i) \cos(\pi n i / N) . \quad C.32$$

By making use of (C.32) with (C.27), the Chebyshev series representation of a function can be computed to a desired accuracy by taking N to be large.

The solution of the Blasius equation represented by a Chebyshev series is attained with this curve-fitting formula. Additionally, for the secondary instability calculations, the primary wave components are represented by a Chebyshev series in the same manner as the Blasius profile described above.

APPENDIX D

NUMERICAL ALGORITHMS

D.1 Introduction

In this section, numerical algorithms or techniques that were used in this thesis will be listed.

D.2 Routines

The following is a 5th-order Runge-Kutta method given by Luther (1966). He referred to this as a Newton-Cotes type. This is given as

$$\begin{aligned}
 y_{n+1} &= y_n + \{7k_1 + 7k_3 + 32k_4 + 12k_5 + 32k_6\}/90, \\
 k_1 &= hf(x_n, y_n), \\
 k_2 &= hf(x_n + h, y_n + k_1), \\
 k_3 &= hf(x_n + h, y_n + \{k_1 + k_2\}/2), \\
 k_4 &= hf(x_n + h/4, y_n + \{14k_1 + 5k_2 - 3k_3\}/64), \\
 k_5 &= hf(x_n + h/2, y_n + \{-12k_1 - 12k_2 + 8k_3 + 64k_4\}/96), \\
 k_6 &= hf(x_n + 3h/4, y_n + \{-9k_2 + 5k_3 + 16k_4 + 36k_5\}/64). \quad D.1
 \end{aligned}$$

where h is the step size. A number of routines are available for usage. This is listed for completeness only.

Used for the shooting approach to find the zero were Newton and three-point inverse Lagrange interpolations listed by Burden and Faires (1985) and False Position method listed by Gear (1978). These are

Newton:

$$\alpha_{i+1} = \alpha_i - (\alpha_i - \alpha_{i-1}) \frac{\Delta_i}{\Delta_i - \Delta_{i-1}} \quad D.2$$

False Position:

$$\alpha_{i+1} = \frac{\Delta_i \alpha_{i-1} - \Delta_{i-1} \alpha_i}{\Delta_i - \Delta_{i-1}} \quad D.3$$

Inverse Lagrange:

$$\begin{aligned} \alpha_{i+1} = & \frac{\alpha_i \Delta_{i-1} \Delta_{i-2}}{(\Delta_i - \Delta_{i-1})(\Delta_i - \Delta_{i-2})} + \frac{\alpha_{i-1} \Delta_i \Delta_{i-2}}{(\Delta_{i-1} - \Delta_i)(\Delta_{i-1} - \Delta_{i-2})} \\ & + \frac{\alpha_{i-2} \Delta_i \Delta_{i-1}}{(\Delta_{i-2} - \Delta_i)(\Delta_{i-2} - \Delta_{i-1})} \end{aligned} \quad D.4$$

where α_{i+1} is the eigenvalue for the next iteration ($i + 1$) and Δ is the matrix determinant of the numerical vector-asymptotic matching which goes to zero as α converges to the proper eigenvalue.

To solve the complex system of equations for the unknown constants to determine the eigenvectors and to determine the determinant of a matrix, two routines are employed from the Press et al. (1986). These are

LUDCMP-LU decomposition

LUBKSB-Solves a linear system

Additionally the following routines were used from IMSL version 9.2. These are

LEQT1C-Solves a linear system (and inverts a matrix)

EIGCC -Determine eigenvalues

From IMSL version 10, the following routines were used.

DLSLCG -Solves a linear system

DEVLCG -Determine eigenvalues

DLINCG -Inverts a matrix

In some circumstances a cubic spline was used. This is determined from the following

$$\begin{pmatrix} x_1^3 & x_1^2 & x_1 \\ x_2^3 & x_2^2 & x_2 \\ x_3^3 & x_3^2 & x_3 \end{pmatrix} \begin{Bmatrix} A \\ B \\ C \end{Bmatrix} = \begin{Bmatrix} p_1 \\ p_2 \\ p_3 \end{Bmatrix} \quad D.5a$$

where x_i are the locations for the spline and p_i are the function values. These equations are solved simultaneously to obtain the coefficients

$$C = \frac{p_3 x_1^2 - p_1 x_3^2}{x_3 x_1^2 - x_3^2 x_1} \quad D.5b$$

$$B = \frac{p_2 x_1^3 - p_1 x_2^3 - C(x_2 x_1^3 - x_1 x_2^3)}{x_1^2 x_2^2 (x_1 - x_2)} \quad D.5c$$

$$A = \frac{p_1 - C x_1 - B x_1^2}{x_1^3} \quad D.5d$$

Additionally, the following Simpson's rules were used

$$\int_{x_0}^{x_2} f(x) dx = \frac{h}{3} [f(x_0) + 4f(x_1) + f(x_2)] - \frac{h^5}{90} f^{(4)}(\zeta) \quad D.6$$

where $x_0 < \zeta < x_2$

$$\int_{x_0}^{x_4} f(x) dx = \frac{2h}{45} [7f(x_0) + 32f(x_1) + 12f(x_2) + 32f(x_3) + 7f(x_4)] - \frac{8h^7}{954} f^{(6)}(\zeta) \quad D.7$$

where $x_0 < \zeta < x_4$.



APPENDIX E

A PROPOSED FORMULATION FOR THE

TURBULENT BOUNDARY LAYER PROBLEM

E.1 Introduction

In this section, we will propose an approach to model the near-wall structure of an incompressible turbulent boundary layer over a flat wall. This approach is novel since it provides an efficient means to model the large-scale and small-scale structure. Additionally compliance is introduced. This approach complements the work of this thesis and with little effort can be directly implemented into the existing primary and secondary instability codes. This is by far not a complete discussion of the turbulent boundary layer problem, rather a proposed model and outline of solution.

In this discussion a derivation of the governing equations is given. The assumptions and any necessary discussion is given. The derivation of equations was taken from Reynolds and Hussain (1972), or R&H. We have chosen their discussion as a reference since it is a complete analysis and they give a few different closure approaches for the large-scale dynamic equations of motion. Additionally they provide an initial means of comparing the rigid and compliant walls. R&H performed a two-dimensional study while we extend their analysis to allow for three-dimensional waves.

Keeping with the notation of R&H, an instantaneous quantity is given as

$$f = \bar{f} + \tilde{f} + f' \quad E.1$$

where \bar{f} is the mean (or time-averaged) contribution, \tilde{f} is the periodic large-scale structure and f' corresponds to the small-scale turbulent fluctuation. A phase

average of the quantity is defined as the average over a large ensemble of points having the same phase with respect to a reference oscillation (e.g. the vibrating ribbon). A phase average of (E.1) is given by

$$\langle f \rangle = \bar{f} + \tilde{f} \quad E.2$$

The phase average $\langle \rangle$ neglects the small-scale background turbulence and extracts the organized large-scale motion from the total signal. As a result of time and phase averaging the following useful properties are found.

$$\langle f \rangle = 0 \quad \bar{f} = 0 \quad \bar{f}' = 0 \quad E.3a$$

$$\bar{f}g = \bar{f}\bar{g} \quad \langle \bar{f}g \rangle = 0 \quad \langle \bar{f}g \rangle = \langle \bar{f}g \rangle \quad E.3b$$

$$\langle \bar{f} \rangle = \bar{f} \quad \langle \bar{f} \rangle = \bar{f} \quad \bar{f}g' = \langle \bar{f}g' \rangle \quad E.3c$$

Although physically this may be unconfirmed, the last term states that the organized periodic motion and background turbulence are uncorrelated.

To define the equations of motion for the mean flow, large-scale organized motion, and small-scale background turbulence, we begin with the nondimensional Navier-Stokes equations.

$$\frac{\partial u_i}{\partial x_i} = 0 \quad E.4$$

$$\frac{\partial u_i}{\partial t} + u_j \frac{\partial u_i}{\partial x_j} = - \frac{\partial p}{\partial x_i} + \frac{1}{R_\delta} \frac{\partial^2 u_i}{\partial x_j \partial x_j} \quad E.5$$

The length scale δ may be taken as the boundary layer thickness and the velocity scale is the mean freestream velocity U_∞ . The Reynolds number is $R_\delta = U_\infty \delta / \nu$. The above equations are assuming incompressible constant-property flows. We follow the decomposition of (E.1), so

$$u_i = \bar{u}_i + \tilde{u}_i + u'_i$$

$$p_i = \bar{p}_i + \tilde{p}_i + p'_i \quad E.6$$

This relates to our secondary instability analysis. We can denote the following similarity

$$u_i = u_i + \bar{u}_i + u'_i = u_o + u_1 + u_3 \quad E.7$$

Other similarities between the laminar and turbulent problem will be given as we proceed.

E.2 Organized Large-scale Motion

The equations for the large-scale motion are found by substituting (E.6) into (E.4, 5). The phase average results in

$$\frac{\partial \bar{u}_i}{\partial x_i} = \frac{\partial \bar{u}_i}{\partial x_i} = \frac{\partial u'_i}{\partial x_i} = 0 \quad E.8$$

$$\begin{aligned} \frac{\partial \bar{u}_i}{\partial t} + \bar{u}_j \frac{\partial \bar{u}_i}{\partial x_j} + \bar{u}_i \frac{\partial \bar{u}_i}{\partial x_j} + \bar{u}_j \frac{\partial \bar{u}_i}{\partial x_j} + \frac{\partial}{\partial x_j} \langle u'_i u'_j \rangle + \frac{\partial}{\partial x_j} (\bar{u}_i \bar{u}_j) \\ = - \left(\frac{\partial \bar{p}}{\partial x_i} + \frac{\partial \bar{p}}{\partial x_i} \right) + \frac{1}{R_\delta} \left(\frac{\partial^2 \bar{u}_i}{\partial x_j \partial x_j} + \frac{\partial^2 \bar{u}_i}{\partial x_i \partial x_j} \right) \end{aligned} \quad E.9$$

If we take the time-average of (E.9) we obtain

$$\bar{u}_j \frac{\partial \bar{u}_i}{\partial x_j} = - \frac{\partial \bar{p}}{\partial x_i} + \frac{1}{R_\delta} \frac{\partial^2 \bar{u}_i}{\partial x_j \partial x_j} - \frac{\partial}{\partial x_j} (\bar{u}'_i \bar{u}'_j) - \frac{\partial}{\partial x_j} (\bar{u}_i \bar{u}_j) \quad E.10$$

This is the equation for the usual mean momentum equation with the addition of a Reynolds stress $-\bar{u}_i \bar{u}_j$ of wave-induced motion. This gives the effect of the waves on the mean motion. Subtracting (E.10) from (E.9) gives

$$\begin{aligned} \frac{\partial \bar{u}_i}{\partial t} + \bar{u}_j \frac{\partial \bar{u}_i}{\partial x_j} + \bar{u}_i \frac{\partial \bar{u}_i}{\partial x_j} = - \frac{\partial \bar{p}}{\partial x_i} + \frac{1}{R_\delta} \frac{\partial^2 \bar{u}_i}{\partial x_j \partial x_j} \\ + \frac{\partial}{\partial x_j} (\bar{u}_i \bar{u}_j - \bar{u}_i \bar{u}_j) + \frac{\partial}{\partial x_j} (\bar{u}'_i \bar{u}'_j - \langle u'_i u'_j \rangle) \end{aligned} \quad E.11$$

Equations (E.8) and (E.11) describe the organized wave. There are terms in equation (E.11) that are not known. These are terms that are the difference between the phase and time-averages of minus the Reynolds stress of the background turbulence, or

$$\bar{r}_{ij} = \langle u'_i u'_j \rangle - \overline{u'_i u'_j} \quad E.12$$

\bar{r}_{ij} can be thought of as the oscillation of the background Reynolds stress due to the passage of the organized structure. Since there is no means to relate \bar{r}_{ij} to \bar{u}_i there is a closure problem in the equation for the disturbance.

To see the importance of these terms R&H developed the dynamic equations for \bar{r}_{ij} . They showed that the closure problem becomes more serious with the introduction of additional unknown terms. Various terms in the equation for \bar{r}_{ij} are of order \bar{u}_i , so that even weak organized motions should expect oscillations in \bar{r}_{ij} of comparable magnitude. This suggests that \bar{r}_{ij} should not be neglected in the solution of (E.11). R&H show energy considerations. Namely that $\bar{r}_{ij} \partial \bar{u}_i / \partial x_j$ represents an energy drain to the turbulent field by the motion of the wave \bar{u}_i . The wave tries to sustain itself with its own Reynolds stresses, but is broken down by the change that the wave itself produces in the background turbulence.

E.3 Linearized Equations for the Organized Motion

In the linearized analysis we neglect higher order terms in \bar{u}_i , but retain terms \bar{r}_{ij} because we expect it to be of importance to first order. Although the boundary layer growth may be of importance, we assume for convenience that the mean flow is parallel and homogenous in the streamwise and spanwise directions. The mean flow is given by $\bar{u}_i = (\bar{u}_1, 0, 0)$. This is similar to the laminar problem. We can arrange the mean flow in a similarity profile with a Reynolds stress forcing

term. In the laminar boundary layer we assume a constant profile while the mean turbulent boundary layer profile is allowed to vary with the organized wave motion. This will be further explained in the final section.

The coefficients of the linearized equation for \hat{u}_i depend on x_2 only and hence yield a normal mode solution which are exponentially dependent on x_1, x_3 and t . We might infer a normal mode wave solution

$$\hat{f} = \frac{1}{2} [\hat{f}(x_2) e^{i(\alpha x_1 + \beta x_3 - \omega t)} + c.c.] \quad E.13$$

\hat{f} represents the complex amplitude of the quantity \hat{f} . α and β are the streamwise and spanwise wavenumbers. Substituting (E.13) into the continuity and momentum equations give

$$i\alpha \hat{u}_1 + D \hat{u}_2 + i\beta \hat{u}_3 = 0 \quad E.14$$

and

$$\begin{aligned} (-i\omega + i\alpha \bar{u}_1) \begin{Bmatrix} \hat{u}_1 \\ \hat{u}_2 \\ \hat{u}_3 \end{Bmatrix} + D \bar{u}_1 \begin{Bmatrix} \hat{u}_2 \\ 0 \\ 0 \end{Bmatrix} &= \begin{Bmatrix} -i\alpha \hat{p} \\ -D \hat{p} \\ -i\beta \hat{p} \end{Bmatrix} \\ + \frac{1}{R_\delta} (D^2 - \alpha^2 - \beta^2) \begin{Bmatrix} \hat{u}_1 \\ \hat{u}_2 \\ \hat{u}_3 \end{Bmatrix} - \begin{Bmatrix} i\alpha \hat{r}_{11} + D \hat{r}_{12} + i\beta \hat{r}_{13} \\ i\alpha \hat{r}_{21} + D \hat{r}_{22} + i\beta \hat{r}_{23} \\ i\alpha \hat{r}_{31} + D \hat{r}_{32} + i\beta \hat{r}_{33} \end{Bmatrix} & \quad E.15 \end{aligned}$$

where $D = \partial/\partial x_2$. By eliminating the pressure, substituting in $\gamma^2 = \alpha^2 + \beta^2$, and introducing normal vorticity the following equations result in terms of normal velocity and vorticity.

$$\begin{aligned} [(\alpha \bar{u}_1 - \omega)(D^2 - \gamma^2) - \alpha D^2 \bar{u}_1] \hat{u}_2 + \frac{i}{R_\delta} (D^2 - \gamma^2)^2 \hat{u}_2 \\ + iD(\alpha^2 \hat{r}_{11} + 2\alpha\beta \hat{r}_{13} + \beta^2 \hat{r}_{33}) + i\gamma^2 D \hat{r}_{22} \\ - (D^2 + \gamma^2)(\alpha \hat{r}_{12} + \beta \hat{r}_{23}) = 0 \quad E.16 \end{aligned}$$

and

$$\begin{aligned} \frac{1}{R_\delta} (D^2 - \gamma^2) \hat{\Omega}_2 - i(\alpha \bar{u}_1 - \omega) \hat{\Omega}_2 - i\beta D \bar{u}_1 \hat{u}_2 \\ + \alpha \beta (\hat{r}_{11} - \hat{r}_{33}) - (\alpha^2 - \beta^2) \hat{r}_{13} \\ - i(\beta D \hat{r}_{12} - \alpha D \hat{r}_{32}) = 0 \end{aligned} \quad E.17$$

The system to solve results in the Orr-Sommerfeld and Squire's equations for the normal velocity and vorticity with the addition of the oscillating Reynolds stress terms \hat{r}_{ij} . To solve this system one needs to find a closure scheme. The boundary conditions are such that far away from the wall the disturbance vanishes, or

$$\hat{u}_2, \hat{u}'_2, \hat{\Omega}_2 \rightarrow 0 \quad \text{as} \quad x_2 \rightarrow \infty \quad E.18$$

At the wall the compliant wall equations hold or at the rigid wall

$$\hat{u}_2 = \hat{u}'_2 = \hat{\Omega}_2 = 0 \quad \text{at} \quad y = 0 \quad E.19$$

As with the laminar boundary layer problem, we regard ω as real and fixed and γ is the complex eigenvalue for the spatial analysis. For temporal, ω is the complex eigenvalue and γ is real and specified.

E.4 Closure Schemes

In this section we introduce the two closure schemes that R&H used. These are used only as a starting point for this approach and are not necessarily the best to provide closure. For the first approach we assume that the viscosity is constant throughout the boundary layer. This is not a bad assumption since R&H found that the variable viscosity and constant viscosity give similar results and the differences were negligible. Also, since the problem is complex enough with

the addition of compliance, we may elect to assume that the viscosity is constant. In the dynamic equations of motion, this results in a modified Reynolds number only.

The simplest model is referred to as the "quasi-laminar" model which implies

$$\tilde{r}_{ij} = 0 \quad E.20$$

This implies that we are solving the Orr-Sommerfeld and Squire's equations with the mean turbulent velocity field \bar{u}_1 . This assumption indicates that the turbulence only affects the wave through the mean velocity profile and not the turbulent stresses. Although R&H showed that this model does not adequately describe the behavior of the waves in turbulent shear flows. It may have a distinct advantage for the compliant wall problem. The solution over compliance can be compared with the solution involving the next closure scheme which accommodates for the Reynolds stress influence. This may show the effect of compliance on the Reynolds stresses and whether the stresses have a significant effect on the wave development over a compliant wall for the turbulent problem.

The second model we choose might be referred to as the Newtonian eddy model. The model goes back to Townsend (1956) who suggests that persistently strained turbulence should develop an equilibrium structure that depends on the type of strain and not the strain-rate magnitude. Lighthill (1956) proposed a constitutive equation for the turbulence structure, based on Townsend's data. Lumley (1967) suggested a similar model which depends on a memory parameter and spatial awareness parameter. He showed that the departure from isotropy is due to the inhomogeneity in the strain-rate. If the strain-rate inhomogeneity is of a sufficient scale and its rate of change is slow then

$$\tilde{r}_{ij} = -2\epsilon \tilde{S}_{ij} \quad E.21$$

is a good approximation where

$$\tilde{S}_{ij} = \frac{\partial \tilde{u}_i}{\partial x_j} + \frac{\partial \tilde{u}_j}{\partial x_i}$$

and

$$\epsilon = \lim_{S_{ij} \rightarrow 0} \frac{1}{2} \left(\overline{u'_i u'_j} S_{ij} / S_{kl} S_{kl} \right)$$

This assumes that the wave causes an oscillation in the turbulent structure and not its energy. We now have (E.21) which is referred to as the Newtonian eddy model. This is substituted into (E.16) and (E.15)

The general wave equations for both models becomes

$$[(\alpha \bar{u}_1 - \omega)(D^2 - \gamma^2) - \alpha D^2 \bar{u}_1] \hat{u}_2 + \frac{i}{R_\delta} (D^2 - \gamma^2)^2 \hat{u}_2 + B_1 = 0 \quad E.22$$

and

$$\frac{1}{R_\delta} (D^2 - \gamma^2) \hat{\Omega}_2 - i(\alpha \bar{u}_1 - \omega) \hat{\Omega}_2 - i\beta D \bar{u}_1 \hat{u}_2 + B_2 \quad E.23$$

where the B_i are found from the closure models

(i) Quasi-laminar: $B_1 = B_2 = 0$

(ii) Newtonian Eddy Model:

$$\begin{aligned} \bar{B}_1 &= i \frac{\nu_t}{\nu} (D^2 - \gamma^2)^2 \hat{u}_2 + 2i \frac{\nu_t'}{\nu} (D^3 - \gamma^2 D) \hat{u}_2 + i \frac{\nu_t''}{\nu} (D^2 + \gamma^2) \hat{u}_2 \\ \bar{B}_2 &= \frac{\nu_t}{\nu} (D^2 - \gamma^2) \hat{\Omega}_2 + \frac{\nu_t'}{\nu} D \hat{\Omega}_2 \end{aligned}$$

where $\frac{\nu_t}{\nu} = 1/R_\epsilon$ is defined as the local eddy-viscosity of the mean flow. Before we discuss the handling of the eddy-viscosity variable and the mean flow, the equations for the small scale background turbulence will be discussed.

E.5 Background Turbulence

The approach for the background turbulence is the same one used for the secondary instabilities discussed earlier in this thesis. The instantaneous velocity is given as

$$u_i = \bar{u}_i + A\bar{u}_i + Bu'_i \quad E.24$$

where A and B are the amplitudes of the large- and small-scale mechanisms. Substituting into the Navier-Stokes equations and subtracting out the mean and large-scale motion, the following equation results

$$\begin{aligned} \frac{\partial u'_i}{\partial t} + \bar{u}_j \frac{\partial u'_i}{\partial x_j} + A\bar{u}_j \frac{\partial u'_i}{\partial x_j} + u'_j \frac{\partial \bar{u}_i}{\partial x_j} + Au'_j \frac{\partial \bar{u}_i}{\partial x_j} \\ = - \frac{\partial p'}{\partial x_i} + \frac{1}{R_\delta} \frac{\partial^2 u'_i}{\partial x_j \partial x_j} + \frac{\partial}{\partial x_j} [\langle u'_i u'_j \rangle - u'_i u'_j] \end{aligned} \quad E.25$$

and

$$\frac{\partial u'_i}{\partial x_i} = 0 \quad E.26$$

This gives the dynamic equations for the small-scale turbulent component of the flow field. This is the same form as given for the secondary instabilities in the laminar boundary layer with the addition of the last two terms in (E.25). This in fact is the phase averaged Reynolds stress and Reynolds stress of the small-scale turbulence. As with the large-scale motion we are using a linear analysis. Since the last two terms of (E.25) are higher order in u'_i they are neglected. So in fact we find that there is no closure problem found for the background turbulence. What remains are precisely the same equations as governed the secondary instabilities in a laminar boundary layer. The difference lies only in the treatment of the basic flow which in this case is the mean turbulent flow and large-scale organized wave motion. The mean turbulent flow and eddy-viscosity are introduced in the next section along with an approach to solve the turbulent problem.

E.6 Turbulent Shear Flow

It is well known that the mean turbulent velocity profile on a rigid wall is composed of a (1) wall law, (2) log law and (3) wake law. As a first approximation to the mean flow we use an empirical relation given in Landahl (1967) as

$$u^+ = \frac{1}{\kappa} \ln(1 + \kappa y^+) + \gamma \left[1 - \exp\left(-\frac{y^+}{11}\right) - \frac{y^+}{11} \exp(-0.33y^+) \right] + 1.3 \left[1 + \sin \frac{\pi}{2} (2\bar{y} - 1) \right] \quad E.27$$

where

$$y^+ = y u_\tau / \nu \quad u^+ = \bar{u} / u_\tau \quad \bar{y} = y / \delta$$

$$\kappa = 0.4 \quad \gamma = 7.4$$

This is a combination of models by Reichardt (1951) and Coles (1956). The friction velocity is chosen from experiments or specified so that $\bar{u}_1 / u_\infty = 0.999$ at $\bar{y} = 1$. In choosing the later approach, the results compare well with Andreopoulos, Durst, Zaric and Jovanovic (1984).

An eddy-viscosity model was given by Cebeci and Smith (1974). This is given as

$$\frac{\nu_t}{\nu} = \kappa^2 y^{+2} \left| \frac{du^+}{dy^+} \right| \left[1 + \exp\left(-\frac{y^+}{A^+}\right) \right]^2 \quad 0 \leq y < y_c$$

$$= 0.0168 \frac{(1 + 0.55) R_\theta H}{1 + 0.55 [1 + \exp(-.243z^{1/2} - .298z)]} \quad y_c \leq y \leq \delta \quad E.28$$

where $z = R_\theta / 425 - 1$, $A^+ = 26$, and $\kappa = 0.4$ R&H found that it made little difference if a constant or variable eddy-viscosity was used.

E.7 Numerical Approach

We could solve the problem in this manner described as such. With the mean velocity profile and eddy-viscosity model given above the large-scale organized wave can be obtained. The results of the large-scale can be used to feed the mean profile which in turn is used to re-solve for the organized wave motion. The number of cycles required needs to be determined. Initially assuming one cycle is sufficient, spectral and shooting methods have been implemented to determine the organized wave using the above mean turbulent velocity and eddy-viscosity profile. The local method proves to be very efficient computationally so a number of further iterations may be performed. The spectral and shooting solutions show agreement.

The background turbulence can be found by the approach used for the secondary instabilities in the laminar boundary layer problem. The assumptions of periodicity in the large-scale motion are similar to those of the primary waves in laminar boundary layers. Additionally, we could assume that the small-scale growth-rates are much greater than the large-scale organized wave. For the background turbulence, the turbulent mean and large-scale wave represent the basic flow for the background turbulence. This can be fed into the secondary instability code to provide a means to solve for the small-scale background turbulence.

The approach should be solved for the rigid wall and compared with other numerical solutions and experimental. Then compliance can be introduced. This approach is computationally efficient compared to DNS and neglects only the higher order terms in the equations. This model will be implemented and discussed in a future investigation.